# Quantitative Measurement and Modeling of the DNA Damage Signaling Network:
# DNA Double-strand Breaks



by

**Andrea R. Tentner**

B.A., Biological Sciences
The University of Chicago, 2003

S.M., Biological Engineering
Massachusetts Institute of Technology, 2006

Submitted to the Department of Biological Engineering
In partial fulfillment of the requirements for the degree of

**Doctor of Philosophy in Bioengineering**
at the
**Massachusetts Institute of Technology**

September 2009


Signature of Author: _____
Department of Biological Engineering
July 24, 2009

Certified by: _____
Michael B. Yaffe
Professor of Biology
Thesis Supervisor

Certified by: _____
Douglas A. Lauffenburger
Professor of Biological Engineering, Biology and Chemical Engineering
Thesis Supervisor

Accepted by: _____
Alan J. Grodzinsky
Professor of Electrical, Mechanical and Biological Engineering
Graduate Program Committee Chairperson

**Quantitative Measurement and Modeling of the DNA Damage Signaling Network: DNA Double-strand Breaks**

by

Andrea R. Tentner

Submitted to the Department of Biological Engineering on July 24, 2009,
in partial fulfillment of the requirements for the degree of
Doctor of Philosophy in Bioengineering

# Abstract

DNA double-strand breaks (DSB) are one of the major mediators of chemotherapy-induced cytotoxicity in tumors. Cells that experience DNA damage can initiate a DNA damage-mediated cell-cycle arrest, attempt to repair the damage and, if successful, resume the cell-cycle (arrest/repair/resume). Cells can also initiate an active cell-death program known as apoptosis. However, it is not known what "formula" a cell uses to integrate protein signaling molecule activities to determine which of these paths it will take, or what protein signaling-molecules are essential to the execution of that decision. A better understanding of how these cellular decisions are made and mediated on a molecular level is essential to the improvement of existing combination and targeted chemotherapies, and to the development of novel targeted and personalized therapies. Our goal has been to gain an understanding of how cells responding to DSB integrate protein signaling-molecule activities across distinct signaling networks to make and execute binary cell-fate decisions, under conditions relevant to tumor physiology and treatment.

We created a quantitative signal-response dataset, measuring signals that widely sample the response of signaling networks activated by the induction of DSB, and the associated cellular phenotypic responses, that together reflect the dynamic cellular responses that follow the induction of DSB. We made use of mathematical modeling approaches to systematically discover signal-response relationships within the DSB-responsive protein signaling network. The structure and content of the signal-response dataset is described, and the use of mathematical modeling approaches to analyze the dataset and discover specific signal-response relationships is illustrated.

As a specific example, we selected a particularly strong set of identified signal-response correlations between ERK1/2 activity and S phase cell-cycle phenotype, identified in the mathematical data analysis, to posit a causal relationship between ERK1/2 and S phase cell cycle phenotype. We translated this posited causal relationship into an experimental hypothesis and experimentally test this hypothesis. We describe the validation of an experimental hypothesis based upon model-derived signal-response relationships, and demonstrate a dual role for ERK1/2 in mediating cell-cycle arrest and apoptosis following DNA damage.

Directions for the extension of the signal-response dataset and mathematical modeling approaches are outlined.

Thesis Supervisor: Michael B. Yaffe
Title: Professor of Biology

Thesis Supervisor: Douglas A. Lauffenburger
Title: Whitaker Professor of Biological Engineering, Biology, and Chemical Engineering

# Biographical Note

Andrea Tentner received a Bachelor in Biological Sciences from The University of Chicago in June 2003. While at The University of Chicago, Andrea worked in the laboratory of Dr. Jean Greenberg, investigating the activation of cell-growth and cell cycle in Arabidopsis thaliana mutants that exhibit one or more aspects of the pathogen-defense response in the absence of pathogen.

In September 2003, Andrea started her graduate work in the Department of Biological Engineering at the Massachusetts Institute of Technology. Under the joint supervision of Michael Yaffe and Douglas Lauffenburger, she conducted a Ph.D. thesis entitled "Quantitative Measurement and Modeling of the DNA Damage Signaling Network: DNA Double-strand Breaks", which was completed in July 2009. For the final three years of her Ph.D. thesis, Andrea was supported by a fellowship from the Integrative Cancer Biology Program.

In October 2009, Andrea will start a postdoctoral fellowship in the Systems Biology Department at Harvard Medical School. Her postdoctoral research will be supervised by Sean Megason and will use zebra-fish as a model system to understand the mechanisms governing cell-fate patterning in spinal cord interneurons.

# Acknowledgements

There are so many people without whom this thesis work would not have been possible. My first thanks go to my advisors, Michael Yaffe and Douglas Lauffenburger. They have afforded me the flexibility to pursue what I found exciting, experimentally and computationally, and have been supportive both scientifically and personally.

I would like to thank Michael especially for being a constant source of enthusiasm from the moment I met him, for hours-long conversations about data, and for guidance in my project and in my career. I would like to thank Doug especially for giving unstinting encouragement and productive feedback throughout, and for fostering a collaborative, thoughtful and scientifically exciting environment in his lab and in the wider BE community. It has been a privilege to be advised by you both.

I would also like to thank my committee members: Forest White, who has unfailingly and generously given me thoughtful feedback on my project as well as encouragement and support, and Leona Samson, who has always been engaged and enthusiastic and served as an amazing role model of a woman in science.

The members of the ICBP and CDP community, especially those from the early days of the group, have provided a great space to talk about the challenges of implementing experimental and computational aspects of quantitative, systems biology investigations. I would like to thank Suzanne Gaudet, Kevin Janes, John Burke and Brian Joughin for particularly helpful discussions at many stages of my project. Other people in the CDP community with whom I have had indispensably helpful discussions about my work include Ericka Noonan, Josh Apgar, Arthur Goldsipe and Pam Kreeger.

The members of the Yaffe Lab, past and present, have been a large part of my experience here at MIT and have helped make it a good one. I want to especially thank the members of the Graduate Student Club: Duaa Mohammed, Sarah Bissonnette, Drew Lowery and Jes Alexander, for discussions on science and on life, and Duaa in particular for being a friend and for showing me the ropes from the moment I stepped into the lab, to now. I would like to thank my bay-mate, Dan Lim, for many snarky comments, for helping me when my computer's hard-drive (inevitably) crashed, for lots of good chats, AND for recommending that I get CorelDRAW to make the figures for my thesis! Gerry Ostheimer edited more versions of my Master's thesis than I can count. Alexandra Gardino has been the best company on long days (and nights) in the Shark Tank and a great source of career advice. Chris Ellson has also been a great source of career advice. I would also like to thank Mary Stewart for keeping the lab running while she was around, and stopping in to check on us every once in a while, even now.

The members of the Lauffenburger lab, past and present, have also been a great part of my experience here, providing essential discussions, lending me reagents and lab space, and always being a great group of people that I enjoy hanging out with. Of those I have not already mentioned, I would like to especially thank Kristin Naegle, Hyung-do Kim, Ben Cosgrove, Matt Lazzara, Ta Hang, Lorenna Lee-Houghton, Megan Palmer, Shannon Alford, Mark Fleury, Aran Parillo and Stacey Pawson.

The Fifth floor of the Cancer Center has been an amazing environment to work in, and past and present members of the Lees, Jacks and Sharp Labs have been my extended lab-mates in many ways.

I would like to thank Alan Grodzinsky and Dalia Gabour for being personally supportive during a particularly rough period in my graduate career. It was, and is, so much appreciated.

My friends, both in Boston and far-flung across the country and world, have supported me face-to-face, by phone and by Facebook. Thank you to Karin Louzada, Karen Kasza, Rana Juster, Justin Sitter, Ali Landman, Jason Wyman, Rachna Khatau and Liju Varghese.

Finally, I would like to thank my family; my parents, Adrian and Felicia, my sister, Karen, my uncle, Sandu, my Grandma Ana, and my boyfriend, Josh. They have been incredibly supportive, and I could not have done this work without them. I want to thank my dad for being one of the best, and most patient sounding boards; he has listened to me talk and brainstorm about my work, thought deeply about it, and given me productive feedback more times than I can count. He has listened to me when I have felt overwhelmed, recognized it, and encouraged me to push on despite it. In my own career, I will strive to have what he has – a never-waning enthusiasm for his own work, and for learning about and tackling new problems. I want to thank my mom for being always enthusiastic about my accomplishments. My sister is one of my best friends, and someone that I learn from every day, and my boyfriend, Josh, is my other best friend; he has been a constant and present support. I want to thank my uncle for forwarding me Cat-of-the-Day e-mails and sending your photos of good food and every-day scenes in exotic places – they make my day! And I want to thank my Grandma Ana, who lives her life the way I want to; strong, independent, but not isolated, and always learning and exploring. You are all amazing and I am so lucky to have you.

## Table of Contents

## List of Figures

## List of Supplementary Figures

## List of Tables



## List of Suplementary Tables

# Chapter 1: Introduction

This thesis investigates the signaling mechanisms governing the cellular response to DNA damage and DNA double-strand breaks (DSB), through the use of quantitative experimental, and computational, molecular and cell biology approaches. This chapter contains background and motivating information for this work, including a contextualization of this work within the questions of the cancer biology field, and an overview of DNA damage- and DSB signaling, the role of inflammatory cytokines in the etiology and treatment of cancer, and systems biology methods and models that we make use of, and extend, within the scope of this thesis.

## DNA damage and DSB: cancer cause and cure

The chromatin integrity network is a highly conserved response, found in all eukaryotes, that is critical to maintaining genomic integrity. Failure of cells to appropriately respond to DNA damage facilitates tumorigenesis [1, 2]. In fact, many mutations commonly found in tumors target and derange the DNA damage response. A failure to respond appropriately to DNA damage also leaves tumor cells susceptible to cell-killing by DNA-damaging agents; these agents are thus used in the clinic to target tumors cells [3-9].

Of the many lesion types that constitute DNA damage, the most lethal is the DNA double-strand break (DSB), and DSB are one of the major mediators of chemotherapy-induced cytotoxicity in tumors [2, 10]. Following induction of DSB, cells respond on a molecular level by activating protein signaling molecules in the core chromatin integrity network or DNA double-strand break response pathway , and in pathways governing general stress response , cell-survival , cell-death and cell-cycle control (Figure 1-1). On the cellular level, the integration of these protein signaling-molecule activities translates into

one of several cell-fate decisions, including induction of cell-cycle arrest, initiation of DNA repair, activation of transcriptional programs, and either apoptosis, necrosis or cell senescence [2, 11]. The two major cellular responses that are explored in this thesis include that of 1) DNA damage-mediated cell-cycle arrest and 2) cell-death via apoptosis.

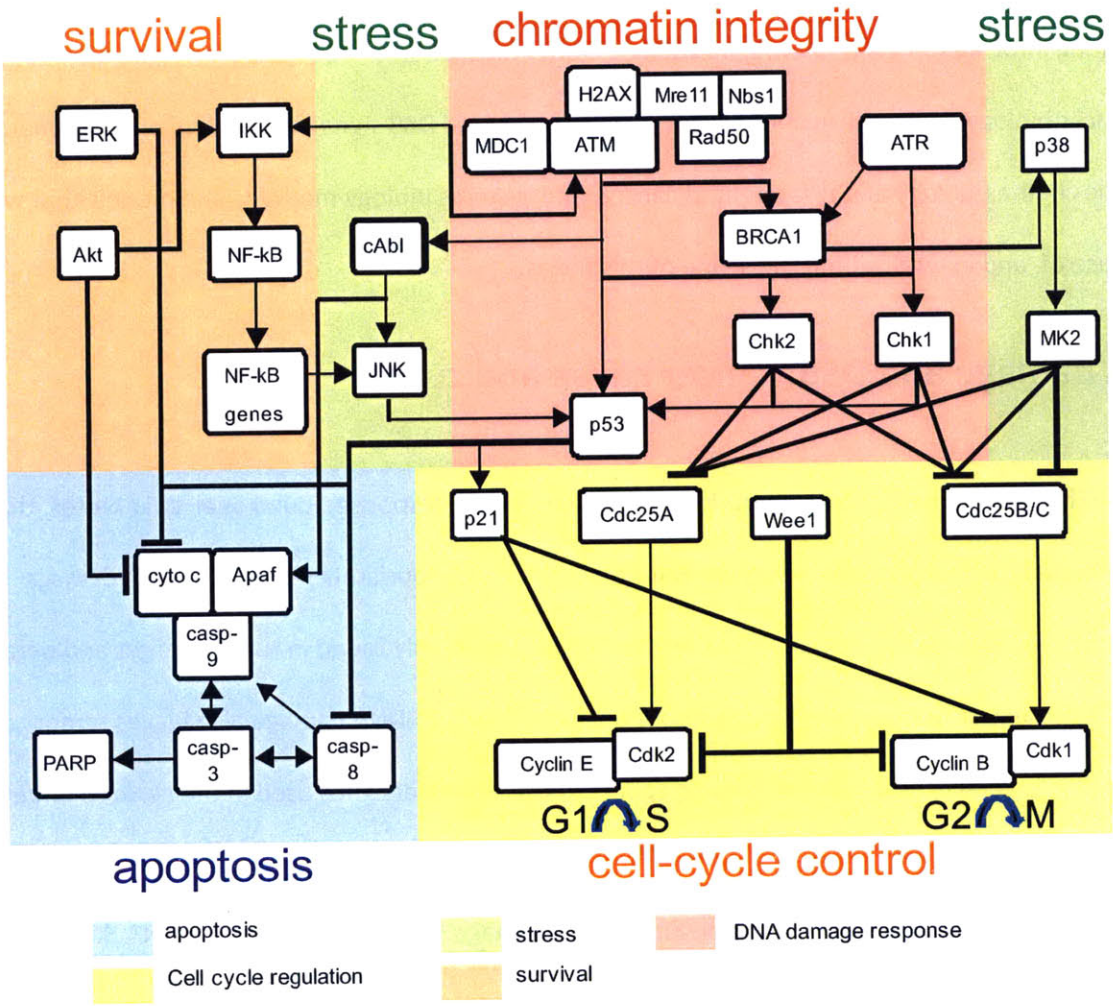


**Figure 1-1.** A schematic DNA damage response signaling network demonstrating the intersection and integration of multiple distinct signaling networks governing the chromatin-integrity response, and general stress, survival, cell-death and cell-cycle regulatory responses.

## Proximal DSB signaling

Following induction of a DSB, inactive ATM dimers in the nucleoplasm auto-phosphorylate, fall apart into active monomers and localize to the site of the break [12, 13]. A complex of three proteins, MRE11, Rad50 and Nbs1, known as the MRN complex, also localizes to the site of the break [14, 15]. Once at the site of the break, ATM phosphorylates the histone variant H2AX at areas surrounding the break and many other chromatin-associated and nucleoplasmic substrates [16-19]. ATM also directly associates with the MRN complex via Nbs1 [20, 21], and ATM and Nbs1 act in a mutual fashion to further, or maintain, the activation status of the other [22-28]. The activation and localization of ATM and Nbs1 to break sites, and of γH2AX to areas surrounding break sites, is required for subsequent recruitment and retention of DNA repair factors, to the site of the break and for activation of downstream signaling molecules necessary for induction of DNA damage mediated cell-cycle arrest and cell-death processes following DNA damage [18, 29]. A few of the better characterized ATM substrates include Chk2 and p53 [30-33]. Chk2 is a checkpoint signaling protein that leads to induction of DNA damage mediated cell cycle arrest via phosphorylation and inactivation of Cdc25A/C phosphatases [34]. p53 is a signaling protein and transcription factor that can lead to maintenance of DNA damage mediated cell cycle arrest via upregulation of the cyclin dependent kinase inhibitor (cki) p21, or to induction of apoptosis via transactivation of pro-apoptotic Bcl-2 protein family members [35-40].

Mutations in many of the proteins involved in the proximal signaling response to DSB, including ATM, H2AX, Chk2, Nbs1 and p53, are commonly found in various cancers and are often clearly associated with increased risk of cancer in mutation-carriers [41, 42].

## Other molecular signals in the DSB response

### *MAPKs*

p38, JNK and ERK kinases are all members of the MAPK (Mitogen Activated Protein Kinase) family. While MAPK family members are not traditionally thought of as part of the specific DNA damage, or DSB, response, these important cellular proteins are widely accepted to be key elements in the regulation of cell fate decisions such as cell cycle control and apoptosis in nearly all cell types. These MAPKs have been shown to be activated by induction of DSB, and they undoubtedly play a role in regulation of cell fate following genotoxic stress.

The MAPK family of signaling pathways is eukaryotic-specific and highly conserved [43-45]. This family of signaling pathways consists of several specific pathways all sharing a general three-kinase signal cascade format in which a MAPKKK (MAPK kinase kinase) serine/threonine kinase is activated, dually phosphorylates and activates a MAPKK (MAPK kinase) dual specificity kinase, that, in turn, dually phosphorylates and activates a MAPK (MAP kinase) serine/threonine kinase on a TXY motif in the MAPK activation loop [44, 46]. MAPKs are serine-threonine kinases with a repertoire of at least 80 substrates consisting of transcription factors, protein kinases and cytoskeletal components [47]. There are just five MAPKs, the best characterized in mammals being p38, JNK, and ERK1/2. However, they are involved in the mediation of such wide-ranging and key cellular processes as cellular growth, differentiation, adaptation to stress, survival and death in response to such diverse stimuli as growth factors, cytokines, cellular adherence status and hypoxic and genotoxic stress [43, 44]. The ability of these few kinases to respond to such a wide variety of stimuli is not fully understood, but is probably facilitated by the MAPK cascade set-up and the ability of several MAPKKK to initiate each cascade [44].

ERK1/2 is usually thought of as a "survival" kinase. It is the MAPK downstream in the three-kinase MAPK pathway consisting of Raf/MEK/ERK [48]. ERK is activated by dual phosphorylation at T202/Y204 by the MAPK kinases MEK1 and MEK2, in response to such growth factors as EGF and PDGF [44, 49]. A role for ERK1/2 in the promotion of cell-survival and proliferation in response to various growth factors and mitogenic signals is well established. However, it is also implicated in both cell cycle control and protection from cell death in some cell types [44, 49], and it is activated in cells following treatment with several genotoxic agents [48, 50].

p38 is usually thought of as a "general stress" kinase. It is a MAPK family member that is activated by dual phosphorylation at T180/Y182 by the MAPK kinases MEK3 and MEK6 [49] in response to cellular stresses, such as genotoxic and osmotic stress, and inflammatory cytokines, such as TNF-$\alpha$ and IL-1 [51]. Its known substrates include the transcription factor ATF2 and the protein kinase MAPK activated protein kinase-2 (MAPKAPK2/Chk3) [51, 52]. p38 has a role in mediating cytokine production and apoptosis [44, 45], as well as in cell cycle checkpoint induction and apoptosis following DNA damage [47, 52]. It has been shown recently by the Yaffe lab and the Fornace lab that the p38 SAPK pathway is activated following UV treatment, and it has been proposed that p38 activation of MAPKAPK2/Chk3 acts as another branch in the DNA damage response, in analogy to the ATM-Chk2 and ATR-Chk1 branches. Indeed, MAPKAPK2/Chk3 shares a high functional similarity to the other Chk effector kinases in mediating cell cycle arrest following UV [52]. MAPKAPK2/CHK3 has been shown to phosphorylate CDC25B/C following UV, generating the 14-3-3 binding site necessary for cytoplasmic sequestration, and it has been shown that loss of MAPKAPK2/Chk3 results in an inability to sustain a G2/M or a G1/S checkpoint following UV-induced DNA damage [52].

JNK is usually thought of as a "general stress" or "death" kinase. It is a MAPK family member that is activated by dual phosphorylation at T183/Y185 by the MAPK kinases MEK4 and MEK7 [49] in response to such cellular stresses as genotoxic (eg UV light, γ-irradiation) and osmotic stess, and in

response to inflammatory cytokines, such as TNF-α and IL-1) [45, 47, 48, 50, 53]. Its known substrates include the Jun-family transcription factors (c-Jun, c-Fos, ATF2) [44, 47]. JNK is implicated in the induction of apoptosis in several cell types .

***Non-MAPKs***

Akt, also known as Protein Kinase B (PKB), is a kinase involved in promotion of survival and regulation of insulin signaling [54, 55]. It is phosphorylated by PDK1 and mTOR-rictor following activation of PI3K by activated RTKs (receptor tyrosine kinases) and requires phosphorylation on T308 and S473 for activity [56-59]. Substrates include FOXO isoforms, BAD, and GSK3. Akt may positively regulate ERK1/2 signaling via GSK3 [60-63]. Mutations that affect Akt regulation are commonly found in cancer, including mutations of PTEN, a negative regulator of Akt, and of PI3K, a positive regulator of Akt [64-67].

NFκB is a transcription factor that is implicated both in promoting survival in response to a wide variety of stresses, including genotoxic stress, and in initiation of inflammatory responses [68-70]. Under normal cellular conditions, NFκB is sequestered in the cytoplasm by the regulatory protein IκBα. When IKK (IκBα kinase, a multi-subunit kinase consisting of two catalytic subunits, IKKα and IKKβ and a non-catalytic subunit, IKKγ or NEMO) is activated, it phosphorylates IκBα, leading to the ubiquitination and degradation of IκBα, and the release of NFκB and its subsequent nuclear translocation [71, 72]. Following DNA damage, ATM may play a key role in activation of NFκB by directly phosphorylating the IKK subunit, NEMO, leading to its activation[73-75].

## Cellular responses to DNA damage/DSB

### *Apoptosis: Programmed cell-death*

Apoptosis is an important cellular response to DNA damage that can prevent the propogation of cells that have sustained irreparable chromatin changes [76-80]. It is an active form of "programmed" cell-death in which cell-elements are broken down and contained in apoptotic membrane-bound vacuoles or blebs. This break-down and containment of cellular elements prevents their release into the surrounding extracellular matrix [78, 81]. Apoptosis does not normally provoke an inflammatory response, as may occur in a relatively unordered and messy alternate mode of cell-death known as necrosis [82-84]. As opposed to other forms of cell-death such as necrosis, or as opposed to non-cell death outcomes such as senescence, apoptosis is the goal cellular outcome of chemotherapeutic treatment regimens as it is thought to be the cellular outcome that most effectively leads to tumor regression [85-87].

Apoptosis can be mediated by two distinct pathways, the extrinsic and intrinsic pathways. In extrinsic pathway activation extracellular ligands bind to death receptors (*e.g.* TNF/TNFR1) and activate a cascade of intracellular signals, leading to the activation of the initiator caspase 8. In intrinsic pathway activation, dysfunction of intracellular organelles (*e.g.* mitochondrial cytochrome c release) due to various cellular stresses leads to activation of the initiator caspase 9 [88-90]. Activation of the initiator caspases via the extrinsic and intrinsic pathways converge to activate the effector cystein protease caspase-3 [91].

Apoptosis is dysregulated in cancer and its dysregulation leads to cancer development and progression [80, 92].

### *Cell cycle checkpoints*

Cell cycle check-points constitute an essential cellular response to DNA damage that can prevent cells from replicating while DNA damage remains unrepaired, thus preventing damaged cells from passing on mutagenic chromatin changes [93, 94]. Cell cycle regulatory elements are commonly dysregulated in cancer and the dysregulation of these elements promotes cancer development and progression [95, 96].

Modulation of cell-cycle regulators may be useful in tumor treatment regimens, alone, or in conjunction with traditional DNA damaging chemotherapeutics. One possible mode of interference is disruption of cell-cycle checkpoints, as bypass of cell-cycle checkpoints normally initiated by DNA damage in tumor cells can lead to cell-death [97-103].

## Doxorubicin

Doxorubicin (Dox) is a naturally occurring, bacterially-derived anthracycline, and is one of the most widely therapeutically applied DNA damage-inducing chemotherapeutics for the treatment of solid and hematopoietic tumors [104-106]. It is a topoisomerase II inhibitor that leads to the induction of DNA double-strand breaks (DSB).

Topoisomerase II is a multifunctional endogenous enzyme that can act as a helicase, nuclease and DNA-religase. It participates primarily during DNA synthesis, but also during transcription, to unwind and cut super-helical DNA, allow DNA and RNA polymerases to pass, and then to relegate DNA following polymerase passage. Doxorubicin binds to topoisomerase II on the DNA and locks it into a conformation that is competent for DNA cleavage, but incompetent for DNA re-ligation. The result is an accumulation of so-called "cleavable-complexes" (ternary complexes of Doxorubicin-topoisomerase II-DNA) marking the sites of protein-linked DNA double-strand breaks [107-109].

Doxorubicin can also mediate cell-killing via oxygen radical production and via DNA intercalation and inhibition of DNA and RNA polymerase [110-113]. Doxorubicin's mode of cytotoxicity has been shown to be dose dependent; at doses above 3 μM the balance shifts from direct strand breaks to oxygen radical production (superoxide production probably results from the transfer of electrons to molecular oxygen by the doxorubicin semiquinone after reduction of the drug by sarcosomal NADPH:cytochrome P-450 reductase; this reaction is accompanied by accumulation of hydrogen peroxide). However, it has been shown that DSB induction (but not SSB induction) is correlated with the cytotoxicity of Doxorubicin [114-117].

## Role of inflammation and inflammatory cytokines in cancer

Tumor cells express and secrete high levels of inflammatory cytokines, including TNF-α, and increased expression of inflammatory cytokines in tumor cells is highly correlated with tumor grade for several tumor types, and is associated with poor prognosis [118-121].

Additionally, some alleles of inflammatory cytokines (TNF) are associated with familial cancers or cancer-prone conditions [122, 123] and suppression of TNF activity or expression in mouse models of cancer has been shown to prevent the development of tumors [124]. Therefore inflammation and inflammatory cytokines are strongly associated with tumor initiation or promotion and tumor progression.

However, TNF has also been shown to have tumoricidal properties. Local high-dose administration of TNF is under investigation as a treatment for some solid tumors [125-127].

## Molecular-Targeted cancer therapeutics: Goals and Challenges

Molecular biological studies have accumulated detailed knowledge about some of the proximal responders to DNA double strand breaks, as well as about signaling molecules that participate canonically in signaling pathways distinct from chromatin-integrity signaling pathways, and that are known to influence the cellular response to DSB (eg signaling molecules that participate in general stress, survival, cell-death regulatory and cell-cycle regulatory pathways). Some of this understanding has led to dramatic, if limited, success in developing targeted cancer therapies.

The most compelling targeted therapy story thus far is perhaps the use of the drug Gefitinib (Iressa) in NSCLS patients. This drug is an EGFR inhibitor and leads to dramatic tumor regression in NSCLC patients whose tumors express EGFR with one of two well-characterized activating mutations. In patients whose tumors do not express a mutated EGFR, Iressa does not lead to substantial tumor regression [128, 129].

Inhibition of signaling from the EGFR leads to inhibition of ERK and Akt signaling, two signaling pathways that lie downstream from the EGFR. Both of these pathways are canonically involved in promoting survival and proliferation. Therefore, that the inhibition of these pathways in cells leads to tumor regression (involving both slowed proliferation and tumor cell death) is a straightforward outcome [130, 131]. However, the signaling networks involved in mediating cell decisions such as that of life versus death are complex, involving positive and negative feedback on many levels, and the outcome obtained from inhibiting a single signaling molecule is often not straightforward [132].

EGFR family member receptors and ligands have been shown to be major drivers of the pathology and progression of breast tumors. However, a large proportion of breast tumors are resistant to treatment with tyrosine kinase inhibitors (TKIs) that target these family members. Mutations in regulatory elements of the Akt signaling pathway are the source of this resistance in some tumors.

Following treatment with TKIs such as Iressa, sensitive tumor cell-lines exhibit decreased phosphorylation/activation of EGFR, ERK and Akt whereas resistant cell-lines exhibit decreased phosphorylation/activation of EGFR and ERK, but maintain Akt signal activation. Loss of PTEN, a negative regulator of Akt, has been shown to result in loss of sensitivity to TKIs. Restoration of PTEN function to PTEN null cells, or direct pharmacologic inhibition of the PI3K/Akt signaling pathway, confers sensitivity to TKIs. In this instance, the context of Akt signaling function (wild-type vs. mutated) is a determining factor between tumor sensitivity and tumor resistance to a targeted chemotherapeutic agent (TKIs) [133-136].

Chemical inhibition of ATM, a master regulator of the DNA damage response, has been proposed as a means to sensitize tumors to treatment with IR and other radiomimetic chemotherapeutic agents [137, 138]. Primary cells from A-T patients and ATM knockout mice are hypersensitive to ionizing radiation (IR) and chemotherapy-induced DNA double strand breaks (DSBs) [139-141]. Additionally, ATM-deficient tumors have been shown to be sensitive to DNA DSB-inducing cancer treatments [142] and some reports show loss of ATM in tumors correlates with beneficial clinical outcomes in patients undergoing chemotherapeutic regimens with DNA damaging agents. However, a large number of studies show the opposite result; certain studies suggest that loss of ATM may correlate with *resistance* to DNA-damaging chemotherapy and poor patient survival [143-145]. Jiang, Reinhardt et al. have recently shown that the mutation status of p53 and ATM, two of the most commonly mutated genes in tumor cells, are crucial elements that interact to determine sensitivity or resistance to DNA damaging chemotherapeutic regimens. Thus, tumors harboring mutations in both p53 and ATM are highly sensitive to the cytotoxic effects of DNA damaging agents, while single mutants in either p53 or ATM are highly resistant. Chemical inhibition of ATM may then be expected to sensitize tumor cells to DNA damaging chemotherapy in the context of a tumor already bearing a p53 mutation. However, in p53 wild-type tumors, adjuvant chemical inhibition of ATM may actually be expected to confer

resistance to the traditional regimen. In tumors already bearing both ATM and p53 mutations, adjuvant ATM inhibition may be expected to not materially contribute to therapeutic outcome.

We do not have a clear understanding of how the integrated signaling response to DNA damage works as a system to make a decision between the alternate cell-fates following DNA damage of cell cycle arrest/repair/ resume or induction of cell death, and to mediate that decision. A better understanding of how these cellular decisions are made and mediated on a molecular level is essential to the improvement of existing combination and targeted chemotherapies, and to the development of novel targeted and personalized therapies. Detailed quantitative systems-level studies of the molecular signaling pathways involved in the cellular decision process following DNA damage are expected to reveal context-dependencies in signaling and cellular decision outcomes. These context dependencies represent crucial knowledge that may reconcile conflicting data in the literature regarding the role of single signaling molecules in the life-death decision following DNA damage. The importance of context to the cellular outcome obtained from a treatment has been demonstrated in many studies, and the relevance to implementation of effective targeted chemotherapeutic regimens is clear [146-149].

## System-biology models to investigate signal-response relationships in cue-responsive biological networks

The collection of systems-level, quantitative signal-response data-sets is an essential step in gaining insight into dynamic, context-dependent signaling mechanisms that may be exploited in design of targeted chemotherapeutic regimens. Just as important is an appropriate analysis methodology for these data. A wide range of computational modeling approaches have been used to study molecular signaling and its regulation of cellular phenotypes. These approaches fall into two broad categories; mechanistic modeling methods and data-driven modeling approaches.

Ordinary differential equation based physicochemical models are a popular implementation of a mechanistic modeling approach. Such models require a detailed knowledge of the mechanisms of interaction among signaling elements modeled that is not available in the context of many studies. The applicability of these models to the analysis of relationships between molecular signaling and resulting cellular phenotype is therefore practically limited [150-153].

Data-driven, relational modeling approaches, including regression analysis approaches such as Partial Least Squares regression (PLSR), Bayesian network analysis and decision tree analysis methods, have been used with success to discover signal-response relationships from quantitative signal-response datasets in the study of biological networks with ill-defined structure that are, therefore, not amenable to modeling in a more explicit fashion using ODE-based modeling approaches.

In PLSR analysis, signaling measurements are cast as a matrix of independent variables, X, across several observations or treatment conditions, and cellular response measurements are cast as a matrix of dependent variables, Y, across the same observations or treatment conditions. The analysis is based on the hypothesis that the measured cellular responses are a definable quantitative function of the measured molecular signaling [151, 154]. Due to technical, time and cost constraints, the number of observations available for analysis is small and generally much smaller than the number of signals we would like to relate to the cellular responses under investigation, prohibiting the calculation of a unique regression solution to the hypothesized relationship $Y = f(X)$.

PLSR reduces the explanatory variable set substantially to an effective explanatory variable set that is made up of orthogonal latent variables, or Principal components (PCs). PCs are linear combinations of the original model independent variables that simultaneously maximally capture variance in the independent variable space and covariance with the dependent variable space. The number of PCs necessary to capture the majority of the variance in the explanatory (independent) variable set is much smaller than the number of original explanatory variables, and smaller than the

number of observations available for analysis. The PCs serve as effective explanatory variables. This effective reduction in the number of explanatory variables allows PLSR to find a unique solution for the signal-response functional relationship [155, 156].

PLSR can be used to identify single signaling elements and combinations of signaling elements that strongly correlate with cellular response. Additionally, it can be used to predict cellular responses to additional treatments or conditions (e.g. following pharmacologic perturbations), using newly measured and/or estimated signaling data. The quality of the model and any predictions it produces rely upon the the original data-set having included: 1) measurements of all essential signaling molecules for the cellular response decision under investigation, 2) measurements across treatment conditions that produce large quantitative changes in activation of signaling elements, and 3) measurements across treatment conditions that produce large qualitative changes in activation of signaling elements [157, 158]. PLSR models have been generated using quantitative molecular signaling and cellular response data from and have been successful at interpreting and predicting signal-response relationships in various contexts, including cytokine- and pathogen-induced epithelial cell apoptosis-survival [154, 157, 159], receptor agonist-induced T-cell and B-cell cytokine release [160, 161], and growth factor-induced mammary epithelial cell proliferation and migration [162].

Stepwise regression (SWR) is a regression method that has been widely used in fields such as sociology and has been used in biology for the analysis of genomic datasets. To our knowledge, it has not been applied for the analysis of network level molecular signaling datasets. Stepwise regression is an iterative algorithm that searches for a subset of explanatory variables, from an original larger set of explanatory variables, that together best explain the variation in the response variable. Sometimes such a subset can be manually chosen by the investigator, to coincide with some explicit hypotheses about the system. A stepwise algorithm can be used to automatically pick out a subset of explanatory variables in the case that there is no a priori hypothesis about which of the possible explanatory

variables might actually best explain the variability in the response variable. Basically, the stepwise technique will take a set of independent variables and put them into a regression one at a time, in a specified manner, until a specified criterion has been met. The criterion is usually one of statistical significance or the improvement in the explained variance. Depending on the strategy used for adding variables to the regression model, multiple stepwise procedures can be used, such as forward, backward, maximum R, etc [163, 164].

The stepwise procedure we use in the analysis of the measured data is a forward stepwise approach. We start with no explanatory variables in the model. We first run all possible univariate regressions, regressing the response variable on each of the possible explanatory variables in turn. For each of these univariate regressions, we determine the significance level of the calculated regression coefficient by calculating first the F statistic, or the ratio of the mean suare deviation between the model and the mean and the mean square deviation between the data and the model. We then calculate the corresponding p-value, or probability that the regression coefficient for that explanatory variable is actually zero given the value of the F statistic, by means of an F-test. If we calculate a p-value less than 0.05 for just one of the univariate regression models, that explanatory variable is added to the model. If we calculate a p-value less than 0.05 for more than one of the univariate regression models, the explanatory variable for which the univariate regression model p-value is lowest is added to the model. Next, all two-variable models that include the first selected explanatory variable are calculated, by adding each of the remaining variables one at a time. For each of these pair-wise regressions, the stepwise procedure determines the significance level of the new variable's ability to explain additional variability in the response variable, by calculating the F statistic for each additional variable, and the p-value, or probability that the regression coefficient for the new variable is actually zero given the F statistic obtained, by means of an F-test. Again, if we calculate a p-value less than 0.05 for more than one of the pair-wise regression models, the new explanatory variable for which the p-value is lowest is

added to the model. This continues, next for all three-variable models, then four-variable models, etc. The procedure stops when all the explanatory variables that satisfy the p-value criterion have been included in the model.

In this thesis, we make use of Stepwise regression within a framework that was developed in the process of analyzing our time-dependent signal-response data and is described in detail in Chapter 3.

The development of data-driven modeling analysis methods for the inference and investigation of network-level signaling and relationship between signaling and cellular phenotype, and for prediction of cellular phenotype under novel treatment conditions, is a rapidly growing area of research. In this thesis, we apply accepted PLSR analysis methods and we develop a novel implementation of another accepted analysis method, SWR, for the discovery of time-dependent network level signaling and signal-response relationships (explained in detail in Chapter 3).

## Thesis Overview

Using quantitative experimental and data-driven computational modeling approaches of a quantitative signal-response data-set, this thesis investigates the relationship between molecular signaling and cellular response phenotype resulting from exposure to DNA damage, and induction of DSB, in a physiologically relevant, inflammatory context.

# Chapter 2: A Systems Approach to DNA Damage Signaling Identifies Phospho-ERK1/2 as a Binary Switch Between S-Phase Progression and Apoptosis

## Introduction

### *DNA damage and DSB: cancer cause and cure*

The chromatin integrity network is a highly conserved response, found in all eukaryotes, that is critical to maintaining genomic integrity. Failure of cells to appropriately respond to DNA damage facilitates tumorigenesis . In fact, many mutations commonly found in tumors target and derange the DNA damage response. But the failure to respond appropriately to DNA damage also leaves tumor cells susceptible to cell-killing by DNA-damaging agents. These agents are thus used in the clinic to target tumors cells.

The DNA double-strand break (DSB) is the most lethal of the many lesion types that constitute DNA damage. DSB are also one of the major mediators of chemotherapy-induced cytotoxicity in tumors. Following induction of DSB, cells respond on a molecular level by activating protein signaling molecules in the core chromatin integrity network or DNA double-strand break response pathway , and in pathways governing general stress response , cell-survival , cell-death and cell-cycle control (Figure 1-1). On the cellular level, the integration of these protein signaling-molecule activities translates into one of two cell-fate decisions. Cells that have experienced DNA damage can initiate a DNA damage-mediated cell-cycle arrest, attempt to repair the damage and, if successful, resume the cell-cycle (arrest/repair/resume). Cells can also initiate an active cell-death program known as apoptosis. However, it is not known what "formula" a cell uses to integrate protein signaling molecule activities in order to determine which of these paths it will take, or what protein signaling-molecules are essential to the execution of that decision. A better understanding of how these cellular decisions are made and

mediated on a molecular level is essential to the improvement of existing combination and targeted chemotherapies, and to the development of novel targeted and personalized therapies. The goal of this work was to gain an understanding of how cells responding to DNA damage (DSB) integrate protein signaling-molecule activities across distinct signaling networks to make and execute binary cell-fate decisions, under conditions relevant to tumor physiology and treatment.

### *DNA Damage signaling and proximal response to DSB*

A large body of research has been devoted to the study of the upstream signaling components in the DNA double strand break response pathway in the 15 years since ATM, a critical first-responder to DSB, was cloned. Following induction of a DSB, inactive ATM dimers in the nucleoplasm auto-phosphorylate, fall apart into active monomers and localize to the site of the break. A complex of three proteins, MRE11, Rad50 and Nbs1, known as the MRN complex, also localizes to the site of the break. Once at the site of the break, ATM phosphorylates the histone variant H2AX at areas surrounding the break and many other chromatin-associated and nucleoplasmic substrates. ATM also directly associates with the MRN complex via Nbs1 and ATM and Nbs1 participate to mutually further activate, or maintain the activation status of, the other. The activation and localization of ATM and Nbs1 to break sites, and of γH2AX to areas surrounding break sites, is required for subsequent activation and recruitment of DNA repair factors, to the site of the break and for activation of signaling molecules necessary for induction of DNA damage mediated cell-cycle arrest and cell-death processes following DNA damage. A few of the better characterized ATM substrates include Chk2, a checkpoint signaling protein that leads to induction of DNA damage mediated cell cycle arrest via phosphorylation and inactivation of Cdc25A/C phosphatases, and p53 , a signaling protein and transcription factor that can lead to maintenance of DNA damage mediated cell cycle arrest via up-regulation of the cyclin dependent kinase inhibitor (cki) p21 , or to induction of apoptosis via trans-activation of pro-apoptotic Bcl-2 protein family members.

Despite some detailed knowledge about some of the proximal responders to DNA double strand breaks, we have an extremely limited understanding of how other distinct signaling pathways and proteins known to influence the response to DSB (e.g. general stress, survival, cell-death regulatory and cell-cycle regulatory pathways) integrate into the pathway. We also have no clear understanding of how this integrated signaling response works as a system to make a decision between the alternate cell-fates following DNA damage of cell cycle arrest/repair/ resume or induction of cell death, and to mediate that decision.

### *DNA Damage signaling network and Linear Regression – a data driven approach to identifying signal-response relationship in a system with ill-defined structure*

The goal of this work was to improve our very limited understanding of the signal to signal, and of the signal to cellular response connectivity in this network, as a whole. Our strategy was to investigate the network biology of the molecular signaling and cellular response to DSB, and to find a systematic way to discover signal-response relationships that are crucial to the cellular response to DSB. As a first step, we created a quantitative signal-response dataset by measuring a set of signals that widely sample the dynamic response of signaling networks activated by the induction of DSB, and the associated cellular responses that together reflect the relevant cell-fate decisions and the cellular phenotypic responses that are mediated, following the induction of DSB, in a physiologically relevant context. In a second step, we made use of mathematical modeling approaches to systematically discover signal-response relationships within the DSB-responsive protein signaling network. Because this network has an as-yet ill-defined structure, we chose to use two data-driven, relational modeling approaches in complement, Partial Least Square Regression (PLSR) and a hypothesis-based, Time-Interval Stepwise Regression analysis (TI-SWR). Both PLSR and TI-SWR can be implemented without a requirement for any imposed structure that is defined by pre-existing knowledge of network

relationships (signal-signal or signal-response), and can be used effectively in complement to identify signal-response relationships in this network. We describe the experimental signal-response dataset and the mathematical modeling approaches used to analyze the data in the following sections.

### *Experimental system: Design and Details*

The goal of the experimental effort was to develop a quantitative signal-response dataset, by measuring signals that widely sample the response of signaling networks activated by the induction of DSB, and the associated cellular phenotypic responses that together reflect the dynamic cellular responses that follow the induction of DSB in a physiologically relevant context.

A pre-requisite for this approach is that we define a system that is biologically and clinically relevant and amenable to mathematical modeling approaches, within which we are able to study and measure the dynamic integrated protein signaling involved in mediating and making the decision between the cellular responses of cell-cycle arrest/repair/resume and cell-death in cells responding to DSB.

We chose to perform this study in U2OS human osteosarcoma cells, which originate from a solid tumor etiology. These cells are p53 wild-type and therefore have intact cell-cycle checkpoints, an important consideration for our study.

In designing our experimental system, there were several important factors we considered critical to allow the acquisition of a dataset that is both clinically relevant and that is amenable to rigorous analysis via quantitative, data-driven mathematical modeling approaches. We considered it critical to include:

- Cues that are biologically, and preferably clinically, relevant to the problem at hand

- Cues that result in *large variations in both the signaling molecules of interest and the cellular responses of interest*

- Multiple cues to elicit combinatorial signaling relevant to the variation in possible physiological start states of cells experiencing the cue in vivo

- Quantitative measurements of molecular signals and cellular responses

Therefore, we chose two biologically/clinically relevant cues- Doxorubicin and TNF-α - that display synergistic effects in mediating cellular response to DSB in vitro to use in tandem to investigate the molecular signaling and cellular response to DSB. Doxorubicin is a topoisomerase II inhibitor that leads to the formation of DNA double strand breaks. It is used extensively as a chemotherapeutic agent in the clinic for the treatment of solid tumors, such as osteosarcoma.

TNF-α is an inflammatory cytokine that is up-regulated in many solid tumors and in the tumor micro-environment and is well correlated with tumor grade in some tumor-types. It is a known context-dependent modulator of cell-survival under various physiologic conditions. In fact, the use of TNF-α as a chemotherapeutic agent in its own right has been explored, and though the side-effects resulting from its systemic administration are far too severe to make it a useful treatment, methods of using TNF in a localized or targeted fashion for the treatment of some tumor types are currently being explored. In our own studies, we observe that exposure of cells to TNF-α alone does not cause cell-death. But when cell populations are simultaneously exposed to Doxorubicin and TNF-α, cell-death is dramatically increased as compared to that observed when cell populations are exposed to Doxorubicin alone. This increase in cell-death in populations treated with Dox plus TNF-α versus populations treated with Dox alone is supra-additive, or synergistic (Supplementary Figure 2-1).

To study the integration of signals across distinct signaling pathways known to contribute to the cellular response decision following DNA damage and their relation to subsequent cellular response, under conditions relevant to tumor physiology and treatment, U2OS human osteosarcoma cells were treated with varying doses of Doxorubicin (at 0, 2, and 10 μM) alone, or in combination with TNF-α , as illustrated in Table 2-1.

**Cue-combination treatments:**

| | Dox (μM) | TNF-α |
|---|---|---|
| 1 | 0 μM | ----- |
| 2 | 0 μM | 100 ng/ml |
| 3 | 2 μM | ----- |
| 4 | 2 μM | 100 ng/ml |
| 5 | 10 μM | ----- |
| 6 | 10 μM | 100 ng/ml |

**Table 2-1.** Table of all 6 cue-combination treatment conditions

Following the exposure of U2OS cells to the 6 distinct cue combination treatment conditions of Dox and TNF-α shown in Table 2-1, cell extracts were collected for quantitative molecular signaling measurements at 10 time-points over 24 hr following treatment. The measurement time points are shown in Table 2-2.

| Measurement # | 1 | 2 | 3 | 4 | 5 | 6 | 7 | 8 | 9 | 10 |
|---|---|---|---|---|---|---|---|---|---|---|
| Time [hr] | 0.25 | 0.5 | 1.0 | 1.5 | 2 | 4 | 8 | 12 | 16 | 24 |

**Table 2-2.** Time points at which cell extracts were collected for molecular signaling measurement

Whole cell samples were collected and fixed for cellular-response measurements at 4 time-points over 48 hr following treatment, as shown in Table 2-3. These conditions define our experimental system going forward.

| Measurement # | 1 | 2 | 3 | 4 |
|---|---|---|---|---|
| Time [hr] | 6 | 12 | 24 | 48 |

**Table 2-3.** Time points at which cell samples were collected for cellular response measurement

### *Experimental Measurements*

We chose a subset of 17 signals to measure that we consider information-rich and/or "strategic" signals in the signaling network (Table 2-4). These signals broadly sample the distinct signaling pathways that are involved in making cell-fate decisions and mediating the cellular response to DSB (Figure 1-1). We included measures of signal activity (via measurement of activating phosphorylation sites, or via direct activity ELISA assay) in many cases, and measures of signal level in others (Table 2-4). Assays for quantitative measurement of these signals were developed and validated. The linear and dynamic ranges for these assays were evaluated, and assays were used for signal measurement in the dataset only if these parameters were deemed satisfactory (Appendix A). From collected cell extracts, we obtained quantitative measurements of 17 signals at each of 10 time-points over 24 hr following treatment (Table 2-2), where all 17 signals measured at each time-point were measured from one cell-extract sample, for each of 6 distinct cue combination treatments shown in Table 2-1. Including replicates, this dataset includes more than 2,500 signaling measurements (Figure 2-1B).

| Signaling molecule | Measurement | Measurement assay | Measurement time-points |
|---|---|---|---|
| pATM (S1981) | activity | quantitative western | 0.25, 0.5, 1, 1.5, 2, 4, 8, 12, 16, 24hr |
| pH2AX (S139)** | activity | quantitative western | 0.25, 0.5, 1, 1.5, 2, 4, 8, 12, 16, 24hr |
| pNbs1 (S343)** | activity | quantitative western | 0.25, 0.5, 1, 1.5, 2, 4, 8, 12, 16, 24hr |
| pp53 (S15)** | activity | quantitative western | 0.25, 0.5, 1, 1.5, 2, 4, 8, 12, 16, 24hr |
| pp38 (T180/Y182)** | activity | quantitative western | 0.25, 0.5, 1, 1.5, 2, 4, 8, 12, 16, 24hr |
| pJNK (T183/Y185)** | activity | quantitative western | 0.25, 0.5, 1, 1.5, 2, 4, 8, 12, 16, 24hr |
| pERK1/2 (T202/Y204)** | activity | quantitative western | 0.25, 0.5, 1, 1.5, 2, 4, 8, 12, 16, 24hr |
| pAkt (S437)** | activity | quantitative western | 0.25, 0.5, 1, 1.5, 2, 4, 8, 12, 16, 24hr |
| total H2AX* | level | quantitative western | 0.25, 0.5, 1, 1.5, 2, 4, 8, 12, 16, 24hr |
| total Nbs1* | level | quantitative western | 0.25, 0.5, 1, 1.5, 2, 4, 8, 12, 16, 24hr |
| total p53** | level/activity | quantitative western | 0.25, 0.5, 1, 1.5, 2, 4, 8, 12, 16, 24hr |
| total JNK* | level | quantitative western | 0.25, 0.5, 1, 1.5, 2, 4, 8, 12, 16, 24hr |
| total ERK1* | level | quantitative western | 0.25, 0.5, 1, 1.5, 2, 4, 8, 12, 16, 24hr |
| total Akt* | level | quantitative western | 0.25, 0.5, 1, 1.5, 2, 4, 8, 12, 16, 24hr |
| total Cyclin A* | level/activity | quantitative western | 0.25, 0.5, 1, 1.5, 2, 4, 8, 12, 16, 24hr |
| total Cyclin B* | level/activity | quantitative western | 0.25, 0.5, 1, 1.5, 2, 4, 8, 12, 16, 24hr |
| NFkB** | activity | ELISA | 0.25, 0.5, 1, 1.5, 2, 4, 8, 12, 16, 24hr |

** included in both PLSR example model and example TI-SWR analysis

* included only in example TI-SWR analysis

**Table 2-4.** Table of protein signals measured, by what assay they were measured, and at what time-points following treatment they were measured, for the quantitative signal-response dataset compiled.

---

We also chose a subset of cellular responses to measure (Table 2-5) that we believe to capture well the relevant cell-fate decisions and mediated cellular responses resulting from exposure to DSB in the context of physiologically relevant inflammatory cytokines.

| Cellular response | Measurement | Measurement assay | Measurement time-point |
|---|---|---|---|
| Cell cycle: % G1* | level | FACS | 6, 12, 24, 48 hr |
| Cell cycle: % S** | level | FACS | 6, 12, 24, 48 hr |
| Cell cycle: % G2-M* | level | FACS | 6, 12, 24, 48 hr |
| Cell cycle: % pH3 | activity | FACS | 6, 12, 24, 48 hr |
| Apoptosis: %CC3+CParp+** | activity | FACS | 6, 12, 24, 48 hr |
| Apoptosis: %CC3-CParp-* | activity | FACS | 6, 12, 24, 48 hr |
| Apoptosis: %CC3+ | activity | FACS | 6, 12, 24, 48 hr |

** included in PLSR example model and individually in example TI-SWR analyses

* included only in example PLSR model

**Table 2-5.** Table of cellular responses measured, by what assay they were measured, and at what time-points following treatment they were measured, for the quantitative signal-response dataset compiled.

---

From collected whole-cell, fixed samples, we obtained quantitative measurements of four measures of cell-cycle phenotypic response and three measures of cell-death/survival phenotypic response (Table 2-5) at each of 4 time-points over 48 hr following treatment shown in Table 2-3. Including replicates, this dataset includes more than 500 cellular response measurements (Figure 2-1B).

The resulting quantitative signal-response dataset provides a comprehensive description of the dynamic response of the cell signaling network following the induction of DSB and forms the biological information foundation for identifying relevant signal-response relationships. We used two distinct data-driven, linear regression analysis modeling approaches, Partial Least Squares Regression (PLSR) and a hypothesis-based, Time-Interval Stepwise Regression analysis (TI-SWR), in complement to identify signal-response relationships from the quantitative signal-response dataset, and to aid in the interpretation of response-response relationships. These mathematical modeling and analysis approaches are described in the following sections. As a specific example, we selected a particularly strong set of identified signal-response correlations between ERK1/2 activity and S phase cell-cycle

phenotype, identified in a TI-SWR analysis, to posit a causal relationship between ERK1/2 and S phase cell cycle phenotype. We translated this posited causal relationship into an experimental hypothesis and then experimentally test this hypothesis. In the following sections we also describe the validation of the experimental hypothesis based upon model-derived signal-response relationships, and demonstrate a role for ERK1/2 as a context-dependent switch between cell-cycle arrest and apoptosis following DNA damage.

A

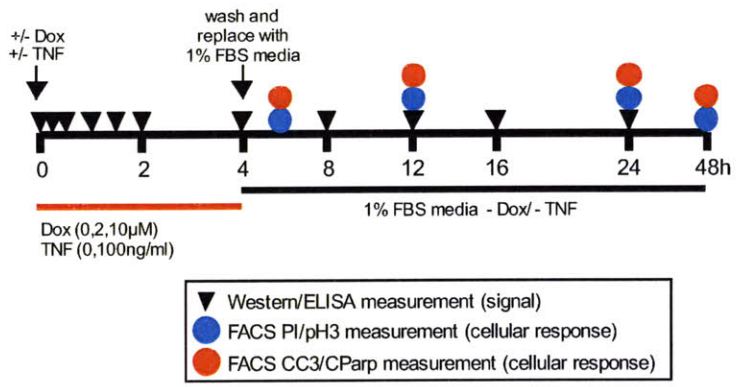


B

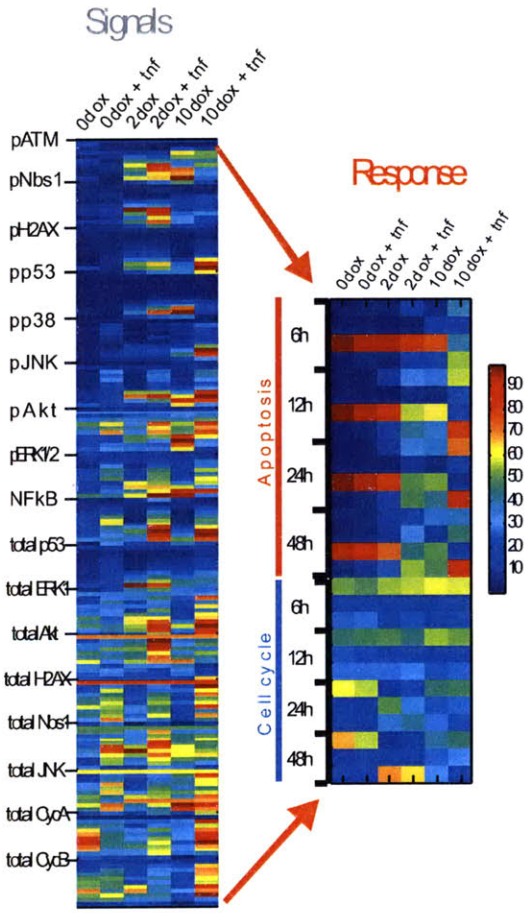


**Figure 2-1.** ***(A)*** Experimental time-line; U2OS cells were seeded at $1.2x10^6$ in media containing 10% FBS (fetal bovine serum) in 10 $cm^2$ tissue culture dishes and incubated for 24 hr. Cells were then treated +/- Dox (0, 2, or 10 μM) and +/- TNF-α (0 or 100ng/ml) and allowed to incubate for 4 hr. Immediately

following treatment, cell-extract and sample collection commences, and proceeds, at appropriate times. 4 hr following treatment, media is aspirated and replaced with media containing 1% FBS. From this point on, cells are NOT further exposed to Dox or TNF-α. Cell-extracts collected for the 4 hr time-point signaling measurements do NOT experience a media change. Cell-extracts for signal measurement were collected at 0.25, 0.5, 1, 1.5, 2, 4, 8, 12, 16 and 24 hr following treatment. Whole cell samples were collected and fixed for cellular-response measurements at 6, 12, 24 and 48 hr following treatment. ***(B)*** Signaling data heatmap and cellular-response data heatmap for all 6 cue-combination treatment conditions investigated. ***Signaling data heatmap;*** 1) Within each single signal measurement set, across the 6 conditions, the 10 time-point measurements of the signal are in consecutive time-order from top to bottom within each column, 2) Within each single signal measurement set, across the 6 conditions, all signal measurement values were normalized to the maximum signal measurement value (the max value ever observed for the measurement of that signal, across conditions and across time-points), such that all values are between 0-1, with dark red denoting high values close to 1 and dark blue denoting low values close to 0. ***Cellular-response data heatmap; 1) Apoptosis section:*** Within each time-point at which apoptosis is measured, across the 6 conditions, 4 measures of apoptosis are represented in order from top to bottom within each column. These 4 measures of apoptosis are: a) % of cells staining positively for both apoptotic markers measured (CC3+CParp+), b) % of cells staining positively for ***only one*** of the markers (CC3+), c) % of cells staining negatively for both apoptotic markers (CC3-CParp-) and d) % of cells staining positively for one apoptotic marker (CC3+), without consideration for the status of staining for the other apoptotic marker (CParp+/-), ***2) Cell-cycle section:*** Within each time-point at which cell-cycle is measured, across the 6 conditions, 3 measures of cell-cycle are represented in order from top to bottom within each column. These 3 measures of cell-cycle are: a) % of cells in G1 phase of the cell-cycle, b) % of cells in S phase of the cell-cycle, and c) % of cells in G2-M phase of the cell-cycle. Data is not normalized and colors are representative as shown in the color-bar at right. All data are means of replicates. Signaling data: n = 2-3. Cellular response data: n = 4-10.

## Materials and Methods

***Cell Culture*** -- U2OS cells were maintained in Dulbecco's modified Eagle medium (DMEM) supplemented with 10% fetal bovine serum, penicillin, streptomycin, 2 mM L-glutamine. Cells were passaged to maintain sub-confluent cell density.

***Cell Stimulation*** -- U2OS cells were seeded at 1.2 x $10^6$ on 10 $cm^2$ tissue-culture dishes in 10 mL DMEM supplemented with 10% fetal bovine serum, penicillin, streptomycin, 2 mM L-glutamine and incubated 20-24 hr. Prior to stimulation, the volume of media left after over-night evaporation was determined for one representative plate; over-night evaporation was almost always 1 mL, leaving a pre-treatment media volume of 9 mL. Cells were stimulated with either 0 or 100 ng/ml TNF-α by spiking in 9 µL of carrier (water) or of 1000x TNF-α stock (stock is 100 µg/mL TNF-α in water; Peprotech). Cell were also stimulated with 0, 2 or 10 µM Doxorubicin by spiking in 9 µL of carrier (water) or of 1000x Doxorubicin stock (for 10 µM treatment), or of a 1:5 dilution of Doxorubicin stock (for 2 µM treatment; 1000x stock is 10 mM Doxorubicin in water; Sigma). Stimulation was always in the order 1) TNF-α and 2) Doxorubicin. Stimulation was accomplished in waves, starting with cells to be collected at latest time-points. Time of stimulation was recorded so that collection-time of samples could be appropriately adjusted to account for treatment-time. Stimulation waves each consisted of equal numbers of plates such that all cells experienced equal amount of time outside of incubation conditions. Cells were incubated for 4 hr following stimulation, and samples were removed as necessary during this time (for treatment time-points before and including the 4 hr time-point). Treatment media was then aspirated and replaced with 8 mL of DMEM supplemented with 1% fetal bovine serum, penicillin, streptomycin, 2 mM L-glutamine. Media replacement was accomplished in waves corresponding to cell-stimulation. Following media replacement, samples were removed as necessary for the duration of the time-course.

***Inhibitor Experiments*** – Methods for inhibitor experiments are as described for ***Cell Stimulation***, except that cells were additionally stimulated with either 0 or 20 μM PD98059 by spiking in 9 μL of carrier (DMSO) or of 1000x PD98059 stock (stock is 20 mM PD98059 in DMSO; Sigma). Stimulation was always in the order 1) PD98059, 2) TNF-α and 3) Doxorubicin. At media replacement (4 hr following initial stimulation), PD98059 is added to the replacement media prior to its application to the cells in the cases where PD9059 was present in the media prior to media replacement.

***Synchronization Experiments*** – U2OS cells were seeded at 5 x $10^5$ on 10 $cm^2$ tissue-culture dishes in 10 mL DMEM supplemented with 10% fetal bovine serum, penicillin, streptomycin, 2 mM L-glutamine and incubated 20-24 hr. Cells were exposed to 2.5 μM thymidine by spiking in 90 μL of 100x thymidine stock (stock is 250 μM thymidine in PBS, filtered; Sigma), and incubated for 18 hr. Media was aspirated, plates were washed 3x with PBS, and replaced with 10 mL DMEM supplemented with 10% fetal bovine serum, penicillin, streptomycin, 2 mM L-glutamine. Cells were incubated for 12 hr. Cells were again exposed to 2.5 μM thymidine by spiking in 90 μL of 100x thymidine stock, and incubated for 18 hr. Media was aspirated, plates were washed 3x with PBS, and replaced with 10 mL DMEM supplemented with 10% fetal bovine serum, penicillin, streptomycin, 2 mM L-glutamine, plus 10 μM aphidicolin (Sigma). Cells were incubated for 1 hr. Methods from this point are as described in ***Cell Stimulation*** and ***Inhibitor Experiments,*** except that at media replacement (4 hr following initial stimulation), PD98059 is added to the replacement media prior to its application to the cells in the cases where PD9059 was present in the media prior to media replacement AND aphidicolin is added to the replacement media prior to its application to the cells in ALL cases. In the case that aphidicolin is "washed off," media was aspirated, cells were washed 3x with PBS and media was replaced with DMEM supplemented with 1% fetal bovine serum, penicillin, streptomycin, 2 mM L-glutamine. Again, PD98059 is added to the

replacement media prior to its application to the cells in the cases where PD9059 was present in the media prior to media replacement.

***Sample Collection for Cell Extracts*** – Cells were removed from the incubator 30 seconds prior to the collection time-point and placed on ice. Media was removed and placed in corresponding 15 mL Falcon tube on ice. 4 mL of ice-cold PBS was added to each plate, moved over plate to rinse cells, then removed and placed in corresponding 15 mL Falcon tube with media. Cells were scraped in residual PBS (usually about 1.5 mL) with non-lysing rubber scrapers. Cells in residual PBS were removed and placed in corresponding 15 mL Falcon tube with media and PBS. Cells/media were centrifuged for 5 min at 1000g, 4C. Supernatant was aspirated. Pellet was brought up in 1 mL ice-cold PBS and transferred to 1.5 mL Eppendorf tube on ice, then micro-centrifuged for 5 min at 4000 rpm, 4C. Supernatant was aspirated and cell-pellets were snap-frozen with liquid nitrogen and transferred to -80C for storage.

***Lysis of Cell-pellets for Cell Extracts*** – Cell pellets were removed from -80C and placed on ice. 350 µL of fresh, ice-cold lysis buffer (1% Triton-X, phosphatase and protease inhibitor tablets (Roche)) was added. Cell-pellets were sonicated for 20-25 duty cycles at 10-20% power. Samples were replaced on ice immediately following sonication. Two aliquots of 12 µL each were removed for use in protein quantification assays; these aliquots were stored at 4C not longer than over-night. One 50 µL aliquot was removed for use in ELISA assays; these aliquots were snap-frozen in liquid nitrogen and stored at - 80C. An aliquot of 55 µL of 6X SDS Sample buffer was added to the remaining lysate and vortexed to mix. Extracts plus sample buffer were snap frozen in liquid nitrogen and stored at - 80C.

***Protein Quantification for Cell Extracts*** – Protein quantification was done using a micro-BCA assay (Pierce) according to the manufacturer's instructions. Standard curves were generated at least in duplicate for every assay plate. Two biological replicates (two aliquots from the original cell-extract) and two assay replicates (two aliquots from the dilution mixture of each original aliquot) were performed for each measurement. Final dilutions of 1:50 and/or 1:100 were used for protein concentration measurements.

***Quantitative Westerns – Gels:*** Gels were always 1.5 mM, 15 lane, 10% acrylamide mini SDS-PAGE gels, except for measurement of p-H2AX/H2AX (12% acrylamide) and p-ATM (6% acrylamide). In general, gels were loaded in the order: 1) ladder, 2) negative control, 3) positive control, 4) empty, 5) 0.25 hr, 6) 0.5 hr, 7) 1 hr, 8) 1.5 hr, 9) 2 hr, 10) 4 hr, 11) 8 hr, 12) 12 hr, 13) 16 hr, 14) 24 hr. The amount of cell-extract loaded in each lane was adjusted according to the data from protein quantification assays in order to load equal amounts of total protein in all lanes. Optimal amount of total protein to load was determined in validation of each of the signaling measurement assays (See Appendix 1). In general, total protein loaded was 10 μg, except for measurement of p-ATM (15 μg). Gels were run out at 180V for 50 min, or until the dye front neared the gel-bottom. For measurement of p-ATM, gels were run out at 180V for 3 hr. ***Transfer:*** Protein was transferred to nitrocellulose membranes in a wet transfer in 10% Methanol (20% Methanol for transfer of p-ATM). Transfer was at 120V for 105 min or at 20V over-night (p-ATM). ***Block/Ab incubation:*** Membranes were blocked for 1 hr with Odyssey Blocking Buffer (OBB; Odyssey) then incubated over-night with the primary antibody in OBB + 0.05% Tween. Membranes were washed 3x, 10min in PBS + 0.1% Tween then incubated for 1 hr with the secondary antibody in OBB + 0.05% Tween. Membranes were again washed 3x, 10min in PBS + 0.1% Tween. ***Visualisation/Quantitation:*** Membranes were visualized on a Licor Odyssey IR-dye scanner. Signal was

quantitated using the Odyssey v2.1 software program. Boxes were drawn around the largest signal band on the blot and duplicated to place around all other signal bands. For each signal band, a duplicate box was created and placed at a point in each lane that did not contain a "background band." The signal reported from this box served as the background signal; this value was subtracted from the signal reported from the corresponding box containing the signal band in that lane. Whenever possible, all background bands were placed at the same point in each lane. Quantitative signal and background data was imported into Excel for further processing. Signaling data is reported as the mean of 2-3 replicates (where error bars are shown, they represent +/- the standard error).

***Sample Collection for Response Measurements (for subsequent FACS analysis)*** – Cells were removed from the incubator 30 seconds prior to the collection time-point and placed in a tissue-culture hood. Media was removed and placed in corresponding 15 mL Falcon tube. 2 mL of PBS was added to each plate, moved over plate to rinse cells, then removed and placed in corresponding 15 mL Falcon tube with media. 1 mL of trypsin was added and cells were replaced in the incubator for 2 min (If many samples are to be collected at one time-point, collection is accomplished in waves. Trypsin incubation in this case is the length of time necessary to accomplish this first step in any other waves). Cells were removed from the incubator again and media from the corresponding 15 mL Falcon was used to quench the trypsin reaction and to resuspend all cell from the plate. Media and cells were then removed and replaced in corresponding 15 mL Falcon tube, and centrifuged for 5 min at 1000g, 4C. From this point, cells were either fixed according to an Ethanol- or Formaldehyde-fixation protocol depending on whether subsequent staining was to be for cell-cycle (Ethanol) or for cell-death outcomes (Formaldehyde).

***Measurement of Cell –cycle Cellular Response (Ethanol-fixation, staining and FACS analysis)*** –

***Fixation:*** Supernatant was aspirated and 200 µL of ice-cold PBS was added. Cell-pellet was re-suspended to a single-cell suspension. 2 mL of ice-cold 70% Ethanol was added drop-by-drop, while vortexing gently. Samples were placed at 4C for storage for at least two hours and not longer than one week. ***Staining:*** Cells were centrifuged for 5 min at 1000g, 4C. Supernatant was aspirated, cells were re-suspended in 200 µL ice-cold PBS and transferred to wells of a V-bottom 96-well plate. Plates were centrifuged for 4 min at 1800 rpm, 4C. Supernatant was flicked off and washed once more with PBS. Cells were re-suspended in 200 µL of ice-cold PBS + 0.25% Triton-X and incubated on ice for 15 min. Cells were centrifuged for 4 min at 1800 rpm, 4C. Supernatant was flicked off and cells were rinsed once with PBS + 1% BSA (200 µL). Cells were re-suspended in 50µL PBS + 1% BSA plus primary antibody (anti phospho-Histone H3, Upstate; 1:100), and incubated overnight at 4C. Cells were washed 2x with PBS + 1% BSA (200 µL) and then re-suspended in 50 µL PBS + 1% BSA plus secondary antibody (488-conjugated anti-Rabbit, Invitrogen Molecular Probes; 1:100), and incubated for one hour at room temperature, protected from light. Cells were washed once with PBS + 1% BSA and once with PBS. Cells were then re-suspended in PBS + 0.1 M boiled RNase + 0.1 mg/mL Propidium iodide. Samples were stored at 4C, protected from light, for at least one hour and not more than overnight. ***Data collection/Analysis:*** Data was collected on a FACScalibur flow-cytometer with Cell-Quest Pro software. Detector parameters were optimized for detection in the FL-1 (for detection of the 488-conjugated secondary antibody) and FL-3 channels (for detection of propidium iodide). Data was analyzed with FlowJo v6.8 for Mac. Cell-cycle data is reported as the mean of at least 4 replicates (where error bars are shown, they represent +/- the standard error).

***Measurement of Apoptosis Cellular Response (Formaldehyde-fixation, staining and FACS analysis) – Fixation:*** Supernatant was aspirated and 400 µL of 4% Formaldehyde (40% stock Formaldehyde diluted 1:10 in PBS; Sigma) was added. Cell-pellet was re-suspended to a single-cell suspension and incubated for 10-15 min. Cells were centrifuged for 5 min at 1000g, 4C. Supernatant was aspirated and 800 µL ice-cold PBS was added. Cells were re-suspended and centrifuged for 5 min at 1000g, 4C. Supernatant was aspirated and 175 µL ice-cold 100% Methanol (Sigma) was added. Cells were re-suspended and samples were placed at -20C for storage for at least two hours and not longer than one week. ***Staining:*** Cells were transferred to wells of a V-bottom 96-well plate. Plates were centrifuged for 4 min at 1800 rpm, 4C. Supernatant was flicked off and cells were re-suspended in 200 µL PBS + 0.1% Tween (PBS-T). Plates were again centrifuged for 4 min at 1800 rpm, 4C. Supernatant was flicked off, and cells were re-suspended in 50µL PBS + 1% BSA + 0.1% Tween (PBS-TB) plus primary antibody (anti Cleaved Caspase-3, Becton Dickinson; 1:500), and incubated for one hour at room temperature. 200 µL PBS-T was added and plates were centrifuged for 4 min at 1800 rpm, 4C. Supernatant was flicked off, cells were washed once with PBS-T (200 µL), and then re-suspended in 50 µL PBS-TB plus primary-conjugated and secondary antibody (647-conjugated anti Cleaved PARP, and 488-conjugated anti-Rabbit, Invitrogen Molecular Probes; 1:250 for both), and incubated for one hour at room temperature, protected from light. 200 µL PBS-T was added and plates were centrifuged for 4 min at 1800 rpm, 4C. Supernatant was flicked off, cells were washed once with PBS-T (200 µL), and then re-suspended in 200 µL PBS-TB. Samples were stored at 4C, protected from light, for at least one hour and not more than overnight. ***Data collection/Analysis:*** Data was collected on a FACScalibur flow-cytometer with Cell-Quest Pro software. Detector parameters were optimized for detection in the FL-1 (for detection of the 488-conjugated secondary antibody) and FL-4 channels (for detection of the 647-

conjugated primary antibody). Data was analyzed with FlowJo v6.8 for Mac. Apoptosis data is reported as the mean of at least 4 replicates (where error bars are shown, they represent +/- the standard error).

# Results

### *Compilation and Evaluation of a Quantitative Signal-Response Dataset: Molecular signaling*

Following 6 distinct Dox/TNF-α cue combination treatment conditions, we observe large quantitative and qualitative ranges of activation for the majority of signals measured, across conditions (Figures 2-2 and 2-3). Signal measurements at each time-point were normalized to that observed in cell populations prior to treatment (untreated cell populations), to yield a "Fold activation." Highest fold-activations ranged from 3-fold in the case of Akt (p-Akt (S473)) to 60-fold in the case of p53 (p-p53(S15)). We observe robust activation of MAPKs and other non-canonical DNA damage responsive signals, such as p-p38, p- JNK, p- ERK1/2 and NFκB, across treatment conditions.

We also observe that much of the cue-activated signaling is resolved, or nearly resolved, by 24 hr, including p-JNK, p-p38, p-Akt and p-ERK1/2 signaling. Notably, cue-activated signaling that is not resolved by 24 hr include signals that are core members of the chromatin-integrity signaling network, and that are involved in the proximal response to DSB, including p-H2AX, p-ATM and p-Nbs1. p53 signaling, as measured by total p53 levels and p-p53 (S15) is also unresolved across several treatment conditions at 24 hr following treatment.

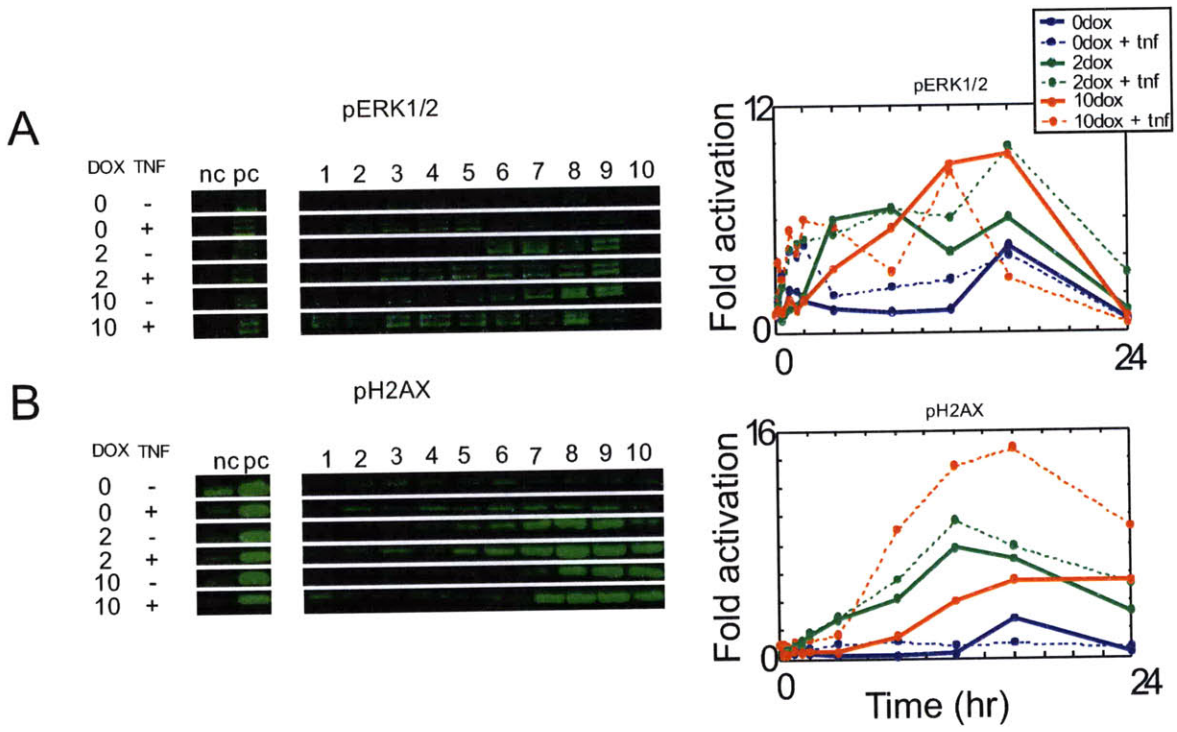


**Figure 2-2.** ***(A)*** Part 1; Represenative quantitative western blots for p-ERK1/2 (T202/Y204) shown for each of the 6 cue-treatment conditions investigated. Negative control (nc) is untreated, asynchronous cells; positive control (pc) is cells that have been serum-shocked for 5 minutes following over-night serum starvation. Lanes 1-10 are cell extracts collected under each of the treatment conditions at 10 time-points following treatment (0.25, 0.5, 1, 1.5, 2, 4, 8, 12, 16 and 24 hr). Part 2; Quantitation of western blot data for p-ERK1/2 (T202/Y204) for each of 6 treatment conditions investigated. Data is the mean of replicates (n=2) and is normalized to the signal measured at 0 hr (prior to treatment) to yield a measure of "Fold activation." ***(B)*** Part 1; Represenative quantitative western blots for p-H2AX (S139) shown for each of the 6 cue-treatment conditions investigated. Negative control (nc) is untreated, asynchronous cells; positive control (pc) is cells that have been exposed to Neocarzinostatin (45 nM) for 1 hr. Lanes 1-10 are cell extracts collected under each of the treatment conditions at 10 time-points following treatment (0.25, 0.5, 1, 1.5, 2, 4, 8, 12, 16 and 24 hr). Part 2; Quantitation of western blot data for p-H2AX (S139) for each of 6 treatment conditions investigated. Data is the mean of replicates (n=3) and is normalized to the signal measured at 0 hr (prior to treatment) to yield a measure of "Fold activation."

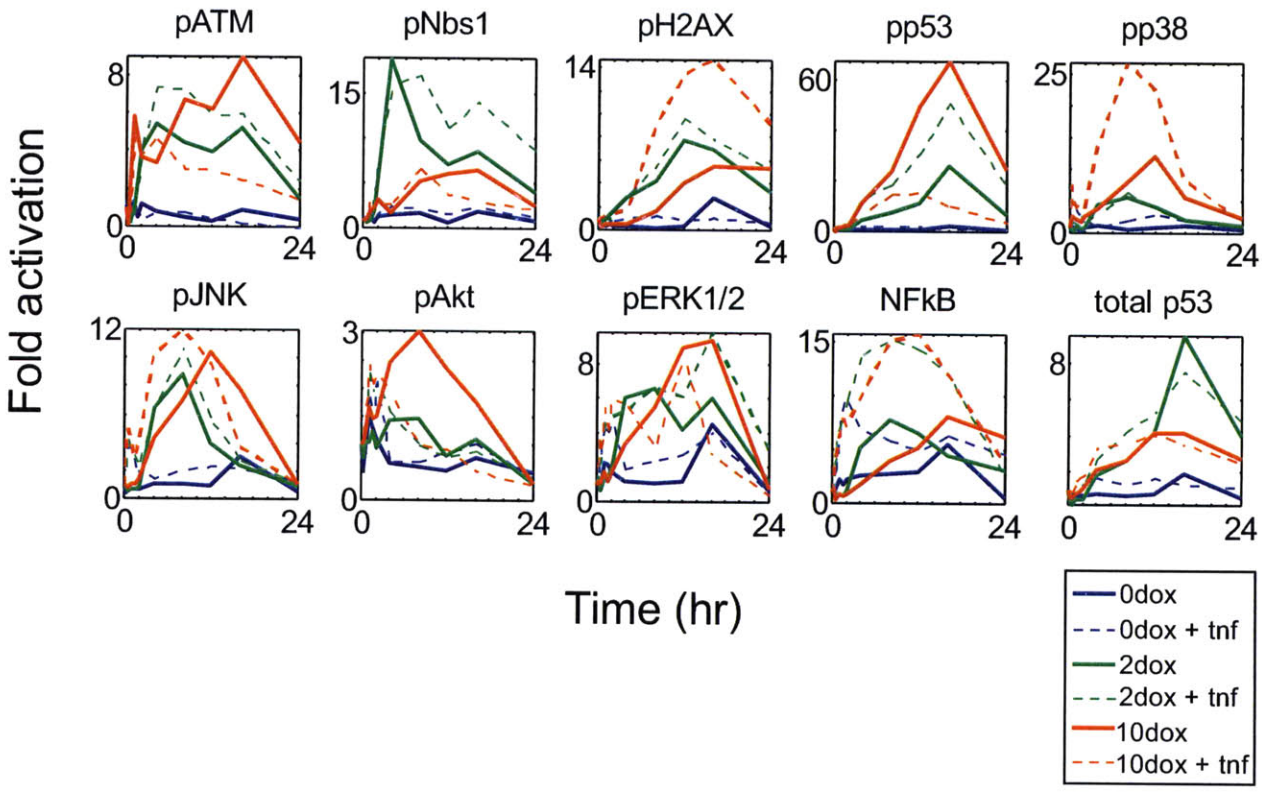


**Figure 2-3.** Quantitation of western blot data for p-ATM (S1981), p-Nbs1 (S343), p-H2AX (S139), p-p53 (S15), p-p38 (T180Y182), p-JNK (T183Y185), p-Akt (S473), p-ERK1/2 (T202/Y204) and total p53 and quantitation of ELISA data for activation of NFkB, for each of 6 treatment conditions investigated. Data is the mean of replicates (n=2 or 3) and is normalized to the signal measured at 0 hr (prior to treatment) to yield a measure of "Fold activation."

---

***Compilation and Evaluation of a Quantitative Signal-Response Dataset: Cellular response***

The single cellular responses of apoptosis and cell-cycle arrest/regulation are both established and essential cellular responses to DNA damage. These cellular responses are intimately and dynamically related cellular responses to DNA damage, such that it is necessary to consider both of

these single measures of cellular response in concert in order to understand the complex, holistic cellular response to DNA damage, on either a single cell or cell population level.

## Apoptosis

Following 6 distinct Dox/TNF-α cue combination treatment conditions, we see a wide quantitative range of apoptosis across the conditions. For example, at 12 hr following treatment, almost 100% of cells stain negatively for both apoptotic markers in cell populations treated with carrier alone, while nearly 80% or cells stain positively for at least one apoptotic marker in cell populations treated with high Dox plus TNF-α. The percent of the cell population that is apoptotic increases with increasing Dox dose. Also, for each Dox dose, the addition of TNF-α synergistically increases apoptosis from that resulting from exposure to Dox alone (Figure 2-4B). The most dramatic changes in observed apoptosis occur between 6 and 24 hr following treatment, and these are likely the most reliable measurements of apoptosis across all six cue combination treatment conditions. At later times, populations treated with high Dox exhibit advanced apoptotic processes including cellular disintegration. The result can be inaccurate determination of the percent of the population that is apoptotic (as illustrated by the apparent decrease in the percent of the population that is apoptotic between 24 and 48 hr in cell populations exposed to either low Dox (2 μM) or high Dox (10 μM) plus TNF-α (Figure 2-5B).

We also observe a range in the qualitative nature of the apoptotic response across the six cue combination treatment conditions. In untreated cell populations, measured apoptosis is minimal over the whole time-course from 6-48 hr (<<5%). Addition of TNF-α to untreated cell populations does not affect apoptosis, which remains minimal at <<5%.

In cell populations treated with low Dox (2 μM) or high Dox (10 μM) ***alone***, the percent of the population that is apoptotic by 6 hr following treatment is minimal (4% and 7% respectively). %

apoptosis quickly rises between 6-12 hr under both of these treatment conditions (in low Dox, from 4% to 15%; in high Dox, from 7% to 30%). % apoptosis then remains nearly constant in cell populations treated with low Dox (2 μM), for the remainder of the time-course, from 12-48 hr. In cell populations treated with high Dox (10 μM), % apoptosis continues to rise through 24 hr, and then remains constant through 48 hr following treatment.

In cell populations treated with low Dox (2 μM) or high Dox (10 μM) ***plus TNF-α***, the percent of the population that is apoptotic by 6 hr following treatment is already quite high (14% and 40% respectively). % apoptosis quickly rises between 6-12 hr under both of these treatment conditions (in low Dox plus TNF-α, from 14% to 32%; in high Dox plus TNF-α, from 40% to 56%). In cell populations treated with low Dox plus TNF-α, % apoptosis remains stationary just above 30% through 24 hr, then decreases between 24-48 hr from 34% to 22%. In cell populations treated with high Dox plus TNF-α, the % of the cell population that is apoptotic continues to rise between 12-24 hr, from 56% to 72%, before sharply decreasing between 24 -48 hr, from 72% to 38% (Figure 2-5B).

A

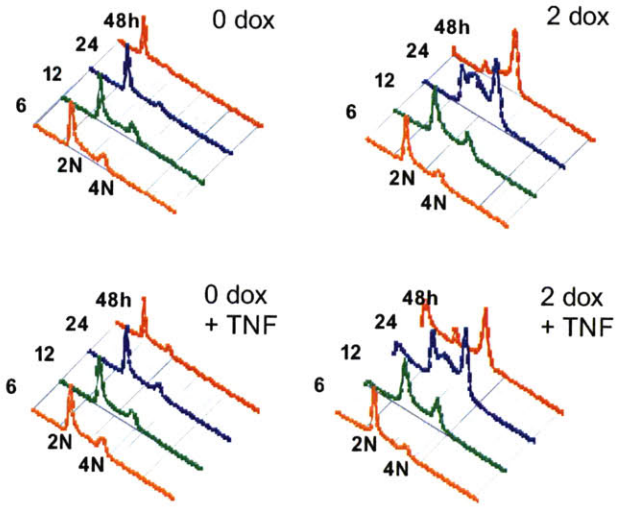

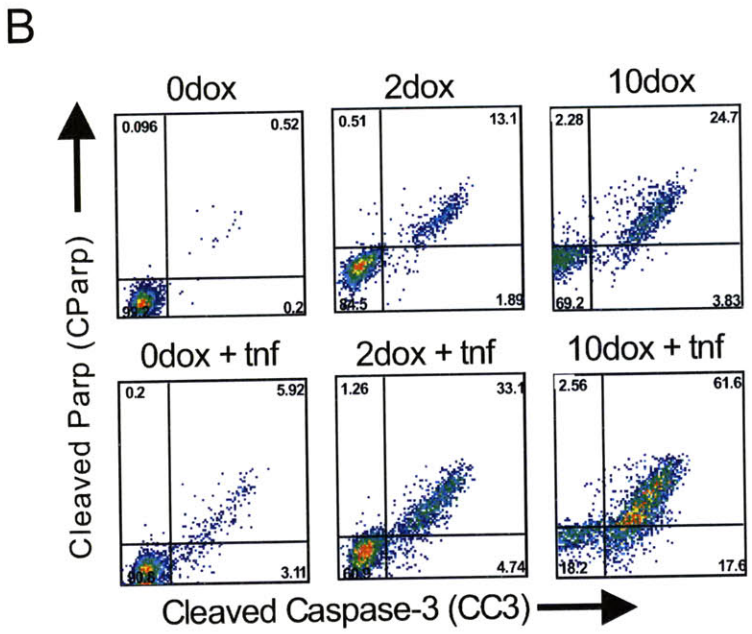


**Figure 2-4.** ***(A)*** Representative FACS PI (propidium iodide) histograms for DNA content for cells exposed to 0 μM Dox +/- TNF-α (left, top and bottom respectively) and to 2 μM Dox +/- TNF-α (right, top and bottom respectively) at 6, 12, 24 and 48 hr following treatment. ***(B)*** Representative FACS scatter plots for cleaved caspase-3 and cleaved Parp, as measured simultaneously in single cells, for all 6 treatment conditions, at 12 hr following treatment.

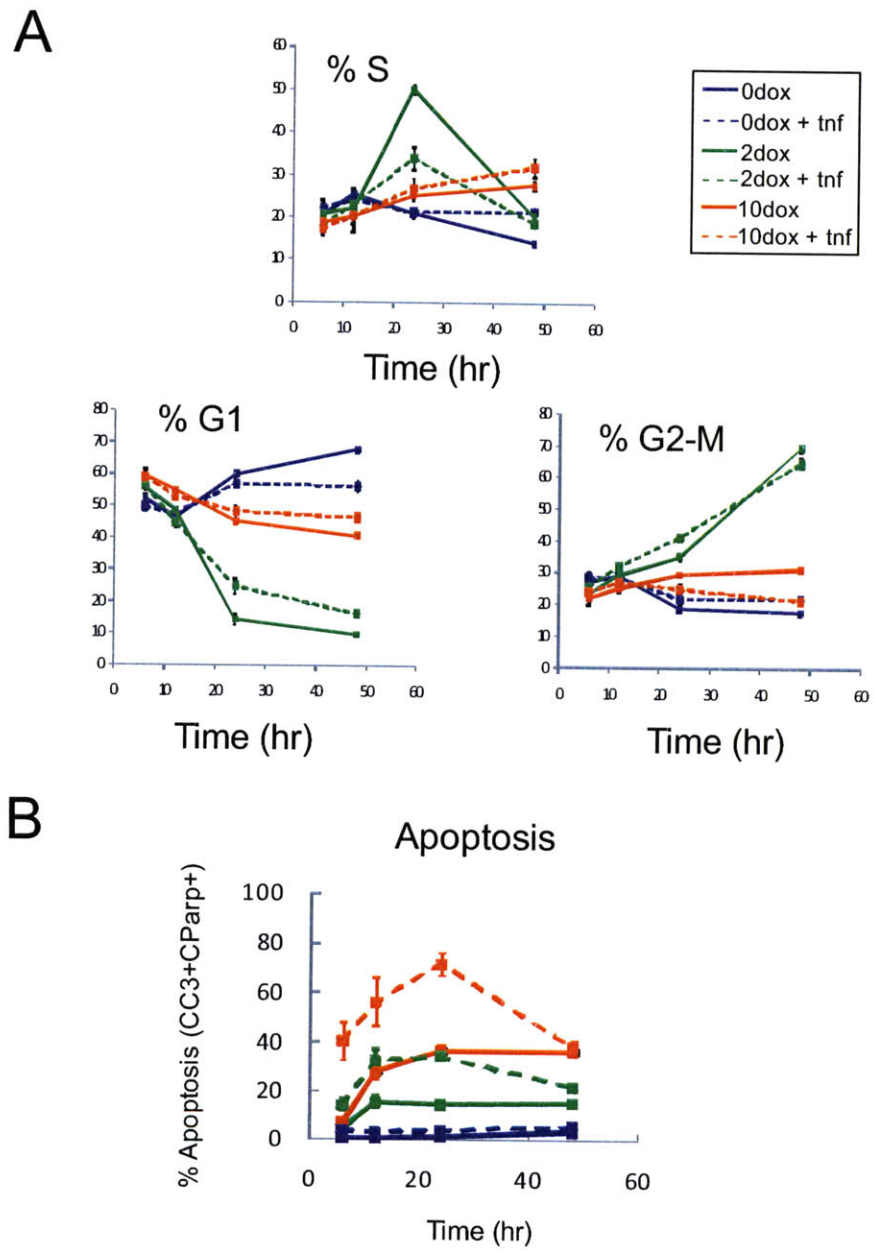


**Figure2-5.** ***(A)*** Quantitation of the % of the cell-population in the S (top), G1 (bottom left) and G2-M (bottom right) phase of the cell-cycle, as measured from FACS PI histogram/DNA content data, for all 6 treatment conditions investigated, at 6, 12, 24 and 48 hr following treatment (Data from at least 4 replicates), ***(B)*** Quantitation of the % of apoptosis in the cell-population (% of the cell-population staining positively for both apoptotic markers, cleaved caspase-3 and cleaved Parp, for all 6 treatment conditions investigated at 6, 12, 24 and 48 hr following treatment.

**Cell-cycle**

Following 6 distinct Dox/TNF-α cue combination treatment conditions, resulting cell-cycle phenotypes track closely with Dox dose, with minimal affect from TNF-α addition. The most dramatic cell cycle phenotypes are observed in cell populations treated with low Dox (2 μM) +/- TNF-α, and are not observable until later times (after 12 hr) (Figure 2-4A and Figure 2-5A).

Untreated cell populations retain a largely similar cell-cycle profile over the full time-course, exhibiting a slight increase in percent of the cell population in G1 (%G1) and parallel decrease in percentage of the cell population in G2-M (%G2-M) by 24 hr. This is an effect that is commonly observed in populations of adherent cells experiencing slowed cell-division due to contact inhibition. In untreated cell-populations, percent of the cell population in S (%S) remains constant throughout the time-course, from 6-48 hr. Cell populations treated with TNF-α alone exhibit cell-cycle profiles similar to those observed in untreated cell-populations at all times (Figure 2-5A).

In cell populations treated with low levels of Dox (2 μM) minus TNF-α, the percent of cells in G1 (%G1) decreases sharply (from 49% of the cell population to 15%) between 12-24 hr following treatment. The %G1 then remains stationary for the rest of the time-course, from 24-48 hr. This sharp decrease in % G1 between 12-24 hr is paralleled by a sharp increase in %S from 12-24 hr that is roughly equal in magnitude and dynamics to the decrease in G1 population, suggesting the shift of a subset of the population from G1 or G1/S to S over this time-period. %S, in this treatment condition, increases sharply (from 22% of the cell population to 50% of the cell population) between 12-24 hr. %S then decreases sharply (from 50% back to 20%)between 24- 48 hr following treatment. Again, this sharp decrease in %S between 24-48 hr is paralleled by a sharp increase in %G2-M between 24-48 hr that is roughly equal in magnitude to the decrease in S population, suggesting a further shift of this "subset"

population from S to G2-M over this time-period. %G2-M sharply increases from 35% of the cell population to 70% of the cell population between 24- 48 hr following treatment.

Cell populations treated with low Dox (2 μM) plus TNF-α exhibit cell-cycle profiles similar to those observed in populations treated with low Dox minus TNF-α at all times, with two significant deviations. The sharp decrease in %G1 between 12-24 hr observed in populations treated with low Dox alone (from 49% to 15%) is less pronounced in populations treated with low Dox plus TNF-α (from 45% to 25%). Likewise, the parallel sharp increase observed in %S over this time period in populations treated with low Dox alone (with a peak of 50% of the cell population in S, decreasing back to 20% by 48 hr) is also less pronounced in populations treated with Dox plus TNF-α (with a peak of 34% of the cell population in S, decreasing back to 19% by 48 hr) (Figure 2-5A).

By 24 hr, cell-cycle profile data is not a reliable measure for cell populations exposed to high dose Dox (10 μM) +/- TNF-α. In these populations, apoptotic processes are very advanced; much of the cell population is fragmented and thus not counted in the measurement. G1, S and G2-M cell-populations are counted as percentages of all cells. Thus, when all cells cannot be counted, inconsistencies in determining % G1, % S and % G2-M may arise.

### *DNA damage-mediated cell cycle arrest in G1 or at the G1/S transition in cell populations treated with low Dox (2 μM) +/- TNF-α*

The observed build-up in S phase population between 12 and 24 hr in cell populations treated with low Dox (2 μM) +/- TNF-α, and the apparent shifts in a subset of the population from G1 to S between 12 and 24 hr and from S to G2-M between 24 and 48 hr is a strong cell-cycle phenotype (Figure 2-4A). Our observations could be the result of a DNA damage-mediated S-phase arrest in cell populations treated with low Dox that we can observe by 24 hr, and that releases sometime after 24 hr

to allow a cohort of cells that have been synchronized by the arrest to enter G2-M by 48 hr. Alternatively, our observations could be the result of a DNA damage-mediated arrest in G1 or at the G1/S transition in cell populations treated with low Dox that releases sometime before 24 hr to allow a cohort of cells that have been synchronized by the arrest to enter S by 24 hr, and then to progress, still synchronously into G2-M by 48 hr.

If these observations were the result of an S phase arrest between 12 and 24 hr, we would expect that %G2-M during this time-period would be stationary, or decreasing (No cells should be moving into G2-M from S if there is an active S phase check-point, and some cells should be moving from G2-M back into G1, unless there is also a G2-M arrest). In fact, we observe the opposite: %G2-M increases over this time-period (Figure 2-5A). These data support a hypothesis that our observed cell-cycle phenotypes can be explained by the induction of a DNA damage-mediated cell cycle arrest in G1 or at the G1/S transition in cell populations treated with low Dox (2 μM) +/- TNF-α that is released before 24 hr to allow progression into S by 24 hr, and into G2-M by 48 hr.

### *Data-driven Mathematical modeling: PLSR and TI-SWR*

We used a PLSR model and a TI-SWR analysis in complement to systematically discover detailed, time-dependent signal-response relationships from the quantitative signal-response dataset described above.

The overarching hypothesis that guides the data-driven mathematical modeling approach is that cue-resultant cellular phenotype, across cue treatments, is a definable function of cue-initiated molecular signaling. Measured molecular signaling can be cast as independent, or explanatory, variables (X) and measured cellular responses can be cast as dependent, or response, variables (Y). Here, X is a data matrix including the measurements of all signals at all time-points, across all cue combination

treatment conditions, and Y is a data matrix including the measurements of all cellular-responses at all time-points, across all cue combination treatment conditions. We would like to gain insight into the nature of the function relating cellular response and molecular signaling (Y and X, respectively) using data-driven computational approaches such as regression analysis. However, in order to do so, and to find a unique solution for the function, traditional regression analysis requires that the number of observations (or cue combination treatment conditions) be greater than the number of explanatory variables (signal measurements) in the model. We are interested in understanding how a relatively large number of signaling molecules contribute, in a dynamic fashion, to cellular response following DSB, and our explanatory variable set is large. Additionally, the number of cue combination treatment conditions we can obtain data for is significantly constrained by cost, in terms of both time and money, and the number of observations we can include in our model is relatively small. These problems have been addressed successfully in previous applications of regression analysis for the discovery of signal-response relationships in biological networks by the use of a Partial Least Squares regression algorithm (PSLR). We extend the utility of PLSR for the discovery of biological network signal-response relationships by using PLSR in tandem with a novel analysis approach, introduced below, that we refer to as hypothesis-based, Time-Interval Stepwise Regression (TI-SWR).

***PLSR***

In PLSR, we reduce our explanatory variable set substantially to an effective explanatory variable set that is made up of orthogonal latent variables, or Principal components (PCs). PCs are linear combinations of the original model independent variables that simultaneously maximally capture variance in the independent variable space and covariance with the dependent variable space (Figure 2-6A). The first principal component (PC1) maximally captures the variance in the independent variable space (conditional on maximizing covariation with the dependent variable space). The second principal

component (PC2) maximally captures the residual variance in the independent variable space (still conditional on maximizing covariation with the dependent variable space), and so on for any additional PCs, such that PCs are orthogonal and uncorrelated. The number of PCs necessary to capture the majority of the variance in the explanatory (independent) variable set is much smaller than the number of original explanatory variables, and should also be chosen to be smaller than the number of observations (samples) available for analysis. These relatively few uncorrelated PCs serve as "super-variables", standing in, as effective explanatory variables, for the large number of often-correlated original explanatory variables. This effective reduction in the number of explanatory variables allows us to use PLSR to find a unique solution for the signal-response functional relationship. We use this approach to investigate the relationships between measured cellular responses of cell-cycle and cell-survival and death that, together, yield a relatively complete picture of the holistic cellular phenotypic response to DSB. We also use this approach to identify some high-level signal-response relationships (Figure 2-6A).

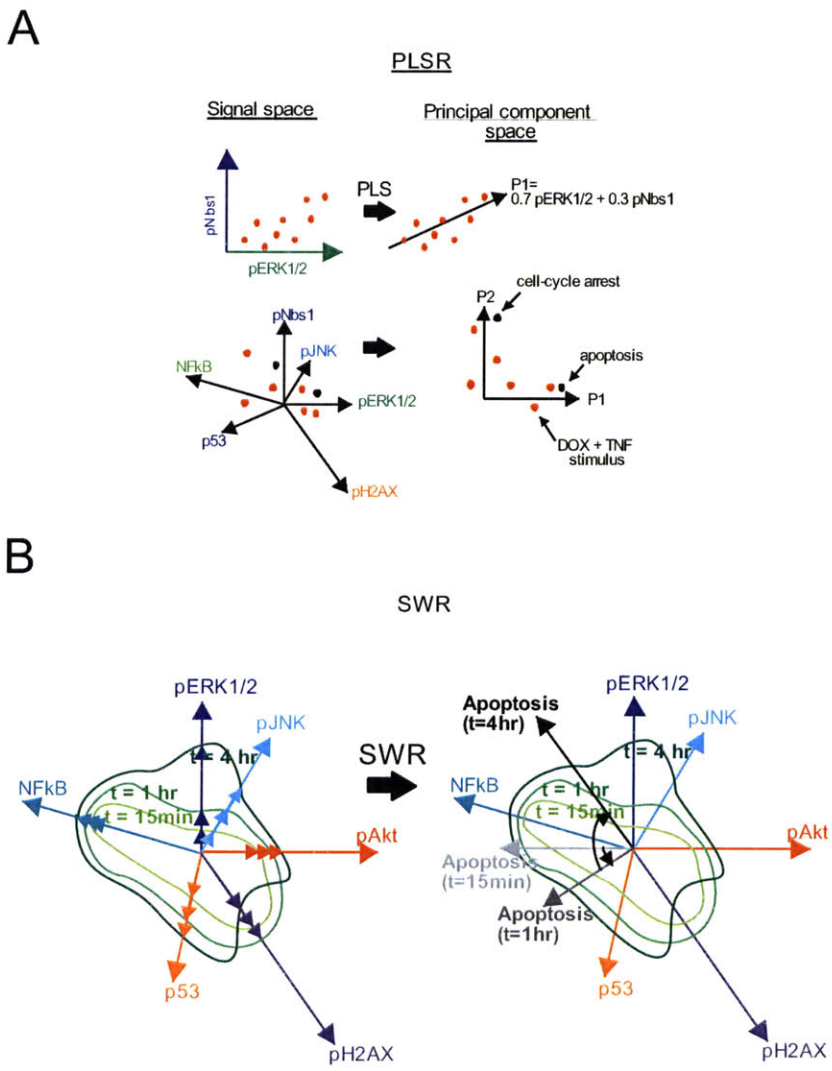


**Figure 2-6.** PLSR (A) and SWR (B) explanatory diagram

### *PLSR: Results*

A PLSR model was constructed, including measures of apoptosis, survival and cell-cycle arrest/regulation across the six treatment conditions investigated as response variables, Y, and time-course signaling measurements across the six treatment conditions as explanatory variables, X. The two principal components model captures 87% of the variation in the response variable space ($R^2 = 0.87$) and has a cross-validated predictive capability of 58% overall ($Q^2 = 0.58$). Cross-validated predictive

capabilities for single cellular-responses in this model vary from high predictive capabilities of 80% for the prediction of the percent of cells in G2-M at 24 hr, and 74% for the prediction of the percent of surviving cells at 6 hr, to lower predictive capabilities of 50% for the prediction of the percent of surviving cells at 12 hr, and 34% for the prediction of the percent of cells in s at 24 hr. Construction of a PLSR model that includes just one measured cellular response as the response variable often results in a model with a higher overall cross-validated predictive capability statistic (e.g. A two-component PSLR model constructed with a single response variable - the measure of percent of cells surviving at 6 hr -has an overall $Q^2$ value of 0.80). However, PLSR gives us a powerful tool with which to visualize the structure of a full data-set; correlations between responses, between signals, and between signals and responses are indicated by proximity in the principal component space. By constructing a PLSR model that includes multiple measures of cellular response as response variables, we can obtain an understanding of the relationships between these cellular responses by examination of the relative locations of the responses in the principal component space. We can also obtain an understanding of the relationships between signaling measurements and multiple cellular responses by examination of the relative locations of the signals and the responses in the principal component space. In the example shown here, the model includes measures of apoptosis and survival at 6 and 12 hr, and measures of cell-cycle status (%G1, %S and %G2-M) at 24 hr as responses (Table 2-2 and Table 2-3).

### *Principal components as Biological response Axes: PC1 is a "Survial/Death" Axis*

Measures of apoptosis at both 6 and 12 hr are highly and ***positively*** weighted in the first principal component, and have low calculated weights in the second principal component. Measures of cell-survival at 6 and 12 hr are highly and ***negatively*** weighted in the first principal component, and have low calculated weights in the second principal component. A plot of these responses in the principal component space (Figure 2-7A), reveals that the first principal component (PC1) is highly correlated with

apoptosis and is highly anti-correlated with measures of survival, such that we may physically interpret PC1 as a "Survival-Death" Axis. Note that the PCs for the proteins (signals) and the PCs for the responses are different, but are directly related when using PLSR. Under this interpretation, we expect that signals that have strong, positive weight in PC1 also correlate with cell-death outcomes and, conversely, that signals that have strong, negative weight in PC1 correlate with cell-survival outcomes.

**A**

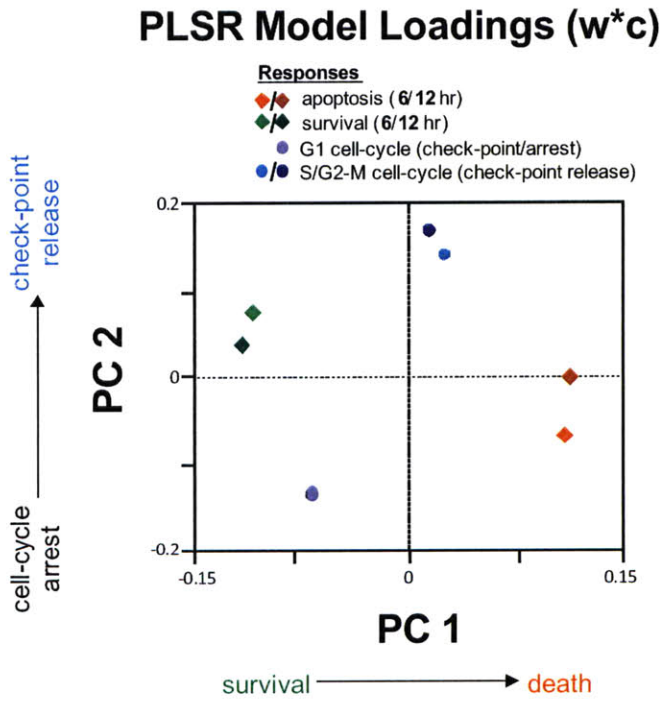

**B**

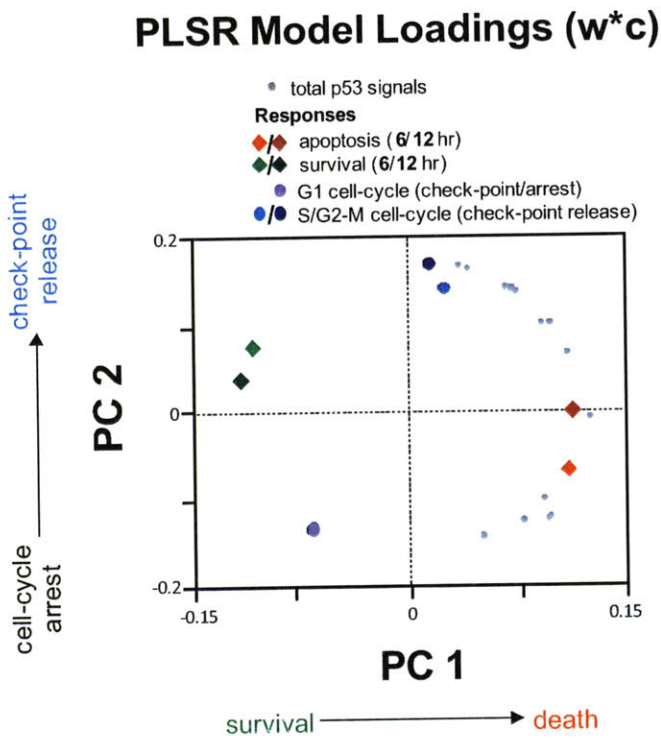


**Figure 2-7.** ***(A)*** Plot of cellular-responses in the Principal component space (Principal component 1 (PC1) vs. Principal component 2 (PC2)) determined by a PLSR model. ***Cellular responses:*** The cellular responses of apoptosis (CC3+CParp+) at 6 and 12 hr following treatment, survival (CC3-CParp-) at 6 and 12 hr following treatment and measures of the G1, S and G2-M cell-cycle populations at 24 hr following treatment are plotted in the Principal component space based on the weights of each of the cellular responses in PC1 and PC2. Apoptotic responses measured at 6 and 12 hr following treatment (red and dark red diamonds respectively) are positively correlated with PC1 and survival responses measured at 6 and 12 hr following treatment (green and dark green diamonds respectively) are negatively correlated with PC1; PC1 is a "Survival-Death" axis. Measurements of S and G2-M cell-cycle populations at 24 hr following treatment (blue and dark blue circles respectively) are positively correlated with PC2 and measurement of G1 cell-cycle population at 24 hr following treatment (light purple circle) is negatively correlated with PC2; PC2 is a "Cell-cycle regulation" axis. ***(B)*** Plot of all time-point measurements of total p53 ("total p53 signals") and cellular-responses in the Principal component space (Principal component 1 (PC1) vs. Principal component 2 (PC2)) determined by a PLSR model. Total p53 measurements (including values of total p53 measured at each of 10 time-points following treatment) are plotted in the principal component space based on their weights in PC1 and PC2 (light grey, small circles). Some total p53 measurements are highly correlated with apoptotic responses only, some are highly correlated with cell-cycle responses only and some are highly correlated with both; this PLSR model allows us to capture the known dual role of p53 in mediating both apoptotic and cell-cycle regulatory responses following DNA damage.

### *Principal components as Biological response Axes: PC2 is a "Cell cycle Arrest/Regulation" Axis*

We also see that the cellular response read-outs of cell-cycle status/arrest spread out along the second principal component (PC2) such that PC2 is highly correlated with a readout of cells in the S phase of the cell-cycle (S populations) and a readout of cells in the G2-M phase of the cell-cycle (G2 population) and is highly anti-correlated with a readout of cells in the G1 phase of the cell cycle (G1 population) (Figure 2-7A). From these observations, we may physically interpret PC2 as a "Cell-cycle Arrest/Regulation" Axis. Under this interpretation, we expect that signals that have strong, positive weight in PC2 also correlate with high S and G2 populations by 24 hr following treatment and, conversely, that signals that have strong, negative weight in PC2 correlate with a high G1 population by 24 hr (or low S and G2 populations by 24 hr). This organization of the responses (G1 is anti-correlated with PC2, ***and separated from*** S and G2-M populations, which lie close together and are correlated with PC2) makes sense in light of our hypothesis that, following DNA damage under the experimental conditions here, a DNA damage-mediated cell cycle arrest in G1 or at the G1/S transition is initiated, and that this arrest releases such that cells can progress into S and G2-M by 24 hr.

### *Signals in the Principal component space: Signal-response relationships*

Using PLSR, we can also obtain an understanding of the relationships between measured molecular signals (explanatory variables, X) and measured cellular responses (response variables, Y) by examining where the signals lie in the principal component space, relative to measured cellular responses.

### *PLSR model confirms a role for p53 in promoting cell-death and cell cycle regulation following DNA damage*

For example, we know that p53 has roles in promoting both cell-death and cell-cycle regulation and in coordinating these responses following DNA damage. Indeed, if we plot total p53 measurements in the principal component space (Figure 2-7B), we can see that some time-point measurements are highly and positively correlated with PC1, the "Survival-Death" Axis and with apoptotic outcomes at 6 and 12 hr. Some time-point measurements of total p53 are highly and positively correlated with PC2, the "Cell-cycle Arrest/Regulation" Axis, and with S and G2 cell populations. And remaining time-point measurements of total p53 are highly and positively correlated with ***both PC1 and PC2.*** Total p53 seems very "informative" in that all time-point measures of total p53 are weighted highly in either PC1 or PC2, or in both. Plotting total p53 signals in principal component space allows us to capture p53's known dual role in both cell-death and cell-cycle regulation following DNA damage.

### *PLSR model suggest a role for ERK in promoting cell-death and in promoting population build-up in S and G2-M following DNA damage*

The MAPK ERK1/2 has an established role in promoting cell-cycle progression through the G1/S transition in normal cell-cycles and in promoting survival following general types of stress. Roles for ERK1/2 in mediating cellular responses of cell-cycle arrest/regulation and/or cell-death in the context of DNA damage are not well-established or specified. If we plot p-ERK signals in the principal component space (Figure 2-8), we can see that some time-point measurements are highly and positively correlated with PC1, the "Survival-Death" Axis and with apoptotic outcomes at 6 and 12 hr. Some time-point measurements of p-ERK are highly and positively correlated with PC2, the "Cell-cycle Arrest/Regulation" Axis, and with S and G2 cell population measurements at 24 hr following treatment. And remaining time-point measurements of p-ERK are highly and positively correlated with ***both PC1 and PC2.*** This

pattern is very similar to that observed for p53 signals. From this pattern we might hypothesize that, despite ERK's established role in promoting cell-survival in some contexts, ERK has a role in both promoting cell-death and in promoting cell-cycle arrest/regulation following DNA damage (p-ERK is correlated with the build-up in S and G2-M populations at 24 hr).

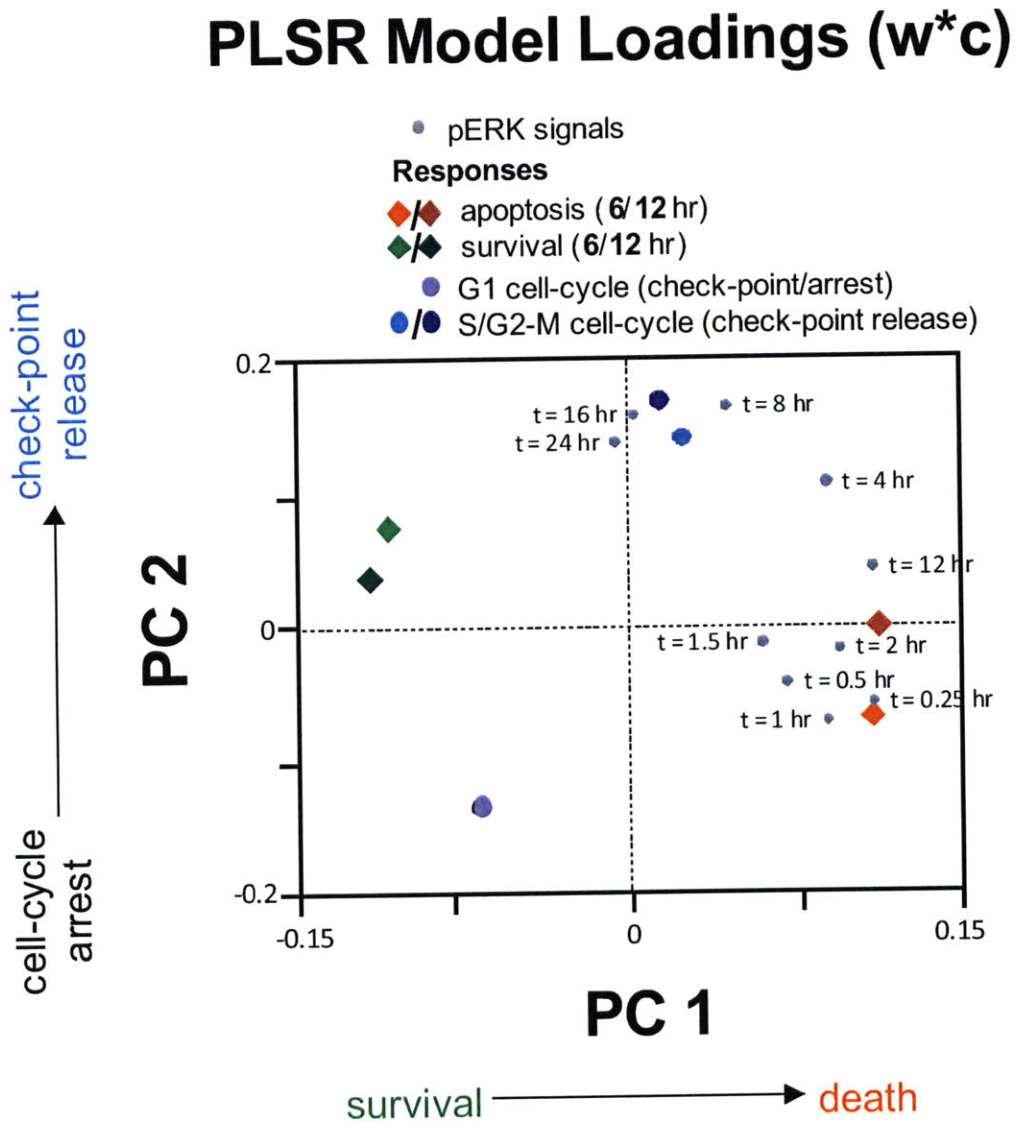


**Figure 2-8.** All p-ERK measurements (including values of p-ERK measured at each of 10 time-points following treatment as well as the max, mean, and equilibrium value of total p53 over the whole time-

course following treatment and the value for the area under the curve (AUC) of p-ERK measured over the full time-course) are plotted in the principal component space based on their weights in PC1 and PC2 (light grey, small circles). Some p-ERK measurements are highly correlated with apoptotic responses only, some are highly correlated with cell-cycle responses only and some are highly correlated with both. These result are reminiscent of those obtained for total p53, and lead us to a hypothesis that, though ERK has an established role in promoting cell-survival and cell-cycle progression under normal or low stress conditions, under DNA damaging conditions, ERK may have a role in promoting apoptosis and cell-cycle regulation.

---

***TI-SWR***

The goal of TI-SWR (Time-Interval Stepwise Regression) is to exploit the time dimension of the dataset to find relatively detailed, time-dependent signal-response relationships, and to significantly decrease the number of explanatory variables in the models we look at, to both allow for the identification of unique functions relating signals and cellular response, and to increase model interpretability.

In TI-SWR, we make our original hypothesis more restrictive in a few ways. Our original hypothesis is that our measured cellular responses are a function of our measured molecular signaling events (including all time-points at which these signals were measured). The hypothesis that a TI-SWR analysis makes is that a subset of the molecular signaling events measured ***at one time-point*** work together to mediate a measured cellular response (Supplementary Figure 2-2). This is a natural hypothesis as a cell integrates information about previous physical/mechanical or signaling events via a physical/chemical encoding of past events in the current status of its signaling components. At any given time a cell uses only the current status of its signaling components and integrates these signals, which occur temporally together, but which also encode past signaling events, in making the decisions which determine future cell actions and eventually the cell fate. E.g., at 1 hr following DNA damage, a cell may

"remember" that ATM was activated at 30 min following damage, even if it is no longer activated at 1 hr following damage, because the ATM activation at 30 min led to H2AX phosphorylation, and H2AX is still phosphorylated at 1 hr.

We first choose just one cellular response of interest to investigate at a time. In order to make this one cellular response variable as "information-rich" as possible, we choose the derivative of the linearized change in a measured cellular response over some time-period as our response variable, instead of the measured cellular response at one time-point. The choice of the derivative of the cellular response as the dependent variable is explained in detail in Chapter 3: Computational Methods.

We next build a set of time-interval models, including one time-interval model for each time-point at which signaling measurements were made. In each time-point specific time-interval model, the response variable is the one that we have chosen to investigate. Explanatory variables include only the measurements of all signals made at the time-point of the time-point specific model.

For the regression step in TI-SWR analysis, we make use of a Stepwise regression algorithm. Stepwise regression is a well-established regression procedure that can be used to select a subset of explanatory variables, from an original larger explanatory variable set, that maximally correlates with the response variable. Explanatory variables that do not add to the model's ability to predict the response variable are excluded from the model (Figure 2-6B). Time-interval models thus have few explanatory (signal) variables and are very likely to have fewer explanatory variables than there are observations in the dataset, thus allowing for the identification of a unique functional relationship between the cellular response and signals at the time-point of the model.

The result of a TI-SWR analysis is a set of time-interval models that are used sequentially for the time-points at which signals were measured to specifically investigate time-dependent signal-response

relationships between signals at each of the time-points and the cellular response being investigated. These time-point specific time-interval models have few explanatory variables and are thus easily interpretable. The sets of time-interval models yield insight into detailed, time-dependent signal-response relationships and greatly facilitate the development of hypotheses regarding signal-response causal relationships as well as the design and execution of hypothesis-motivated experiments to test and validate these hypotheses.

### *TI-SWR: Results*

We pursued the investigation of signal-response relationships related to the dramatic cell-cycle phenotypes we observed for cell populations treated with low Dox +/- TNF-α using the TI-SWR methodology. We chose the change in the percent of the cell population in S phase between 12 and 24 hr following treatment (Δ %S, 12-24 hr) as the response variable in a TI-SWR analysis.

When we choose this response variable (Δ %S, 12-24 hr) as the subject of a TI-SWR analysis, the result is a set of 5 time-point specific time-interval models (Table 2-6). At five out of the 10 time-points at which signals were measured, no signal-response relationships reach a level of significance (These time-points include the 0.25, 0.5, 1, 1.5 and 12 hr time-points). That is, no signals at these time-points are found to significantly correlate with the response variable. Therefore, the Stepwise regression algorithm excludes all signals from these time-interval regression models and no model is reported at these time-points.

Y : Δ % S phase, 12-24h

| Time-point (hr) | Signal correlates in decreasing order of $R^2$ |
|---|---|
| 0.25h | ---- |
| 0.5h | ---- |
| 1h | ---- |
| 1.5h | ---- |
| 2h | + pH2AX, - total H2AX, + pERK1/2, - pNbs1 |
| 4h | + pERK1/2, - total p53, - total JNK, - pp53 |
| 8h | + pERK1/2 |
| 12h | ---- |
| 16h | + total p53 |
| 24h | + total p53 |

**Table 2-6.** Table of results from a TI-SWR (Time-Interval Stepwise regression) analysis investigating the change in S phase cell-cycle population between 12 and 24 hr following treatment (Δ %S, 12-24 hr) as the cellular response variable. Rows present an overview of the results for each of the 10 time-point specific Time-Interval models constructed (For each of the time-point specific Time-Interval models, the response variable is Δ %S, 12-24 hr and the explanatory variable set is all signals measured at that time-point). For each Time-interval model, signal names are listed in order of decreasing $R^2$ (ability to explain the variability in the response variable), within the single optimal model calculated. Where no signals are listed, no signal-response relationships reached an acceptable level of significance ($p < 0.05$). p-ERK (red) is positively correlated with Δ %S, 12-24 hr at 2, 4 and 8 hr following treatment. These data strengthen our hypothesis that ERK has a role in mediating cell-cycle regulatory phenotypes following DNA damage. For further details on individual Time-Interval models in this set, and on the full TI-SWR analysis, reference Supplemental Figure 3-1 through 3-8.

### *TI-SWR analysis suggests that ERK promotes population build-up in S phase following DNA damage*

The five time-point specific models that do result from the TI-SWR analysis are for signaling at 2, 4, 8, 16 and 24 hr (Table 2-6). Interestingly, we find that H2AX and ERK1/2 are correlated with the response variable (Δ %S, 12-24 hr) at relatively early times (2 hr). H2AX is excluded from the model by the 4 hr time-point, but ERK1/2 remains in the 4 hr time-point model. In the 4 hr time-point model, ERK1/2 has a much higher correlation with the response variable (Δ %S, 12-24 hr) than in the 2 hr time-point model, and now works in concert with p53. ERK1/2 is also still retained in the 8 hr time-point model. In the 8 hr time-point model, ERK1/2 is highly correlated with the response variable and is the ***only*** signal at this time-point that is correlated with the response variable. By the 12 hr time-point, ERK1/2 is excluded from the time-point model, and is not included in models for either of the later time-point models (16 and 24 hr time-point models). Time-point specific models for the 16 and 24 hr time-point exclude all signals except for total p53, indicating that only total p53 is significantly correlated with the response variable at these late times.

### *Translating a Model-derived relationship into an experimentally testable Hypothesis*

The results of a TI-SWR analysis with Δ %S, 12-24 hr as the response variable, indicate that p-ERK1/2 activity at 2, 4 and 8 hr following treatment is correlated with the change in the percentage of the population in S phase between 12 and 24 hr (Δ %S, 12-24 hr). This correlation is particularly strong at the 4 and 8 hr time-points, with p-ERK1/2 showing up as the only signal correlate with the Δ %S from 12-24 hr at the 8 hr time-point (Supplementary Figures 3-1 through 3-5).

We can indeed see that there is robust activation of ERK1/2 over the time-period from 2-8 hr following treatment under many of the treatment conditions examined (Figure 2-2A). In untreated cell

populations ERK1/2 activity is minimal over this time-period. In cell populations treated with TNF-α, there is an early period of ERK1/2 activity, with pERK1/2 rising to 3 fold over untreated by 30 min following treatment, up to nearly 5 fold by 2 hr following treatment, then rapidly decreasing to a low activity level of about 2 fold over untreated by 4 hr and remaining at this low levels at least through the 8 hr time-point. Cell populations treated with low Dox (2 μM) alone exhibit low levels of ERK1/2 activity early in the time-course following, but pERK1/2 begins to rise to 2 fold over untreated by 2 hr following treatment and rapidly increases between 2-4 hr, exhibiting activity levels 6 fold over untreated by 4 hr and 7 fold over untreated by 8 hr. Cell populations treated with low Dox (2 μM) plus TNF-α exhibit an early rise in ERK1/2 activity nearly identical in dynamics and magnitude to that observed in populations treated with TNF- α alone. However, whereas in populations treated with TNF- α alone this ERK1/2 activity is not sustained beyond 2 hr following treatment, in cell populations treated with low Dox plus TNF- α, early ERK1/2 activity is sustained beyond 2 hr, remaining at a consistently high 5-6 fold over untreated activation level through 12 hr following treatment (these mid-time range kinetics are nearly identical to those observed in populations treated with low Dox alone). Cell populations treated with high Dox alone (10 μM) exhibit low early ERK1/2 activity levels, followed by a slow, continuous ascent from 1.7 fold by 2 hr following treatment to 5.5 fold by 8 hr.

Because of these differential ERK1/2 activity dynamics over the time-period from 2-8 hr following treatment, we posited that, in addition to the correlation between the activity of ERK1/2 at each of the 2, 4 and 8 hr time-points and Δ %S from 12-24 hr, that there would also be a correlation between the integrated ERK1/2 activity over the time-period from 2-8 hr and Δ %S from 12-24 hr. In fact, the regression coefficient from a univariate linear regression analysis of these two variables was 0.8, revealing a high positive correlation between the integrated ERK1/2 activity over the time-period from 2-8 hr following treatment and Δ %S from 12-24 hr (Supplementary Figure 2-3).

We posited that if this correlation represents a causal relationship between pERK1/2 from 2-8 hr and Δ %S from 12-24 hr, then a lower pERK1/2 from 2-8 hr would result in a lower Δ %S from 12-24 hr. Thus, we hypothesized that if we experimentally inhibit ERK1/2 over the time-period between 2-8 hr following DNA damage, we would expect a lower Δ %S from 12-24 hr than if we do not inhibit ERK1/2 over this time-period.

### *Experimentally Testing a Model-derived Hypothesis*

Cell populations treated with low Dox (2 μm) exhibit the largest Δ %S from 12-24 hr (Figure 2-5A) and the largest integrated ERK1/2 activity over the time-period from 2-8 hr following treatment (Figure 2-2A). Therefore, we chose to pursue the validation of our hypothesis under this treatment condition. We used PD98059, an ATP-competitive inhibitor of MKK2/MEK1, the only known activating kinase of ERK1/2, to inhibit ERK1/2 activity over the time-period between 2-8 hr following treatment with low Dox (2 μm).

We hypothesized that we would observe a lower Δ %S from 12 to 24 hr in cell populations treated with PD98059 in the time period from 2-8 hr following treatment with low Dox (2 μm) than we would observe in cell populations treated with low Dox alone. We reasoned that this decrease in the Δ %S from 12 to 24 hr would manifest itself as either an observed decrease in the %S at 24 hr, an observed increase in the %S at 12 hr, or as both of these effects. We considered that an observed decrease in the %S at 24 hr would be an unsurprising result; ERK1/2 has an established role as a positive regulator of proliferation and the G1/S transition, so that its inhibition could reasonably be expected to prevent cells from entering S, thus decreasing the observed %S at some time following its inhibition. By the same reasoning, an observed increase in %S at 12 hr would be an unexpected result. The combination of these two results would be equally unexpected.

### *Inhibition of ERK results in a decrease in Δ %S between 12 and 24 hr*

Cells were treated with Dox as before (Figure 2-1A), and PD98059 or carrier alone was added at either the same time as Dox (0 hr) or at 2 hr following Dox treatment, to more specifically test the hypothesis that ERK1/2 activity in the time period from 2-8 hr is crucial for this cellular response phenotype. In cell populations treated with Dox plus PD98059 at 0 hr, or plus PD98059 at 2 hr, we observed both a statistically significant decrease in %S at 24 hr and a statistically significant increase in %S at 12 hr as compared to cells treated with Dox, plus carrier alone (Figure 2-9A). Thus, experimental inhibition of ERK1/2 in the time period from 0-8 hr or in the time period from 2-8 hr following Dox treatment results in lower Δ %S from 12 to 24 hr than is observed following Dox treatment without inhibition of ERK1/2, confirming our model-derived hypothesis.

These results were surprising and suggested a novel role for ERK1/2 in cell-cycle regulation following DNA damage. Therefore, we chose to pursue a more detailed study of cell-cycle dynamics in cell populations treated with low Dox in the presence and absence of ERK1/2 inhibition.

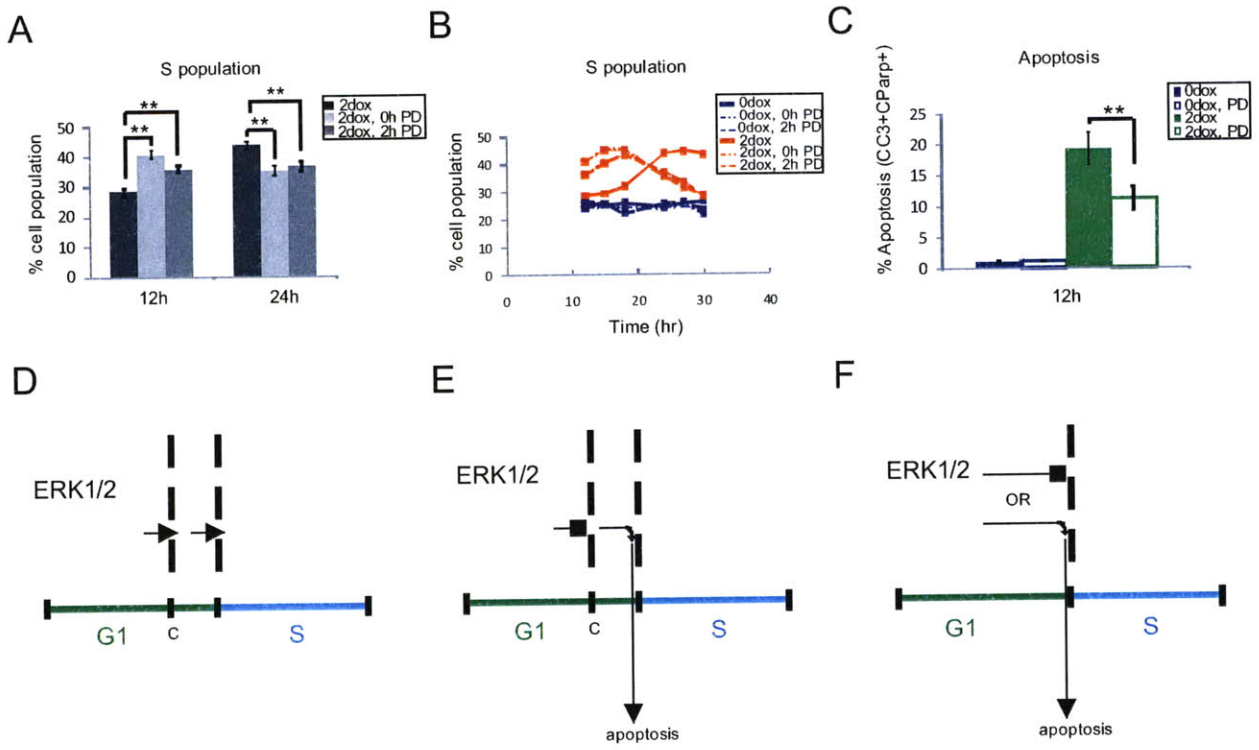


**Figure 2-9.** ***(A)*** A plot of the % of the total cell population that is observed to be in the S phase of the cell-cycle at 12 and 24 hr following treatment with 2 μM Dox +/- PD98059 (20 μM), added simultaneously with Dox (0 h) or added 2 hr following Dox treatment (2 h). U2OS cells were treated with 2 μM Dox plus PD98059 (20 μM) at 0 hr following Dox treatment or at 2 hr following Dox treatment. Treatment protocol was as described in Figure 2-1. (A), except that PD98059 was either never added, added simultaneously with Dox, or added 2 hr following Dox treatment. An additional divergence from the previously described protocol is that, following media aspiration and replacement with media containing 1% FBS, in this case media also contained PD98059 if it already contained PD98059 prior to the media change. Whole cell samples were collected and fixed at 12 and 24 hr following treatment and stained with PI (propidium iodide) for FACS measurement of DNA content. FACS cell-cycle histograms were gated to distinguish fractions of the total cell population in G1, S or G2-M cell-cycle phase, and these gates were subsequently quantified. ***(B)*** A plot of the % of the total cell population that is observed to be in the S phase of the cell-cycle at 12, 15, 18, 24, 27 and 30 hr following treatment with 2 μM Dox +/- PD98059 (20 μM), added simultaneously with Dox (0 h) or added 2 hr following Dox treatment (2 h). ***(C)*** A plot of the % of the total cell population that is observed to be apoptotic at 12 hr following treatment with 2 μM Dox +/- PD98059 (20 μM), added simultaneously with Dox. U2OS cells were treated as described in (A). Whole cell samples were collected and fixed at 12 and 24 hr following treatment and stained for FACS measurement of cleaved caspase-3 and cleaved Parp. FACS dot plots were gated to distinguish fractions of the total cell population staining positively for one, none or both apoptotic markers, and these gates were subsequently quantified. Here, cells staining positively for both apoptotic markers (CC3+CParp+) were considered to be apoptotic. **(D)** ERK1/2 has an established role in promoting cell-survival and cell-cycle progression under normal or low stress conditions. ***(E)*** Model 1: ERK1/2 has a role in promoting apoptosis and maintenance of a cell-cycle

check-point/arrest in G1 or at the G1/S transition following DNA damage; ERK1/2 switches between promotion of the maintenance of a cell-cycle check-point and promotion of apoptosis based upon the cell-cycle context at the time of damage. That is, if damage is induced prior to a cell-cycle check-point in G1 or at the G1/S transition, ERK1/2 promotes maintenance of this check-point once it has been engaged. If damage is induced post cell-cycle check-point, ERK1/2 promotes apoptosis. ***(F)*** Model 2: ERK1/2 has a role in promoting apoptosis and maintenance of a cell-cycle check-point/arrest in G1 or at the G1/S transition following DNA damage; ERK1/2 switches between promotion of the maintenance of a cell-cycle check-point and promotion of apoptosis based upon the damage context of the cell. That is, ERK1/2 promotes maintenance of a cell-cycle check-point in G1 or at the G1/S transition in the case that damage is below some threshold in terms of amount and/or complexity and ERK1/2 promotes apoptosis in the case that damage is above some threshold in terms of amount and/or complexity.

---

### *Inhibition of ERK results in early release from a DNA damage-mediated cell cycle arrest in G1 or at the G1/S transition*

Cells were treated with Dox as before, and PD98059 or carrier alone was added at either the same time as Dox (0 hr) or at 2 hr following Dox treatment. The cell-cycle status of these populations was determined by FACS analysis at 6 time-points over 30 hr following treatment, including 3 "early" time-points (12, 15 and 18 hr) and three "late" time-points (24, 27 and 30 hr). In untreated cell populations, the percentage of the cell population in S phase (% S) remains nearly constant over the full 18 hr time course at about 25%. Adding PD98059 to untreated cell populations either at the same time as mock treatment (0 hr) or 2 hr following mock treatment does not change the percentage of the cell population in S phase (%S) or the constant dynamics of the %S over the full 18 hr time course. (In both of these treatment conditions, the %S also remains nearly constant over the full 18 hr time course and overlays almost exactly that of untreated cell populations that never see PD98059 with a constant %S of approximately 25% over the full time course.) (Figure 2-9B)

In cell populations treated with low Dox (2 μM), %S remains relatively constant at levels just above those observed in untreated cell populations (28% at 12 hr; 29% at 15 hr) through 15 hr following

treatment. %S begins to increase to levels above those observed in untreated cell populations by 18 hr following treatment (32%). The percent of the cell population in S rises dramatically between 18 hr following treatment and 24 hr following treatment, such that 44% of the cell population is observed to be in S phase at 24 hr following treatment. The %S peaks just above this value at 45% of the cell population in S at 27 hr following treatment and may start to decrease by 30 hr following treatment, with an observed %S of 43% at 30 hr following treatment.

As observed previously, in cell populations treated with low Dox plus PD98059 at the time of Dox treatment (0 hr), %S was observed to be higher at 12 hr following treatment than that observed in cell populations treated with Dox minus PD98059 (Figure 2-9A). %S at 12 hr following treatment in this population was 41% (compared to 28% for the cell population treated with Dox minus PD98059, rose to 45% by 15 hr following treatment and remained at 45% through 18 hr following treatment before beginning a steady descent over the remaining 12 hr in the time course back to levels just above those seen in untreated cell populations, and equivalent to those seen in Dox treated cell populations minus PD98059 at 12 hr following treatment (28%), by 30 hr following treatment. Results for cell populations treated with low Dox plus PD98059 at 2 hr following treatment were nearly identical to those observed for cell populations treated with Dox plus PD98059 at the time of Dox treatment (0 hr), with somewhat lower values observed for %S at 12 and 15 hr following treatment than that observed in cell populations treated with Dox plus PD98059 at 0 hr (36% vs. 41% and 40% vs. 45%, respectively), though still significantly higher than values observed in untreated cell populations or populations treated with Dox minus PD98059 (Figure 2-9B).

From examination of the cell-cycle profiles, we determined that the increase in S phase at 12 hr following Dox treatment plus PD989059 that we quanitify in Figure 2-9B is due to a population moving synchronously out of G1 into S. This population is a "shoulder" off of the G1 peak in a cell-cycle

histogram staining for PI at 12 hr, but by 15-18 hr this large cohort of the population has moved synchronously into mid S phase (Supplementary Figure 2-4). By 24 hr, this cohort population is moving from S into G2-M, and by 30 hr, this cohort has completed its transition into G2-M.

We previously noted, and again observed, this "cohort "effect of cells moving synchronously through the cell cycle in cell populations treated with low Dox alone. Our data are consistent with the hypothesis that this cohort effect is likely due to a population build-up at a DNA damage mediated cell cycle checkpoint in G1 or at the G1/S transitions, followed by a release of the cell-cycle checkpoint that allows the now synchronized population, or cohort, to continue through the cell cycle together. In cell populations treated with low Dox alone (no PD) this "cohort" moves from G1 into S by 27 hr, and from S into G2-M by 48 hr. In cell populations treated with low Dox ***plus PD***, this "cohort" moves from G1 into S by 15-18 hr, and from S into G2-M by 24.

Addition of the PD drug then results in an early release of the "cohort" from a DNA damage mediated cell cycle arrest in G1 or at the G1/S transition. From these observations we reasoned that ERK1/2 may be involved in the maintenance of a DNA damage mediated cell-cycle checkpoint in G1 or at the G1/S, transition, as its inhibition appears to result in an early release from a cell-cycle check-point.

### *Inhibition of ERK reduces apoptosis following DNA damage*

We also examined the apoptotic phenotype of cell populations treated with low Dox plus or minus PD. In untreated cell populations, apoptosis as measured by positivity for both apoptotic markers, cleaved Caspase-3 and cleaved PARP, is minimal (<<5%). In untreated populations, addition of PD98059 does not affect apoptosis; these populations also exhibit minimal apoptosis (<<5%) (Figure 2-9C). In cell populations treated with Dox (2μM), nearly 20% of the population is apoptotic at 12 hr following treatment. In cell populations treated with Dox (2μM) plus TNF-α, nearly 40% of the population is apoptotic at 12 hr following treatment. Addition of PD98059 at the time of Dox treatment to cell populations treated with Dox alone or Dox plus TNF-α significantly decreases apoptosis in these populations at 12 hr following treatment, from nearly 19% to 11% and from 39% to 25% respectively Figure 2-9C and data not shown). Similar results were found at 24 hr following treatment, with addition of PD98059 decreasing apoptosis from 13% to 8% in populations treated with Dox alone, and from 28% to 17% in populations treated with Dox plus TNF-α (Data not shown). These results indicated to us that ERK1/2 might be involved in promoting apoptosis following DNA damage, as its inhibition results in dramatically decreased apoptosis following DNA damage.

### *Inhibition of ERK reduces apoptosis in G1 or at the G1/S transition following DNA damage*

In cell populations treated with low Dox plus TNF-α, the % apoptosis is dramatically higher than that observed in cell populations treated with low Dox alone at all time-points examined (Figure 2-5B). The cell-cycle "cohort" effect observed in cell populations treated with Dox alone is likewise observed in cell populations treated with low Dox plus TNF-α. However, the cohort that is released from G1 into S by 24 hr and that leaves S to progresses into G2-M by 48 hr is a significantly smaller population in cell

populations treated with low Dox plus TNF-α than is observed in populations treated with low Dox alone (Figure 2-5A and Supplementary Figure 2-6).

We reasoned that this cohort might be smaller in populations treated with low Dox plus TNF-α than in populations treated with low Dox alone because the complement of this cohort is dying by apoptosis prior to release of the cohort into S, either in G1 or at the G1/S transition, and that this apoptosis is ERK1/2 dependent. This is consistent with the observations that in cell populations treated with low Dox plus TNF-α, 1) apoptosis is dramatically higher than that observed in populations treated with low Dox alone, 2) the population cohort that makes its way from G1 into S by 24 hr following Dox plus TNF- α is smaller than that observed in populations treated with low Dox alone, and 3) Inhibition of ERK1/2 in populations treated with low Dox plus TNF-α results in both significant inhibition of apoptosis, and in an increase in the size of the population cohort that is released from G1 into S by 12 hr (Supplementary Figure 2-6).

### *Model*

ERK1/2 has an established role in promoting cell-survival and progression through the cell-cycle under normal and/or low stress conditions (Figure 2-9D). These data thus suggested that ERK1/2 is involved in both 1) promotion of apoptosis, and 2) maintenance of a cell-cycle checkpoint in G1 or at the G1/S transition following DNA damage. We further hypothesized that 3) ERK1/2 activity switches between promotion of apoptosis, or maintenance of a cell-cycle arrest in G1 or at the G1/S transition, in a single cell based on the either the ***cell-cycle context*** in which the cell sustained DNA damage (e.g. whether damage is sustained pre-G1 or G1/S checkpoint or post-checkpoint) (Figure 2-9E), or based on the ***damage context*** of the cell following DNA damage (e.g. the extent/type of damage a cell has sustained) (Figure 2-9F).

### *ERK promotes apoptosis in G1 or at the G1/S transition following DNA damage without requiring progression through S phase*

We proceeded to directly test the hypothesis that ERK1/2 is involved in promotion of apoptosis in G1 or at the G1/S transition following DNA damage. We synchronized cells in G1 via a double thymidine block, released into aphidicolin to prevent progression into S phase, then treated G1-synchronized populations with Dox (2μM), or Dox plus TNF-α, plus or minus PD and measured apoptosis at 8 hr following Dox treatment, without ever allowing cells to progress through S phase (Figure 2-10A).

In untreated, G1-synchronized cell populations, apoptosis as measured by positivity for both apoptotic markers, cleaved Caspase-3 and cleaved PARP, is minimal (<<5%). In untreated G1-synchronized populations, addition of PD98059 does not affect apoptosis; these populations also exhibit minimal apoptosis (<<5%). In G1-synchronized cell populations treated with Dox (2μM), 33% of the population is apoptotic at 8 hr following Dox treatment when the population is blocked from

progression into S phase by the presence of aphidicolin. In G1-synchronized cell populations treated with Dox (2μM) plus TNF-α, 55% of the population is apoptotic at 8 hr following Dox treatment when the population is blocked from progression into S phase by the presence of aphidicolin. In both of these populations, addition of PD98059 significantly reduces apoptosis in the population, from 33% to 17% (a 48% reduction) and from 55% to 35% (a 36% reduction) respectively (Figure 2-10B and data not shown).

These data support our hypothesis that ERK1/2 is involved in promotion of apoptosis in G1 or at the G1/S transition following DNA damage. However, in order to rule out the "chattering" effect at the G1/S boundary that has been observed to occur in cells blocked from entering S by incubation with aphidicolin (minimal levels of origin firing may occur during incubation with aphidicolin) as a necessary condition for this observed apoptosis, we repeated this experiment, this time allowing progression into S phase by removing aphidicolin (Figure 2-10C). If origin firing and progression into S is a necessary condition for ERK1/2 dependent promotion of apoptosis following DNA damage, we would expect that G1-synchronized cell populations treated with Dox that are allowed to progress into S by removal of aphidicolin will exhibit higher absolute levels of apoptosis than is observed in G1-synchronized cell populations treated with Dox that are never allowed to progress into S phase. We also might expect a greater margin of saving (reduction in apoptosis) by ERK1/2 inhibition in cell populations that are allowed to progress into S.

In G1-synchronized cell populations treated with Dox (2μM), 17% of the population is apoptotic at 7 hr following Dox treatment when the population is allowed to progress into S phase for 1 hr following release from an aphidicolin block, accomplished at 6 hr following Dox treatment. In G1-synchronized cell populations treated with Dox (2μM) plus TNF-α, 48% of the population is apoptotic at 7 hr following Dox treatment when the population is allowed to progress into S phase for 1 hr following release from an aphidicolin block, accomplished at 6 hr following Dox treatment. In both of these

populations, addition of PD98059 significantly reduces apoptosis in the population, from 17% to 11% (a 35% reduction) and from 48% to 31% (a 35% reduction) respectively (Figure 2-10D and data not shown).

These data thus support our hypothesis that ERK1/2 is involved in promotion of apoptosis in G1 or at the G1/S transition following DNA damage, and that this ERK1/2 dependent promotion of apoptosis in G1 or at the G1/S transition does not require progression into S phase.

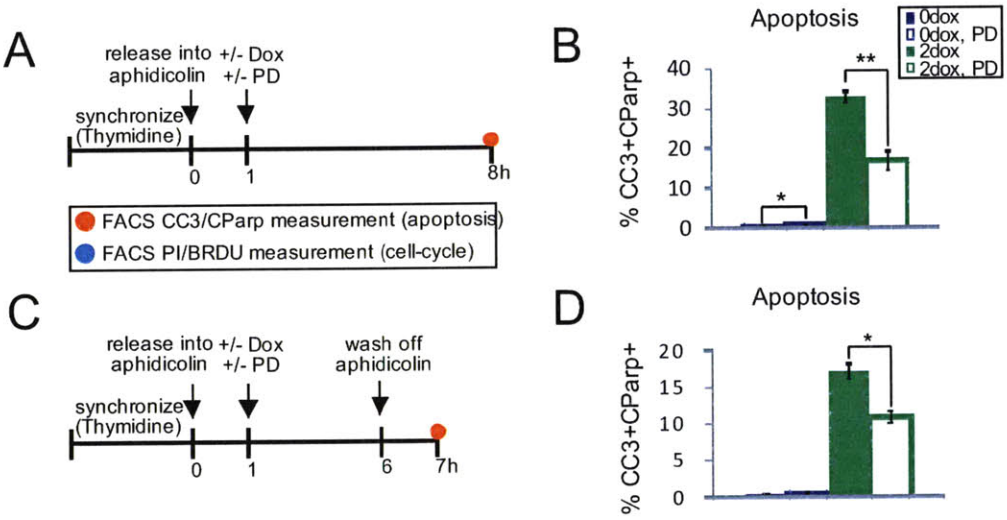


**Figure 2-10.** ***(A)*** Time-line of experiment; data is in (B). U2OS cells were synchronized in late G1 via a double thymidine block and released into fresh media containing aphidicolin (10 μM) to prevent progression into the S phase of the cell cycle. One hour following release into aphidicolin, cells were treated +/- Dox (0 or 2 μM) and +/- PD98059 (20 μM). At 4 hr following treatment, treatment media was aspirated and replaced with media containing 1% FBS and +/- PD98059 according to whether PD98059 was present or not prior to media exchange, and ***plus aphidicolin***. Whole cell samples were collected and fixed at 8 hr following treatment, then stained for FACS measurement of cleaved caspase-3 and cleaved Parp. ***(B)*** A plot of the % of the total cell population that is observed to be apoptotic at 8 hr following treatment in cell populations that were treated in late G1, and never allowed to progress into S phase, as described in (A). FACS dot plots of cleaved caspase-3 vs. cleaved Parp were gated to distinguish fractions of the total cell population staining positively for one, none or both apoptotic markers, and these gates were subsequently quantified. Here, cells staining positively for both apoptotic markers (CC3+CParp+) were considered to be apoptotic. ***(C)*** Time-line of experiment; data is in (D). U2OS cells were synchronized in late G1 via a double thymidine block and released into fresh media containing aphidicolin (10 μM) to prevent progression into the S phase of the cell cycle. One hour following release into aphidicolin, cells were treated +/- Dox (0 or 2 μM) and +/- PD98059 (20 μM). At 4 hr following treatment, treatment media was aspirated and replaced with media containing 1% FBS and

+/- PD98059 according to whether PD98059 was present or not prior to media exchange, and ***plus aphidicolin***. At 6 hr following treatment, media was aspirated and replaced with media containing 1% FBS ***without aphidicolin***, to allow progression into S phase. Whole cell samples were collected and fixed at 7 hr following treatment, then stained for FACS measurement of cleaved caspase-3 and cleaved Parp. ***(D)*** A plot of the % of the total cell population that is observed to be apoptotic at 7 hr following treatment in cell populations that were treated in late G1, but subsequently allowed to progress into S phase, as described in (C). FACS dot plots of cleaved caspase-3 vs. cleaved Parp were gated to distinguish fractions of the total cell population staining positively for one, none or both apoptotic markers, and these gates were subsequently quantified. Here, cells staining positively for both apoptotic markers (CC3+CParp+) were considered to be apoptotic.

---

### *Future Experiments: ERK promotes maintenance of a DNA damage mediated cell cycle checkpoint in G1 or at the G1/S transition*

In future experiments, we will provide further evidence of our hypothesis that ERK1/2 is involved in maintenance of a cell cycle checkpoint in G1 or at the G1/S transition following DNA damage. Similarly to previous experiments described, we will synchronize cells in G1 via a double thymidine block, release into aphidicolin to prevent progression into S phase. We will then treat G1-synchronized populations with Dox (2μM), or Dox plus TNF-α, plus or minus PD, remove aphidocolin at 6 hr following Dox treatment to allow for progression into S phase, and make measurements of the cell-cycle profiles of these populations at 3 hr intervals following release from aphidicolin (at 6, 9 and 12 hr following Dox treatment). BRDU will be added 1 hr prior to sample collection for cell cycle profile measurement to rigorously assess entry into S (Supplementary Figure 2-7). We expect that cell populations treated with Dox or Dox plus TNF-α in the absence of PD will exhibit a cell-cycle arrest in G1 and will not progress into S following release from aphidicolin within the time-period of this experiment (up to 12 hr following Dox). On the other hand, we expect that cell populations treated with Dox or Dox plus TNF-α in the presence of PD will not exhibit a cell-cycle arrest in G1 and will progress into S following release from aphidicolin within the time-period of this experiment (up to 12 hr following Dox).

***Future Experiments: ERK switches between promoting maintenance of a DNA damage mediated cell cycle checkpoint and promoting apoptosis in G1 or at the G1/S transition based on either the cell-cycle context or the damage context***

In future experiments, we will also attempt to distinguish between our two proposed models for ERK1/2's role in mediating cellular responses following DNA damage. Our first model proposes that ERK1/2 activity switches between a role in promotion of apoptosis or maintenance of a cell-cycle arrest in G1 or at the G1/S transition in a single cell following DNA damage based on the damage context of that cell (the extent/type of damage sustained). A second model proposes that ERK1/2 activity switches between a role in promotion of apoptosis or maintenance of a cell-cycle arrest in G1 or at the G1/S transition in a single cell following DNA damage based on the cell-cycle context of that cell (pre- or post-cell cycle checkpoint at the time of damage).

We will synchronize cell populations in metaphase via a nocodazol block, remove nocodazol to release this metaphase-synchronized population to progress into G1. At 4 hr following release, greater than 90% or the population is expected to have progressed into G0/G1 (early G1). Starting at 4 hr following release, and at 2 hr intervals thereafter, through 10 hr following release (until progression through G1 is complete – G1 is approximately 6 hr in length), we will treat separate cell populations with Dox, or Dox plus TNF-α, plus or minus PD, and measure apoptosis in, and cell-cycle profiles of, these populations at 6 hr following treatment (Supplementary Figure 2-8A).

If the switch in ERK1/2 role is cell-cycle context dependent, such that in cells damaged pre- cell cycle checkpoint ERK1/2 promotes maintenance of a cell cycle checkpoint and in cells damaged post-cell cycle checkpoint ERK1/2 promotes apoptosis, then we expect that populations treated with Dox at early times following release from nocodazol will exhibit a robust cell cycle arrest phenotype (a population build-up in G1 or at the G1/S transition) and minimal apoptosis (Supplementary Figure 2-8B

and Supplementary Figure 2-8C). Populations treated with Dox at later times following release from nocodazol should exhibit an increasingly robust apoptotic phenotype (larger proportions of apoptotic cells) as larger proportions of the cell population progress to a point in G1 that is post- cell cycle checkpoint. Presumably, populations treated with Dox at 10 hr following release from nocodazol, wherein the whole population should have progressed to a point in G1 that is post- cell cycle checkpoint (late G1 or G1/S), will exhibit a very robust apoptotic phenotype, and addition of PD will result in a robust saving (reduction in apoptosis) (Supplementary Figure 2-8D and Supplementary Figure 2-8E).

If the switch in ERK1/2 role is damage context dependent, such that in cells that experience low-level or simple damage ERK1/2 promotes maintenance of a cell cycle checkpoint and in cells that experience high-level or complex damage ERK1/2 promotes apoptosis, then we expect that there will be no change in the magnitude or proportion of cell-cycle arrest and apoptotic phenotypes exhibited by cell populations treated with Dox at different points in G1.

One caveat to this projection is that if cells are more susceptible to damage at different points in G1, then we would expect results similar to those projected in the case that our cell-cycle dependent model is true. Therefore we might erroneously conclude that ERK1/2 switches its role in mediation of cellular response following DNA damage in a cell-cycle context dependent manner, even if the true model is that ERK1/2 switches its role in a damage-context dependent manner, IF extent/type of damage is cell-cycle dependent.

In order to avoid such erroneous conclusions, we will additionally collect cell-extracts at 4 hr following treatment with Dox in all cases and measure extent of damage by probing for γH2AX. If we observe results consistent with a cell-cycle context dependent model and equal levels of γH2AX across cell populations treated with Dox at different point in G1, then we will conclude that we have strong

evidence for a cell-cycle context dependent model. However, if we observe results consistent with a cell-cycle context dependent model and levels of γH2AX across cell populations treated with Dox at different point in G1 are not equal, then we will conclude that we have strong evidence for a damage context dependent model.

## Discussion

We have collected a large, quantitative signal-response dataset investigating network level signaling and cellular responses following DNA damage, under inflammatory and non-inflammatory treatment conditions. We used two distinct and complementary data-driven computational modeling approaches to systematically investigate network level relationships between signals and cellular phenotype in the data-set.

Data-driven computational modeling approaches are still in the early stages of development and application in biology. Techniques such as PLSR and Bayesian network analysis have been used successfully to gain insight into network level signal-response relationships, and as tools for prediction of cellular response under novel treatment conditions. Janes et. al have used PLSR analyses of a large quantitative signal-response dataset of population level, time-series signal and response measurements to identify autocrine cascades involved in cytokine-induced apoptosis in HT-29 colon carcinoma cells [165]. Kemp et. al have used PLSR analysis of a quantitative signal-response dataset of population level, time-series signal and response measurements to predict the production of IL-2 in a T-cell hybridoma cell line stimulated with altered peptide ligands of varying antigenicity [160]. More recently, Janes et. al have developed a method they call "Model break-point analysis" that they use in conjunction with PLSR analysis to further probe similar quantitative signal-response datasets to identify signaling that is essential in a context (treatment)-specific manner (bounded by the treatments described in the dataset) [166]. In this work, they show that break-point analysis allows for the identification of signals that are

essential for cellular responses, such as apoptosis, under specific treatment conditions and not for others, where the results from PLSR analysis alone does not identify the signal as essential for the cellular response overall.

Sachs et. al have used Bayesian network analysis of a quantitative signaling dataset of single-cell level signaling data measured at one time-point (including inhibitor-perturbed treatment conditions) to reconstruct network level signaling relationships and to discover novel interpathway network causalities following activation of human primary naïve $CD4^+$ T-cells via CD3, CD28 and LFA-1 receptors [167]. A major drawback to a Bayesian approach, as pointed out by the authors, was the inability of the analysis to identify cyclic signaling relationships, such that several well-established feed-back relationships in the signaling network were missed in the signaling network reconstruction. More recently, Sachs et. al have developed a Generalized Bayesian network analysis approach to infer signaling network structure from a quantitative signaling dataset of single-cell level, time-course signaling data; this generalized analysis approach, applied to time-course data, aims to allow for inference of cyclic relationships in signaling networks [168].

These examples demonstrate that 1) data-driven analysis methods can be successfully used to discover network-level signaling relationships and signal-response relationships, 2) different data analysis methods can be usefully applied depending on the type of data collected (conversely, the type of data to be collected in an experimental investigation should be thoughtfully considered before-hand, with an eye to what data-analysis methods will be applied), and 3) more than one data-driven analysis method may be applied to a single dataset and the consideration of results from these analyses together can greatly increase the depth of insight gained from the data (e.g. as in the consideration of break-point analysis and PSLR analysis together).

In this work, we applied PLSR and TI-SWR methods to study DNA damage signaling. This work represents the first application of data-driven computational modeling to the analysis of signaling events

following genotoxic stress. Results from the construction of a PLSR model suggested a role for ERK1/2 in mediating both cell-cycle regulatory effects (increase in S phase and G2-M populations at 24 hr) and in mediating apoptotic effects following DNA damage. A TI-SWR analysis identified a strong correlation between ERK1/2 activity at 2, 4 and 8 hr following damage, and the change in percent of the cell population in S phase between 12 and 24 hr (Δ %S, 12-24 hr). To our knowledge, this use of TI-SWR is the first systematic application of SWR to investigate time-specific network-level relationships between signals and cellular phenotypes.

ERK has a well-established role in promoting survival and progression into the cell-cycle under normal and/or low-stress conditions [169-172]. A role for ERK1/2 following DNA damage has not been well established, with some studies reporting a pro-survival role, and a few reporting a pro-apoptotic role, for ERK1/2 following DNA damage. Tsakiridis et. al have shown that detection of active ERK in samples of NSCLC tumors correlates with poor radiologic response [173], and Nishioka et. al have shown that inhibition of ERK enhances apoptosis in acute myelogenous leukemia cells concurrently exposed to the DNA damaging chemotherapeutic agent cytaribine [174]. Tang et. al have suggested that ERK contributes to maintenance of a G2/M arrest following low dose etoposide treatment and to promotion of apoptosis following high dose etoposide [175]. Yan et. al have suggested that ERK is necessary for the induction of a G2/M checkpoint following irradiation in MCF-7 cells, and mediates the G2/M checkpoint via activation of ATR [176]. We demonstrate that ERK1/2 plays a role in promoting apoptosis following DNA damage, and also plays a role in maintaining a DNA damage-mediated cell-cycle arrest following DNA damage. Thus our data point to a context specific role for ERK following DNA damage that is in opposition to the role it plays under non-DNA-damaging conditions.

Two of the key steps in tumor development include acquisition of the ability to evade apoptosis and the acquisition of the ability to proliferate in an uncontrolled manner. Consistent with ERK's role in promoting survival and proliferation under non-DNA damaging conditions, upstream components of the

ERK cascade, including Ras, Raf and the EGFR are often mutated in cancer [177, 178], and the dysregulation and hyper-activation of these pathways has been shown to be pathological in many tumors, conferring resistance to therapy [179]. There has been a large effort to design rational therapies to inhibit this pathway. Several MEK inhibitors are under development and EGFR inhibitors have been some of the first targeted therapies to be approved and used in the clinic [178]. The success of these agents had been surprisingly limited and has highlighted the complexity of this signaling mechanism.

If the predominant role of ERK1/2 is to promote apoptosis under DNA damaging conditions, inhibition of ERK1/2 (via, for example, application of a MEK inhibitor) should lead to inhibition of apoptosis and could result in ***increased resistance*** to DNA damaging chemotherapy. If, on the other hand, the predominant role of ERK1/2 is to promote cell-cycle checkpoint maintenance under DNA damaging conditions, inhibition of ERK1/2 should lead to bypass of that checkpoint and result in increased sensitization to DNA damaging chemotherapy [180]. We have demonstrated that ERK1/2 promotes apoptosis and maintenance of a checkpoint following DNA damage. It is crucial to determine under what conditions the predominant effect of ERK1/2 is to promote apoptosis and under what conditions the predominant effect of ERK1/2 is to promote maintenance of checkpoints, in order to effectively implement chemotherapeutic regimens that combine DNA damaging chemotherapeutic agents with MEK inhibitors.

Two hypotheses, consistent with our data, are that within a single cell ERK1/2 switches between promotion of apoptosis and promotion of maintenance of a DNA damage-mediated cell-cycle checkpoint based on either 1) the extent of damage sustained, or 2) the cell-cycle status at the time damage was sustained. In the case where the predominant effect of ERK1/2 is determined by the extent of damage sustained, ERK1/2 may promote checkpoint maintenance when low damage levels are sustained, and ERK1/2 may promote apoptosis when high damage levels are sustained. If this is correct,

adjuvant therapy with MEK inhibitors may be effective in combination with doses of DNA damaging chemotherapeutic agents that inflict only low levels of damage, but should be avoided in regimens that include high doses of DNA damaging chemotherapeutics. In the case where the predominant effect of ERK1/2 is determined by the cell-cycle status at the time damage was sustained, ERK1/2 may promote checkpoint maintenance when damage was sustained prior to a DNA damage checkpoint in G1 or at the G1/S transition, and ERK1/2 may promote apoptosis when damage was sustained after a DNA damage checkpoint in G1 or at the G1/S transition. If this is correct, the timing of the administration of both the DNA damaging agent and MEK inhibitors may be crucial for the effectiveness of the treatment. It may be effective to attempt to synchronize tumor cells using cdk inhibitors, such as Roscovitin, prior to administration of DNA damaging agents and MEK inhibitors.

Further elucidation of the context dependent activity of ERK following DNA damage will provide clinicians with better guidelines in designing chemotherapeutic regimens that combine DNA damaging chemotherapeutic agents and MEK inhibitors for the treatment of a wide range of tumors. Elucidation of other such network signaling context dependencies through experimental and computational systems level analysis of DNA damage responsive signaling networks will be crucial to the effective implementation of treatment regimens that exploit the combination of traditional DNA damaging chemotherapeutic agents and the broad range of targeted chemotherapeutics now under development.

### *Discussion of potential ERK mechanisms*

#### ERK and Cyclin D1

Nuclear Cyclin D1 levels increase via Raf-Mek-Erk dependent transcriptional upregulation [181-184], PI3K/Akt dependent translational upregulation and decreased degradation [62, 185, 186] during G1 in a mitogen dependent fashion [187]. In complex with ckd4 and cdk6, Cyclin D1 leads to the

phosphorylation and inactivation of Rb, resulting in the activation of E2F transcription factors and transcription of genes such as Cyclin E that are necessary for the transit from G1 to S [188-192].

Following G1/S transition, Cyclin D1 is phosphorylated on T286, exported from the nucleus and degraded in the cytoplasm via the 26S proteosome. Nuclear export and degradation are both essential for normal progression into S phase [186, 193, 194].

Inhibition of Cyclin D1 nuclear export results in re-replication of DNA and chromosomal instability and uncontrolled proliferation and is highly transforming [195-199]. Inhibition of Cyclin D1 degradation in the cytoplasm results in delayed entry into S phase [194].

In a normal cell cycle, GSK3β is implicated as the kinase that phosphorylates T286 on Cyclin D1. Phosphorylation of T286 allows interaction of Cyclin D1 with a nuclear export factor, CRM1, and subsequent nuclear export of Cyclin D1. T286-phosphorylated Cyclin D1 in the cytoplasm is recognized by the F-box protein, Fbx4, and a co-factor, alphaB crystalline, resulting in its polyubiquitilation and subsequent degradation by the 26S proteosome [193].

Okabe et al have also suggested that ERK serves as the primary kinase that phosphorylates T286 in normal S phase progression. They show that ERK interacts with Cyclin D via a D domain in Cyclin D and phosphorylates it on T286 and that in cells expressing a mutant Cyclin D1 lacking a D domain, Cyclin D1 is not efficiently phosphorylated. They also show that inhibition of ERK activity leads to increased stability of Cyclin D1 in S phase cells. In this study, they suggest that the F-box protein required for recognition, polyubiquitilation and proteosomal degradation of T286-phosphorylated Cyclin D1 is FBXW8 [194].

In addition to occurring in the course of normal cell cycle progression, Cyclin D1 degradation is also a well characterized stress response mechanism that is essential for proper cell-cycle checkpoint induction or cell-cycle exit following various cellular stresses, including osmotic and genotoxic stress.

Human kidney cells induce a transient cell cycle arrest that is p38 dependent following exposure to osmotic stress and oxidative stress [200-202]. Under these conditions, cells also degrade Cyclin D1. GSK3β is not required for Cyclin D1 degradation under these conditions. In fact, Casanovas et al showed that, under these two stress conditions, p38 phosphorylates Cyclin D1 on T286, leading to its ubiquitilation and proteosomal degradation [203].

Human melanoma cells degrade Cyclin D1 following exposure to irradiation and many other types of genotoxic stress. Under these conditions, cells also induce a cell cycle arrest at the G1/S transition that is dependent on Cyclin D1 phosphorylation on T286 and on its degradation. Santra et al show that ATM phosphorylation and stabilization of the F-box protein FBXO31 is required for ubiquitilation and proteosomal degradation of Cyclin D1. They also show that GSK3β kinase activity is dispensable for the degradation of Cyclin D1 under these conditions, but that ERK kinase activity is required for the degradation of Cyclin D1 under these conditions [204].

This study suggests that, in addition to promoting degradation of Cyclin D1 in the course of normal S phase progression, ERK may also have a role in promoting degradation of Cyclin D1 in the context of genotoxic-stress induced cell-cycle arrest. By blotting for Cyclin D1 levels in cells treated with low Doxorubicin plus or minus PD98059, we can investigate whether this mechanism may be operating in our system.

### ERK and Myc

As discussed above, ERK activity is necessary for the transcriptional upregulation of Cyclin D1 in the G1 phase of the cell cycle, and therefore, for normal cell-cycle progression from G1 into S phase. One mechanism by which ERK upregulates Cyclin D1 is via stabilization of the Myc transcription factor. Myc protein participates directly in the transcriptional induction of Cyclin D1, promoting cell-cycle progression [205].

The strict regulation of Myc protein levels is essential to normal cell cycle progression. Myc is absent in quiescent cells, and is upregulated both transcriptionally and via Ras dependent increase in stability following mitogenic stimulation, as cells enter G1 [206]. Homozygous deletion of myc genes results in embryonic lethality [207, 208]. On the other hand, constitutive overexpression of myc protein cultured cells or transgenic animals blocks differentiation and induces neoplastic transformation [209, 210].

Down-regulation of c-Myc is also associated with induction of cell-cycle arrest or cell-cycle exit phenotypes in tumor cells. Benaud et al show that downregulation of c-Myc is required for a G1 cell cycle arrest following loss of adhesion in mammary epithelial cell lines [211]. Janardhanan et al show that treatment of human neuroblastoma cells with the combination of N-(4-hydroxyphenyl) retinamide (4-HPR, 0.5muM) and genistein (GST, 25muM) resulted in cell-cycle exit to a neuronal differentiation phenotype that required downregulation of n-Myc [212].

Myc is a highly unstable molecule with a half-life of about 30 minutes [213, 214], and is rapidly degraded via the proteosomal pathway in a ubiquitin mediated fashion [215-217]. Myc's stability is regulated in a post-transcriptional fashion, by two adjacent N-terminal phosphorylation sites, T58 and S62. These sites have opposing roles in the control of Myc protein stability. Phosphorylation of Myc at S62 by ERK stabilizes Myc protein. Subsequent phosphorylation of Myc at T58 requires the prior phosphorylation on S62, is accomplished by GSK3β, and promotes degradation of Myc via a PP2A and Pin1 dependent mechanism [206, 218-222].

Pin1 induces conformational changes in S62/T58-dually phosphorylated Myc that allow PP2A to dephosphorylate the S62 site on Myc, resulting in T58-singly phosphorylated Myc. T58-singly phosphorylated Myc is rapidly degraded via ubiquitilation and proteosomal degradation [219].

In normal cell cycle progression, Ras pathway activation by mitogens leads to the activation of both ERK and Akt. ERK phosphorylates Myc at S62, and Akt likely phophorylates GSK3β, preventing phosphorylation of Myc at T58, overall increasing Myc protein stability [206, 223-225].

These studies suggests that, in addition to promoting stabilization of Myc in the course of normal cell cycle progression, ERK may also have a role in promoting degradation of Myc and subsequent cell cycle arrest or exit under some conditions. ERK phosphorylation of Myc at 62 is a "stabilizing" phosphorylation, but it also primes Myc for degradation. Where Akt activity is not present or strong enough to antagonize GSK3β, and where PP2A activity is high, phosphorylation of Myc at S62 by ERK could have a net destabilizing effect. Additionally, Sears et al note that ERK may be capable of phosphorylating both S62 and T58 on Myc [226, 227]. Therefore, in the presence of especially high ERK activity, it is possible that ERK could be the perpetrator of both the "priming" phosphorylation on S62 and the degradation-promoting phosphorylation on T58. By blotting for Myc levels in cells treated with low Doxorubicin plus or minus PD98059, we can investigate whether this mechanism may be operating in our system.

**ERK and Mcl-1**

ERK pathway signaling plays a major role in promoting survival in many tumor cell types [170, 228-231]. One of the major mechanisms by which signaling in the ERK pathway regulates survival is via regulation of Bcl-2 family members [232].

Bcl-2 family members consist of multi-domain members that are anti-apoptotic (Bcl-2, Bcl-xL, and Mcl-1) and proapoptotic (Bax and Bak) and of BH3 domain-only pro-apoptotic members (BOPs).

In viable cells, pro-apoptotic multi-domain members, Bax and Bak, are bound to and sequestered by anti-apoptotic multi-domain partners. In response to stress, BOPs are either expressed or activated and bind to anti-apoptotic multi-domain members, promoting release of pro-apoptotic

multi-domain members, which can then oligomerize among themselves leading to mitochondrial outer membrane permeabilization, release of cytochrome C and initiation of apoptosis [91, 233, 234].

BIM is a BOP that is negatively regulated by ERK on at least two levels. First, it is well established that ERK activation leads to the repression of BIM mRNA levels [235]. Nuclear entry of the transcription factor FOXO3A, for example, following cytokine withdrawal, leads to the transcriptional upregulation of pro-apoptotic BIM [236]. Yang et al have recently shown that ERK can phosphorylate FOXO3A, targeting it for proteosomal degradation, thereby preventing BIM accumulation [237]. A second mechanism by which ERK regulates BIM is via direct phosphorylation of BIM on S69, which targets BIM for proteosomal degradation [238-242]. The relevant E3 ligase necessary for BIM degradation is unclear. Finally, ERK appears to inhibit the binding of $BIM_{EL}$ to anti-apoptotic multi-domain Bcl-2 family members such as BCL-xL and Mcl-1, functionally inhibiting $BIM_{EL}$, as BOPs must interact with pro-survival family members to kill cells [240, 243].

ERK also directly participates in the regulation of the anti-apoptotic Mcl-1. Mcl-1 has a short half life and turnover is regulated by phosphorylation at two sites within an N-terminal PEST domain. ERK directly phosphorylates Mcl-1 on T163 within the PEST domain of Mcl-1, and this phosphorylation is generally thought to result in increased Mcl-1 stability [244]. However, Maurer et al show that this "stabilizing" phosphorylation at T163 also acts as a "priming" phosphorylation for the second site in the PEST domain, S159, to be phosphorylated by GSK3β. Phosphorylation of this second site promotes polyubiquitilation and proteosomal degradation of Mcl-1 [245]. The relevant E3 ligase necessary for Mcl-1 degradation is unclear. Thus, as in the case of ERK regulation of Myc stability, there is a fine balance deciding when ERK promotes stabilization and when destabilization of Mcl-1, and there is room for ERK to mediate a pro-apoptotic effect via destabilization of Mcl-1. By blotting for Mcl-1 levels in cells treated with low Doxorubicin plus or minus PD98059, we can investigate whether this mechanism may be operating in our system.

# Chapter 3: Computational Methods

## Introduction

Here we will review, and show example results for, two data-driven, computational methods, Partial Least Squares regression (PLSR) and a hypothesis-based, iterative Time-Interval Stepwise regression (TI-SWR), that can be used successfully in complement to systematically discover signal-response relationships from quantitative signal-response datasets that address biological network questions. In designing a system in which to collect such a signal-response dataset, we consider that when cells are exposed to a cue of interest (treatment, or other environmental perturbation), molecular signaling across signaling pathways is activated, and this molecular signaling is integrated in some fashion by the cell to make and mediate cell-fate decisions regarding resultant phenotype. The overarching hypothesis guiding this approach is that cue-resultant cellular phenotype is a function of cue-initiated molecular signaling and that we can gain insight into the nature of this function using data-driven computational approaches such as regression analysis.

There are several prerequisites for successfully using data-driven modeling of quantitative signal-response datasets as a means to address biological network questions. One requirement is that the biological network question is part of a relatively well defined system where a significant fraction of the components involved in mediating cellular responses of interest in response to cues of interest are known. A corollary to this is that participant molecules should be relatively well characterized in their own right, at least in some contexts. A second requirement is the identification of an appropriate system, with clear physiological relevance to the problem at hand, in which to compile a signal-response dataset that includes observations, wherein the range of both signal and response measurements is maximized in quantitative and qualitative variability. A final requirement is the ability to measure

network signaling, and cellular responses to the cues of interest that define the system, in a rigorously quantitative fashion.

Our goal in this project was to systematically discover signal-response relationships in the DNA damage signaling network response to DNA double-strand breaks, from a quantitative signal-response dataset, using data-driven modeling approaches. The DNA damage signaling network response to DNA double-strand breaks is a relatively well-studied response, such that most proteins involved in the proximal signaling response have been identified. Additionally, many other signaling molecules with established roles in mediating cell-death, cell-survival, cell-cycle checkpoints and general stress responses following wide ranges of stimuli have been shown to be activated by DSB. These molecules are also thought to be involved in mediating cellular responses to DSB, such as apoptosis and cell-cycle arrest (Figure 1-1).

We treated U2OS human osteosarcoma cells with 6 distinct cue treatment combinations of Doxorubicin and TNF-α (Table 2-1), that together expose cells to a range of DSB, in two different physiologically relevant contexts. We did work to compile a quantitative signal-response dataset using this system, consisting of 17 distinct and quantitative signal measures at 10 timepoints over 24 hr following treatment (Table 2-4 and Figure 2-1A, Figure 2-1B) and 7 distinct and quantitative response measures at 4 timepoints over 48 hr following treatment (Table 2-5 and Figure 2-1A, Figure 2-1B).

In this chapter we will review computational approaches we have used in the investigation of this quantitative signal-response dataset with the goal of systematically discovering signal-response relationships. The computational approaches used include Partial Least Squares regression (PLSR) and a hypothesis-based, iterative, Time-Interval Stepwise regression (TI-SWR) for discovery of both signal-response and signal-signal relationships. We will discuss challenges, and solutions that may easily

generalize to other biological problems investigated in a like manner, illustrated by examples from our specific study.

## Challenges

There are several major technical challenges to using traditional data-driven modeling approaches such as Multiple Linear regression (MLR) for the analysis of quantitative signal-response datasets that address biological network questions. Some of these challenges include high dimensionality in the independent variable set, small numbers of observations, potential high collinearity in the dataset, and an inability to consider multiple response variables together.

High dimensionality and a low number of observations in the dataset pose two major problems. First, each additional independent variable results in an additional degree of freedom in finding a solution to the regression; there is no unique solution for a regression in which independent variables outnumber observations. Especially in the context of low numbers of observations (in our example, 6 observations), this high dimensionality (in our example 170-dimensional; 17 signal measurements x 10 time-points) can be crippling if all signals measured are considered simultaneously in the analysis of any given outcome. Second, high dimensionality introduces noisy independent variables into the regression that result in degradation of solution quality. And finally, even in the best of circumstances, high dimensionality will lead to a regression solution that is difficult to interpret. High dimensionality with respect to number of observations will inherently be a problem that must be addressed in analysis of signal-response datasets addressing biological network problems, at least for the foreseeable future. Data for additional observations is time-consuming and costly to obtain, and we want to understand how relatively large networks of proteins and other signaling elements work together, over a time-course, to mediate cellular responses of interest to cues of interest, leading to large independent variable sets.

High collinearity in the dataset is a problem if we want to use our regression solution to infer the contributions that individual signals (independent variables) make to the response of interest (dependent variable), as collinearity results in inaccurate and inconsistent estimation of independent variable coefficients, and high confidence intervals on coefficients. If, for example, three of our consecutive time-point ERK1/2 activity measurements contribute highly to cell-death outcomes, and the ERK1/2 activity measurements are also highly correlated with each other, then removing any one of these ERK1/2 measurements does not lead to a significant degradation of the model. The result is that each of these ERK1/2 measurements is assigned a low coefficient in the resulting regression model. There are two main ways to deal with the distorting effects of collinearity on coefficient determination in regression models. One approach is to increase the observation size which will reduce coefficient confidence intervals despite collinearity. Another way to deal with the effect of collinearity is to identify the source of collinearity and to remove it by either removing or combining variables in some way that makes sense in the context of the application. Multicollinearity will inherently be a problem that must be addressed in analysis of quantitative signal-response datasets addressing biological network problems. The largest source of collinearity in our signal-response dataset comes from measures of single signals at each of 10 time-points. These measurements are clearly not independent of each other and are likely highly correlated in many cases. Additionally, while the signals we chose to measure for this dataset were chosen at least partly to minimize redundancy of information between measured signals, we still expect that some of these signals will not be completely independent of each other.

Finally, classical regression approaches such as MLR do not allow multiple response variables to be considered together in a single regression model. This poses a problem in the analysis of quantitative signal-response datasets addressing biological network problems as cellular responses of interest are often complex phenotypes that are best described by a combination of measurements of more than one

single cellular response, considered together. In the case of our specific study, for example, the cellular responses of apoptosis, survival, and cell-cycle arrest/regulation are intimately entwined in such a way that it is difficult to describe the holistic cellular phenotypic response to DNA damage without measuring and considering each of these individual measures of the phenotype together.

The data-driven modeling approaches for analysis of quantitative signal-response datasets addressing biological network problems that we discuss here (PLSR and TI-SWR) each address these challenges to varying extents and effects.

## PLSR

Prinicipal Component regression (PCR) is a combined method using Principal Component Analysis (PCA) and MLR. In PCR, PCA is used to compute Principal Components (PCs). PCs are linear combinations of model independent variables that maximally capture variance in the independent variable space. PC1 maximally captures the variance in the independent variable space. PC2 maximally captures the residual variance, and so on for any additional PCs, such that PCs are orthogonal and uncorrelated (Figure 2-6A top panels). The number of PCs necessary to capture the majority of the variance in the explanatory (independent) variable set is smaller than the number of original explanatory variables, and should also be chosen to be smaller than the number of observations (samples) available for analysis. These relatively few uncorrelated PCs serve as "super-variables", standing in for the large number of often-correlated original explanatory variables, and in a second step, response variables are regressed against these "super-variables" using OLS (ordinary least squares).

PCR thus allows for a significant reduction in dimensionality and elimination of collinearity in the effective independent variable set, from many, correlated explanatory (independent) variables to a few, uncorrelated PCs. A major limitation of PCR is that PCs are calculated without consideration of the

dependent variable set. This has no bearing on the ability to compute a regression model with high predictive capability. However, in the context of a biological network problem, where explanatory (independent) variables are measures of molecular signaling and response (dependent) variables are measures of cellular responses, we care about understanding the contribution of individual signals to individual cellular responses or to all measured cellular responses together. It is then often useful to be able to assign some physical/biological meaning to PCs (which can be thought of as "directions in signaling space") that is also relevant to cellular response (e.g. If we follow a particular "direction in signaling space" we will get to a particular cellular response). When PCs are calculated without consideration for response variables, the result is often PCs that are difficult to interpret in this manner (e.g. they may be "directions in signaling space" that do not lead to any of the measured cellular responses).

PLSR is a conceptually similar method that addresses this problem by calculating PCs that simultaneously maximize the variation in the independent variable set, and the covariation with the dependent variable set. The result is a method that significantly reduces dimensionality and collinearity in the signal dataset and that also results in PCs in the response space to which we can often assign some physical/biological meaning that is relevant to cellular response and that we can interpret as a "direction in signaling space" that leads to a specific cellular response. The PCs in the independent variable (signal) space and in the dependent variable (response) space are defined as linear combinations of the original signals and responses, respectively, as shown in Equations 1 and 2.

Principal components for the signals (signals, 1 to j)

$$PC_i^S = \sum_j C_{i,j} * S_j \qquad (1)$$

Principal components for the responses (responses, 1 to m)

$$PC_i^R = \sum_m C_{i,m} * R_m \qquad (2)$$

PLSR can provide a fast overview of the overall structure of the data, and insight into some generalized relationships among the cellular responses measured in the dataset and between the signals and the cellular responses measured in the dataset (Figure 2-6A bottom panels).

### *PLSR Results: Response-Response Relationships*

Our example model includes measures of apoptosis (cell-death) and cell-cycle arrest/regulation as cellular responses to DNA damage. These single cellular responses are both established and essential cellular responses to DNA damage. Apoptosis and cell-cycle arrest are intimately and dynamically related cellular responses to DNA damage, such that it is really necessary to consider both of these single measures of cellular response in concert in order to understand the complex, holistic cellular response to DNA damage, on either a single cell or cell population level. Using PLSR, we can get some understanding of the relationship between these responses by examining where each of these responses lie in the principal component space. In the example shown here, the model includes measures of apoptosis and survival at 6 and 12 hr, and measures of cell-cycle status at 24 hr as responses.

When we plot these responses in the principal component space (Figure 3-1), we can see that the first principal component (PC1) is highly correlated with apoptosis and is highly anti-correlated with measures of survival, such that we may physically interpret PC1 as a "Survival-Death" Axis. Note that the $PC^S_i$ for the proteins (signals) and the $PC^R_i$ for the responses are different, but are directly related when using PLSR. Under this interpretation, we expect that signals that have strong, positive weight in PC1 also correlate with cell-death outcomes and, conversely, that signals that have strong, negative weight in PC1 correlate with cell-survival outcomes.

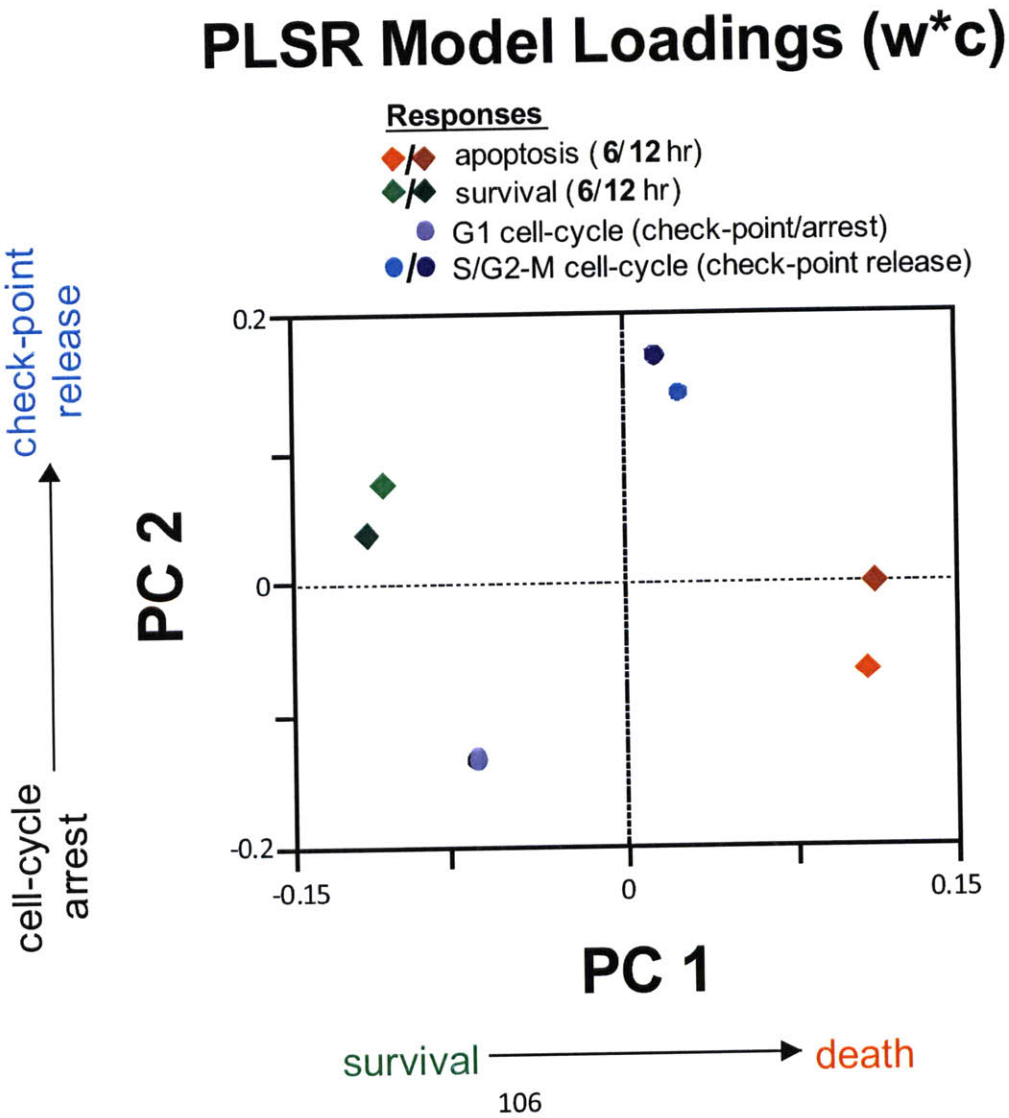

**Figure 3-1.** Plot of selected cellular-responses in the Principal component space (Principal component 1 (PC1) vs. Principal component 2 (PC2)) determined by a PLSR model. ***Cellular responses:*** The cellular responses of apoptosis (CC3+CParp+) at 6 and 12 hr following treatment, survival (CC3-CParp-) at 6 and 12 hr following treatment and measures of the G1, S and G2-M cell-cycle populations at 24 hr following treatment are plotted in the Principal component space based on the weights of each of the cellular responses in PC1 and PC2. Apoptotic responses measured at 6 and 12 hr following treatment (red and dark red diamonds respectively) are positively correlated with PC1 and survival responses measured at 6 and 12 hr following treatment (green and dark green diamonds respectively) are negatively correlated with PC1; PC1 is a "Survival-Death" axis. Measurements of S and G2-M cell-cycle populations at 24 hr following treatment (blue and dark blue circles respectively) are positively correlated with PC2 and measurement of G1 cell-cycle population at 24 hr following treatment (light purple circle) is negatively correlated with PC2; PC2 is a "Cell-cycle regulation" axis.

---

We also see that the cellular response read-outs of cell-cycle status/arrest spread out along the second principal component (PC2) such that PC2 is highly correlated with a read-out of cells in the S phase of the cell-cycle (S populations) and with a read-out of cells in the G2-M phase of the cell-cycle (G2 population), and is highly anti-correlated with a readout of cells in the G1 phase of the cell cycle (G1 population). From these observations, we may physically interpret PC2 as a "Cell-cycle Arrest/Regulation" Axis. Under this interpretation, we expect that signals that have strong, positive weight in PC2 also correlate with high S and G2 populations by 24 hr following treatment and, conversely, that signals that have strong, negative weight in PC2 correlate with a high G1 population by 24 hr (or low S and G2 populations by 24 hr).

Another interesting feature we can observe is a reversal of timing in apoptosis and cell-survival responses along PC2, our "Cell-cycle Arrest/Regulation" axis. From this observation (and some knowledge of the system), we may hypothesize that in this system, cell-cycle arrest and regulation modulate the timing of cell-death and survival responses.

One final observation regarding response-response relationships is that cell-survival responses and S and G2 populations are all positively correlated along PC1, while cell-death and G1 populations are both negatively correlated along PC1, suggesting that cell-survival may be associated with S and G2 cell populations and that cell-death may be associated with G1 cell populations.

### *PLSR Results: Signals-Response Relationships*

Our quantitative signal-response dataset includes measures of signals in the chromatin integrity network that are involved in the proximal response to DNA Double-strand breaks (DSB), as well as measures of signals involved in distinct signaling networks governing cell-cycle arrest, cell-death and cell-survival and general stress responses that have been shown to be activated by DSB. Signals in the example model include: p-Nbs1, p-H2AX, p-Nbs1, p-p53, total p53, p-p38, p-JNK, active NFkB, p-ERK1, p-ERK2, and p-Akt. The measured value for each of these signals at each of the 10 time-points over a period of 24 hrs following treatment was included in the dataset, and a measure of the mean, maximum, and total area under the curve for each signal was also included, resulting in a model with greater than 100 explanatory variables.

These signals are known to respond to DSB, and some have established roles in mediating the cellular responses of cell-cycle arrest/regulation and/or apoptosis, at least in some contexts. For example, NFkB has an established role in modulating cell-survival following many types of stressors and p38 and JNK have established roles in mediating apoptosis following many types of stressors. p53 has an established role in mediating both cell-cycle arrest (at both G1 and G2/M DNA damage check-points), specifically in the context of DNA damage, and in mediating cell-death outcomes in many physiological contexts, including DNA damage. However, the majority of these signaling molecules do not have

established ***or well-specified*** roles in mediating the cellular responses of cell-cycle arrest/regulation and/or apoptosis specifically in the context of DNA damage.

Using PLSR, we can gain an understanding of the relationships between these signals and measured cellular responses by examining where the signals lie in the principal component space, relative to measured cellular responses when both signals and responses are plotted in the principal component space based on their respective weights in each of the principal components. Loadings for all signals and responses included in this example model, in each of the two Principal components included in the final model, are listed in Supplementary tables 3-1, 3-2 and 3-3. Supplementary Table 3-1 is unsorted, while Supplementary Table 3-2 lists loadings sorted by positive weight in the first Principal component and Supplementary Table 3-3 lists loadings sorted by positive weight in the second Principal component.

For example, we know that p53 has roles in promoting both cell-death and cell-cycle regulation and in coordinating these responses following DNA damage. Indeed, if we plot total and p-p53 measurements in the principal component space (Figure 3-2), we can see that, for total p53 measurements, some time-point measurements are highly and positively correlated with PC1, the "Survival-Death" Axis and with apoptotic outcomes at 6 and 12 hr. Some time-point measurements of total p53 are highly and positively correlated with PC2, the "Cell-cycle Arrest/Regulation" Axis, and with S and G2 cell populations. And remaining time-point measurements of total p53 are highly and positively correlated with ***both PC1 and PC2.*** Total p53 seems very "informative" in that all time-point measures of total p53 are weighted highly in either PC1 or PC2, or in both. We can see that p-p53 follows the same pattern as total p53, with some time-point measures correlated mostly with PC1, some correlated mostly with PC2, and some time-point measures correlated with both. p-p53 signals are weighted less highly than total p53 signals and p-p53 signal measurements may be somewhat less

informative in general than total p53 measurements in determining the holistic cellular phenotypic response to DNA damage. Plotting total and p-p53 signals in principal component space allows us to capture p53's known dual role in both cell-death and cell-cycle regulations following DNA damage.

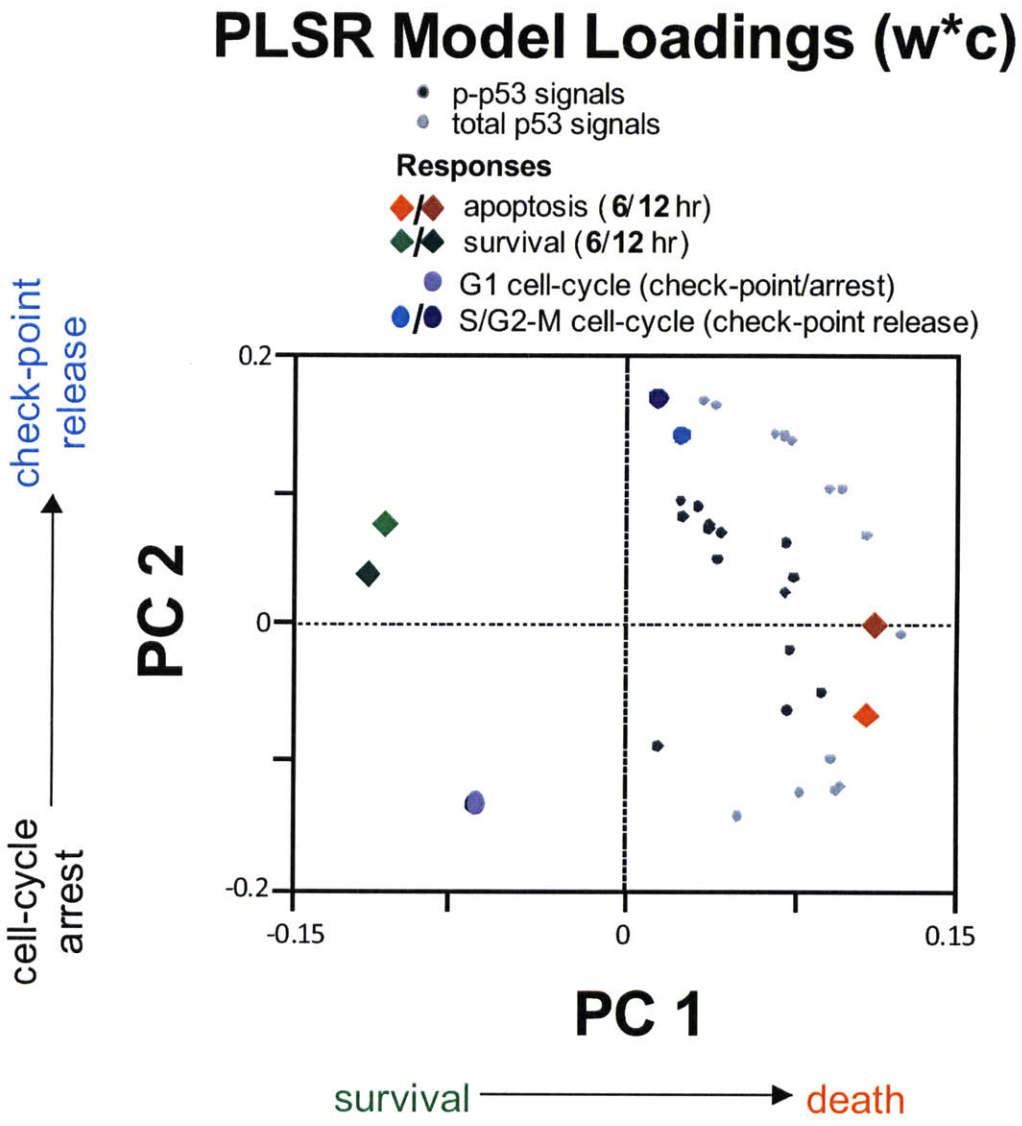


**Figure 3-2.** Plot of selected signals and cellular-responses in the Principal component space (Principal component 1 (PC1) vs. Principal component 2 (PC2)) determined by a PLSR model. ***Cellular responses:*** Refer to Figure 3-1 for further explanation. ***Signals:*** All total p53 measurements (including values of total p53 measured at each of 10 time-points following treatment as well as the max, mean, and equilibrium value of total p53 over the whole time-course following treatment and the value for the area under the curve (AUC) of total p53 measured over the full time-course) are plotted in the principal

component space based on their weights in PC1 and PC2 (light grey, small circles). Some total p53 measurements are highly correlated with apoptotic responses only, some are highly correlated with cell-cycle responses only and some are highly correlated with both; this PLSR model allows us to capture the known dual role of p53 in mediating both apoptotic and cell-cycle regulatory responses following DNA damage. All p-p53 measurements (including values of p-p53 measured at each of 10 time-points following treatment as well as the max, mean, and equilibrium value of p-p53 over the whole time-course following treatment and the value for the area under the curve (AUC) of p-p53 measured over the full time-course) are plotted in the principal component space based on their weights in PC1 and PC2 (dark grey, small circles). Measurements of p-p53 show patterns similar to those observed for total p53 measurements, but are less informative. That is, some measurements of p-p53 are correlated with apoptosis alone, some are correlated with cell-cycle regulatory responses alone, and some are correlated with both. However, measurements of p-p53 are, overall, not as highly correlated with these cellular responses as measurements of total p53.

---

The MAPK p38 has an established role in mediating apoptotic outcomes following general types of stress to the cell, such as osmotic stress. However, a role for p38 in mediating cellular responses following DNA damage (e.g. promoting apoptosis or cell-cycle arrest/regulation) is not well-established or specified. If we plot p-p38 signals in our principal component space (Figure 3-3), we can see that, in opposition to the pattern displayed by signal measurements of total p53, p38 signals all cluster close to apoptotic response outcomes, being highly and positively correlated with PC1 (the "Survival-Death" Axis) almost exclusively. We might hypothesize from this pattern that p38 likely (and unsurprisingly) has a role in promoting cell-death in the context of DNA damage.

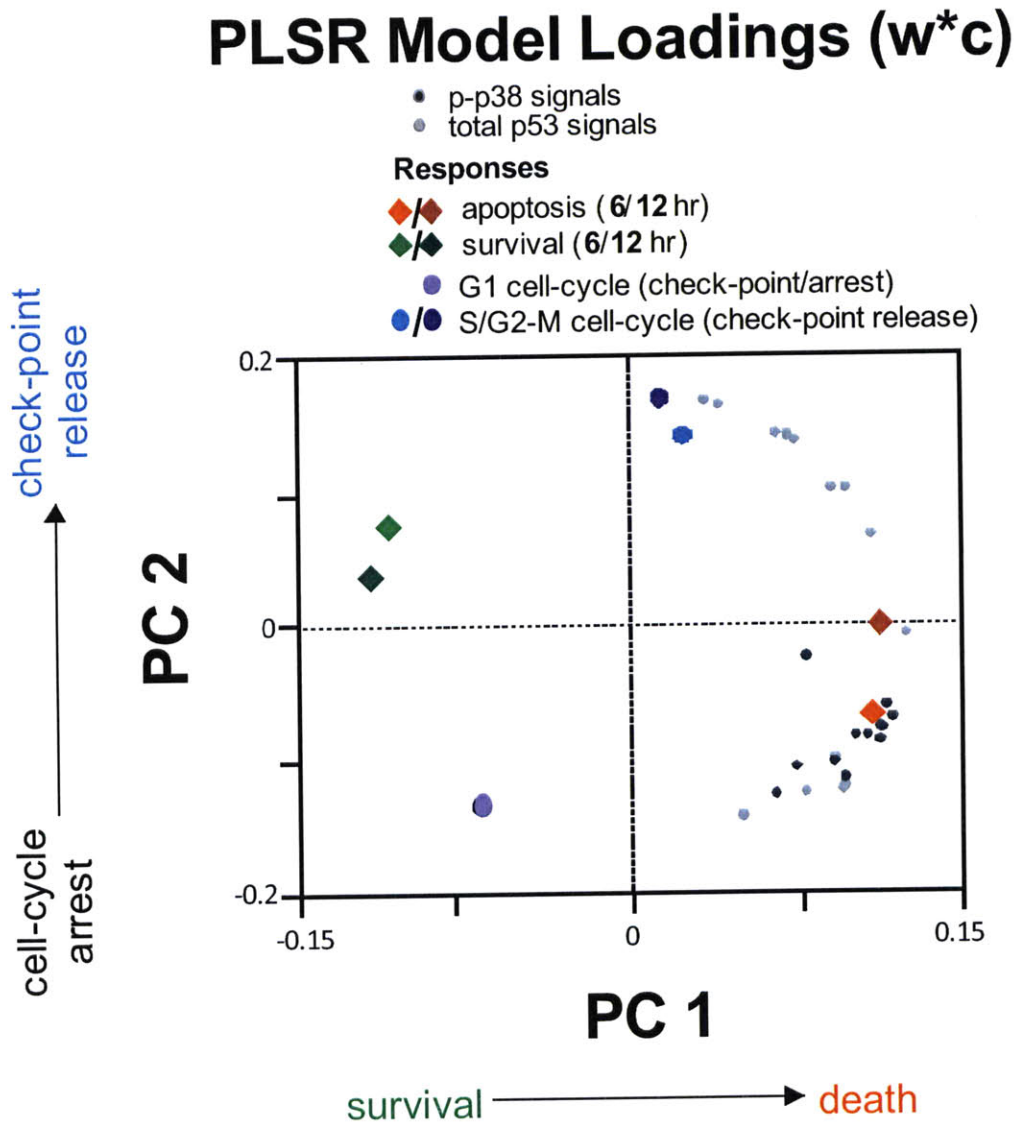


**Figure 3-3.** Plot of selected signals and cellular-responses in the Principal component space (Principal component 1 (PC1) vs. Principal component 2 (PC2)) determined by a PLSR model. ***Cellular responses:*** Refer to Figure 3-1 for further explanation. ***Signals:*** All total p53 measurements (including values of total p53 measured at each of 10 time-points following treatment as well as the max, mean, and equilibrium value of total p53 over the whole time-course following treatment and the value for the area under the curve (AUC) of total p53 measured over the full time-course) are plotted in the principal component space based on their weights in PC1 and PC2 (light grey, small circles). Some total p53 measurements are highly correlated with apoptotic responses only, some are highly correlated with cell-cycle responses only and some are highly correlated with both; this PLSR model allows us to capture the known dual role of p53 in mediating both apoptotic and cell-cycle regulatory responses following DNA damage. All p-p38 measurements (including values of total p-p38 measured at each of 10 time-points following treatment as well as the max, mean, and equilibrium value of total p-p38 over the whole time-course following treatment and the value for the area under the curve (AUC) of p-p38 measured over

the full time-course) are plotted in the principal component space based on their weights in PC1 and PC2 (dark grey, small circles). All p-p38 measurements are highly correlated with apoptotic responses; this PLSR model allows us to capture the known role of p-p38 in mediating apoptotic responses in general, although the role of p-p38 in mediating apoptosis specifically following DNA damage has not been well characterized.

---

The MAPK JNK also has an established role in mediating apoptotic outcomes following general types of stress and the MAPK ERK1/2 has an established role in promoting cell-cycle progression through the G1/S transition in normal cell-cycles and in promoting survival following general types of stress. Roles for these MAPKs in mediating cellular responses of cell-cycle arrest/regulation and/or cell-death in the context of DNA damage are not well-established or specified. If we plot p-JNK signals in our principal component space (Figure 3-4), we can see that p-JNK signals for the most part cluster closely with apoptotic response outcomes, being highly and positively correlated with PC1 (the "Survival-Death" Axis) almost exclusively. We might hypothesize from this pattern that JNK, like p38, likely (and unsurprisingly) has a role in promoting cell-death in the context of DNA damage. If we plot p-ERK signals in the principal component space (Figure 3-4), we can see that some time-point measurements are highly and positively correlated with PC1, the "Survival-Death" Axis and with apoptotic outcomes at 6 and 12 hr. Some time-point measurements of p-ERK are highly and positively correlated with PC2, the "Cell-cycle Arrest/Regulation" Axis, and with S and G2 cell populations. And remaining time-point measurements of p-ERK are highly and positively correlated with ***both PC1 and PC2.*** This pattern is very similar to that observed for p53 signals. From this pattern, we might hypothesize, despite ERK's established role in promoting survival in some contexts, that ERK has a role in both promoting cell-death and in promoting cell-cycle arrest/regulation following DNA damage.

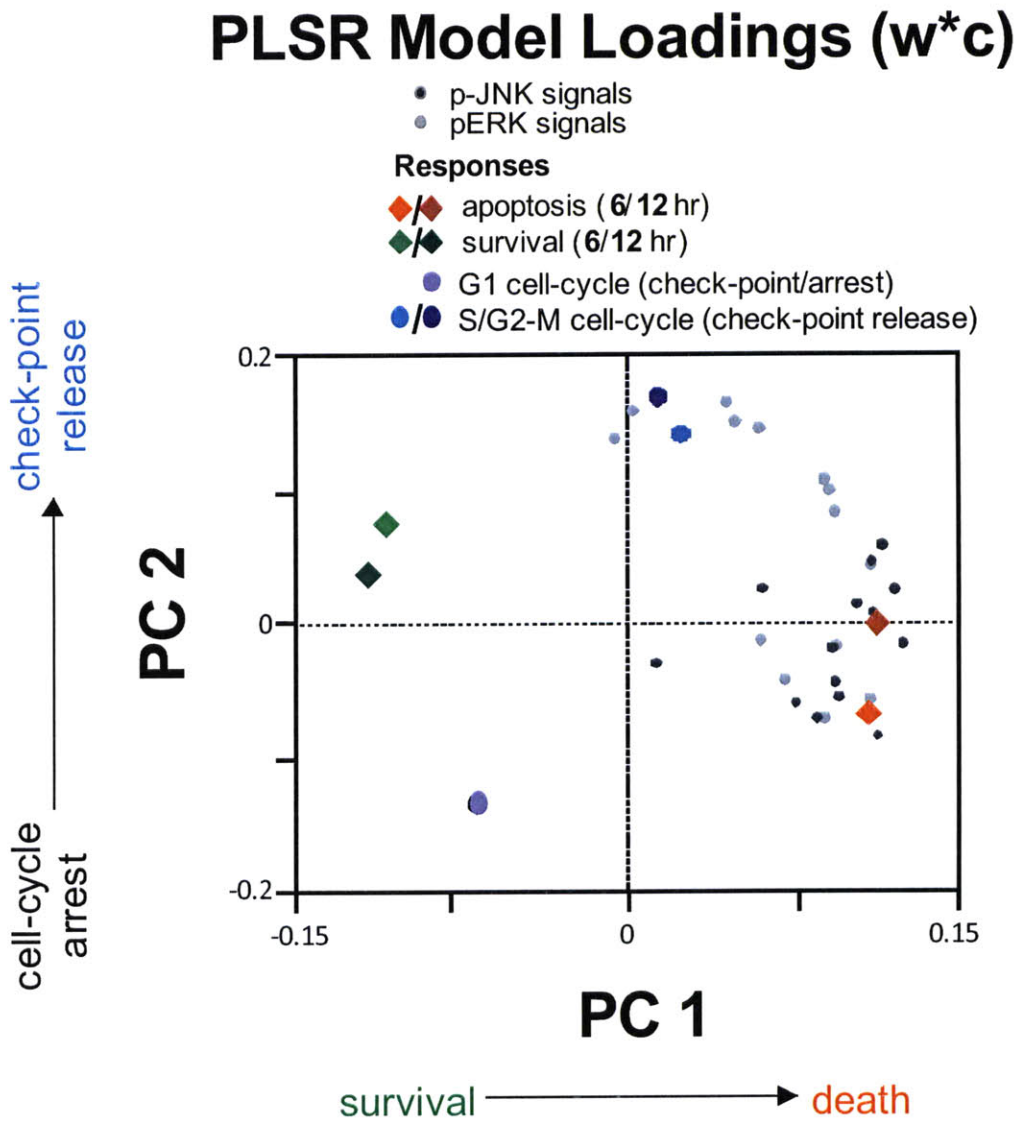


**Figure 3-4.** Plot of selected signals and cellular-responses in the Principal component space (Principal component 1 (PC1) vs. Principal component 2 (PC2)) determined by a PLSR model. ***Cellular responses:*** Refer to Figure 3-1 for further explanation. ***Signals:*** All p-ERK measurements (including values of p-ERK measured at each of 10 time-points following treatment as well as the max, mean, and equilibrium value of total p53 over the whole time-course following treatment and the value for the area under the curve (AUC) of p-ERK measured over the full time-course) are plotted in the principal component space based on their weights in PC1 and PC2 (light grey, small circles). Some p-ERK measurements are highly correlated with apoptotic responses only, some are highly correlated with cell-cycle responses only and some are highly correlated with both. These result are reminiscent of those obtained for total p53, and lead us to a hypothesis that, though ERK has an established role in promoting cell-survival and cell-cycle progression under normal or low stress conditions, under DNA damaging conditions, ERK may have a

role in promoting apoptosis and cell-cycle regulation. All p-JNK measurements (including values of p-JNK measured at each of 10 time-points following treatment as well as the max, mean, and equilibrium value of p-JNK over the whole time-course following treatment and the value for the area under the curve (AUC) of p-JNK measured over the full time-course) are plotted in the principal component space based on their weights in PC1 and PC2 (dark grey, small circles). Nearly all p-JNK measurements are highly correlated with apoptotic responses and is very similar to the pattern observed for p-p38 measurements (See Figure 3-3); this PLSR model allows us to capture a known role for p-JNK in mediating apoptotic responses in general, although the role of p-JNK in mediating apoptosis specifically following DNA damage has not been well characterized.

---

Members of the chromatin-integrity network and proximal responders to DNA double-strand break (DSB) damage, H2AX and Nbs1, have established roles in initiating and sustaining the signaling response to DSB, including recruiting repair factors and activating downstream signaling components such as p53. However, there is no established role for these molecules in mediating the cellular responses of cell-cycle arrest/regulation and/or cell-death following damage. If we plot p-H2AX signals in our principal component space (Figure 3-5), we can see that p-H2AX signals for the most part cluster closely with apoptotic response outcomes, being highly and positively correlated with PC1 (the "Survival-Death" Axis) almost exclusively. On the other hand, If we plot p-Nbs1 signals in our principal component space (Figure 3-5), we can see that p-Nbs1 signals are highly and positively correlated with PC2 (the "Cell-cycle Arrest/Regulation" Axis) almost exclusively, for the most part clustering closely with measures of S and G2 cell populations. From these patterns, we might hypothesize that, despite their overlapping and complementary roles as proximal responders to DSB, H2AX and Nbs1 influence the cellular response to DNA damage in distinct ways, with H2AX primarily having a role in mediating cell-death outcomes following damage, and with Nbs1 primarily having a role in mediating cell-cycle arrest/regulation following damage.

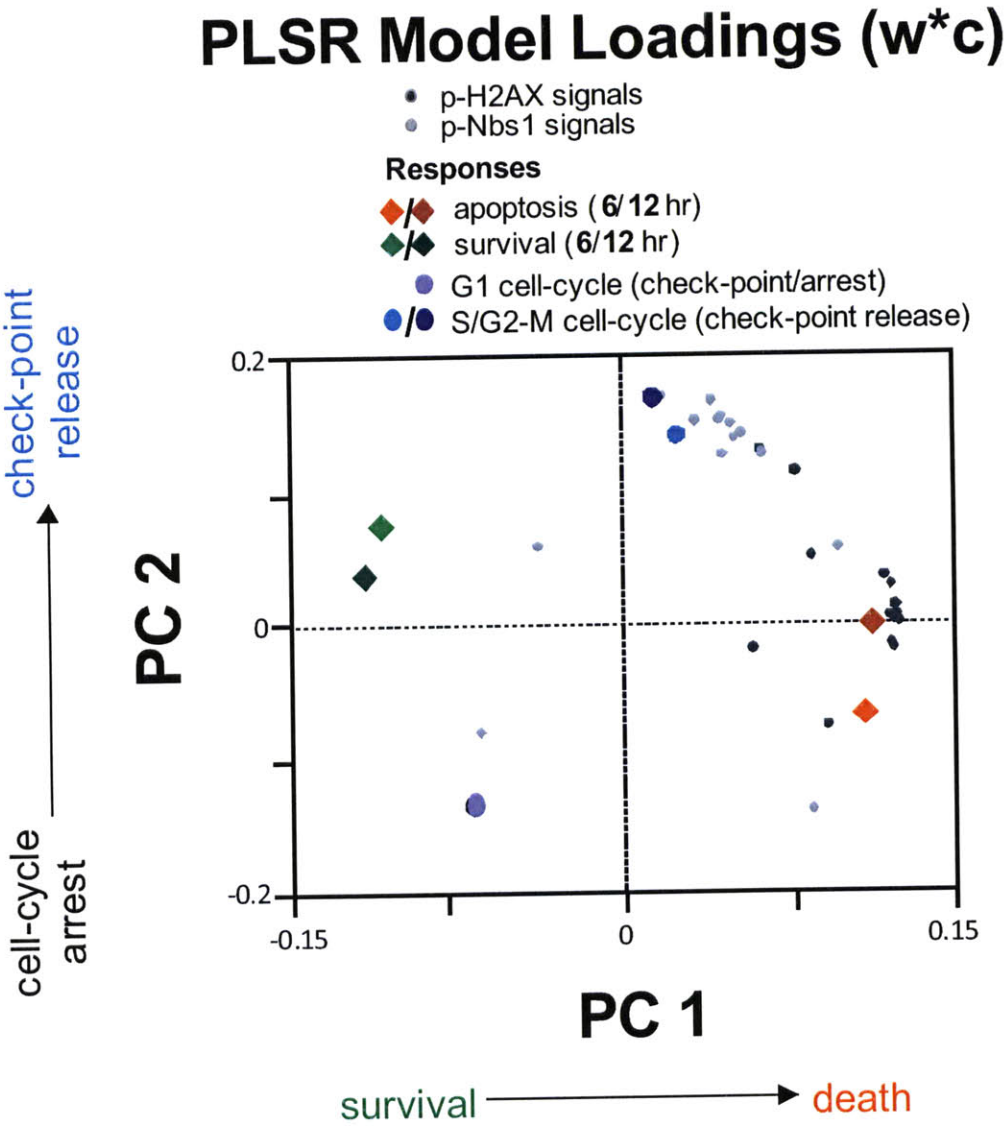


**Figure 3-5.** Plot of selected signals and cellular-responses in the Principal component space (Principal component 1 (PC1) vs. Principal component 2 (PC2)) determined by a PLSR model. ***Cellular responses:*** Refer to Figure 3-1 for further explanation. ***Signals:*** All p-Nbs1 measurements (including values of p-Nbs1 measured at each of 10 time-points following treatment as well as the max, mean, and equilibrium value of p-Nbs1 over the whole time-course following treatment and the value for the area under the curve (AUC) of p-Nbs1 measured over the full time-course) are plotted in the principal component space based on their weights in PC1 and PC2 (light grey, small circles). Nearly all p-Nbs1 measurements are highly correlated with cell-cycle regulatory responses (measurements of S and G2-M population at 24 hr following treatment). There is no known/well-characterized role for p-Nbs1 in mediating cell-cycle regulatory and/or apoptotic responses following DNA damage. However, these data suggest that Nbs1 may have a role in mediating cell-cycle regulation following DNA damage. All p-H2AX measurements

(including values of p-H2AX measured at each of 10 time-points following treatment as well as the max, mean, and equilibrium value of p-H2AX over the whole time-course following treatment and the value for the area under the curve (AUC) of p-H2AX measured over the full time-course) are plotted in the principal component space based on their weights in PC1 and PC2 (dark grey, small circles). Nearly all p-H2AX measurements are highly correlated with apoptotic responses and this pattern is similar to the pattern observed for p-p38 and p-JNK measurements (See Figure 3-3 and 3-7). There is no known/well-characterized role for p-H2AX in mediating cell-cycle regulatory and/or apoptotic responses following DNA damage. However, these data suggest that p-H2AX may have a role in mediating apoptotic responses following DNA damage.

---

### *PLSR: Strengths and Weaknesses*

PLSR is a fast method to get an understanding of the overall structure of a signal-response dataset. We can use our full signal-response dataset, including explanatory variables consisting of all signals measured at all times and including response variables consisting of all cellular responses measured at all times. It does not require any manual "weeding" of the data or further hypothesis formulation. It allows us to look at multiple measured cellular responses in a single analysis and therefore can give us some insight into complex cellular response phenotypes that are combinations of single measured cellular responses. Using PLSR, we can often calculate PCs to which we can assign biological/physical meaning that is relevant to cellular response. In this case, we can also use explanatory variable (signal) coefficients in each of the PCs to which we have assigned a physical/biological meaning that is relevant to cellular response to gain an understanding of relationships between signals and cellular responses, or between signals and complex phenotypes that are combinations of measured cellular responses.

However, the ability to encompass and integrate a large amount of wide-ranging data, which is the main strength of PLSR, is also a weakness. Large numbers of original explanatory (signal) variables can result in PCs with difficult to interpret explanatory variable (signal) coefficients due to an overload of simultaneous information. The coefficient for a given signal may give an accurate idea of how well that

signal is correlated to a specific cellular response relative to other signals in the model. However, the coefficient for a given signal does not necessarily give an accurate idea of how well that signal is correlated to a specific cellular response in an absolute fashion. A relatively high absolute correlation can be hidden by inclusion of highly collinear signals in the independent variable set. For example, if signal A measured at time-point #2 is very highly correlated with cell-death, and signal B measured at time-point #2 is also quite highly correlated with cell-death, but measures of signal A at 6 of the other time-points are highly correlated with signal A measured at time-point #2, then these other measures of signal A may be assigned higher coefficients than signal B at time-point #2. This coefficient assignment may or may not be reflective of the true value of these signals in the model. That is, it is possible that several measurements of signal A together powerfully influence cell-death and so the inclusion of all is necessary to the model. It is also possible that any one of the measures of signal A is powerfully predictive of cell-death. In this case, the inclusion of more than one measure of signal A is redundant and artificially lowers coefficients on explanatory variables that are somewhat less highly correlated with cell-death. This quality can lead to difficulties in using PLSR model results to identify precise signal-response relationships and to formulate hypotheses to drive specific experiments to test these identified signal-response relationship.

We can address this problem to some extent by building smaller models using PLSR with subsets of our signal-response dataset to get a better idea of what signals have important relationships with measured cellular responses, as we will briefly illustrate here, and by using other analysis methods such as TI-SWR in conjunction with PLSR to get a better idea of when a particular signal is important and what other signals might also be important at that time, which we will discuss later.

### *PLSR Results: Signals-Response Relationships from small models*

We can build small models where all explanatory variables (signals) are excluded, except for all of the measurements of one single signal, and ask how well all of the measurements of this one signal together predict a cellular response or group of responses. Here we have built small models for each of the signals in our large example model for both cell-cycle arrest/regulation cellular outcomes and for cell-death/cell-survival outcomes. The results of the small models built with the cellular response of cell-cycle arrest/regulation as the response variable are quite informative. We can see that more than half of our original signal explanatory variable sets are not predictive of cell-cycle arrest/regulation outcomes ***at all*** (Figure 3-6A). In fact, p-ERK1/2, p-Nbs1 and total p53 clearly have the highest predictive capabilities for cell-cycle arrest/regulation, such that only three of the original nine signal explanatory variable sets contain the majority of the information about this cellular response. The results of the small models built with the cellular response of cell-survival/cell-death as the response variable are less informative. Only one of our original nine signal explanatory variable sets is not predictive at all of cell-death. We can perhaps say something about the relative strength of the relationship between the remaining signal explanatory variable sets based on their relative predictive capabilities; p-p38 and p-JNK may be very important in mediating the cell-death response, whereas p-H2AX, total p53, NFkB, pAkt and pERK1/2 play secondary, but still important roles in this process (Figure 3-6B). The main conclusion though from these small models is that relatively few of our measured signaling molecules (p-ERK1/2, p-Nbs1 and total p53) play a role in mediating cell-cycle arrest/regulation following DNA damage, whereas nearly the full complement of measured signaling molecules plays a role in mediating cell-death following DNA damage.

A

**Y: G1, S and G2 cell population, 24 hr**

| Signaling Molecule | $Q^2$ (PC1) |
|---|---|
| p-ERK1/2 (T202/Y204) | 64% |
| p-Nbs1 (S343) | 64% |
| total p53 | 62% |
| p-H2AX (S139) | 21% |
| p-Akt (S437) | ----- |
| p-JNK (T183/Y185) | ----- |
| p-p38 (T180/Y182) | ----- |
| p-p53 (S15) | ----- |
| NFkB | ----- |

B

**Y: CC3+/CParp+ and CC3-/CParp-, 6, 12 and 24 hr**

| Signaling Molecule | $Q^2$ (PC1) |
|---|---|
| p-p38 (T180/Y182) | 81% |
| p-JNK (T183/Y185) | 71% |
| p-H2AX (S139) | 55% |
| total p53 | 48% |
| NFkB | 47% |
| p-Akt (S437) | 41% |
| p-ERK1/2 (T202/Y204) | 32% |
| p-p53 (S15) | 13% |
| p-Nbs1 (S343) | ----- |

**Figure 3-6.** PLSR "small-model" results for PLSR small models built with a response variable set including measurements of G1, S and G2-M populations at 24 hr following treatment (A) or including measurements of apoptosis (CC3+CParp+) and survival (CC3-CParp-) at 6, 12 and 24 hr following treatment (B). PLSR small models were built with these respective response variable sets and with

explanatory variable sets that include all measurements (including values measured at each of 10 time-points following treatment as well as the max, mean, and equilibrium value over the whole time-course following treatment and the value for the area under the curve (AUC) measured over the full time-course) of ***one single signaling molecule*** (e.g. all measurements of p-ERK). Small models were built for each signaling molecule and the resulting PLSR model were forced to include only one single Principal component. The predictive capability ($Q^2$) of each model was determined via an automated "leave one out" cross-validation process, and this predictive capability is reported. ***(A)*** Only four out of 9 single-signaling molecule PLSR "small models" have any ability to predict this response set that includes measures of G1, S and G2-M populations at 24 hr following treatment. These data support a substantial individual contribution to cell-cycle regulatory responses following DNA damage from p-ERK, p-Nbs1 and total p53. ***(B)*** Eight out of 9 single- signaling molecule PLSR "small models" have at least some ability to predict this response set that includes measures of apoptosis (CC3+CParp+) and survival (CC3-CParp-) at 6, 12, and 24 hr following treatment. The single-signaling molecule models that have the highest predictive capability are those built on explanatory variable sets including p-p38 and p-JNK measurement. These data imply that many more signaling molecules have a role in determining apoptotic responses following DNA damage than have a role in determining cell-cycle regulatory responses, and that apoptotic response regulation may be dominated by the activity of (and information integrated by) general stress kinases in the cell. Together, these data support a potential *dual* role for p-ERK, total p53 and p-H2AX, in mediating both cell-cycle regulatory responses and apoptotic responses following DNA damage.

---

We can also try to look for more detailed signal-response relationships, such as time-dependence of signal-response relationships, by plotting the time-point measurements of all the signals and responses in the principal component space and looking by eye at what falls close together. This is a tedious and tenuous process; it is hard, and likely to yield hard to interpret results. An easier and more systematic approach to this problem is afforded by a second analysis approach, TI-SWR.

## TI-SWR

In this section we introduce Time-Interval Stepwise regression (TI-SWR), a novel approach that was used in this work to investigate the relationships between the measured cell responses and signals and the dynamic interactions between various signals. The goal of TI-SWR (Time Interval Stepwise Regression) is to use the established Stepwise Regression method in a manner designed to exploit the time dimension of the dataset in order to find relatively detailed, time-dependent signal-response and

signal-signal relationships, and to dramatically decrease the number of explanatory variables in the models we look at, and thus increase model interpretability. In this approach, the time domain is discretized in a series of time intervals, corresponding to the time intervals between successive measurements.

The basic steps of the approach are to 1) choose a single measured cellular response to investigate, 2) make the hypothesis that the measured signals at one time-point work in concert to mediate the selected cellular response at some later time, and 3) regress the single cellular response against all of the signal measurements at that time-point (Figure 2-6B and Figure 3-7A).

---

**A**

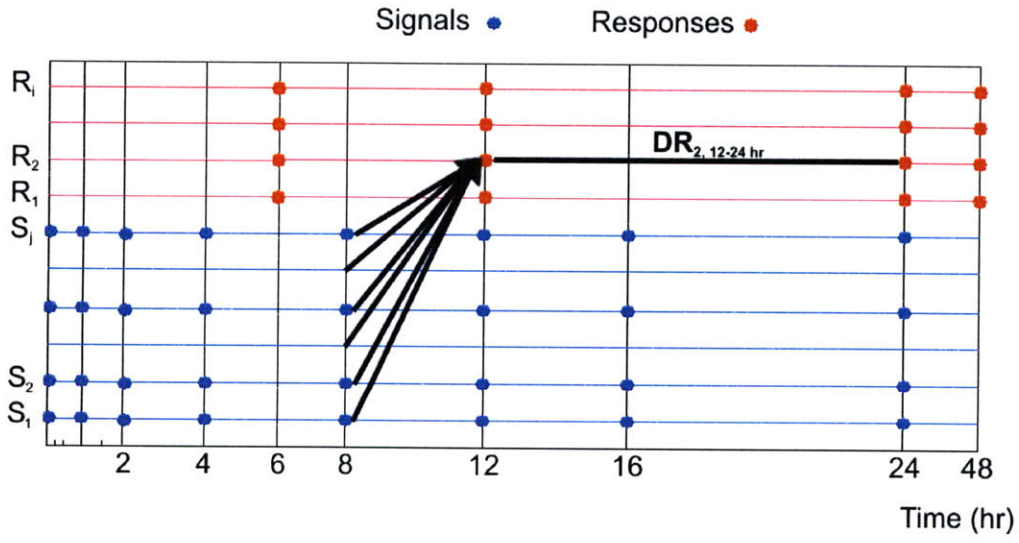

**B**

Y : Δ % S phase, 12-24h

| Time-point (hr) | Signal correlates in decreasing order of $R^2$ |
|---|---|
| 0.25h | ---- |
| 0.5h | ---- |
| 1h | ---- |
| 1.5h | ---- |
| 2h | + pH2AX, - total H2AX, + pERK1/2, - pNbs1 |
| 4h | + pERK1/2, - total p53, - total JNK, - pp53 |
| 8h | + pERK1/2 |
| 12h | ---- |
| 16h | + total p53 |
| 24h | + total p53 |

**C**

Y : Δ % apoptosis (CC3+CParp+), 6-12h

| Time-point (hr) | Signal correlates in decreasing order of $R^2$ |
|---|---|
| 0.25h | + pAkt |
| 0.5h | ---- |
| 1h | ---- |
| 1.5h | ---- |
| 2h | ---- |
| 4h | + pAkt |
| 8h | + pp53, + total JNK |
| 12h | + pERK1/2 |
| 16h | N/A |
| 24h | N/A |

**Figure 3-7.** ***(A)*** Illustration of the hypothesis that each time-point specific, Time-Interval model in a TI-SWR (Time-Interval Stepwise regression) analysis set makes. In a TI-SWR analysis set, there is one cellular response of interest under investigation and there are as many time- point specific, Time-Interval models in the set as there are time-points at which signaling is measured that precede the cellular response of interest. For each of these time-point specific, Time-Interval models, the response variable is the cellular response under investigation and the possible explanatory variable set includes all of the signaling measurements made at that time point. Here is illustrated a time-point specific, Time-Interval model for which the response variable is the change in the cellular response $R_2$ between 12 and

24 hr and for which the possible explanatory variable set includes all signaling measurements taken at the 8 hr time-point ($S_{1,\ 8hr}$ through $S_{j,\ 8hr}$). ***(B)*** Table of results from a TI-SWR (Time-Interval Stepwise regression) analysis investigating the change in S phase cell-cycle population between 12 and 24 hr following treatment (Δ %S, 12-24 hr) as the cellular response variable. Rows present an overview of the results for each of the 10 time-point specific Time-Interval models constructed (For each of the time-point specific Time-Interval models, the response variable is Δ %S, 12-24 hr and the explanatory variable set is all signals measured at that time-point). For each Time-interval model, signal names are listed in order of decreasing $R^2$ (ability to explain the variability in the response variable). Where no signals are listed, no signal-response relationships reached an acceptable level of significance ($p < 0.05$). p-ERK (red) is positively correlated with Δ %S, 12-24 hr at 2, 4 and 8 hr following treatment. These data strengthen our hypothesis that ERK has a role in mediating cell-cycle regulatory phenotypes following DNA damage. For further details on individual Time-Interval models in this set, and on the full TI-SWR analysis, reference Supplementary Figures 3-1 through 3-8. ***(C)*** Table of results from a TI-SWR (Time-Interval Stepwise regression) analysis investigating the change in apoptosis between 6 and 12 hr following treatment (Δ % apoptosis (CC3+CParp+), 6-12 hr) as the cellular response variable. Here cells staining positively for both apoptotic markers (CC3+CParp+) are considered apoptotic. Rows present an overview of the results for each of the 10 time-point specific Time-Interval models constructed (For each of the time-point specific Time-Interval models, the response variable is Δ %apoptosis, 6-12 hr and the explanatory variable set is all signals measured at that time-point). For each Time-interval model, signal names are listed in order of decreasing $R^2$ (ability to explain the variability in the response variable). Where no signals are listed, no signal-response relationships reached an acceptable level of significance ($p < 0.05$). Where N/A is listed, the time-point is later than the cellular response under investigation. p-ERK1/2 at 12 hr is positively correlated with Δ %apoptosis between 6-12 hr following treatment. In a TI-SWR analysis investigating apoptosis at later times (between 12 and 24 hr following treatment) p-ERK1/2 at 12 hr is also positively correlated with this apoptotic response. These data suggest that ERK1/2 activity between 8 and 12 hr following treatment may have a role in promoting apoptosis following DNA damage, and further supports a dual role for p-ERK1/2 in mediating both cell-cycle regulatory and apoptotic responses following DNA damage. For further details on individual Time-Interval models in this set, and on the full TI-SWR analysis, reference Supplementary Figures 3-9 through 3-15. For details on a TI-SWR analysis investigating apoptosis at later times (between 12 and 24 hr following treatment), reference Supplementary Figures 3-16 through 3-25 and Supplementary Table 3-4.

---

### *Cellular response: maximizing information*

The first step in TI-SWR is to choose a single measured cellular response to investigate. Using this method, we investigate one cellular response at a time. We choose the cellular response that we investigate strategically, to be as informative as possible. Specifically, we choose a specific cellular response measure that is particularly interesting, and we also choose to investigate the change in a measured cellular response over some time-period of interest, rather than choosing the actual

measured cellular response. The reason for selecting the change in the cellular response over a period of time - i.e. the derivative of the linearized response during the selected time interval - as the dependent variable in the regression analysis is explained below.

Assume that, for a given time interval $\Delta t^n = t^{n+1} - t^n$ we define $C^n_{ij}$ as the change in response i due to $S^n_j$ - the protein j at time n - per unit time and per unit of protein j at the beginning of the time interval. Then, the response i at the end of the time interval can be written as;

$$R_i^{n+1} = R_i^n + \sum_j C_{i,j}^n * S_j^n * (t^{n+1} - t^n): \qquad (3)$$

We can re-arrange eq. 3, moving $R^n_{i,}$ on the LHS, and dividing by $\Delta t^n$ to obtain:

$$DR_i^n = \sum_j C_{i,j}^n * S_j^n \qquad (4)$$

Where $DR^n_i$ is the derivative of response i over the time interval n, defined as:

$$DR_i^n = (R_i^{n+1} - R_i^n)/(t^{n+1} - t^n) \qquad (5)$$

We note that equation 4 is now in the exact form of the multiple linear regression equation, where the independent variables are the measured values of the protein i at time n, and the dependent variable is $DR^n_i$ the derivative of response i over the time interval n, which can be calculated from the measured data using equation 5. This means that the coefficients $C^n_{i,j}$ calculated by the multiple linear regression have a clearly defined meaning, i.e. they represent the change in response i over the selected time interval due to $S^n_j$ - the protein j at time n - per unit time and per unit of protein j at the beginning of the time interval.

A notable advantage of this formulation of the multiple linear regression equation is that the coefficients $C^n_{i,j}$ represent changes in response i per unit time, during the time interval n. This means that although our measurements – and corresponding regressions – have been performed for intervals of time of different length, the regression coefficients, which represent change per unit time, can be compared across multiple time intervals to provide a measure of the change in specific response-protein dependence over time. This approach results in response variables that are as densely informative as possible.

For the example TI-SWR model we show here, we chose to investigate a cell-cycle regulation phenotype that we had identified as being of interest. In two of our treatment instances (cell-populations exposed to low levels of DNA damage, in the presence or absence of TNF-α), we observed a dramatic build-up in S-phase populations by 24 hr following treatment, and hypothesized that this was due to a DNA-damage mediated cell-cycle arrest in G1 or at the G1/S transition, followed by a release from that arrest that allows a cohort population of cells to enter S phase synchronously by 24 hr following treatment. In order to capture this phenotype as fully as possible, we chose to use the change in S population between 12 hr (when S population is approximately equal across cue treatment conditions) and 24 hr (when S population is dramatically higher in cell-populations exposed to low levels

of DNA damage) following treatment as the response variable in a TI-SWR model. We will refer to this response variable as Δ S, 12-24 hr.

### *Hypothesis: Selecting the explanatory variable sets*

The second step in TI-SWR is to make the hypothesis that the measured signals at one time-point work in concert to mediate this cellular response (Figure 3-7A). In general, we expect that the closer in time the selected set of measured signal are to the time interval of interest, the more likely it is that the assumption of linear dependence between the dependent variable and the set of independent variables applies. We can, for example, make the hypothesis that all of the signals we measure (pH2AX, p-Nbs1, total p53, p-p53, p-p38, p-Akt, p-ERK1/2, p-JNK and NFkB) work together at 12 hr following treatment to mediate the cell-cycle regulation phenotype that we have captured with our response variable, Δ S, 12-24 hr.

A cell integrates information about previous physical/mechanical or signaling events via a physical/chemical encoding of past events in the current status of its signaling components. At any given time a cell uses only the current status of its signaling components and integrates these signals, which occur temporally together, but which also encode past signaling events, in making the decisions which determine future cell actions and eventually the cell fate. E.g., at 1 hr following DNA damage, a cell may "remember" that ATM was activated at 30 min following damage, even if it is no longer activated at 1 hr following damage, because the ATM activation at 30 min led to H2AX phosphorylation, and H2AX is still phosphorylated at 1 hr. Then the hypothesis that the measured states of all signaling molecules at one time-point are integrated by the cell to make decisions that eventually mediate the cellular response is a logical and natural hypothesis.

Making this hypothesis significantly reduces the size of the model. In our example model, we have a regression model with one response variable (Δ S, 12-24 hr) and 9 potential explanatory (signal) variables (the measurement of each of 9 signals at the 12 hr time-point), as compared to our PLSR model, with 7 response variables and over 100 explanatory (signal) variables. The reduction in dimensionality (size) results in a far more tractable and interpretable model. Also along with this reduction in size comes a very desirable significant reduction in multicollinearity and associated problems in the determination of model coefficients.

The hypothesis that the measured states of all signaling molecules at one time-point are integrated such that, together, they mediate a cellular response is a logical and natural hypothesis. However, we do not have to limit our investigation to only the relationship between the signaling at one time-point and the cellular response of interest. We will exclude the time-points that are after the time interval of the selected cellular response, but we can build multiple small time-interval regression models to investigate the relationship between the selected time interval cellular response and the signal sets at each of the time-points that precede, or overlap with, the selected cellular response time interval, in an iterative fashion.

We build one model for every time-point at which signals were measured and at which we may reasonably hypothesize that a causal relationship between the signaling at that time-point and the cellular response of interest exists. It is worth noting that the closer in time the small-model time-point is to the cellular response of interest, the more likely it is that identified relationships between signals and cellular response are direct, and linear in nature. This iterative approach allows us to systematically discover specific, time-dependent signal-response relationships from our signal-response dataset using sets of small, interpretable, time-interval models.

### *Regression: Filtering the explanatory variables*

The third step in TI-SWR is to run the regressions for all of these time-point specific models, regressing the single cellular response against all of the signal measurements at a previous time-point, iteratively, for each of the time-points at which signals were measured. In the example TI-SWR model we present here, our response variable is the change in S population between 12 and 24 hr (Δ S, 12-24 hr), and signals were measured at 10 time-points over 24 hr following treatment. None of these time-points are at times after the cellular response of interest, and we have no other reason to believe that signaling at any of the time-points is uninformative to the cellular response decision. Therefore our TI-SWR model is a set of 10 small models; one for each measured signal time-point, each having 9 potential explanatory (signal) variables (Figure 3-7B).

However, we can further reduce the number of explanatory variables in each of our models if we make another very natural hypothesis; that only a subset of the signals at a time-point are working in concert to mediate a later cellular response. That is, not all signals contribute to the cell-fate decision at all times. For example, perhaps the activity of hypothetical signals A, B, and C at 2 hr following treatment are important for the cell-fate decision and the cellular response that we measure between 12 and 24 hr. At 4 hr following treatment (the next measured time-point), the activity of hypothetical signals A and B are no longer "important", but the activity of hypothetical protein C is still important, and the activity of hypothetical protein D and E are also important now. This situation might arise if, for example, the activities of hypothetical signals A and B at 2 hr cooperate to activate hypothetical protein D by 4 hr, and this is their only important function in the cell-fate decision process. This hypothesis implies that in each of our small, time-interval models, not all explanatory (signal) variables should be represented in the final regression model; signals that are important ***at the time-interval model time-***

***point*** for the cell-fate decision and the later cellular response should be represented and signals that are not important should be dropped from the model.

In order to incorporate this hypothesis, we make use of a Stepwise regression algorithm in the regression step for each of our time-interval models. Stepwise regression is a well-established regression procedure that can be used to select a subset of explanatory variables, from an original larger explanatory variable set, that maximally correlates with the response variable. Explanatory variables that do not add to the model's ability to predict the response variable are excluded from the model.

The combination of these three steps defines the approach we call hypothesis-based, Time Interval Stepwise regression (TI-SWR). TI-SWR exploits the time-dimension of the signal-response dataset by systematically exploring time-dependent signal-response relationships for each chosen cellular response. The result is a set of time-interval models that are low dimensional and thus easily interpretable. These sets of time-interval models yield insight into detailed, time-dependent signal-response relationship and greatly facilitate the development of hypotheses about signal-response causal relationships as well as the design and execution of hypothesis-motivated experiments to test and validate these hypotheses.

### *TI-SWR: signal-response correlations*

In this example, we have used TI-SWR to investigate signal-response relationships for the cell-cycle regulation phenotype previously described, which we capture with a response variable that is a readout of the change in S population between 12 and 24 hr (Δ S, 12-24 hr). For every time-point at which signals were measured (0.25, 0.5, 1, 1.5, 2, 4, 8, 12,16, and 24 hr), we iteratively regressed the response variable, Δ S, 12-24 hr, against all of the signal measured at that time-point, using a Stepwise regression algorithm in each case to build each of our time-point specific, time-interval regression

models. The result is a set of 10 time-point specific time-interval models that reveal detailed, time-dependent relationships between the signals we have measured (p-H2AX, p-Nbs1, p-p53, total p53, p-p38, p-JNK, p-ERK1/2, p-Akt, and NFkB) and the response variable we have investigated here.

In fact, in this example, the result is a set of 5 time-point specific small models (Figure 3-7B). At five out of the 10 time-points at which signals were measured, no signal-response relationships reach a required level of significance (These time-points include the 0.25, 0.5, 1, 1.5 and 12 hr time-points). That is, no signals at these time-points are found to significantly correlate with the response variable. Therefore, the Stepwise regression algorithm excludes all signals from these time-interval regression models and no model is reported at these time-points. The signaling at these time-points is perhaps "uninformative" to the cell in determining cell-fate and cellular response. A possible explanation is that at these times other proteins, not included in the measured set, play a dominant role in the dynamic signaling, while the measured proteins are temporarily not important.

The five time-point specific models that do result from the hi-SWR analysis are for signaling at 2, 4, 8, 16 and 24 hr. Interestingly, we find that H2AX, in concert with ERK1/2, appears to be important at relatively early times (2 hr). H2AX is excluded from the model by the 4 hr time-point, but ERK1/2 remains in the 4 hr time-point model. In the 4 hr time-point model, ERK1/2 has a much higher correlation with the response variable and now works in concert with p53. ERK1/2 is also still present in the 8 hr time-point model. In the 8 hr time-point model, ERK1/2 is highly correlated with the response variable and is the only signal at this time-point that is correlated with the response variable. By the 12 hr time-point, ERK1/2 is excluded from the time-point model, and is not included in models for either of the even later time-point models (16 and 24 hr time-point models). Time-point specific models for the 16 and 24 hr time-point exclude all signals except for total p53, indicating that only total p53 is significantly correlated with the response variable at these late times. Why do we find a relationship

between H2AX at one early time, but not at any later times? It is possible that H2AX activity at the 2 hr time-point is critical for regulating the activation of ERK1/2 at that time. Once ERK1/2 has been activated, the critical role of H2AX activity in the cell-fate decision is passed. H2AX activity at later time-points is no longer important or necessarily related to cellular response. The critical information has been "passed" from H2AX to ERK1/2 and it is between ERK1/2 activity and the cellular response that we find significant relationships at a later time. A similar reasoning can be used to hypothesize that ERK1/2 activity may be critical in regulating the activation of p53 under these damaging conditions, as we identify significant relationships between ERK1/2 and cellular response in 2, 4 and 8 hr time-point specific models, but lose this significant relationship in later time-point specific models, as we gain significant relationships between total p53 and cellular response. It is at least possible then, to hypothesize that we are identifying direst "transfer of critical information" relationships between these signals. However, another explanation for "losing" significant relationships between a given signal and cellular response in later time-point specific models, after having observed a significant signal-response relationship in earlier time-point specific models, is that, for example, H2AX activity at the 2 hr time-point is critical for regulating the activation of some signal that we have not measured. This is perhaps more likely than the hypothesis that H2AX directly acts to regulate activation of ERK1/2, as these two molecules have not been reported in the literature to directly interact. If our hi-SWR model results do not indicate that H2AX directly regulates the activation of ERK1/2 (direct critical information transfer), then there are two additional things that the model results could indicate. One is that H2AX indirectly regulates the activation of ERK1/2, via some molecule that we have not measured (indirect critical information transfer). A second possibility is that H2AX has no role in regulating activation of ERK1/2, and that H2AX is critically involved in regulating some other signaling in parallel to ERK1/2 signaling that is critical for cellular response (parallel critical information transfer).

In another example of TI-SWR analysis, we chose the change in cell-death between 6 and 12 hr following treatments (Δ % apoptosis, 6-12 hr) as the cellular response of interest (Figure 3-7C). In this analysis, the final model set resulting from the analysis consists of only 4 time-point specific small models. Two of the time-points at which we have measured signals fall after our cellular response (the 16 and 24 hr time-points). It is not possible for signaling at these later time-points to have a causal relationship with the cellular response that came before, so we exclude these time-points from the analysis. At four of the eight remaining time-points, there are no significant relationships found between signals and our response variable (Δ % apoptosis, 6-12 hr). The time-points specific small models which do result from this analysis are for the time-points of 0.25, 4, 8 and 12 hr.

It is worth noting here that p53 is included in the time-point specific small model at 8 hr and p-ERK1/2 is included, to the exclusion of all other signals, in the 12 hr time-point specific small model. Both of these signals were included in time-point specific small models for the previously discussed cell-cycle phenotype cellular response TI-SWR analysis. Thus these TI-SWR analyses suggest that both p53 and ERK1/2 are involved in making and mediating cell-fate decisions governing cell-cycle arrest/regulatory phenotypes and cell-death phenotypes. Our PLSR analysis also suggested that both p53 and p-ERK1/2 have roles in mediating both of these cell-fate decisions. This is just one example to illustrate that results from TI-SWR and PLSR analysis are often mutually confirming methods. This dual confirmation raises our confidence level in the specific case of overlapping results, but also raises our confidence in the case of results that can only be produced by either PLSR or TI-SWR analysis, such as response-response relationship inferences in the case of PLSR, or systematic, time-dependent relationships between signals and cellular response in the case of TI-SWR.

### *TI-SWR: signal-signal correlations*

TI-SWR can also be used to investigate dynamic signal-signal relationships. The methodology for investigating the signal-signal relationships is similar to that described above for the study of signal-response relationships, with the proteins (signals) being viewed as "responses" to the previous sets of signals. We choose a dependent variable of interest as before, which is now the change in a particular cell signal (protein) divided by the time interval ($t^{n+1} - t^n$), i.e. the derivative of the linearized signal over the selected time interval. The explanation for this choice is presented below, and follows the same approach presented above for the cell responses.

For a given time interval $\Delta t^n = t^{n+1} - t^n$ we define $C^n_{ij}$ as the change in protein i due to $S^n_j$ - the protein j at time n - per unit time and per unit of protein j at the beginning of the time interval. Then, the protein i at the end of the time interval can be written as;

$$S_i^{n+1} = S_i^n + \sum_j C_{i,j}^n * S_j^n * (t^{n+1} - t^n): \qquad (6)$$

We can re-arrange eq. 6, moving $S^n_i$ on the LHS, and dividing by $\Delta t^n$ to obtain:

$$DS_i^n = \sum_j C_{i,j}^n * S_j^n \qquad (7)$$

Where $DS^n_i$ is the derivative of protein i over the time interval n, defined as:

$$DS_i^n = (S_i^{n+1} - S_i^n)/(t^{n+1} - t^n) \qquad (8)$$

We note that equation 7 is now in the exact form of the multiple linear regression equation, where the independent variables are the measured values of the proteins j at time n, and the dependent variable is $DS^n_i$ the derivative of protein i over the time interval n, which can be calculated from the measured data using equation 8. This means again that the coefficients $C^n_{i,j}$ calculated by the multiple linear regression have a clearly defined meaning, i.e. they represent the change in protein i over the selected time interval due to $S^n_j$ - the protein j at time n - per unit time and per unit of protein j at the beginning of the time interval.

As noted previously for the responses, a significant advantage of this formulation of the multiple linear regression equation is that the coefficients $C^n_{i,j}$ represent changes in protein i per unit time, during the time interval n. This means that although our measurements – and corresponding regressions – have been performed for intervals of time of different length, the regression coefficients, which represent change per unit time, can be compared across multiple time intervals to provide a measure of the change in specific protein-protein dependence over time.

The dynamic signal-signal relationships can be investigated in either a "walk-back" fashion or in a systematic fashion, as described below.

### *A "Walk-Back" approach for linking cell responses with dynamic signal (protein) changes and for the investigation of signal-signal relationships*

The "walk-back" approach provides an approach to studying the dynamic signal (protein) changes associated with a selected cellular response. In this case, we choose a cellular response of interest as before, which is the derivative of the linearized selected cellular response over a time interval n, between the times $t^n$ and $t^{n+1}$. Then we make the hypothesis that the signals at the time-point $t^n$ (the starting time-point for the time interval of the cellular response of interest) are integrated by the cell to make and mediate the cell-fate decision and cellular response of interest. Measured signal sets at other time points that precede the selected time interval can also be selected as independent variables, but as we noted before, the closer in time the independent variables (protein signal set) are to the cellular response of interest, the more likely any identified relationships between signals and cellular responses are to be direct, and linear in nature.

We regress the cellular response of interest against the signal measurements at $t^n$ using the Stepwise regression algorithm, as before, to identify signal-response relationships between signals at $t^n$ and the cellular response. The cellular response at the end of the interval n, time $t^{n+1}$, is given by:

$$R_i^{n+1} = R_i^n + DR_i^n * (t^{n+1} - t^n) \qquad (11)$$

where the response derivative $DR^n_i$ is obtained from the TI-SWR as a function of the explanatory proteins at time n:

$$DR_i^n = \sum_j C_{i,j}^n * S_j^n \qquad (12)$$

The explanatory proteins in Equation 12 can now be expressed as a function of the signals at time $t^{n-1}$:

$$S_j^n = S_j^{n-1} + DS_j^{n-1} * (t^n - t^{n-1}) \qquad (13)$$

Next we choose $DS^{n-1}_j$ as our response variable. Here the dependent variable is no longer the derivative of a cellular response over a time-period, but the derivative of a linearized measured signal over the time interval n-1. We can continue "walking back" in time to investigate what signals are related to the signals that have been identified as being related to the change in the selected cell response. This method has the advantage that all models are constructed in a manner that maximizes the probability of finding signal-response and signal-signal relationships that are direct, and linear in nature (Figure 3-8A).

A

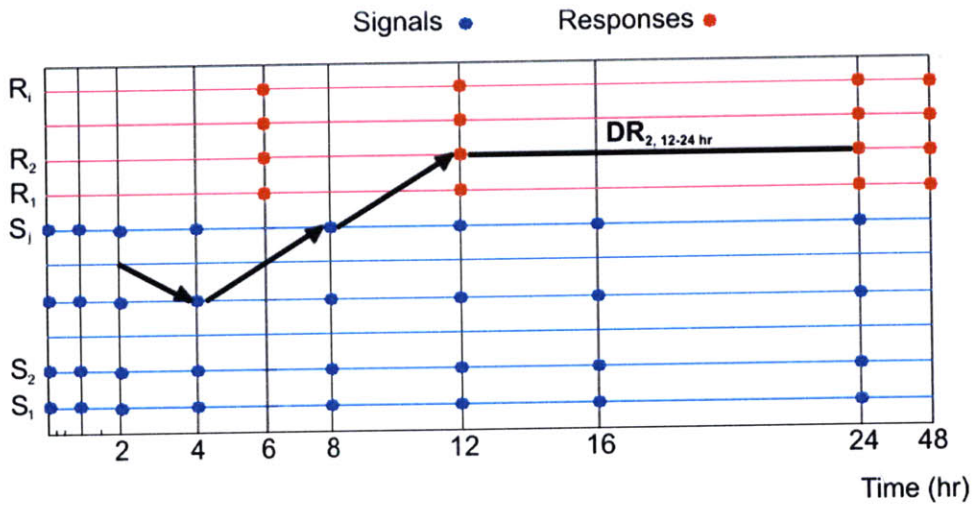


B

| Y: response variable | X: top correlate | X: p val | X: $R^2$ |
|---|---|---|---|
| Y: Δ CC3+, 12-24 hr | p-p38, 16 hr | 0.03 | 0.69 |
| Y: Δ p-p38, 12-16hr | p-p38, 12 hr/p-Akt, 12 hr | 8e-6/0.01 | 0.99/0.004 |
| Y: Δ p-p38, 8-12 hr | NFkB, 8 hr | 0.03 | 0.70 |
| Y: Δ NFkB, 4-8 hr | p-JNK, 4hr/NFkB, 4 hr | 0.008/0.02 | 0.85/0.12 |

**Figure 3-8.** ***(A)*** Illustration of the "walk back" approach to TI-SWR (Time-Interval Stepwise regression) analysis. In a "walk back" approach, start with a cellular response of interest and construct just one time-point specific, Time-Interval model for a time-point that is close in time to the cellular response of interest. This model has the cellular response of interest as a response variable and all of the signaling measurements made at one time-point as the potential explanatory variable set (In the illustration, the response variable for this first model is the change in the cellular response, $R_2$, between 12 and 24 hr following treatment and the potential explanatory variable set includes all signaling measurements made at 8 hr following treatment). The top signal correlate/s from this model now specifies the response variable in a new time-point specific, Time-Interval model that we can construct. In this

model, the response variable no longer refers to a change in a cellular response over a time-interval, but to a change in a signal over a time-period. Specifically, the response variable for this next model is the change in the top-correlate signal between the time-point immediately preceding the first time-point specific model, to the time-point of the first time-point specific model (In the illustration, the response variable for this second model is the change in $S_j$ between 4 and 8 hr following treatment and the potential explanatory variable set includes all signaling measurements made at 4 hr following treatment). Again, the top signal correlate/s from this model specifies the response variable in a new time-point specific, Time-Interval model that steps us back one more time-point. This "walk back" in the time-space, following first the chain of signal-response relationship, then signal-signal relationships, can be continued as long as the signal-signal relationship chain is unbroken (until we reach a time-point specific, Time-Interval model for which no signal-signal relationships reach a required level of significance; $p<0.05$). In the illustration, we stop after the 2 hr time-point specific model (for which the response variable is the change in the signal $S_{j-2}$ between 2 and 4 hr following treatment and for which the potential explanatory variable set includes all signaling measurements at 2 hr following treatment), because this model yields no significant signal-signal relationships to follow further back in time.
***(B)*** Table of results from a "walk back" TI-SWR (Time-Interval Stepwise regression) analysis investigating the change in apoptosis between 12 and 24 hr following treatment (Δ %apoptosi (CC3+), 12-24 hr) as the cellular response variable. Cells staining positively for one of the apoptotic markers (CC3+) regardless of whether they stained positively for another apoptotic marker (+/- CParp) were considered apoptotic in this analysis. Rows present an overview of the results for each of the time-point specific Time-Interval models constructed. For each of the time-point specific Time-Interval models, the response variable is listed first and models are listed in time-space "walk back" order. The potential explanatory variable set is all signaling measurements made at the time-point that defines the beginning of the response variable time-interval, except in the case of the first model that begins with the cellular response of interest. ***For this first model in the "walk back" analysis, the potential explanatory variable set includes all signaling measurements made at the 16 hr time-point***, which is a time-point that falls ***within*** the time-interval of the cellular response of interest (12-24 hr following treatment). For each Time-interval model, the top signal correlate/s are listed in order of decreasing $R^2$ (ability to explain the variability in the response variable). The significance levels of top signal correlate/s are listed, as are $R^2$ values. For further details on individual Time-Interval models in this set, reference Supplemental Figure 3-26 through 3-29.

---

As an example, we chose to investigate the change in apoptosis between 12 and 24 hr following treatment (Δ %apoptosis (CC3+), 12-24 hr) using a "walk back" TI-SWR approach (Figure 3-8B and Supplementary Figures 3-26 through 3-29). In the "first step" model, this cellular response is the response variable, and the potential set of explanatory variables are all signal measurements at 16 hr following treatment (a time-point that falls within the cellular response time-interval). The top signal correlate identified from the first step model is p-p38, 16 hr. In the second step model, the change in p-

p38 between 12 and 16 hr following treatment (Δ p-p38, 12-16hr) serves as the response variable, and the potential set of explanatory variables are all signal measurements at 12 hr following treatment. The top signal correlates identified from the second step model are p-p38, 12 hr and p-Akt, 12 hr. However, p-Akt, 12 hr contributes almost no additional ability to explain the variability in the response variable (Supplementary Figure 3-27) and so we do not pursue that path, but continue with a third step model in which the response variable is the change in p-p38 between 8 and 12 hr following treatment, and the potential set of explanatory variables are all the signal measurements at 8 hr following treatment. The top signal correlate identified from the third step model is NFkB, 8 hr. In a fourth step model then, the change in NFkB between 4 and 8 hr serves as the response variable, and the potential set of explanatory variables are all signal measurements at 4 hr following treatment. The top signal correlates identified from the fourth step model are p-JNK, 4 hr and NFkB, 4 hr. Both significantly contribute ability to explain variability in the response variable (Supplementary Figure 3-29). Therefore, either/both may be followed back (e.g. fifth step models with either the change in p-JNK between 2 and 4 hr following treatment as the response variable or the change in NFkB between 2 and 4 hr following treatment as the response variable, with a potential explanatory variable set of all signal measurements at 2 hr in both cases). However, in neither case do we identify any further significant signal-signal relationships. This is then the end of a "walk back" TI-SWR analysis, where this analysis has yielded insight into some dynamic, time-dependent signal-signal relationships, and has yielded further insight into potential mechanisms of signal-signal-cellular response trajectories.

### *A systematic approach to studying signal-signal relationships*

We can also take a "systematic" approach to finding signal-signal relationships. In this case we do not start with a cellular response of interest. Instead, we start with the first signal time-point measurements. For each of the signals we have measured we say that the change in that signal

between the first and second time-point is a function of all of the signals measured at the first time-point, build a time-interval regression model with the linearizied signal derivative as the response variable and signal measurements at the first time-points as explanatory variables to find which signals are related to the change in our response variable signal. For each signal measured, we can "step forward" and build time-interval regression models to identify which signals are identified as related to the change in any measured signal over any of the time-periods for which we have measured data (Figure 3-9). If we execute this for all measured signals over all measured time-periods, then the result is a systematic identification of time-dependent signal-signal relationships that can be discovered in the dataset. Models to identify signal-response relationships can also be included in this systematic "step forward" approach over appropriate time intervals. The ability to identify signal-signal relationships can help to clarify identified signal-response relationships and may yield clues to the mechanism of identified signal-response relationships.

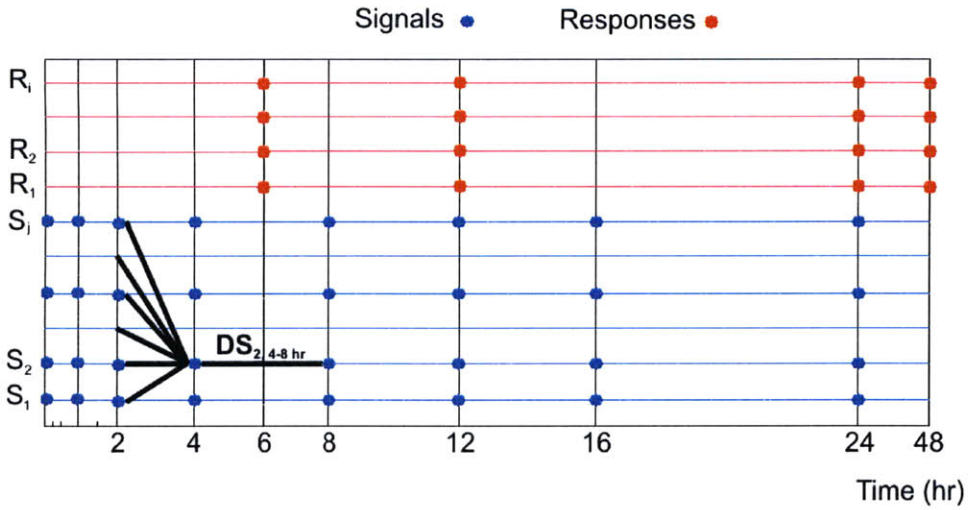


**Figure 3-9.** Illustration of the systematic, forward approach to TI-SWR (Time-Interval Stepwise regression) analysis. In a systematic, forward approach, ***do NOT*** start with a cellular response of interest. Instead start at the earliest time-points at which signaling measurements were made. The response variable for the first time-point specific, Time-Interval model constructed will be the change in one of the signals measured over this first time interval; the potential explanatory variable set will be all of the signaling measurements made at the beginning of this time-interval. This model construction in repeated for all signals measured. The result is a set of time-point specific, Time-Interval models that specifies the relationship between all of the signals measured at the first time-point and the change in each of the signals over the first time-interval. The next step is to move to the next time-interval over which signals were measured and repeat the process for all time intervals over which signals were measured. The result is a systematic investigation of all time-dependent signal-signal relationships captured in the dataset. Cellular responses can be included as either response variables or potential explanatory variables as appropriate.

---

## Discussion

Computational modeling approaches are necessary tools to facilitate our progress towards a deeper and more complete understanding of how specific biological networks function, and of how biological networks function in general.

This type of biological network study is part experimental study, part computational modeling/analysis. It is a highly iterative process. The modeling gives us insight into the biology we have measured and points us in the direction of where we should be looking – what parts of our data are important. However, the other direction is at least as important. And oftentimes, close examination of the original data, or subsequently obtained data, can illuminate features of the model that were previously unclear.

Quantitative measurement of signaling data is becoming more accessible, high (or higher) throughput data is also becoming more accessible. It is clear that network level biology that addresses how signaling molecules within and across canonical signaling pathways work in concert to mediate complex cellular and cell-population phenotypes is an area of study that is critically important for the understanding of complex human pathologies and for the development of targeted therapies to treat these pathologies.

# Chapter 4: Future Directions

In this work we have developed a quantitative signal-response data set that allows the study of the dynamic response of the cell signaling network following DSB. We have also developed a promising analytical methodology, TI-SWR, which could open the way to a better understanding of the functioning of the cell signaling networks. The efficacy of the TI-SWR techniques is expected to improve significantly as the signal and response measurements are spaced closer in time, discretizing the cellular response and making the linear approximation of the network dependencies an increasingly accurate approximation. Thus, a future direction for continuing this work is to expand the quantitative signal response data base by making additional measurements at shorter time intervals for the selected treatments. We also recommend a better discretization of the treatments, in order to understand better the importance of the DSB level on the cellular response. As demonstrated in this work, the application of TI-SWR to such a dataset can generate interesting hypothesis about the cellular response that can suggest specific time-dependent treatment interventions. Experiments involving such time-dependent treatments can be planned in the future to allow the systematic study of treatments where both the dose of the treatments and the time-dependent treatment interventions are varied systematically; signaling and response measurements collected under these treatment conditions may be added to a continuously expanding quantitative, DNA damage signal-response data base.

It would be interesting to much more fully explore the interaction between the cellular responses of cell-cycle arrest and cell-death following DNA damage. The relationship between these responses is complex and has been under-explored, especially in light of the relevance of this interaction to cancer therapy. Many studies focus on measuring either cell-death or cell-cycle arrest outcomes, and even then only measure at a single time-point. Additionally, often studies investigate one or two levels of DNA damage based on the phenotype they are more interested in. DNA damage is either very high in

studies that primarily investigate apoptosis or relatively low in studies that primarily investigate cell-cycle checkpoints.

However, it is clear that these are continuously evolving and interacting processes. Cell-populations that have been subjected to DNA damage may arrest at more than one DNA damage-mediated cell-cycle checkpoint at different times following DNA damage, and cell-death is often not a linear function with respect to time, but may occur in a burst or bursts. DNA damage mediated cell cycle checkpoints are initiated and/or maintained in a cell in order to stop DNA synthesis (prevent a cell from replicating its DNA while damaged and thus passing on mutations) and to allow for DNA repair. The accepted view is that when DNA has been repaired, checkpoints are released and the cell re-enters the cell-cycle. On the other hand, when DNA cannot be repaired, in a normally functioning cell, apoptotic processes are initiated. It seems clear that there must be feedback between the cell-cycle checkpoints and apoptotic processes, but the interactions between these two processes, even on the cell-biologic level of cellular phenotype has not been explored in any depth.

A first step might be to find a set of conditions that covered a spectrum of the balance between cell-cycle arrest and apoptotic phenotypes (ranging from mild cell-cycle arrest and high apoptosis to very robust cell-cycle arrest phenotypes and very low apoptosis, concentrating more on the lower end of apoptosis). Under these conditions, it would be interesting to carry out detailed dynamic studies of cell-cycle and apoptotic phenotypes. It would also be interesting to explore other parameters in a dynamic fashion, including 1) the dynamics and spectrum of DNA damage being induced, 2) dynamics and mode of DNA repair, 3) dynamics of autophagy and 4) dynamics of other modes of cell-death such as necrosis.

The measurement of cell-cycle phenotypes could be expanded to more precisely understand the cell-cycle and checkpoint status at the time of measurement; phase-specific cyclin levels and localizations and cdk activities may be measured, BRDU incorporation levels may be measured to

determine S phase fraction, and cki levels may also be measured. The spectrum of DNA damage (and perhaps DNA repair) could be monitored by pulsed gel electrophoresis (for single and double strand DNA breaks), measurement of various DNA adducts via mass spectrometry, and measurement of H2AX localization and phosphorylation via live-cell imaging or IF. The dynamics of DNA repair may be captured by these same measurements. The mode of DNA repair could be monitored by measurement of recruitment of repair mode-specific factors (e.g. recruitment of XRCC4, DNA ligase IV and Artemis would indicate repair via non-homologous end joining). Autophagy could be monitored by cleavage of the marker protein LC3B or by IF staining for LC3B foci, in the case that the cell type under investigation natively expresses adequate levels of LC3B. Necrosis may be monitored by concurrent measurement of Annexin V staining of phospatidyl-serine on the cell-surface and of membrane permeability to propidium iodide. Such a dataset could be explored extensively and in a detailed time-dependent fashion using the TI-SWR methods outlined in Chapter 3 of this thesis, where each of these measured cellular phenotypes, at almost any time-point at which it was measured, can move freely between consideration as an explanatory and as a response variable. This study would give us a much stronger understanding of the interaction between these dynamic and interacting processes on a phenomenological level, and could serve as a strong basis for more detailed signaling studies to investigate the molecular signaling governing these outcomes.

Another interesting avenue would be to explore the autocrine/paracrine networks stimulated by DNA damage, and also to further explore how the effect of DNA damage on cells changes based on the extra-cellular milieu.

We did not investigate autocrine/paracrine factors in this thesis. However, tumor cells are noted for their production of both inflammatory and anti-inflammatory cytokines and these factors have been associated with tumor grade and implicated in aiding tumor cells to evade immune recognition and attack. Some interesting questions include: 1) what factors are released; are they

inflammatory/anti-inflammatory/mitogenic?, 2) do the factors that are released change with treatment condition? with any of the cellular responses discussed above?, 3) if the factors (or combinations of factors) that are released change, how do these various factor-combinations affect the ability of adaptive immune cells to be activated by cognate antigen or to avoid anergy or tolerization? How do they affect the ability of endothelial cells to vascularize?, 4) do released factors (or combinations of factors) promote genomic instability and/or increased proliferation in tumor cells? (factors released by tumor cells could be associated with tumor grade because they directly affect tumor cells and allow tumor cells to accumulate additional advantageous mutations via increased genomic instability, or because they allow tumor cells to proliferate in an unregulated manner via increased stimulation to proliferate, or because they indirectly affect tumor cells and prevent adaptive immune cells from recognizing and attacking them or stimulate endothelial cells to promote vascularization...) and 5) can the addition of an additional factor or neutralization of a factor moderate or reverse these outcomes?

We did investigate how the effect of DNA damage on cells changes based on the extracellular milieu (by adding the inflammatory cytokine TNF-α). However, it would be interesting to deeply investigate this effect by testing the effect of a panel of single inflammatory and/or mitogenic factors as well as combinations of these factors. An additional dimension to add might be seeding tumor cells to be treated on various extracellular matrix component combinations to vary the nature of the mechanical contacts the cell makes with the surface it rests on. Tumor cells could be seeded in a 3-D matrix system and even co-seeded with non-tumor stromal cells to investigate the effect of the 3D nature of a true tumor environment and the interaction of tumor cells with non-tumor cells in its surroundings.

Another interesting avenue would be to extend the work done in this thesis by replicating the dataset in a panel of U2OS cell-lines with defined mutations or stably transfected with shRNA against

key signaling molecules or stably transfected with constitutively active versions of key signaling molecules.

# Appendix 1: Signaling Assay Validation

The most informative data for the purposes of analysis via data-driven mathematical modeling approaches, such as linear regression, are quantitative data. Therefore, we validated all signaling assays used in this work to collect molecular signaling data, for their ability to provide a quantitative, linear signal with increasing activity or level of the relevant signaling molecule present.

We validated quantitative Western assays for over 17 measurements of either phosphorylated signaling proteins or total protein levels and one quantitative ELISA assay for measurement of the activation of the NFkB transcription factor. Quantitative western assays validated include those for: p-ATM (S1981), p-Nbs1 (S343), total Nbs1, p-H2AX (S139), total H2AX, p-p53 (S15), p-p53 (S20), total p53, p-p38 (T180/Y182), p-JNK (T183/Y185), total JNK, p-ERK1/2 (T202/Y204), total ERK1 and p-Akt (S473).

Below are data from the validation of these assays, including the full blots and the quantification of the identified relevant signal.

A

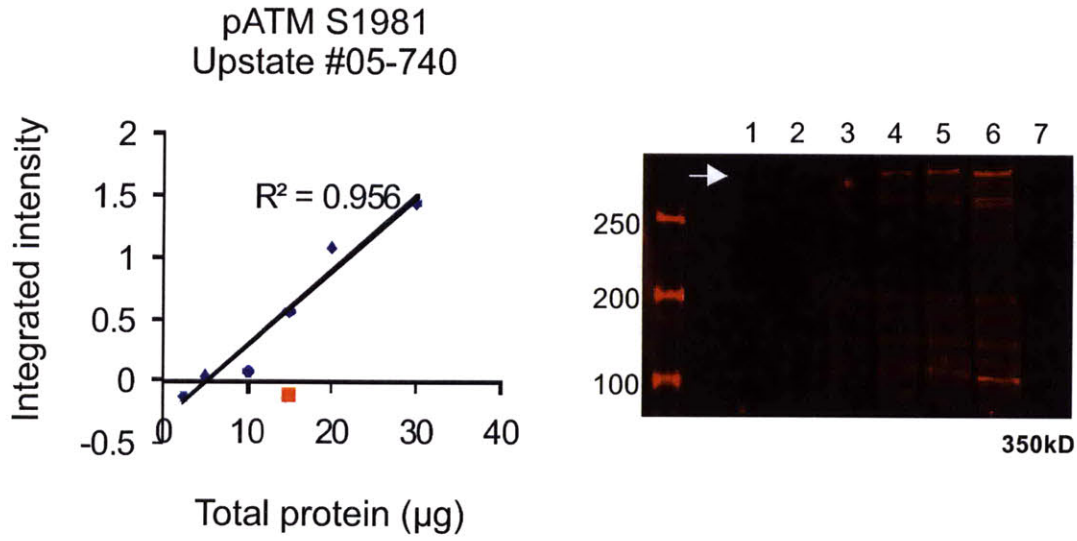
pATM S1981
Upstate #05-740
Integrated intensity
2
1.5
1
0.5
0
-0.5
R² = 0.956
0
10
20
30
40
Total protein (µg)
1 2 3 4 5 6 7
250
200
100
350kD

B

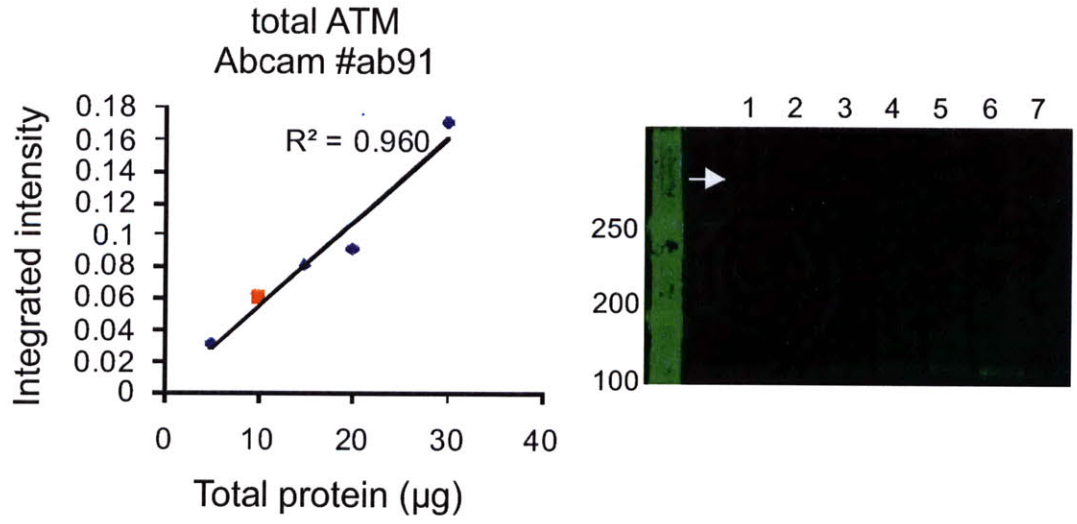
total ATM
Abcam #ab91
Integrated intensity
0.18
0.16
0.14
0.12
0.1
0.08
0.06
0.04
0.02
0
R² = 0.960
0
10
20
30
40
Total protein (µg)
1 2 3 4 5 6 7
250
200
100

**Figure A1-1.** Quantitative western blots for p-ATM (S1981) (A) and for total ATM (B). For both (A) and (B) blue circles on the plots are signal obtained from positive control lysates; red circles on the plots are signal obtained from negative control lysates. Positive control lysates are extracts from asynchronous U2OS cells treated with Neocarzinostatin (45 nM) for 1 hr. Negative control lysates are extracts from asynchronous U2OS cells that are untreated and sub-confluent. For both (A) and (B) Lanes 1-6 on membrane images are increasing amounts of total protein loaded from positive control lysates for p-ATM (S1981). Lanes 1-6 are 2.5, 5, 10, 15, 20 and 30 μg of total protein loaded in that order. Lane 7 is 15 μg of total protein loaded from negative control lysates for p-ATM (S1981). ***(A)*** Signal for p-ATM (S1981) increases in a linear fashion with increasing amounts of total protein loaded (from 2.5-30 μg of total protein loaded) from positive control extracts (blue circles on plot; regression coefficient of 0.95). Signal to background is high (compare blue circle and red circle on plot at 15 ug of total protein loaded) and signal is easy to distinguish by eye at 15 μg of total protein loaded (lane 4 on membrane image). All subsequent measurements of p-ATM were carried out using 15 μg of total protein from the sample lysate and include positive and negative controls on the blot (also 15 μg of total protein loaded) as described here, for comparison and normalization. ***(B)*** Signal for total ATM increases in a linear fashion with increasing amounts of total protein loaded (from 2.5-30 μg of total protein loaded) from positive control extracts (blue circles on plot; regression coefficient of 0.96). 15 ug of total protein loaded from negative control extracts (lane 7 on membrane image) gives the same signal as that obtained from positive control extracts (compare to lane 3 on membrane image), implying that there is no regulation of total levels of protein under these conditions. All subsequent measurements of total ATM were carried out using 15 μg of total protein from the sample lysate and include positive and negative controls on the blot (also 15 μg of total protein loaded) as described here, for comparison and normalization.

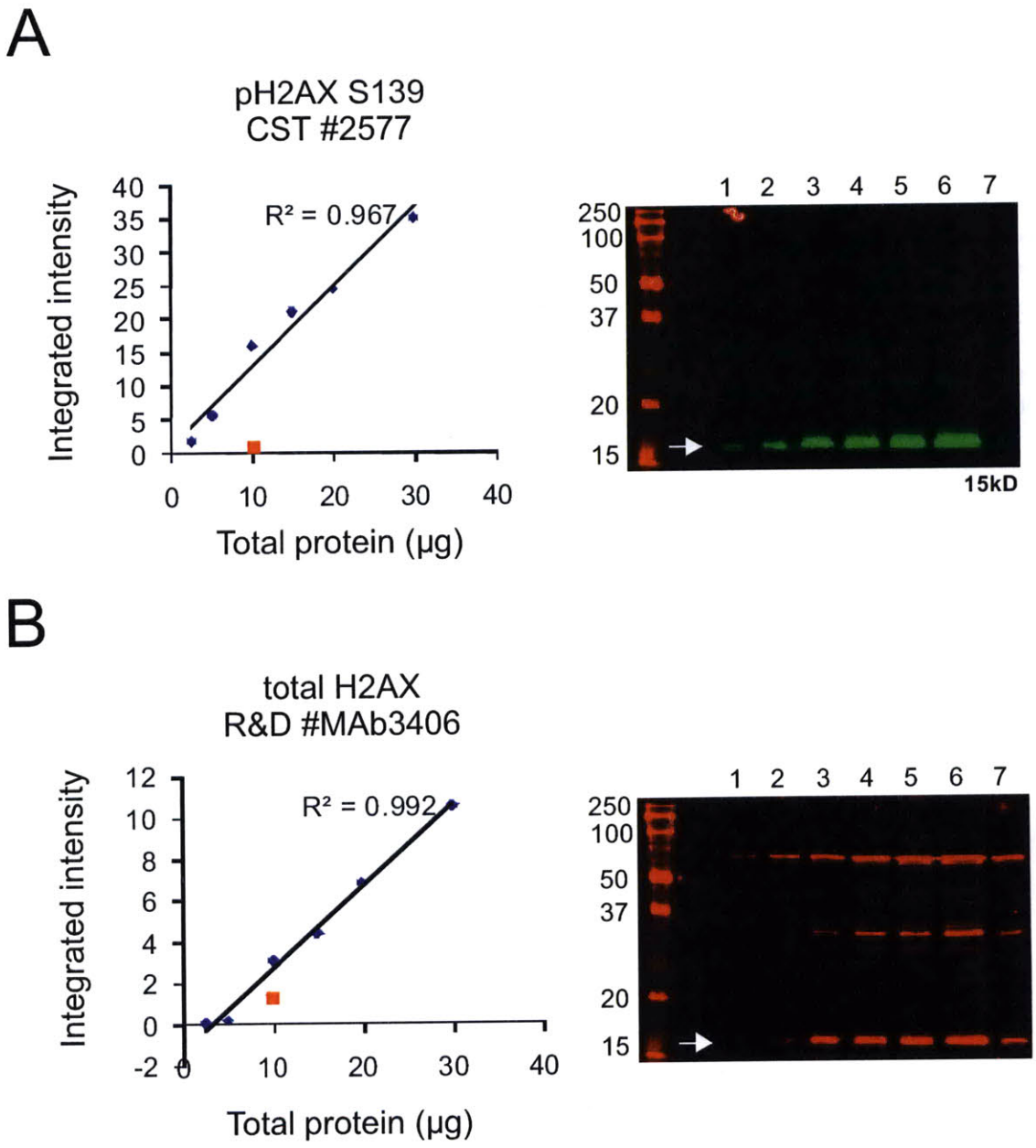


**Figure A1-2.** Quantitative western blots for p-H2AX (S139) (A) and for total H2AX (B). For both (A) and (B) blue circles on the plots are signal obtained from positive control lysates; red circles on the plots are signal obtained from negative control lysates. Positive control lysates are extracts from asynchronous U2OS cells treated with Neocarzinostatin (45 nM) for 1 hr. Negative control lysates are extracts from asynchronous U2OS cells that are untreated and sub-confluent. For both (A) and (B) Lanes 1-6 on membrane images are increasing amounts of total protein loaded from positive control lysates for p-H2AX (S139). Lanes 1-6 are 2.5, 5, 10, 15, 20 and 30 µg of total protein loaded in that order. Lane 7 is

10 μg of total protein loaded from negative control lysates for p-H2AX (S139). ***(A)*** Signal for p-H2AX (S139) increases in a linear fashion with increasing amounts of total protein loaded (from 2.5-30 μg of total protein loaded) from positive control extracts (blue circles on plot; regression coefficient of 0.96). Signal to background is high (compare blue circle and red circle on plot at 10 ug of total protein loaded) and signal is easy to distinguish by eye at 10 μg of total protein loaded (lane 3 on membrane image). All subsequent measurements of p-H2AX were carried out using 10 μg of total protein from the sample lysate and include positive and negative controls on the blot (also 10 μg of total protein loaded) as described here, for comparison and normalization. ***(B)*** Signal for total H2AX increases in a linear fashion with increasing amounts of total protein loaded (from 2.5-30 μg of total protein loaded) from positive control extracts (blue circles on plot; regression coefficient of 0.99). 10 ug of total protein loaded from negative control extracts (lane 7 on membrane image) gives a lower signal than that obtained from positive control extracts (compare to lane 3 on membrane image), implying that there may be regulation of total levels of protein under these conditions (up-regulation of total H2AX under DNA damaging conditions). All subsequent measurements of total H2AX were carried out using 10 μg of total protein from the sample lysate and include positive and negative controls on the blot (also 10 μg of total protein loaded) as described here, for comparison and normalization.

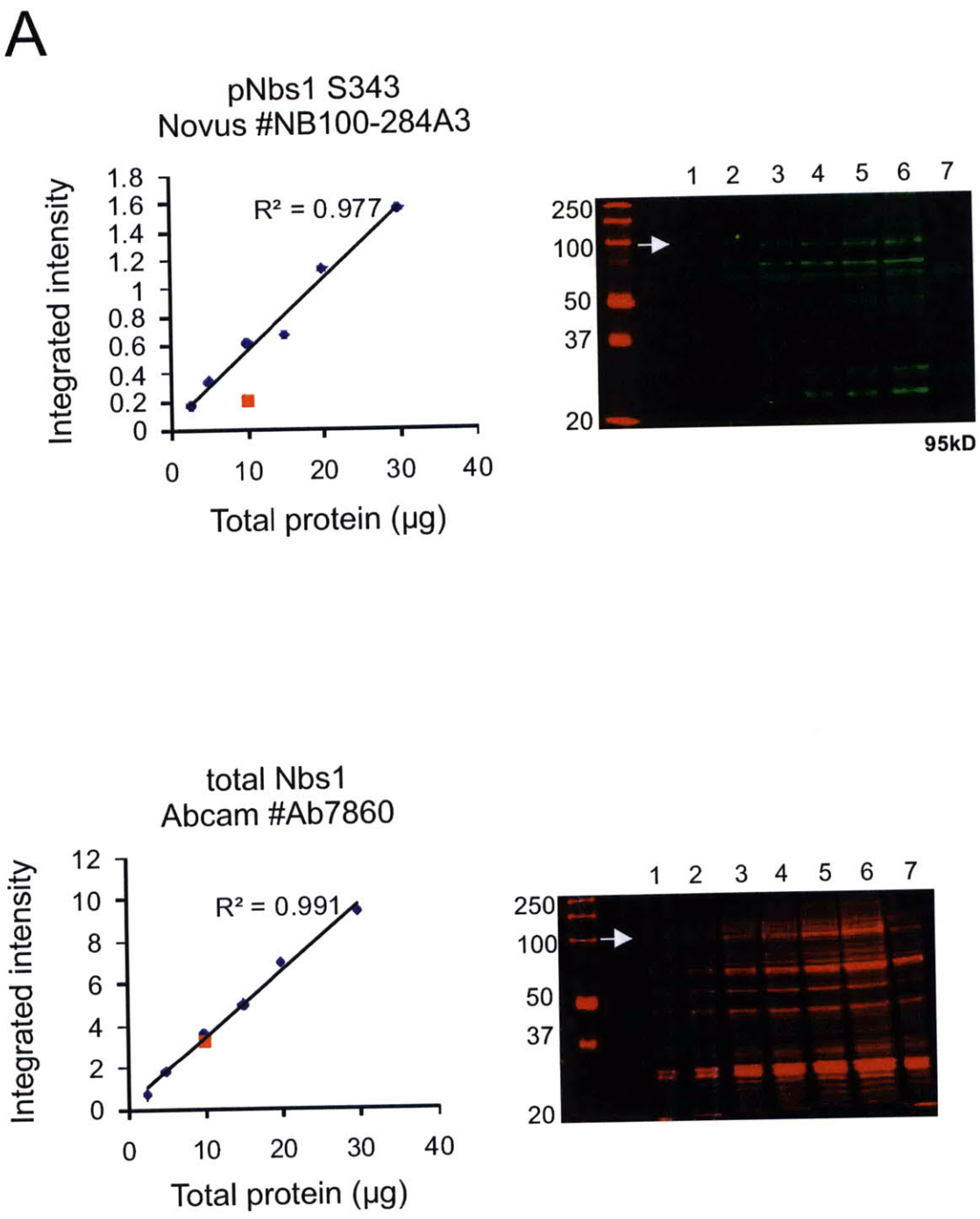


**Figure A1-3.** Quantitative western blots for p-Nbs1 (S343) (A) and for total Nbs1 (B). For both (A) and (B) blue circles on the plots are signal obtained from positive control lysates; red circles on the plots are signal obtained from negative control lysates. Positive control lysates are extracts from asynchronous U2OS cells treated with Neocarzinostatin (45 nM) for 1 hr. Negative control lysates are extracts from asynchronous U2OS cells that are untreated and sub-confluent. For both (A) and (B) Lanes 1-6 on

membrane images are increasing amounts of total protein loaded from positive control lysates for p-Nbs1 (S343). Lanes 1-6 are 2.5, 5, 10, 15, 20 and 30 μg of total protein loaded in that order. Lane 7 is 10 μg of total protein loaded from negative control lysates for p-Nbs1 (S343). ***(A)*** Signal for p-Nbs1 (S343) increases in a linear fashion with increasing amounts of total protein loaded (from 2.5-30 μg of total protein loaded) from positive control extracts (blue circles on plot; regression coefficient of 0.97). Signal to background is high (compare blue circle and red circle on plot at 10 ug of total protein loaded) and signal is easy to distinguish by eye at 10 μg of total protein loaded (lane 3 on membrane image). All subsequent measurements of p-Nbs1 were carried out using 10 μg of total protein from the sample lysate and include positive and negative controls on the blot (also 10 μg of total protein loaded) as described here, for comparison and normalization. ***(B)*** Signal for total Nbs1 increases in a linear fashion with increasing amounts of total protein loaded (from 2.5-30 μg of total protein loaded) from positive control extracts (blue circles on plot; regression coefficient of 0.99). 10 ug of total protein loaded from negative control extracts (lane 7 on membrane image) gives the same signal as that obtained from positive control extracts (compare to lane 3 on membrane image), implying that is no regulation of total levels of protein under these conditions. All subsequent measurements of total Nbs1 were carried out using 10 μg of total protein from the sample lysate and include positive and negative controls on the blot (also 10 μg of total protein loaded) as described here, for comparison and normalization.

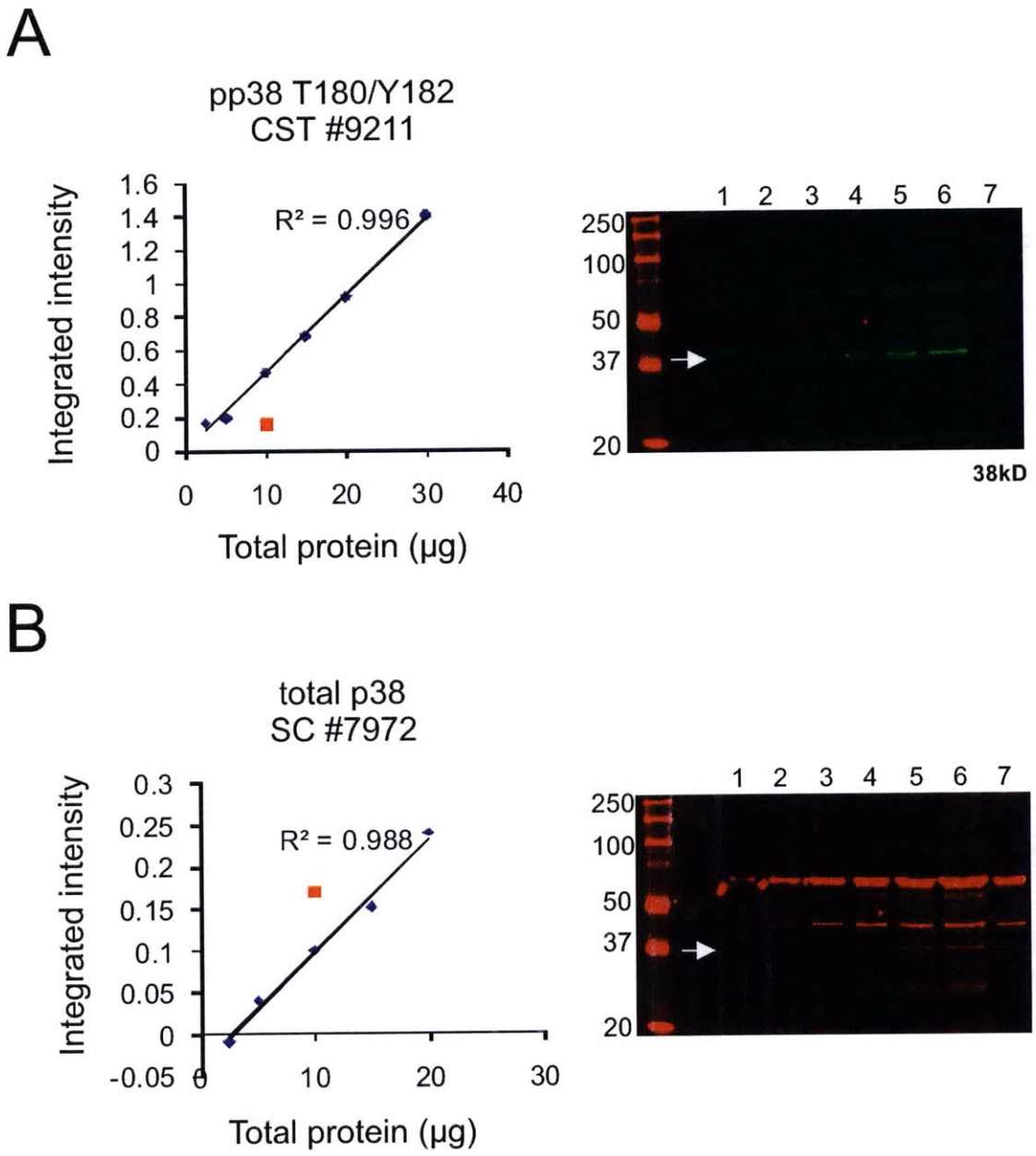


**Figure A1-4.** Quantitative western blots for p-p38 (T180/Y182) (A) and for total p38 (B). For both (A) and (B) blue circles on the plots are signal obtained from positive control lysates; red circles on the plots are signal obtained from negative control lysates. Positive control lysates are extracts from asynchronous U2OS cells treated with UV (50 J/m$^2$) and collected 1 hr later. Negative control lysates are extracts from asynchronous U2OS cells that are untreated and sub-confluent. For both (A) and (B) Lanes 1-6 on membrane images are increasing amounts of total protein loaded from positive control lysates for p-p38 (T180/Y182). Lanes 1-6 are 2.5, 5, 10, 15, 20 and 30 µg of total protein loaded in that order. Lane 7 is 10 µg of total protein loaded from negative control lysates for p-p38 (T180/Y182). ***(A)*** Signal for p-p38 (T180/Y182) increases in a linear fashion with increasing amounts of total protein loaded

(from 2.5-30 μg of total protein loaded) from positive control extracts (blue circles on plot; regression coefficient of 0.99). Signal to background is high (compare blue circle and red circle on plot at 10 ug of total protein loaded) and signal is easy to distinguish by eye at 10 μg of total protein loaded (lane 3 on membrane image). All subsequent measurements of p-p38 were carried out using 10 μg of total protein from the sample lysate and include positive and negative controls on the blot (also 10 μg of total protein loaded) as described here, for comparison and normalization. ***(B)*** Signal for total p38 increases in a linear fashion with increasing amounts of total protein loaded (from 2.5-20 μg of total protein loaded) from positive control extracts (blue circles on plot; regression coefficient of 0.98). 10 ug of total protein loaded from negative control extracts (lane 7 on membrane image) gives a higher signal than that obtained from positive control extracts (compare to lane 3 on membrane image), implying that there may be regulation of total levels of protein under these conditions (down-regulation of total p38 levels under UV treatment conditions). All subsequent measurements of total p38 were carried out using 10 μg of total protein from the sample lysate and include positive and negative controls on the blot (also 10 μg of total protein loaded) as described here, for comparison and normalization.

A

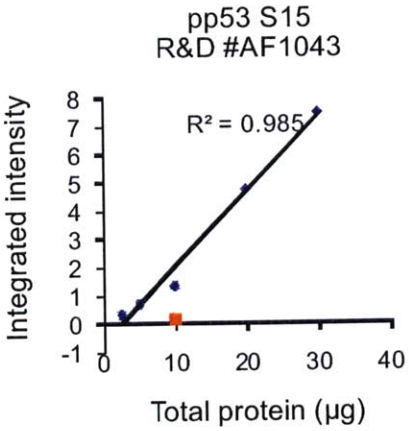
pp53 S15
R&D #AF1043
Integrated intensity
R² = 0.985
Total protein (µg)

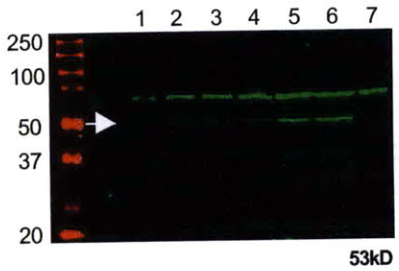
1 2 3 4 5 6 7
250
100
50
37
20
53kD

B

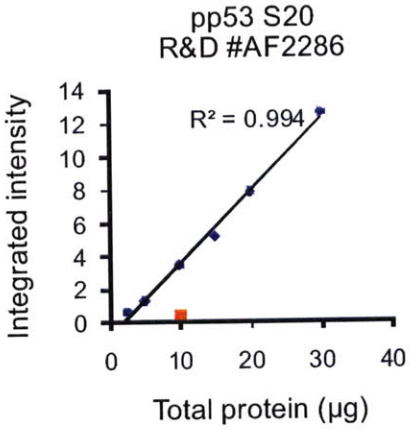
pp53 S20
R&D #AF2286
Integrated intensity
R² = 0.994
Total protein (µg)

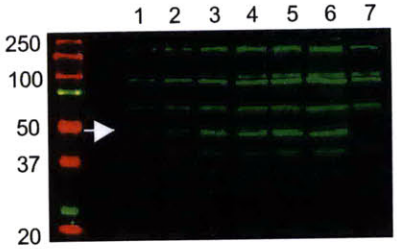
1 2 3 4 5 6 7
250
100
50
37
20

C

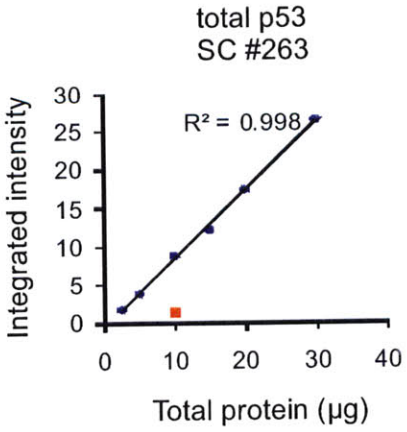
total p53
SC #263
Integrated intensity
R² = 0.998
Total protein (µg)

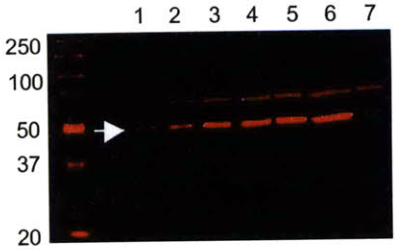
1 2 3 4 5 6 7
250
100
50
37
20

**Figure A1-5.** Quantitative western blots for p-p53 (S15) (A), p-p53 (S20) (B) and for total p53 (C). For (A), (B) and (C) blue circles on the plots are signal obtained from positive control lysates; red circles on the plots are signal obtained from negative control lysates. Positive control lysates are extracts from asynchronous U2OS cells treated with Doxorubicin (10 μM) for 8 hr. Negative control lysates are extracts from asynchronous U2OS cells that are untreated and sub-confluent. For both (A) and (B) Lanes 1-6 on membrane images are increasing amounts of total protein loaded from positive control lysates for p-p53 (S15 and/or S20). Lanes 1-6 are 2.5, 5, 10, 15, 20 and 30 μg of total protein loaded in that order. Lane 7 is 10 μg of total protein loaded from negative control lysates for p-p53 (S15 and/or S20). ***(A)*** Signal for p-p53 (S15) increases in a linear fashion with increasing amounts of total protein loaded (from 2.5-30 μg of total protein loaded) from positive control extracts (blue circles on plot; regression coefficient of 0.98). Signal to background is high (compare blue circle and red circle on plot at 10 ug of total protein loaded) and signal is easy to distinguish by eye at 10 μg of total protein loaded (lane 3 on membrane image). All subsequent measurements of p-p53 were carried out using 10 μg of total protein from the sample lysate and include positive and negative controls on the blot (also 10 μg of total protein loaded) as described here, for comparison and normalization. ***(B)*** Signal for p-p53 (S20) increases in a linear fashion with increasing amounts of total protein loaded (from 2.5-30 μg of total protein loaded) from positive control extracts (blue circles on plot; regression coefficient of 0.99). Signal to background is high (compare blue circle and red circle on plot at 10 ug of total protein loaded) and signal is easy to distinguish by eye at 10 μg of total protein loaded (lane 3 on membrane image). All subsequent measurements of p-p53 were carried out using 10 μg of total protein from the sample lysate and include positive and negative controls on the blot (also 10 μg of total protein loaded) as described here, for comparison and normalization. ***(C)*** Signal for total p53 increases in a linear fashion with increasing amounts of total protein loaded (from 2.5-30 μg of total protein loaded) from positive control extracts (blue circles on plot; regression coefficient of 0.99). 10 ug of total protein loaded from negative control extracts (lane 7 on membrane image) gives a much lower signal than that obtained from positive control extracts (compare to lane 3 on membrane image), implying that there is regulation of total levels of protein under these conditions (up-regulation of total p53 levels under DNA damaging conditions). All subsequent measurements of total p53 were carried out using 10 μg of total protein from the sample lysate and include positive and negative controls on the blot (also 10 μg of total protein loaded) as described here, for comparison and normalization.

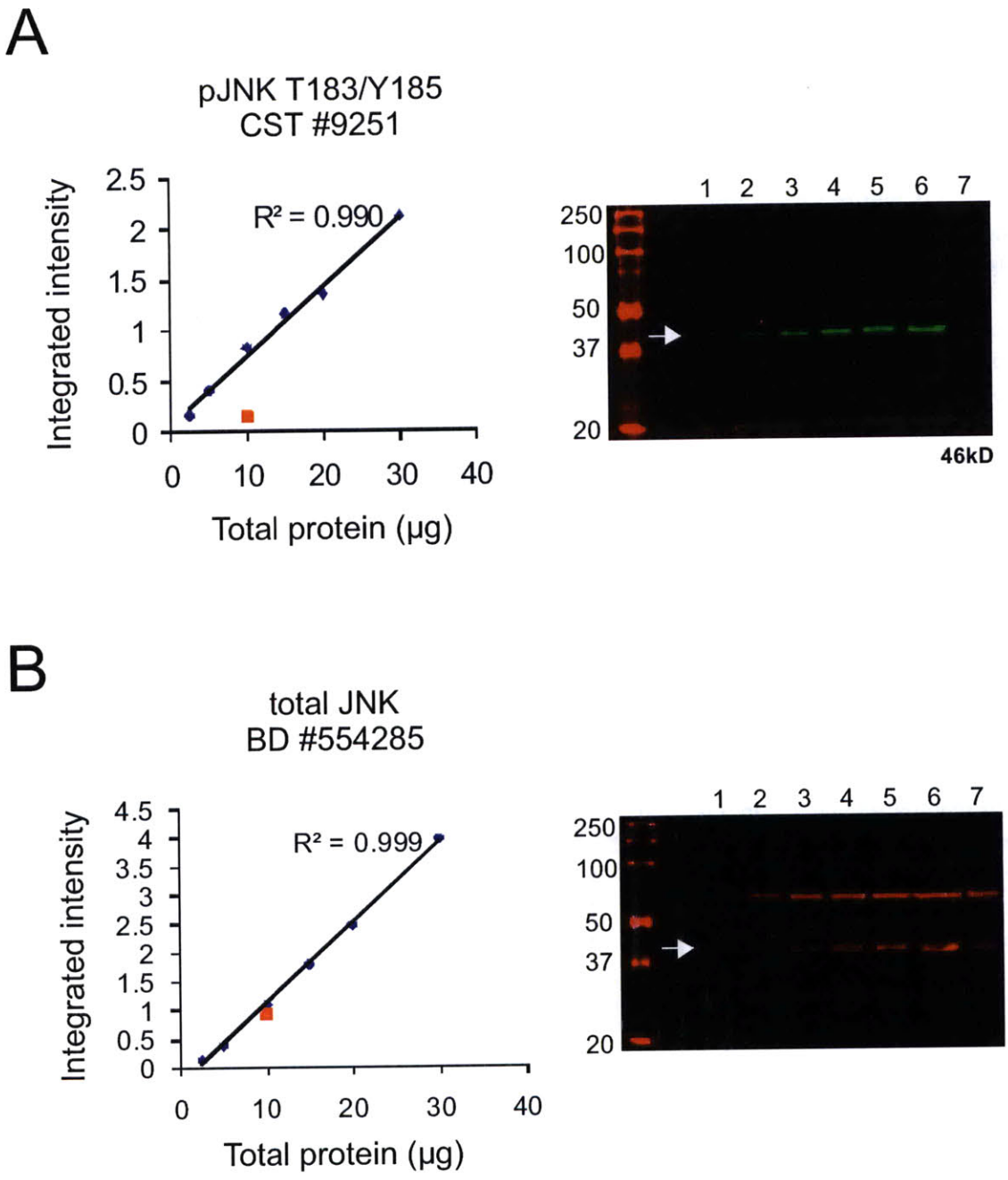


**Figure A1-6.** Quantitative western blots for p-JNK (T183/Y185) (A) and for total JNK (B). For both (A) and (B) blue circles on the plots are signal obtained from positive control lysates; red circles on the plots are signal obtained from negative control lysates. Positive control lysates are extracts from asynchronous U2OS cells treated with UV (50 J/m$^2$) and collected 1 hr later. Negative control lysates are extracts from asynchronous U2OS cells that are untreated and sub-confluent. For both (A) and (B) Lanes 1-6 on membrane images are increasing amounts of total protein loaded from positive control lysates for p-JNK (T183/Y185). Lanes 1-6 are 2.5, 5, 10, 15, 20 and 30 µg of total protein loaded in that order.

Lane 7 is 10 μg of total protein loaded from negative control lysates for p-JNK (T183/Y185). ***(A)*** Signal for p-JNK (T183/Y185) increases in a linear fashion with increasing amounts of total protein loaded (from 2.5-30 μg of total protein loaded) from positive control extracts (blue circles on plot; regression coefficient of 0.99). Signal to background is high (compare blue circle and red circle on plot at 10 ug of total protein loaded) and signal is easy to distinguish by eye at 10 μg of total protein loaded (lane 3 on membrane image). All subsequent measurements of p-JNK were carried out using 10 μg of total protein from the sample lysate and include positive and negative controls on the blot (also 10 μg of total protein loaded) as described here, for comparison and normalization. ***(B)*** Signal for total JNK increases in a linear fashion with increasing amounts of total protein loaded (from 2.5-30 μg of total protein loaded) from positive control extracts (blue circles on plot; regression coefficient of 0.99). 10 ug of total protein loaded from negative control extracts (lane 7 on membrane image) gives the same signal as that obtained from positive control extracts (compare to lane 3 on membrane image), implying that there is no regulation of total levels of protein under these conditions. All subsequent measurements of total JNK were carried out using 10 μg of total protein from the sample lysate and include positive and negative controls on the blot (also 10 μg of total protein loaded) as described here, for comparison and normalization.

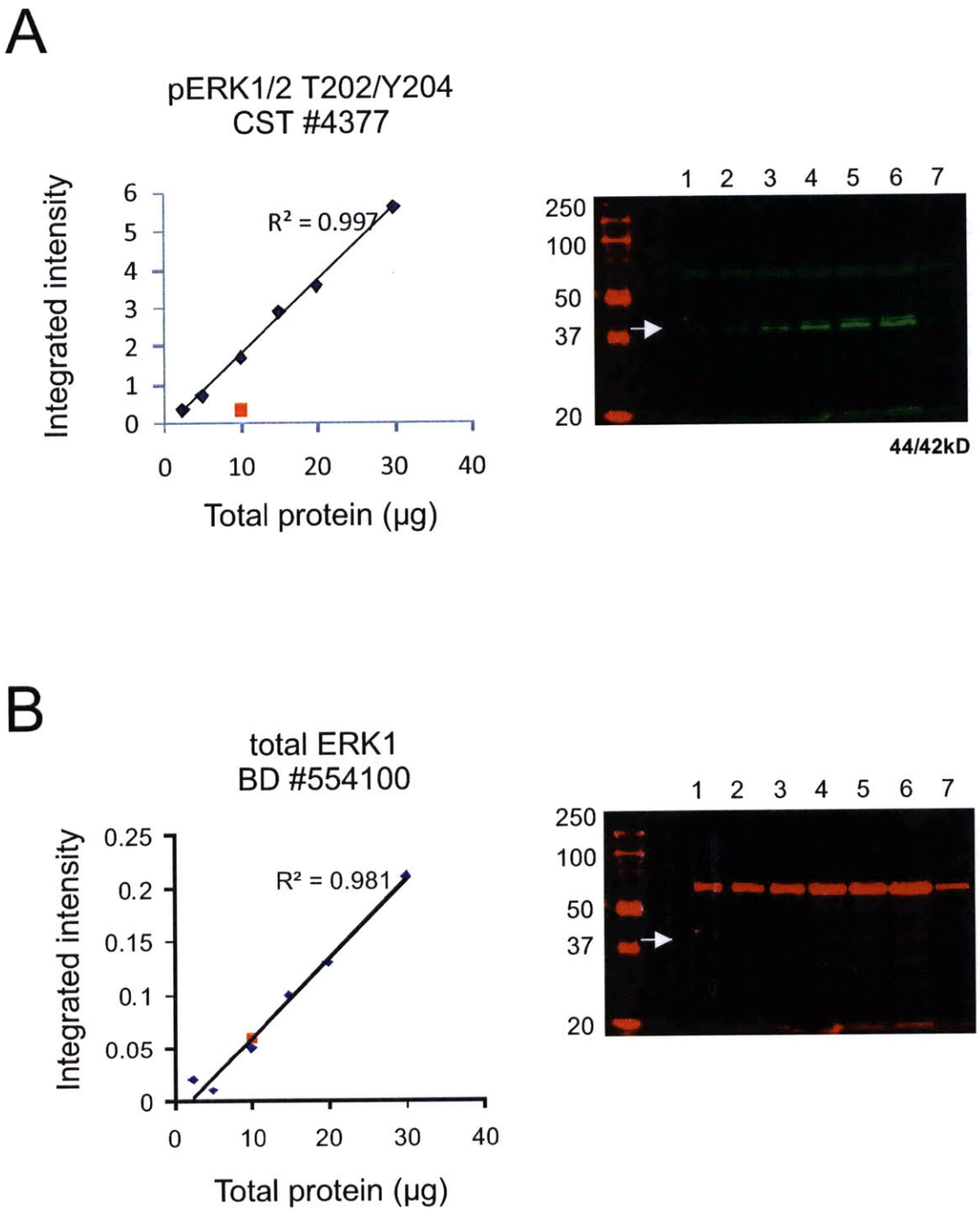


**Figure A1-7.** Quantitative western blots for p-ERK1/2 (T202/Y204) (A) and for total ERK1 (B). For both (A) and (B) blue circles on the plots are signal obtained from positive control lysates; red circles on the plots are signal obtained from negative control lysates. Positive control lysates are extracts from asynchronous U2OS cells serum starved overnight and then placed in 100% FBS for 5 min. Negative control lysates are extracts from asynchronous U2OS cells that are untreated and sub-confluent. For both (A) and (B) Lanes 1-6 on membrane images are increasing amounts of total protein loaded from positive control lysates for p-ERK1/2 (T202/Y204). Lanes 1-6 are 2.5, 5, 10, 15, 20 and 30 µg of total

protein loaded in that order. Lane 7 is 10 μg of total protein loaded from negative control lysates for p-ERK1/2 (T202/Y204). ***(A)*** Signal for p-ERK1/2 (T202/Y204) increases in a linear fashion with increasing amounts of total protein loaded (from 2.5-30 μg of total protein loaded) from positive control extracts (blue circles on plot; regression coefficient of 0.99). Signal to background is high (compare blue circle and red circle on plot at 10 ug of total protein loaded) and signal is easy to distinguish by eye at 10 μg of total protein loaded (lane 3 on membrane image). All subsequent measurements of p-ERK1/2 were carried out using 10 μg of total protein from the sample lysate and include positive and negative controls on the blot (also 10 μg of total protein loaded) as described here, for comparison and normalization. ***(B)*** Signal for total ERK1 increases in a linear fashion with increasing amounts of total protein loaded (from 2.5-30 μg of total protein loaded) from positive control extracts (blue circles on plot; regression coefficient of 0.98). 10 ug of total protein loaded from negative control extracts (lane 7 on membrane image) gives the same signal as that obtained from positive control extracts (compare to lane 3 on membrane image), implying that there is no regulation of total levels of protein under these conditions. All subsequent measurements of total ERK1 were carried out using 10 μg of total protein from the sample lysate and include positive and negative controls on the blot (also 10 μg of total protein loaded) as described here, for comparison and normalization.

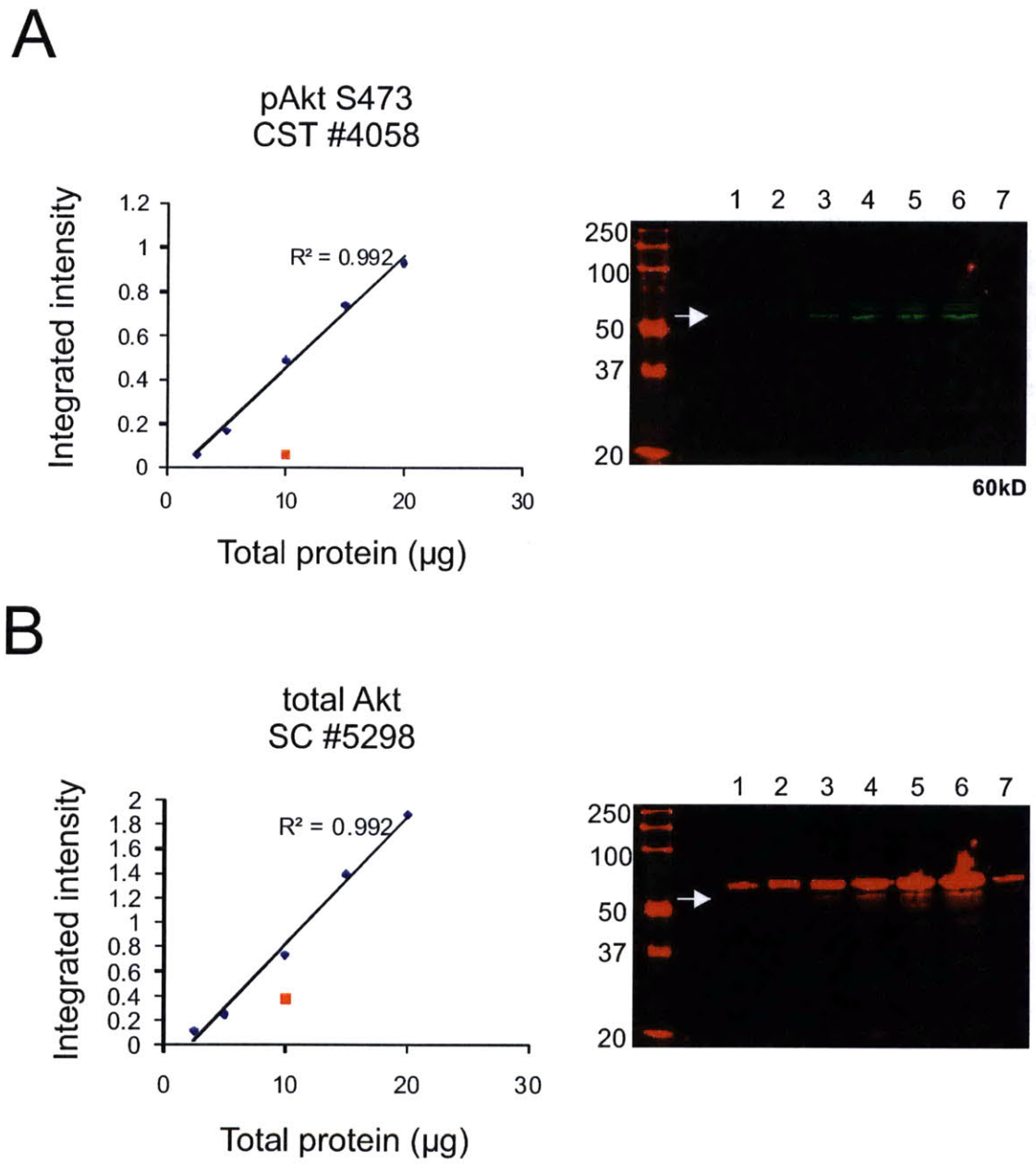


**Figure A1-8.** Quantitative western blots for p-Akt (S473) (A) and for total Akt (B). For both (A) and (B) blue circles on the plots are signal obtained from positive control lysates; red circles on the plots are signal obtained from negative control lysates. Positive control lysates are extracts from asynchronous U2OS cells serum starved overnight and then placed in 100% FBS for 5 min. Negative control lysates are extracts from asynchronous U2OS cells that are untreated and sub-confluent. For both (A) and (B) Lanes 1-6 on membrane images are increasing amounts of total protein loaded from positive control lysates for p-Akt (S473). Lanes 1-6 are 2.5, 5, 10, 15, 20 and 30 µg of total protein loaded in that order. Lane 7 is 10 µg of total protein loaded from negative control lysates for p-Akt (S473). ***(A)*** Signal for p-Akt (S473) increases in a linear fashion with increasing amounts of total protein loaded (from 2.5-20 µg of

total protein loaded) from positive control extracts (blue circles on plot; regression coefficient of 0.99). Signal to background is high (compare blue circle and red circle on plot at 10 ug of total protein loaded) and signal is easy to distinguish by eye at 10 μg of total protein loaded (lane 3 on membrane image). All subsequent measurements of p-Akt were carried out using 10 μg of total protein from the sample lysate and include positive and negative controls on the blot (also 10 μg of total protein loaded) as described here, for comparison and normalization. ***(B)*** Signal for total Akt increases in a linear fashion with increasing amounts of total protein loaded (from 2.5-20 μg of total protein loaded) from positive control extracts (blue circles on plot; regression coefficient of 0.99). 10 ug of total protein loaded from negative control extracts (lane 7 on membrane image) gives a lower signal than that obtained from positive control extracts (compare to lane 3 on membrane image), implying that there may be regulation of total levels of protein under these conditions (up-regulation of total Akt under serum shock conditions). All subsequent measurements of total Akt were carried out using 10 μg of total protein from the sample lysate and include positive and negative controls on the blot (also 10 μg of total protein loaded) as described here, for comparison and normalization.

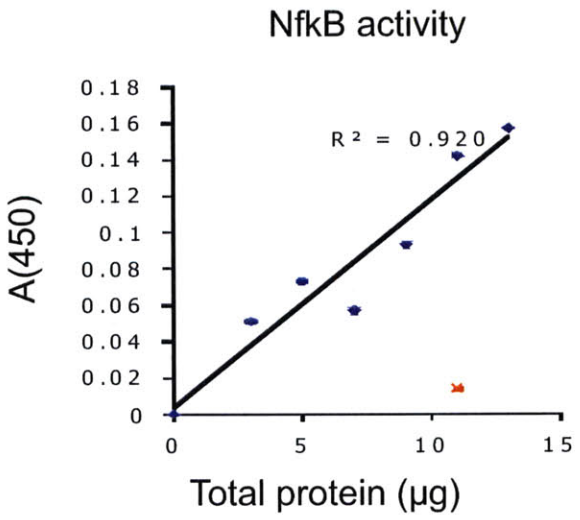


**Figure A1-9.** Plot of ELISA assay validation results for quantification of NFkB activation. Blue circles on the plots are signal obtained from positive control lysates; red circles on the plots are signal obtained from negative control lysates. Positive control lysates are extracts from asynchronous U2OS treated with TNF-α (100 ng/ml) for 30 min. Signal for active NFkB increases in a linear fashion with increasing amounts of total protein loaded (from 3-13.5 µg of total protein loaded) from positive control extracts (blue circles on plot; regression coefficient of 0.92). Signal to background is high (compare blue circle and red circle on plot at 11 ug of total protein loaded) and signal is easy to distinguish by eye at 11 µg of total protein loaded (Data not shown). All subsequent measurements of NFkB activity were carried out using 15 µg of total protein from the sample lysate and include positive and negative controls in the ELISA plate (also 15 µg of total protein loaded) as described here, for comparison and normalization.

# Appendix 2: Chapter 2 Supplementary Figures

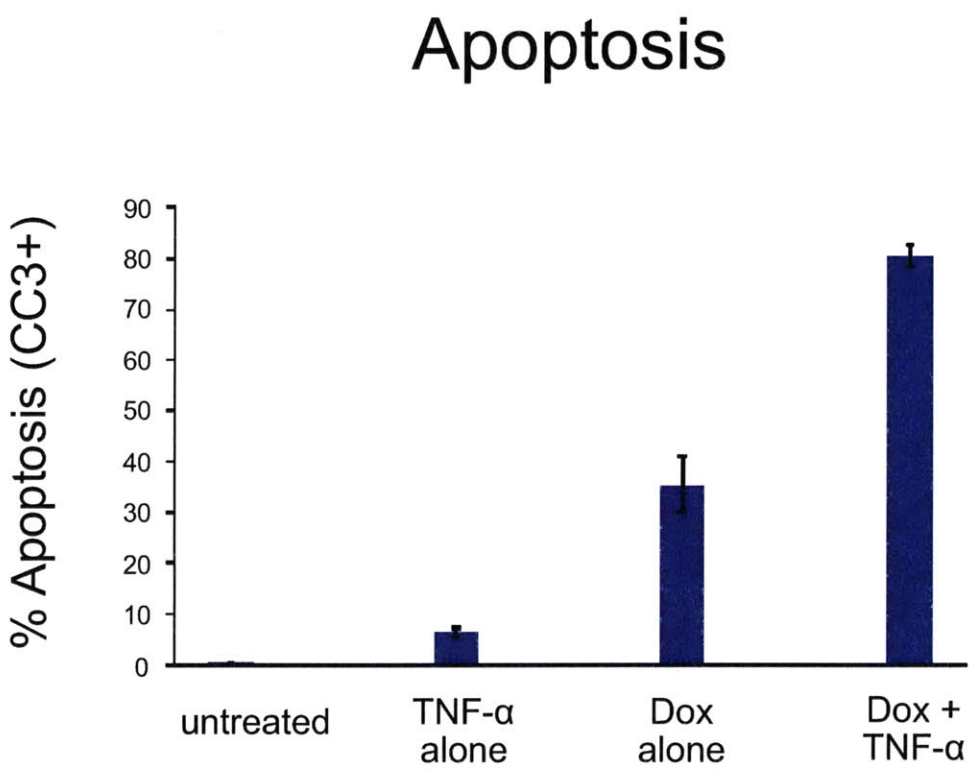


**Supplementary Figure 2-1.** Plot of % of total cell population that is apoptotic at 24 hr following Dox treatment (10 μM) +/- TNF-α (100ng/ml). U2OS cells were treated as described in Figure 2-1 (A). Whole cell samples were collected and fixed at 24 hr following treatment and stained for FACS measurement of cleaved caspase-3 and cleaved Parp. FACS dot plots of cleaved caspase-3 vs. cleaved Parp were gated to distinguish fractions of the total cell population staining positively for one, none or both apoptotic markers, and these gates were subsequently quantified. Here, cells staining positively for the apoptotic marker, CC3+, were considered to be apoptotic.

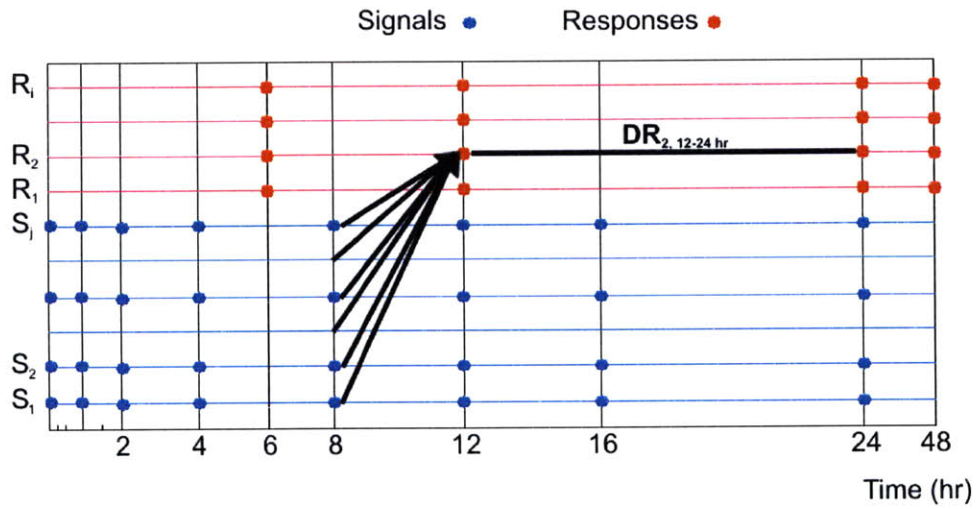


**Supplementary Figure 2-2.** Illustration of the hypothesis that each time-point specific, Time-Interval model in a TI-SWR (Time-Interval Stepwise regression) analysis set makes. In a TI-SWR analysis set, there is one cellular response of interest under investigation and there are as many time- point specific, Time-Interval models in the set as there are time-points at which signaling is measured that precede the cellular response of interest. For each of these time-point specific, Time-Interval models, the response variable is the cellular response under investigation and the possible explanatory variable set includes all of the signaling measurements made at that time point. Here is illustrated a time-point specific, Time-Interval model for which the response variable is the change in the cellular response $R_2$ between 12 and 24 hr and for which the possible explanatory variable set includes all signaling measurements taken at the 8 hr time-point.

A

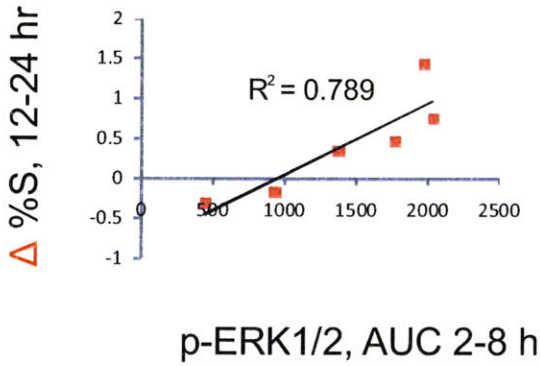


B

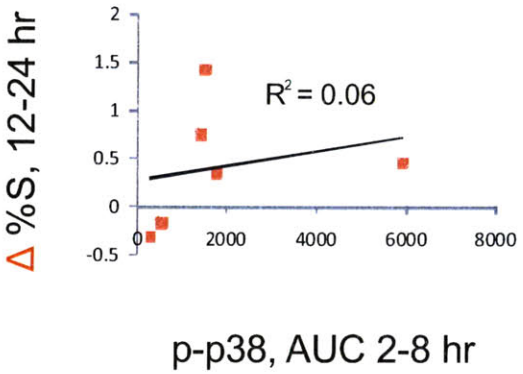


**Supplementary Figure 2-3.** ***(A)*** Regression plot showing the change in the % of the cell-population observed to be in the S phase of the cell-cycle between 12 and 24 hr following treatment (Δ %S, 12-24 hr - the cellular response investigated in the previous TI-SWR analysis) vs. the integrated area under the curve for the measurement of p-ERK1/2 between 2 and 8 hr following treatment (p-ERK1/2, AUC 2-8 hr). The regression coefficient ($R^2$ = 0.789) and the positive slope of the regression line indicates a strong and positive relationship between p-ERK1/2 (2-8 hr following treatment) and the cell-cycle phenotype captured by the change in the percentage of the cell-population in S phase between 12 and 24 hr (Δ %S, 12-24 hr). ***(B)*** Regression plot showing the change in the % of the cell-population observed to be in the S phase of the cell-cycle between 12 and 24 hr following treatment (Δ %S, 12-24 hr - the cellular response investigated in the previous TI-SWR analysis) vs. the integrated area under the curve for the measurement of p-p38 between 2 and 8 hr following treatment (p-p38, AUC 2-8 hr). The regression coefficient ($R^2$ = 0.06) indicates that there is no discernible relationship between p-p38 (2-8 hr following treatment) and the cell-cycle phenotype captured by the change in the percentage of the cell-population in S phase between 12 and 24 hr (Δ %S, 12-24 hr).

A

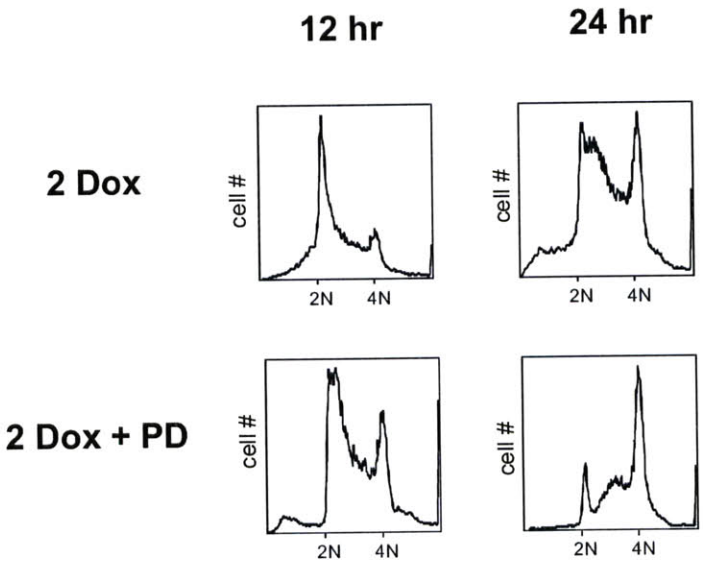


B

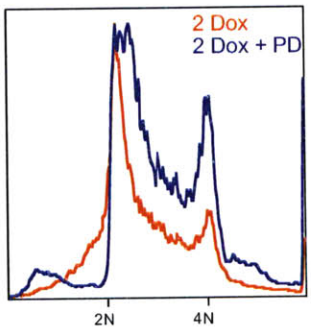


**Supplementary Figure 2-4.** ***(A)*** Cell-cycle profiles of U2OS cell-populations treated with Dox (2 μM) alone (upper boxes) or with Dox (2 μM) plus PD98059 (20 μM) (lower boxes) at 12 and 24 hr following treatment. Populations treated with Dox alone show a clear build-up in early/mid-S phase population by 24 hr following treatment. Populations treated with Dox plus PD show a clear build-up in early-S phase population by 12 hr following treatment, but by 24 hr following treatment, this built-up population has progressed through S phase and is observed to be in mid/late-S phase. ***(B)*** Overlay of a cell-cycle profile of U2OS cell-populations treated with Dox (2 μM) alone (red trace) or with Dox (2 μM) plus PD98059 (20 μM) (blue trace) at 12 hr following treatment. There is a clear build-up in early-S phase population in populations treated with Dox plus PD as compared to populations treated with Dox alone. This build-up is a "shoulder" off of the G1 peak of the cell-cycle profile.

A

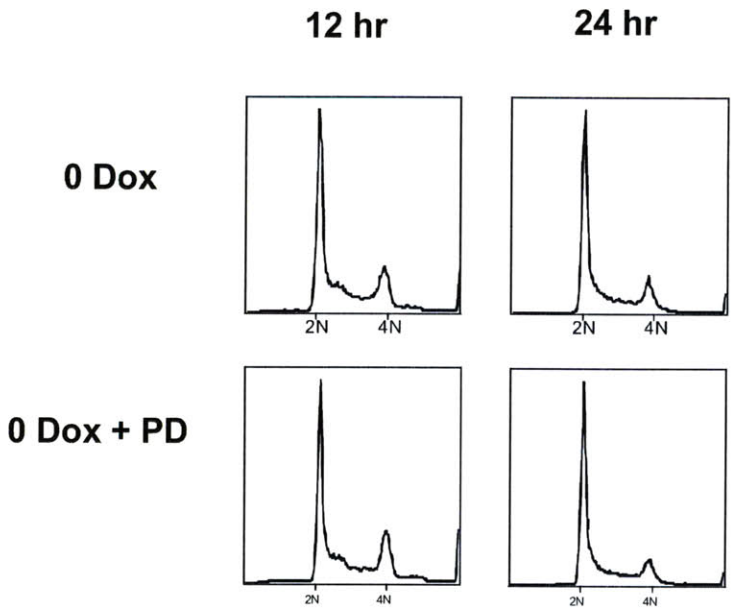


B

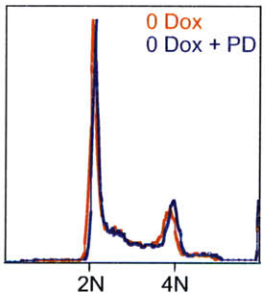


**Supplemenary Figure 2-5.** ***(A)*** Cell-cycle profiles of U2OS cell-populations treated with carrier alone (upper boxes) or treated with carrier plus PD98059 (20 μM) (lower boxes) at 12 and 24 hr following treatment. Populations treated with carrier plus PD show no discernible differences in cell-cycle profile as compared to populations treated with carrier alone, at 12 or 24 hr following treatment. ***(B)*** Overlay of a cell-cycle profile of U2OS cell-populations treated with carrier alone (red trace) or with carrier plus PD98059 (20 μM) (blue trace) at 12 hr following treatment. Cell-cycle profiles for populations treated with carrier alone or with carrier plus PD almost exactly overlay.

A

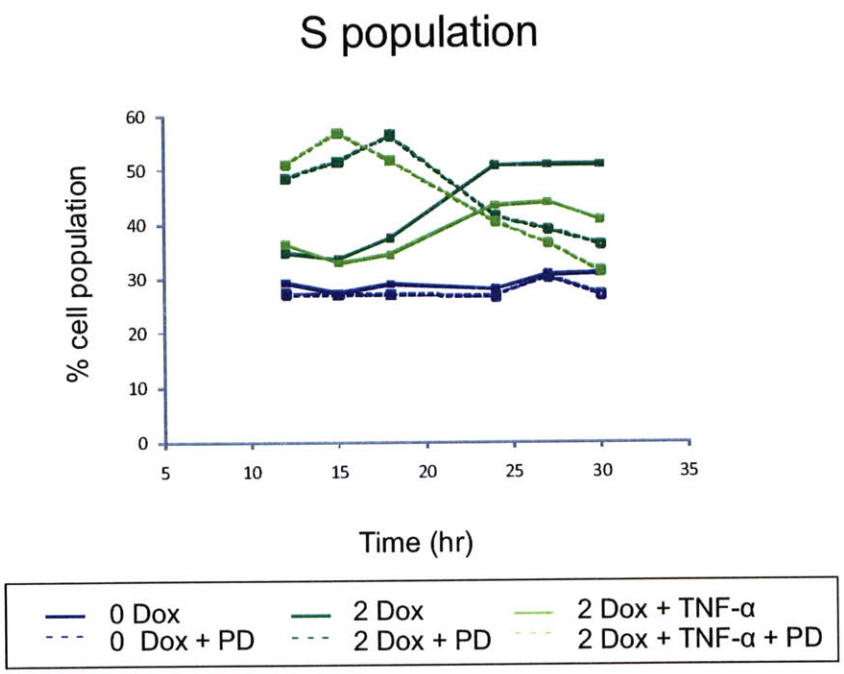


B

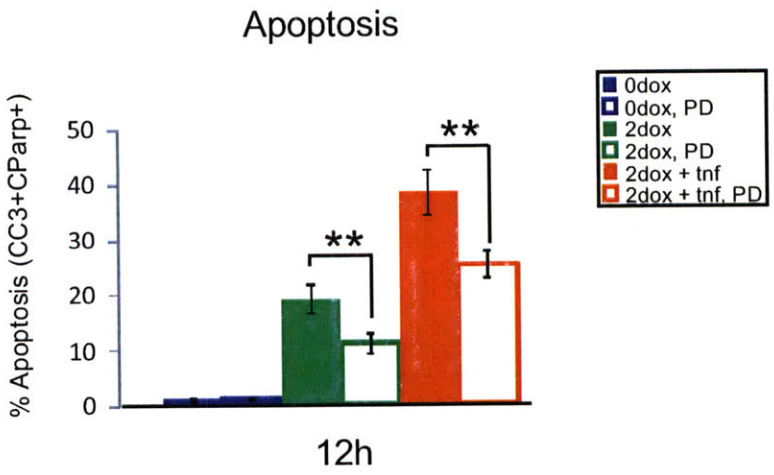


**Supplementary Figure 2-6.** ***(A)*** A plot of the % of the total cell population that is observed to be in the S phase of the cell-cycle at 12, 15, 18, 24, 27 and 30 hr following treatment with 2 μM Dox +/- PD98059 (dark green dash and solid lines respectively), 2 μM Dox + TNF-α (100ng/ml) +/- PD98059 (light green dash and solid lines respectively) or carrier (0 μM Dox) +/- PD98059 (blue dash and solid lines respectively). PD98059 added simultaneously with Dox treatment. There is a build-up in the S phase of the cell-cycle by 24 hr following treatment with Dox or Dox plus TNF-α. The build-up in S phase is smaller in magnitude in populations treated with Dox plus TNF-α as compared to populations treated

with Dox alone. When PD98059 is added simultaneously with Dox to populations treated with Dox alone, the population that builds up in S phase does so earlier than in the absence of PD98059 (by 12-15 hr following treatment), and the population build-up is of roughly equal magnitude. When PD98059 is added simultaneously with Dox to populations treated with Dox plus TNF-α, the population that builds up in S phase also does so earlier than in the absence of PD98059 (by 12-15 hr following treatment), but the population build-up is greater in magnitude than it is in the absence of PD98059, and is roughly equal in magnitude to that observed in populations treated with Dox alone. ***(B)*** A plot of the % of the total cell population that is observed to be apoptotic at 12 hr following treatment with 2 μM Dox +/- TNF-α and +/- PD98059 (20 μM), added simultaneously with Dox. U2OS cells were treated as described in Figure 2-9A. Whole cell samples were collected and fixed at 12 hr following treatment and stained for FACS measurement of cleaved caspase-3 and cleaved Parp. FACS dot plots were gated to distinguish fractions of the total cell population staining positively for one, none or both apoptotic markers, and these gates were subsequently quantified. Here, cells staining positively for both apoptotic markers (CC3+CParp+) were considered to be apoptotic.

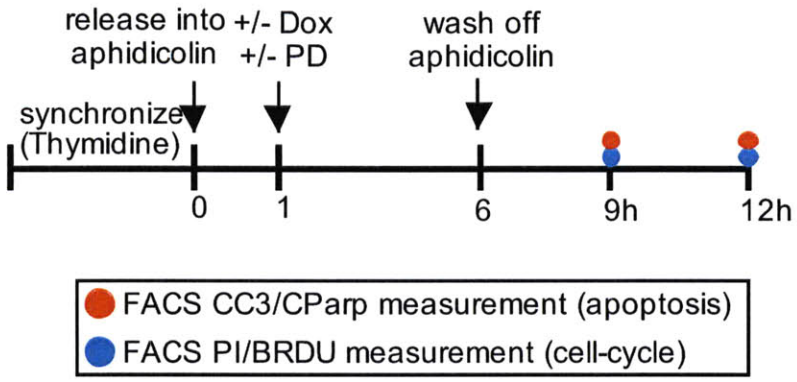


**Supplementary Figure 2-7.** Experimental time-line for Future Experiment #1 which aims to provide further evidence that ERK1/2 acts in G1 or at the G1/S transition to promote maintenance of a cell-cycle check-point following DNA damage. U2OS cells will be synchronized in late G1 via a double thymidine block and released directly into fresh media containing aphidicolin to prevent progression into S phase. One hour following release into aphidicolin, cells will be treated +/- Dox (2 μM) and +/- PD98059 (20 μM). At 4 hr following treatment, media will be aspirated and replaced with media containing 1% FBS, +/- PD98059 according to whether PD98059 was present prior to media replacement, and aphidicolin. At 6 hr following treatment, media will be aspirated and replaced with media containing 1% FBS ***without aphidicolin***, to allow progression into S phase. Whole cell samples will be collected and fixed at 9 and 12 hr following treatment and stained for FACS measurement of cell-cycle profile and apoptosis. We expect that, over the course of this experiment, we ***will not*** see substantial progression of the cell population that was treated with Dox in late G1, from late G1 into S phase. We also expect that, over the course of this experiment, we ***will*** see substantial progression of the cell population that was treated with Dox plus PD98059 in late G1, from late G1 into S phase.

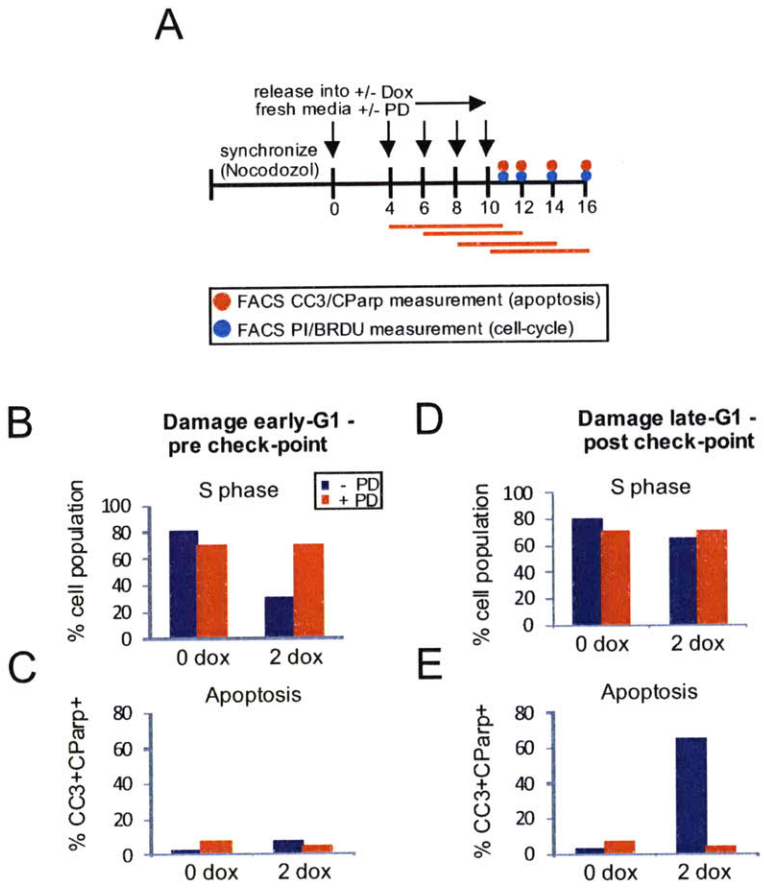


**Supplementary Figure 2-8.** ***(A)*** Experimental time-line for Future Experiment #2, which aims to provide evidence either for or against the cell-cycle context dependent model for ERK1/2 role-switching between promotion of maintenance of a cell-cycle check-point and promotion of apoptosis following DNA damage presented in Figure 2-9 (E). U2OS cells will be synchronized in metaphase via a nocodazol arrest and mitotic shake-off, replated in fresh media and incubated for 4 hr to allow progression into early G1. Cells will be treated +/- Dox and +/- PD98059 at 4, 6, 8 or 10 hr following re-plating, and whole cell sample will be collected, fixed and stained for measurement of cell-cycle profile and apoptosis 6 hr following treatment. ***(B)-(C)*** Hypothetical data for cell populations treated in early G1 (pre- cell cycle check-point), if the cell-cycle context dependent model is true. Plots of % of the cell population in S phase (B) and % of the cell population that is apoptotic (C). We expect a robust cell-cycle phenotype (cell-cycle checkpoint in G1 or at the G1/S transition) in populations treated with Dox, and that this check-point can be overcome by addition of PD98059. We also expect minimal apoptosis in populations treated with Dox. ***(D)-(E)*** Hypothetical data for cell populations treated in late G1 (post- cell cycle check-point), if the cell-cycle context dependent model is true. Plots of % of the cell population in S phase (D) and % of the cell population that is apoptotic (E). We expect a minimal cell-cycle phenotype (cell-cycle checkpoint in G1 or at the G1/S transition) in populations treated with Dox. We also expect signigicant apoptosis in populations treated with Dox, and that this apoptotic phenotype can be largely overcome by addition of PD98059.

# Appendix 3: Chapter 3 Supplementary Figures

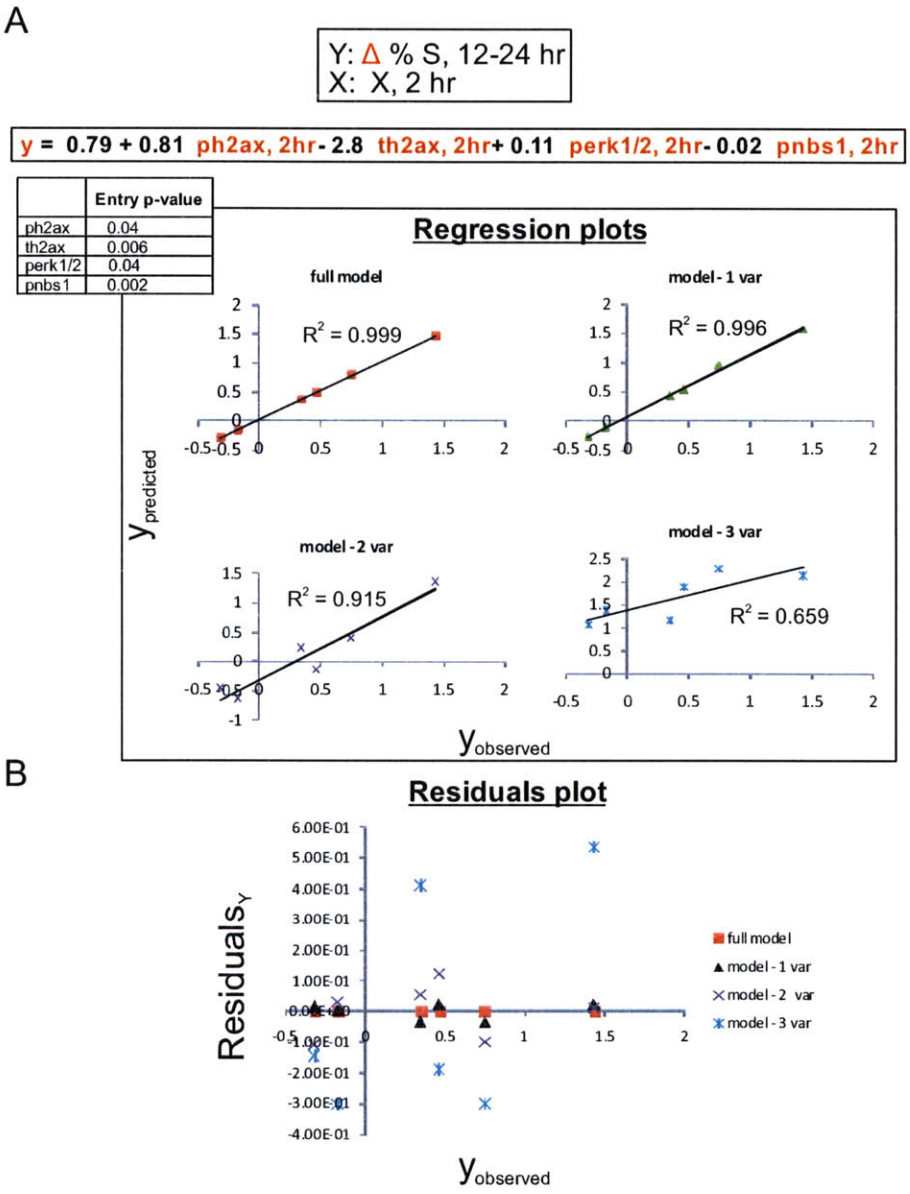


**Supplementary Figure 3-1.** ***(A)*** Full model equation and regression plots for the 2 hr time-point specific, Time-Interval model from the TI-SWR analysis set investigating the change in the percentage of the cell-population in S phase between 12 and 24 hr following treatment (Δ %S, 12-24 hr) as the response variable. The full model as determined by a Stepwise regression algorithm includes 4 signals and these ***signals are listed in decreasing order of $R^2$ (ability to explain variability in the response variable) in the full model equation***. The regression plot for the full model, the model minus one

variable ("model – 1 var"), the model minus two variables ("model – 2 var"), and the model minus three variables ("model – 3 var") is shown where variables are subtracted in order, starting with the signal with the lowest $R^2$. ***(B)*** Residuals plot for the 2 hr time-point specific, Time-Interval model.

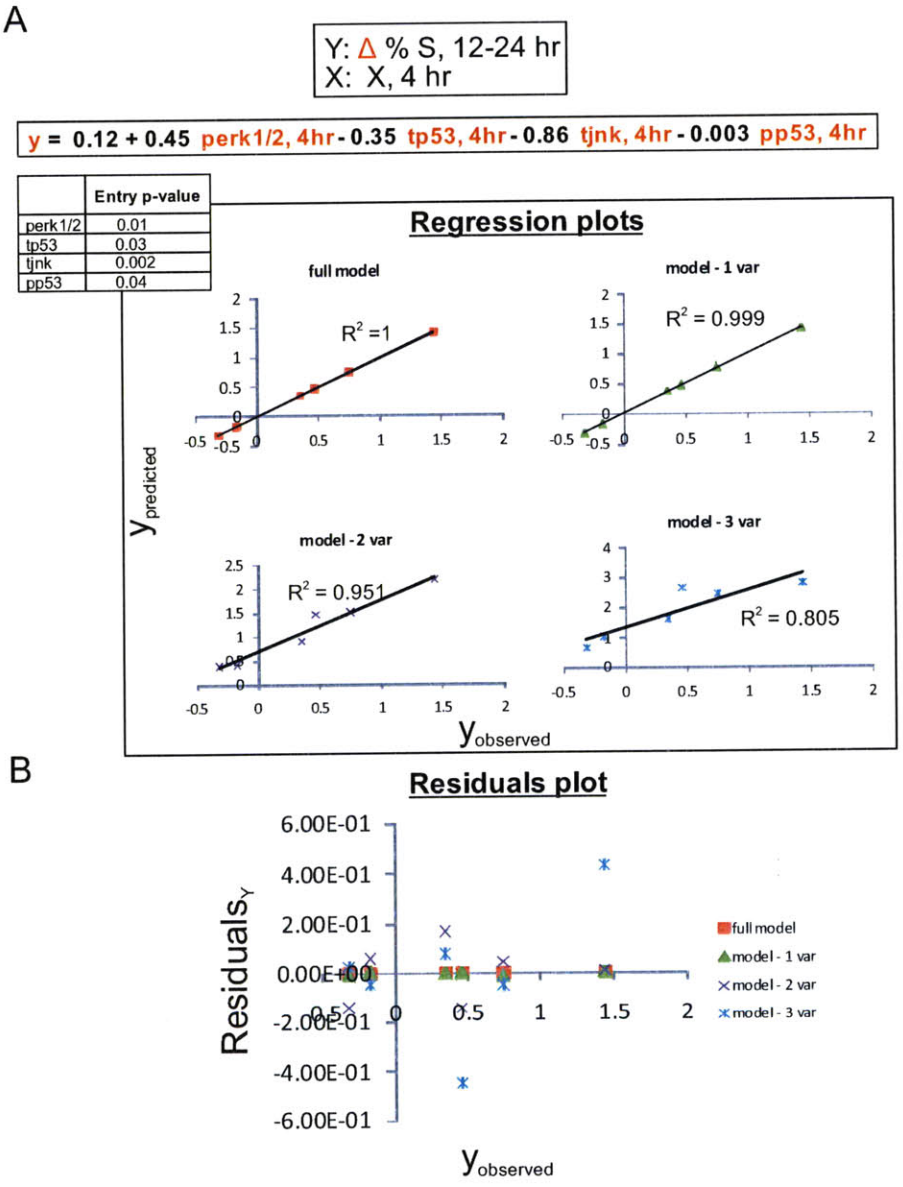


**Supplementary Figure 3-2.** ***(A)*** Full model equation and regression plots for the 4 hr time-point specific, Time-Interval model from the TI-SWR analysis set investigating the change in the percentage of the cell-population in S phase between 12 and 24 hr following treatment (Δ %S, 12-24 hr) as the response variable. The full model as determined by a Stepwise regression algorithm includes 4 signals and these ***signals are listed in decreasing order of $R^2$ (ability to explain variability in the response***

***variable) in the full model equation***. The regression plot for the full model, the model minus one variable ("model – 1 var"), the model minus two variables ("model – 2 var"), and the model minus three variables ("model – 3 var") is shown where variables are subtracted in order, starting with the signal with the lowest $R^2$. ***(B)*** Residuals plot for the 4 hr time-point specific, Time-Interval model.

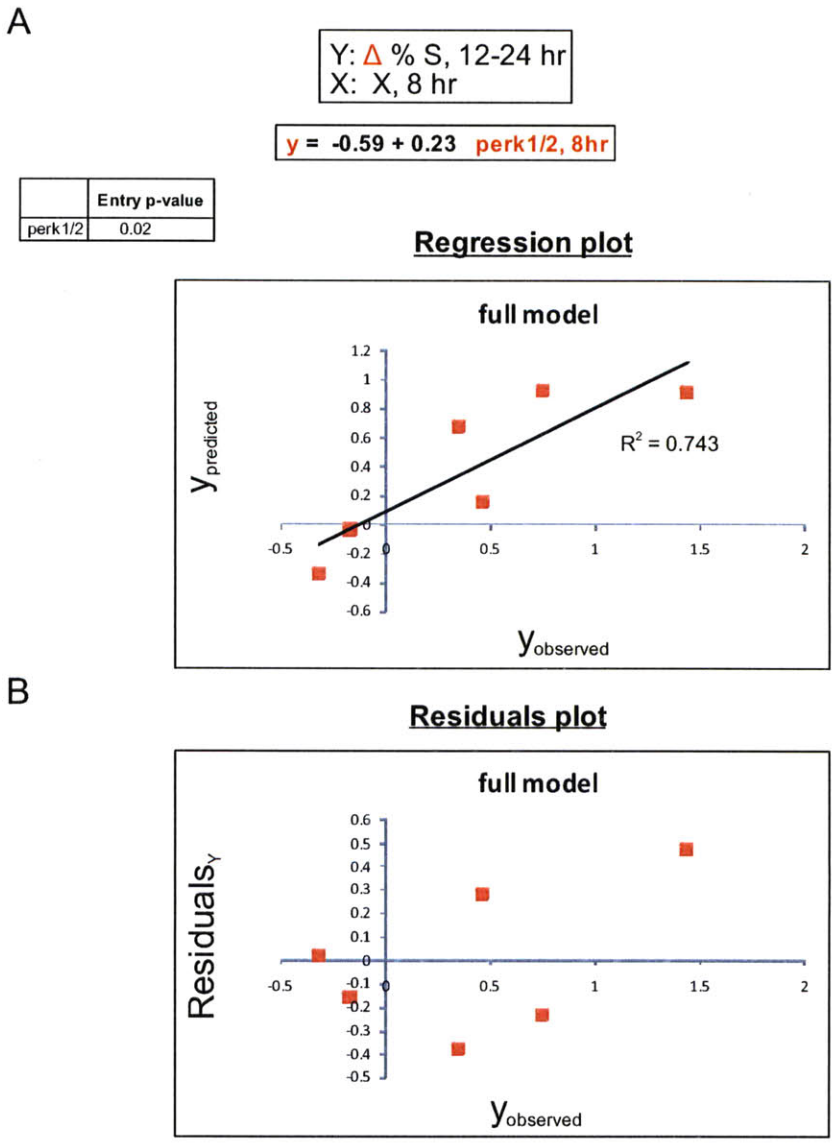


**Supplementary Figure 3-3.** ***(A)*** Full model equation and regression plots for the 8 hr time-point specific, Time-Interval model from the TI-SWR analysis set investigating the change in the percentage of the cell-population in S phase between 12 and 24 hr following treatment (Δ %S, 12-24 hr) as the response variable. The full model as determined by a Stepwise regression algorithm includes only one

signal. The regression plot for the full model is shown. ***(B)*** Residuals plot for the 8 hr time-point specific, Time-Interval model.

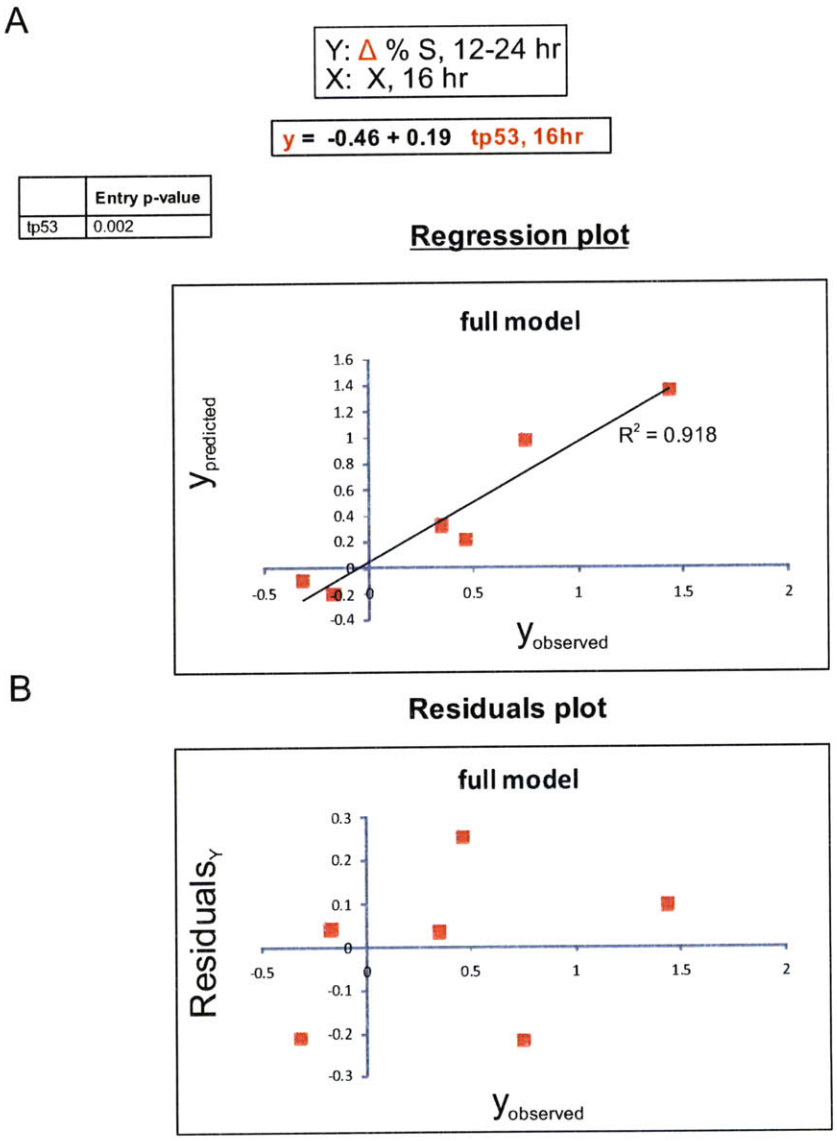


**Supplementary Figure 3-4.** ***(A)*** Full model equation and regression plots for the 16 hr time-point specific, Time-Interval model from the TI-SWR analysis set investigating the change in the percentage of the cell-population in S phase between 12 and 24 hr following treatment (Δ %S, 12-24 hr) as the response variable. The full model as determined by a Stepwise regression algorithm includes only one signal. The regression plot for the full model is shown. ***(B)*** Residuals plot for the 16 hr time-point specific, Time-Interval model.

A

Y: Δ % S, 12-24 hr
X: X, 24 hr

y = -0.46 + 0.34 tp53, 24hr

| | Entry p-value |
|---|---|
| tp53 | 0.02 |

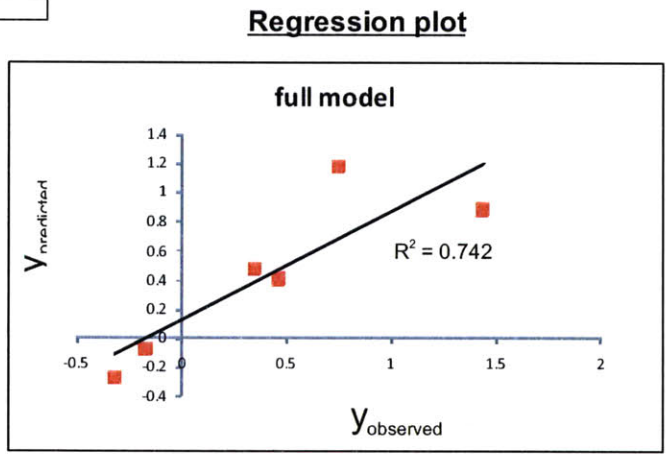


B

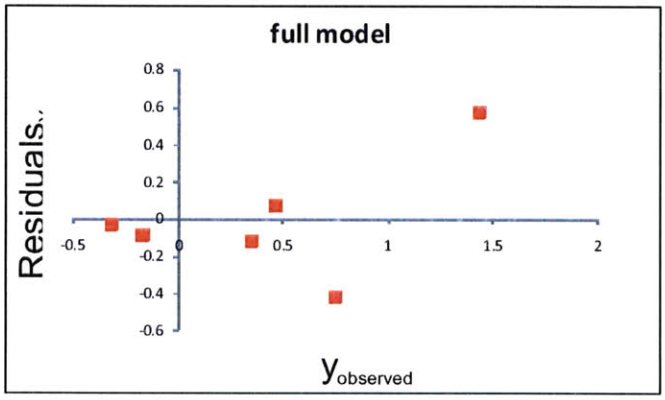


**Supplementary Figure 3-5.** ***(A)*** Full model equation and regression plots for the 24 hr time-point specific, Time-Interval model from the TI-SWR analysis set investigating the change in the percentage of the cell-population in S phase between 12 and 24 hr following treatment (Δ %S, 12-24 hr) as the response variable. The full model as determined by a Stepwise regression algorithm includes only one signal. The regression plot for the full model is shown. ***(B)*** Residuals plot for the 24 hr time-point specific, Time-Interval model.

A

Y: Δ % S, 12-24 hr
X: X, combined time-point

| | Time-point | $R^2$ |
|---|---|---|
| ph2ax | 2 hr | 0.65 |
| th2ax | 2 hr | 0.26 |
| perk1/2 | 4 hr | 0.80 |
| tp53 | 4 h | 0.151 |
| perk1/2 | 8 hr | 0.74 |
| tp53 | 16 hr | 0.91 |

**y = -0.46 + 0.18 tp53, 16hr**

| | Entry p-value |
|---|---|
| tp53, 16hr | 0.002 |

**Regression plot**

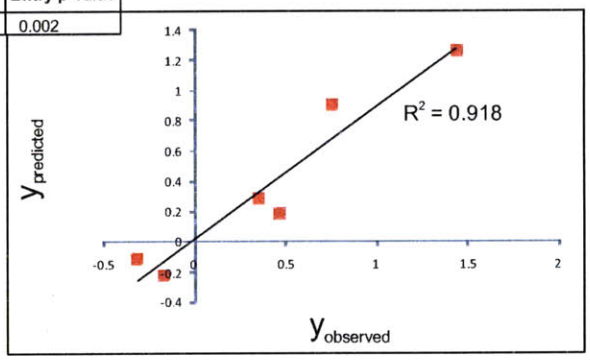


B

**Residuals plot**

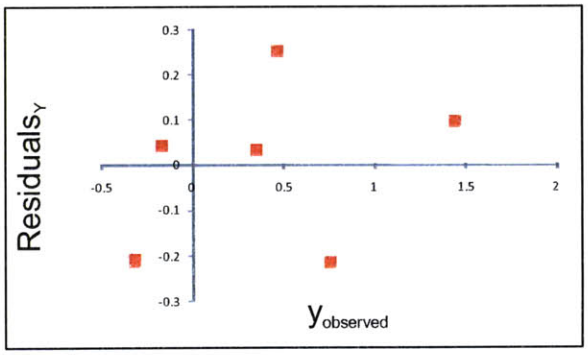


**Supplementary Figure 3-6.** ***(A)*** Full model equation and regression plots for a combined time-point model using top signal correlates from the TI-SWR analysis set investigating the change in the percentage of the cell-population in S phase between 12 and 24 hr following treatment (Δ %S, 12-24 hr) as the response variable, as the potential explanatory variable set. The full potential explanatory variable set is listed (top table) along with the $R^2$ of each within the time-point specific model in which they were determined to be top signal correlates with the cellular response of interest. The response variable for this model is Δ %S, 12-24 hr. The full model as determined by a Stepwise regression algorithm includes only one signal. The regression plot for the full model is shown. ***(B)*** Residuals plot for the "combined time-point" model.

A

Y: Δ % S, 12-24 hr
X: X, combined time-point

| | Time-point | $R^2$ |
|---|---|---|
| ph2ax | 2 hr | 0.65 |
| perk1/2 | 4 hr | 0.80 |
| perk1/2 | 8 hr | 0.74 |
| tp53 | 16 hr | 0.91 |

**OLS**

y = -0.62 - 0.26 ph2ax, 2hr
+ 0.17perk1/2, 4 hr
- 0.01perk1/2, 8 hr
+ 0.15tp53, 16 hr

| $R^2$ | F stat | p val |
|---|---|---|
| 0.97 | 10.3 | 0.22 |

B

Y: tp53, 16 hr
X: perk1/2, 8 hr

**OLS**

y = -0.58 + 1.2 perk1/2, 8hr

| $R^2$ | F stat | p val |
|---|---|---|
| 0.78 | 14.6 | 0.01 |

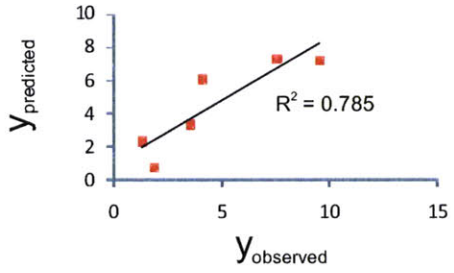


**Supplementary Figure 3-7.** ***(A)*** Full model equation for a combined time-point model using top signal correlates from the TI-SWR analysis set investigating the change in the percentage of the cell-population in S phase between 12 and 24 hr following treatment (Δ %S, 12-24 hr) as the response variable, as the explanatory variable set. A subset has been chosen to decrease the number of potential explanatory variables to be less that the number of observations in the dataset (6 observations). The full explanatory variable set is listed (top table) along with the $R^2$ of each within the time-point specific model in which they were determined to be top signal correlates with the cellular response of interest. The response variable for this model is Δ %S, 12-24 hr. The full model as determined by OLS (Ordinary Least squares) regression does not reach a required level of significance ($p<0.05$). ***(B)*** Model equation and regression plot for a regression model relating two of the potential explanatory signal measurements in the "combined time-point" model investigating Δ %S, 12-24 hr (Response variable is total p53 at 16 hr; explanatory variable is p-ERK1/2 at 8 hr). A high degree of collinearity is demonstrated between the two signal measurements.

A

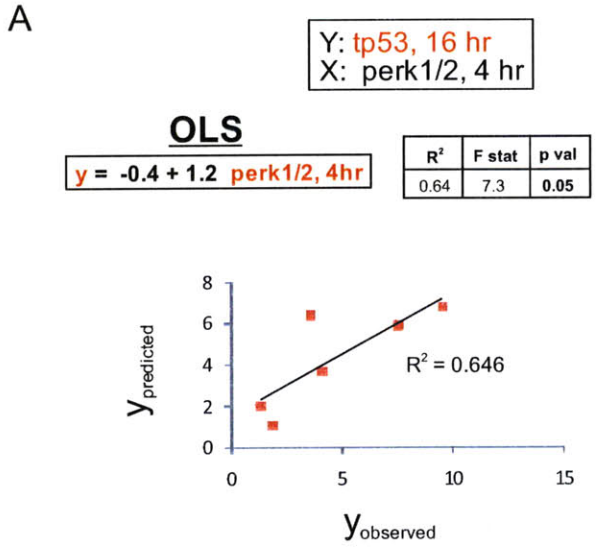


B

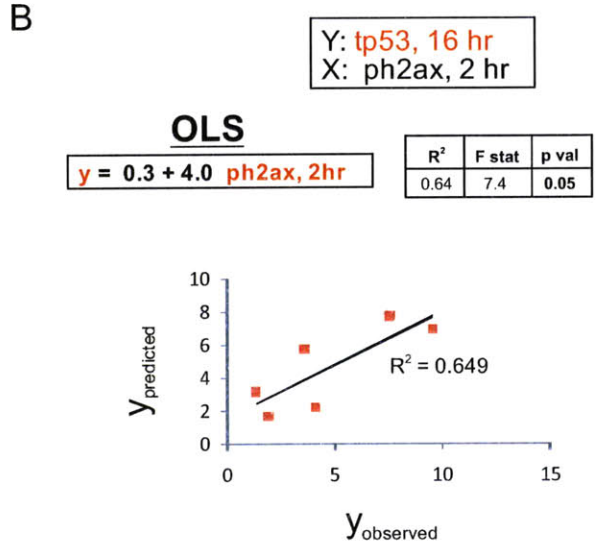


**Supplementary Figure 3-8.** ***(A)*** Model equation and regression plot for a regression model relating two of the potential explanatory signal measurements in the "combined time-point" model investigating Δ %S, 12-24 hr. (Response variable is total p53 at 16 hr; explanatory variable is p-ERK1/2 at 4 hr). A high degree of collinearity is demonstrated between the two signal measurements. ***(B)*** Model equation and regression plot for a regression model relating two of the potential explanatory signal measurements in the "combined time-point" model investigating Δ %S, 12-24 hr (Response variable is total p53 at 16 hr, explanatory variable is p-H2AX at 2 hr). A high degree of collinearity is demonstrated between the two signal measurements.

A

Y: Δ % CC3+CParp+, 6-12 hr
X: X, 0.25 hr

y = -2.3 + 5.2 pakt, 0.25hr

| | Entry p-value |
|---|---|
| pakt | 0.02 |

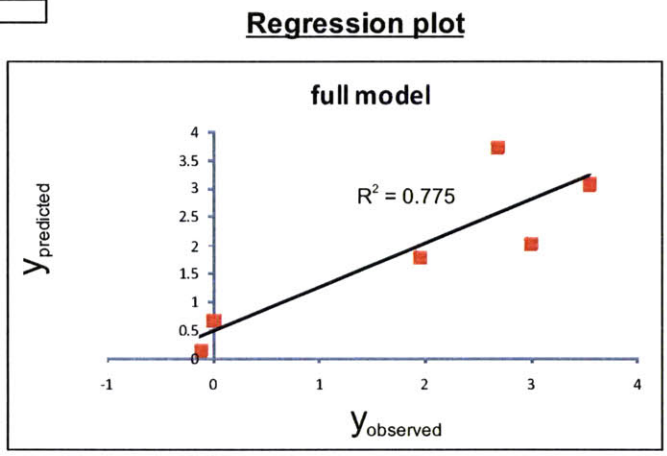


B

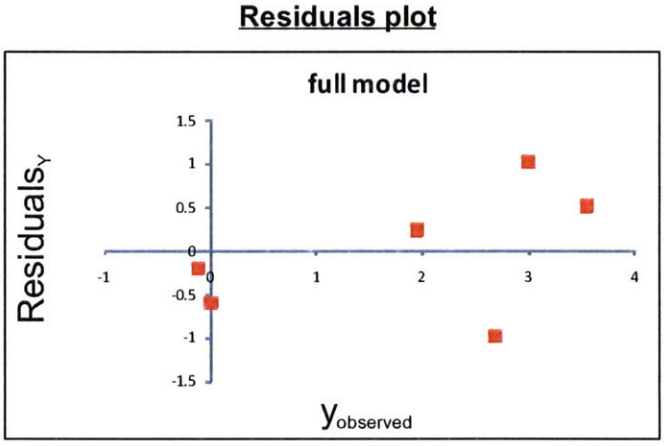


**Supplementary Figure 3-9.** ***(A)*** Full model equation and regression plots for the 0.25 hr time-point specific, Time-Interval model from the TI-SWR analysis set investigating the change in the percentage of apoptosis in the cell-population between 6 and 12 hr following treatment (Δ %apoptosis (CC3+CParp+), 6-12 hr) as the response variable. The full model as determined by a Stepwise regression algorithm includes only one signal. The regression plot for the full model is shown. ***(B)*** Residuals plot for the 0.25 hr time-point specific, Time-Interval model.

A

Y: Δ % CC3+CParp+, 6-12 hr
X: X, 4 hr

y = -1.3 + 2.1 pakt, 4hr

| | Entry p-value |
|---|---|
| pakt | 0.003 |

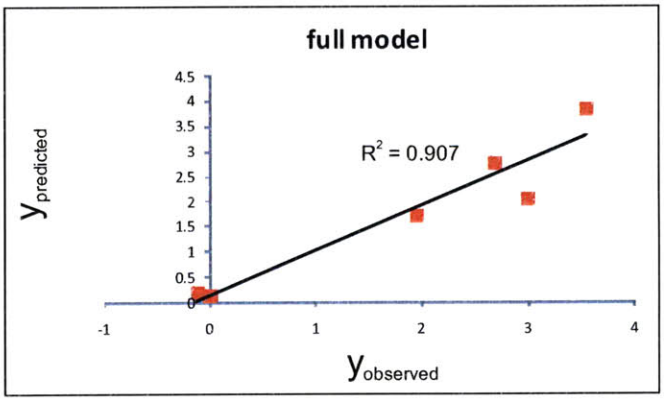


B

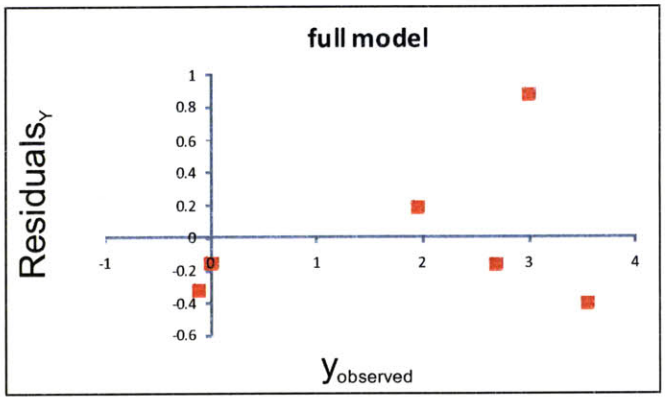


**Supplementary Figure 3-10.** ***(A)*** Full model equation and regression plots for the 4 hr time-point specific, Time-Interval model from the TI-SWR analysis set investigating the change in the percentage of apoptosis in the cell-population between 6 and 12 hr following treatment (Δ %apoptosis (CC3+CParp+), 6-12 hr) as the response variable. The full model as determined by a Stepwise regression algorithm includes only one signal. The regression plot for the full model is shown. ***(B)*** Residuals plot for the 4 hr time-point specific, Time-Interval model.

A

Y: Δ % CC3+CParp+, 6-12 hr
X: X, 8 hr

y = -2.2 + 0.10 pp53, 8hr+3.1 tjnk, 8hr

| | Entry p-value |
|---|---|
| pp53 | 0.002 |
| tjnk | 0.01 |

**Regression plots**

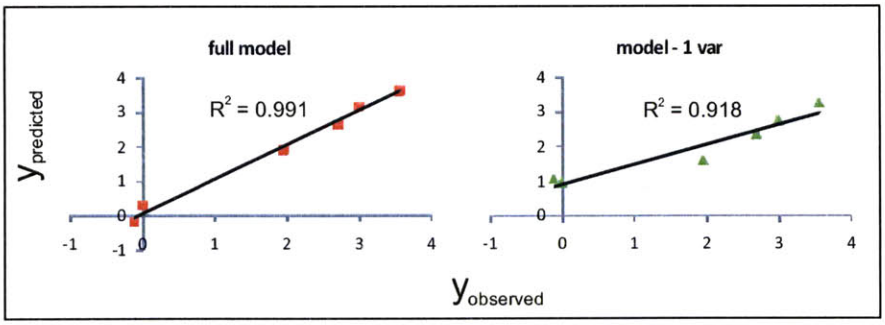


B

**Residuals plot**

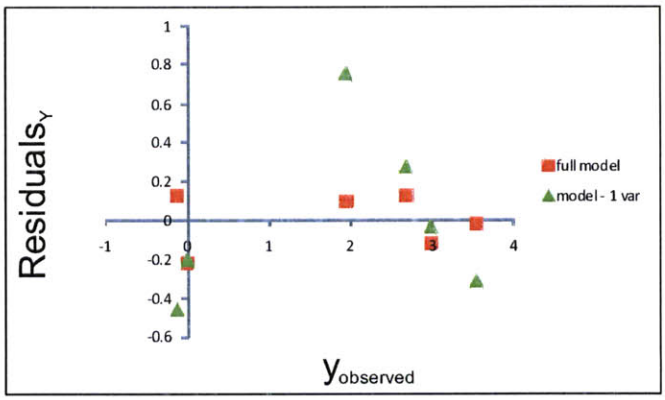


**Supplementary Figure 3-11.** ***(A)*** Full model equation and regression plots for the 8 hr time-point specific, Time-Interval model from the TI-SWR analysis set investigating the change in the percentage of apoptosis in the cell-population between 6 and 12 hr following treatment (Δ %apoptosis (CC3+CParp+), 6-12 hr) as the response variable. The full model as determined by a Stepwise regression algorithm includes 2 signals and these ***signals are listed in decreasing order of $R^2$ (ability to explain variability in the response variable) in the full model equation***. The regression plot for the full model and the model minus one variable ("model – 1 var") is shown where variables are subtracted starting with the signal with the lowest $R^2$. ***(B)*** Residuals plot for the 8 hr time-point specific, Time-Interval model.

A

Y: Δ % CC3+CParp+, 6-12 hr
X: X, 12 hr

y = -0.6 + 0.46 perk1/2, 12hr

| | Entry p-value |
|---|---|
| perk1/2 | 0.01 |

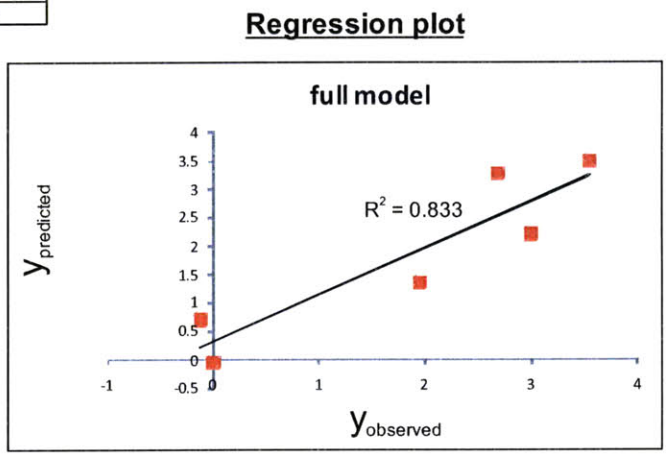


B

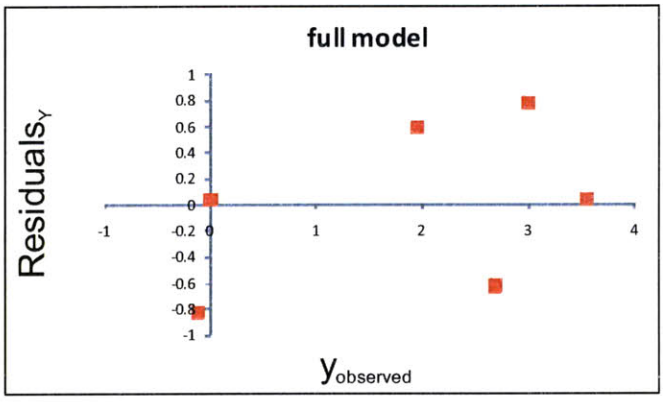


**Supplementary Figure 3-12.** ***(A)*** Full model equation and regression plots for the 12 hr time-point specific, Time-Interval model from the TI-SWR analysis set investigating the change in the percentage of apoptosis in the cell-population between 6 and 12 hr following treatment (Δ %apoptosis (CC3+CParp+), 6-12 hr) as the response variable. The full model as determined by a Stepwise regression algorithm includes only one signal. The regression plot for the full model is shown. ***(B)*** Residuals plot for the 12 hr time-point specific, Time-Interval model.

A

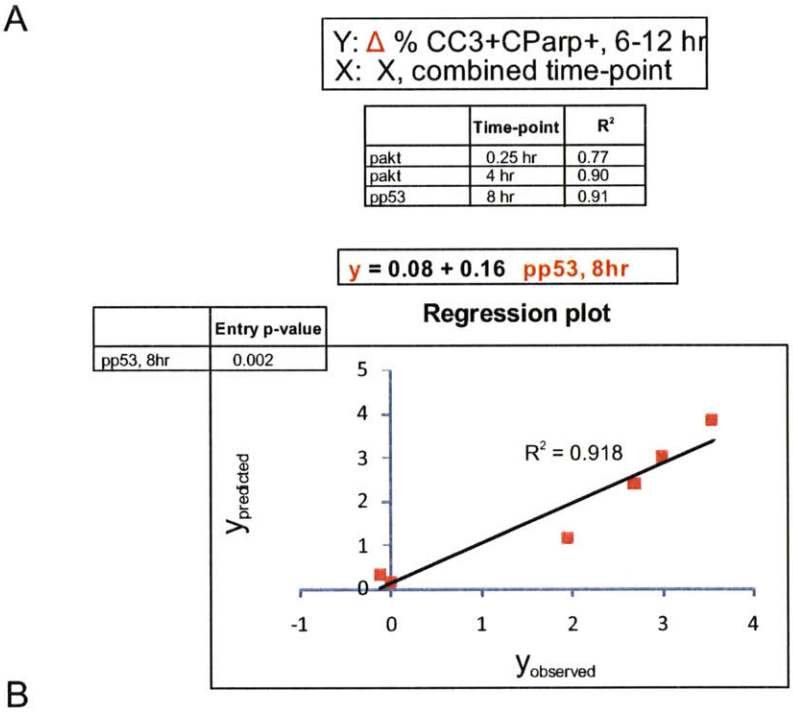


B

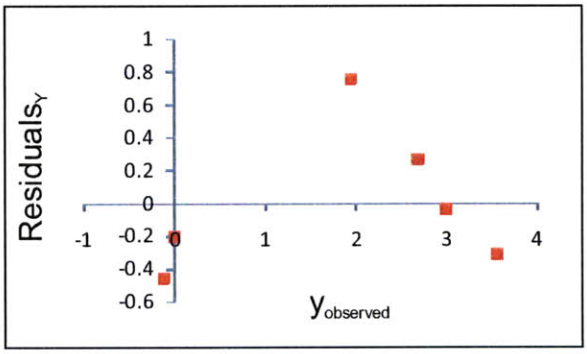


**Supplementary Figure 3-13.** ***(A)*** Full model equation and regression plots for a combined time-point model using top signal correlates from the TI-SWR analysis set investigating the change in the percentage of apoptosis between 6 and 12 hr following treatment (Δ %apoptosis (CC3+CParp+), 6-12 hr) as the response variable, as the potential explanatory variable set. The full potential explanatory variable set is listed (top table) along with the $R^2$ of each within the time-point specific model in which they were determined to be top signal correlates with the cellular response of interest. The response variable for this model is Δ %apoptosis (CC3+CParp+), 6-12 hr. The full model as determined by a Stepwise regression algorithm includes only one signal. The regression plot for the full model is shown. ***(B)*** Residuals plot for the "combined time-point" model.

A

Y: Δ % CC3+CParp+, 6-12 hr
X: X, combined time-point

| | Time-point | $R^2$ |
|---|---|---|
| pakt | 0.25 hr | 0.77 |
| pakt | 4 hr | 0.90 |
| pp53 | 8 hr | 0.91 |

**OLS**

y = -0.90 + 1.3 pakt, 0.25hr
+ 0.37 pakt, 4 hr
+ 0.10 pp53, 8 hr

| $R^2$ | F stat | p val |
|---|---|---|
| 0.94 | 12.5 | 0.07 |

B

Y: pp53, 8 hr
X: pakt, 4 hr

**OLS**

y = -7.5 + 12.5 pakt, 4hr

| $R^2$ | F stat | p val |
|---|---|---|
| 0.87 | 29.1 | **0.005** |

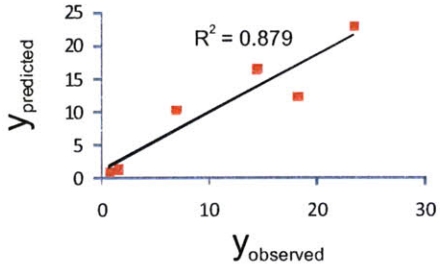


**Supplementary Figure 3-14.** ***(A)*** Full model equation for a combined time-point model using top signal correlates from the TI-SWR analysis set investigating the change in the percentage of apoptosis between 6 and 12 hr following treatment (Δ %apoptosis (CC3+CParp+), 6-12 hr) as the response variable, as the explanatory variable set. A subset has been chosen to decrease the number of potential explanatory variables to be less that the number of observations in the dataset (6 observations). The full explanatory variable set is listed (top table) along with the $R^2$ of each within the time-point specific model in which they were determined to be top signal correlates with the cellular response of interest. The response variable for this model is Δ %apoptosis (CC3+CParp+), 6-12 hr. The full model as determined by OLS (Ordinary Least squares) regression does not reach a required level of significance ($p<0.05$). ***(B)*** Model equation and regression plot for a regression model relating two of the potential explanatory signal measurements in the "combined time-point" model investigating Δ %apoptosis (CC3+CParp+), 6-12 hr (Response variable is p-p53 at 8 hr; explanatory variable is p-Akt at 4 hr). A high degree of collinearity is demonstrated between the two signal measurements.

A

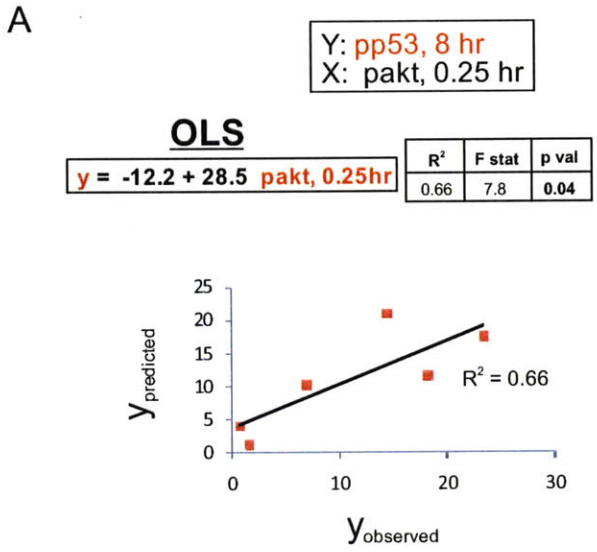


B

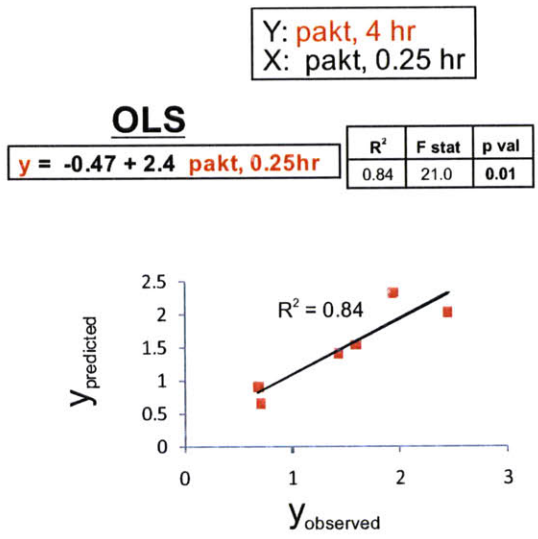


**Supplementary Figure 3-15.** ***(A)*** Model equation and regression plot for a regression model relating two of the potential explanatory signal measurements in the "combined time-point" model investigating Δ %apoptosis (CC3+CParp+), 6-12 hr. (Response variable is p-p53 at 8 hr; explanatory variable is p-Akt at 0.25 hr). A high degree of collinearity is demonstrated between the two signal measurements. ***(B)*** Model equation and regression plot for a regression model relating two of the potential explanatory signal measurements in the "combined time-point" model investigating Δ %apoptosis (CC3+CParp+), 6-12 hr (Response variable is p-Akt at 4 hr, explanatory variable is p-Akt at 0.25 hr). A high degree of collinearity is demonstrated between the two signal measurements.

A

Y: Δ % CC3+, 12-24 hr
X: X, 0.25 hr

**y = -0.55 + 1.15 pakt, 0.25hr**

| | Entry p-value |
|---|---|
| pakt | 0.007 |

**Regression plot**

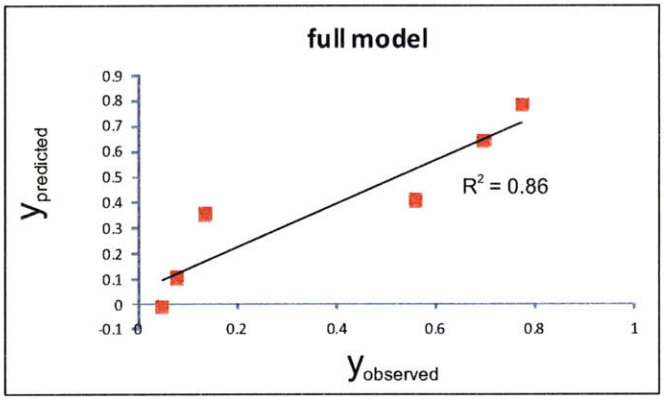


B

**Residuals plot**

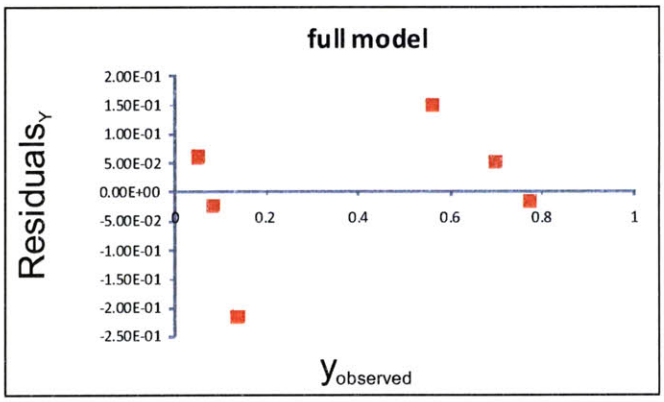


**Supplementary Figure 3-16.** ***(A)*** Full model equation and regression plots for the 0.25 hr time-point specific, Time-Interval model from the TI-SWR analysis set investigating the change in the percentage of apoptosis in the cell-population between 12 and 24 hr following treatment (Δ %apoptosis (CC3+), 12-24 hr) as the response variable. The full model as determined by a Stepwise regression algorithm includes only one signal. The regression plot for the full model is shown. ***(B)*** Residuals plot for the 0.25 hr time-point specific, Time-Interval model.

A

Y: Δ % CC3+, 12-24 hr
X: X, 0.5 hr

y = -0.62 + 1.23 tnbs1, 0.5hr

| | Entry p-value |
|---|---|
| tnbs1 | 0.04 |

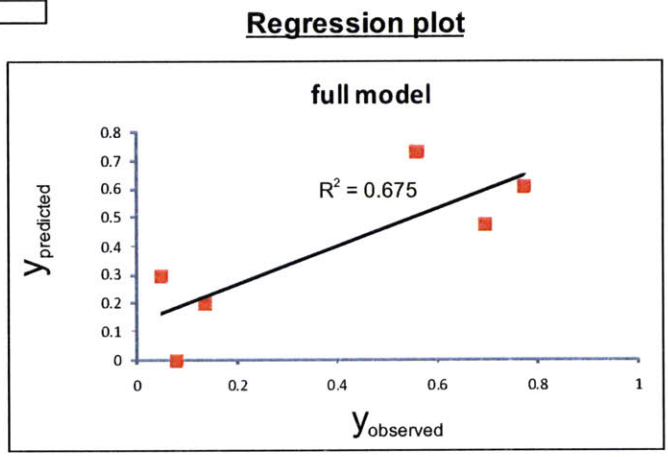


B

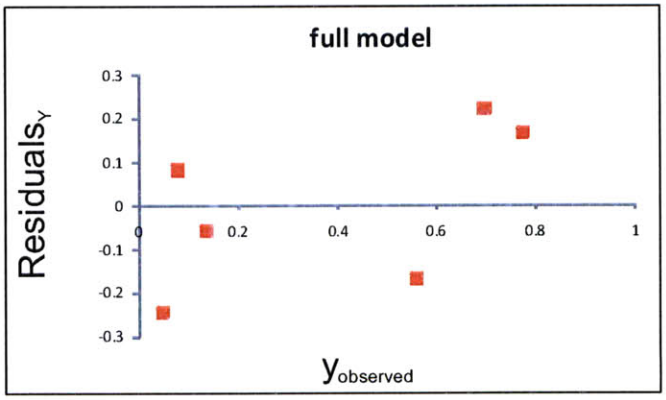


**Supplementary Figure 3-17.** ***(A)*** Full model equation and regression plots for the 0.5 hr time-point specific, Time-Interval model from the TI-SWR analysis set investigating the change in the percentage of apoptosis in the cell-population between 12 and 24 hr following treatment (Δ %apoptosis (CC3+), 12-24 hr) as the response variable. The full model as determined by a Stepwise regression algorithm includes only one signal. The regression plot for the full model is shown. ***(B)*** Residuals plot for the 0. 5 hr time-point specific, Time-Interval model.

A

Y: Δ % CC3+, 12-24 hr
X: X, 4 hr

**y = -0.23 + 0.42 pakt, 4hr**

| | Entry p-value |
|---|---|
| pakt | 0.01 |

**Regression plot**

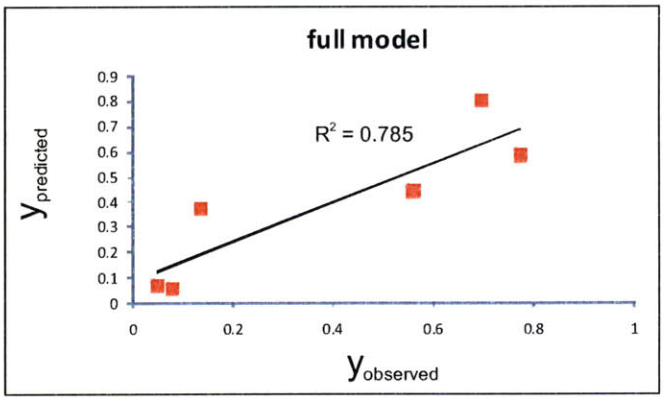


B

**Residuals plot**

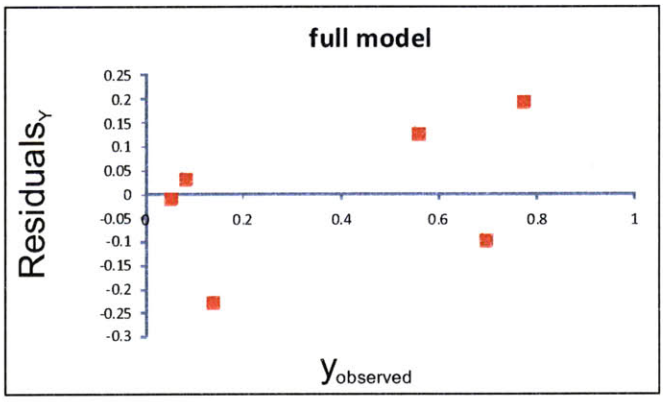


**Supplementary Figure 3-18.** ***(A)*** Full model equation and regression plots for the 4 hr time-point specific, Time-Interval model from the TI-SWR analysis set investigating the change in the percentage of apoptosis in the cell-population between 12 and 24 hr following treatment (Δ %apoptosis (CC3+), 12-24 hr) as the response variable. The full model as determined by a Stepwise regression algorithm includes only one signal. The regression plot for the full model is shown. ***(B)*** Residuals plot for the 4 hr time-point specific, Time-Interval model.

A

Y: Δ % CC3+, 12-24 hr
X: X, 8 hr

**y = -0.01 + 0.02 pp53, 8hr+ 0.01 pp38, 8hr**

| | Entry p-value |
|---|---|
| pp53 | 0.01 |
| pp38 | 0.02 |

**Regression plots**

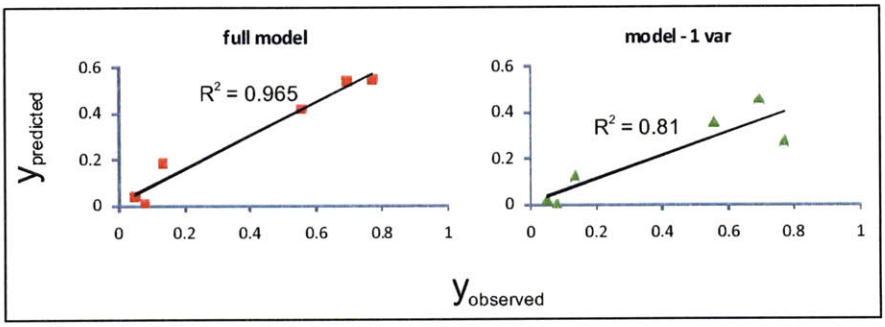


B

**Residuals plot**

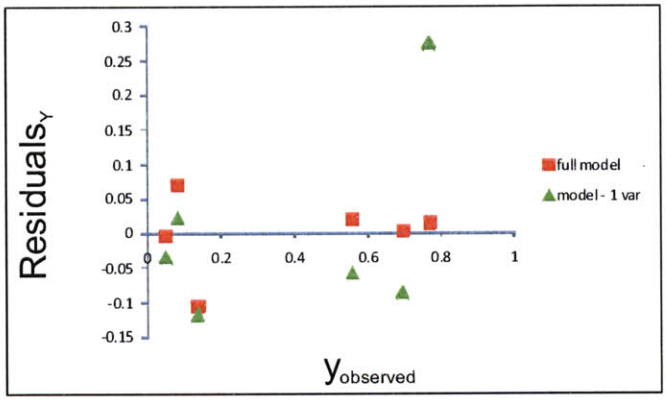


**Supplementary Figure 3-19.** ***(A)*** Full model equation and regression plots for the 8 hr time-point specific, Time-Interval model from the TI-SWR analysis set investigating the change in the percentage of apoptosis in the cell-population between 12 and 24 hr following treatment (Δ %apoptosis (CC3+), 12-24 hr) as the response variable. The full model as determined by a Stepwise regression algorithm includes 2 signals and these ***signals are listed in decreasing order of $R^2$ (ability to explain variability in the response variable) in the full model equation***. The regression plot for the full model and the model minus one variable ("model – 1 var") is shown where variables are subtracted starting with the signal with the lowest $R^2$. ***(B)*** Residuals plot for the 8 hr time-point specific, Time-Interval model.

A

Y: Δ % CC3+, 12-24 hr
X: X, 12 hr

y = -0.15 + 0.1 perk1/2, 12hr

| | Entry p-value |
|---|---|
| perk1/2 | 0.003 |

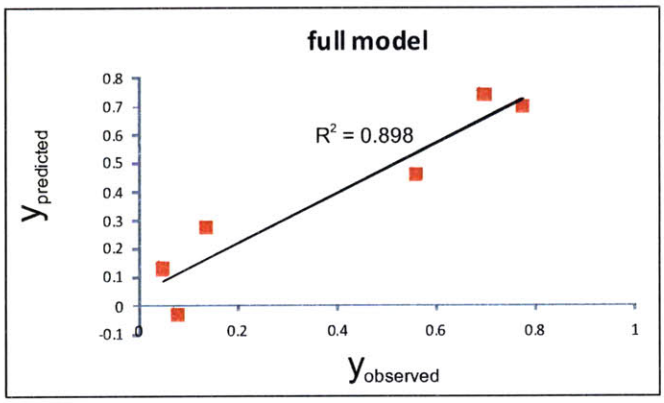


B

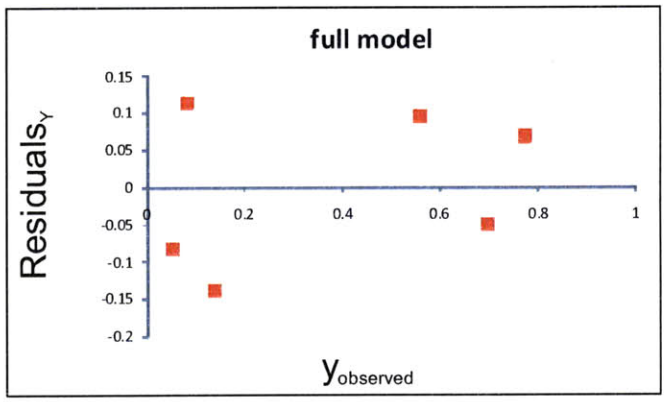


**Supplementary Figure 3-20.** ***(A)*** Full model equation and regression plots for the 12 hr time-point specific, Time-Interval model from the TI-SWR analysis set investigating the change in the percentage of apoptosis in the cell-population between 12 and 24 hr following treatment (Δ %apoptosis (CC3+), 12-24 hr) as the response variable. The full model as determined by a Stepwise regression algorithm includes only one signal. The regression plot for the full model is shown. ***(B)*** Residuals plot for the 12 hr time-point specific, Time-Interval model.

A

Y: Δ % CC3+, 12-24 hr
X: X, 16 hr

**y = 0.03 + 0.09 pp38, 16hr**

| | Entry p-value |
|---|---|
| pp38 | 0.03 |

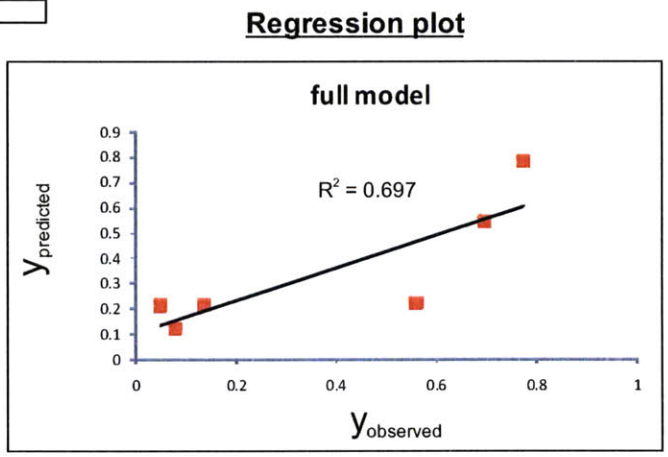


B

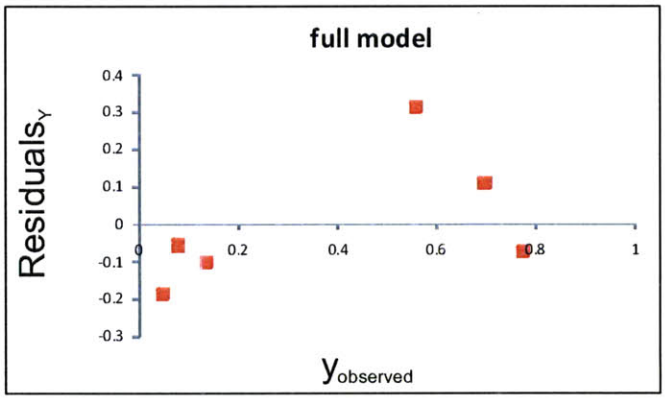


**Supplementary Figure 3-21.** ***(A)*** Full model equation and regression plots for the 16 hr time-point specific, Time-Interval model from the TI-SWR analysis set investigating the change in the percentage of apoptosis in the cell-population between 12 and 24 hr following treatment (Δ %apoptosis (CC3+), 12-24 hr) as the response variable. The full model as determined by a Stepwise regression algorithm includes only one signal. The regression plot for the full model is shown. ***(B)*** Residuals plot for the 16 hr time-point specific, Time-Interval model.

A

Y: Δ % CC3+, 12-24 hr
X: X, 24 hr

y = -0.34 + 0.10 ph2ax, 24hr+ 0.69 tnbs1, 24hr

| | Entry p-value |
|---|---|
| ph2ax | 0.008 |
| tnbs1 | 0.03 |

**Regression plots**

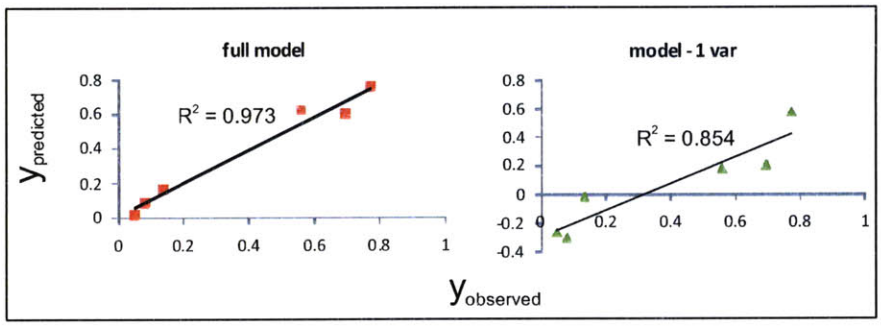


B

**Residuals plot**

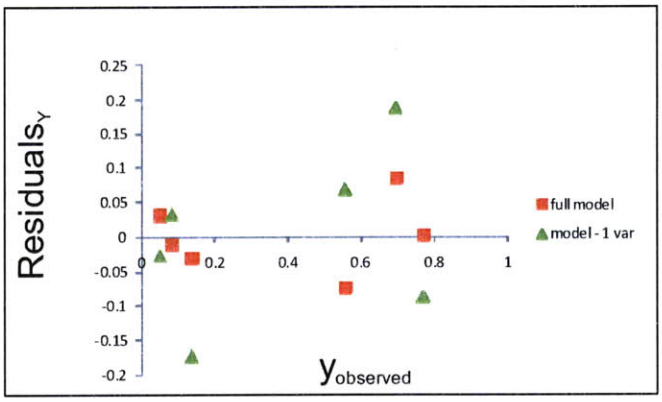


**Supplementary Figure 3-22.** ***(A)*** Full model equation and regression plots for the 24 hr time-point specific, Time-Interval model from the TI-SWR analysis set investigating the change in the percentage of apoptosis in the cell-population between 12 and 24 hr following treatment (Δ %apoptosis (CC3+), 12-24 hr) as the response variable. The full model as determined by a Stepwise regression algorithm includes 2 signals and these ***signals are listed in decreasing order of $R^2$ (ability to explain variability in the response variable) in the full model equation***. The regression plot for the full model and the model minus one variable ("model – 1 var") is shown where variables are subtracted starting with the signal with the lowest $R^2$. ***(B)*** Residuals plot for the 24 hr time-point specific, Time-Interval model.

A

Y: Δ % CC3+, 12-24 hr
X: X, combined time-point

| | Time-point | $R^2$ |
|---|---|---|
| pakt | 0.25 hr | 0.86 |
| tnbs1 | 0.5 hr | 0.67 |
| pakt | 4 hr | 0.78 |
| pp53 | 8h | 0.81 |
| pp38 | 8 hr | 0.15 |
| perk/12 | 12 hr | 0.89 |
| pp38 | 16 hr | 0.69 |

**y = -0.15 + 0.1 perk1/2, 12hr**

| | Entry p-value |
|---|---|
| perk1/2, 12 hr | 0.004 |

**Regression plot**

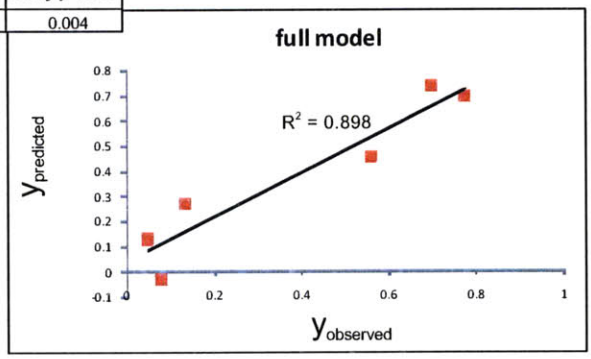


B

**Residuals plot**

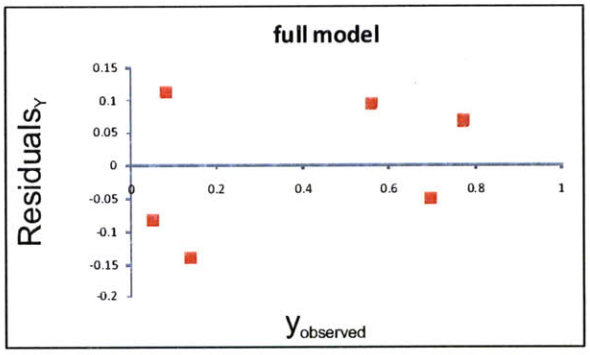


**Supplementary Figure 3-23.** ***(A)*** Full model equation and regression plots for a combined time-point model using top signal correlates from the TI-SWR analysis set investigating the change in the percentage of apoptosis between 12 and 24 hr following treatment (Δ %apoptosis (CC3+), 12-24 hr) as the response variable, as the potential explanatory variable set. The full potential explanatory variable set is listed (top table) along with the $R^2$ of each within the time-point specific model in which they were determined to be top signal correlates with the cellular response of interest. The response variable for this model is Δ %apoptosis (CC3+), 12-24 hr. The full model as determined by a Stepwise regression algorithm includes only one signal. The regression plot for the full model is shown. ***(B)*** Residuals plot for the "combined time-point" model.

A

Y: Δ % CC3+, 12-24 hr
X: X, combined time-point

| | Time-point | $R^2$ |
|---|---|---|
| pakt | 0.25 hr | 0.86 |
| pakt | 4 hr | 0.78 |
| pp53 | 8h | 0.81 |
| perk/12 | 12 hr | 0.89 |

**OLS**

y = -0.24 + 0.94 pakt, 0.25hr
- 0.51pakt, 4 hr
+ 0.02pp53, 8 hr
+ 0.06perk1/2, 12 hr

| $R^2$ | F stat | p val |
|---|---|---|
| 0.98 | 13.8 | 0.19 |

B

Y: perk1/2, 12 hr
X: pp53, 8 hr

**OLS**

y = 1.9 + 0.3 pp53, 8hr

| $R^2$ | F stat | p val |
|---|---|---|
| 0.83 | 20.8 | 0.01 |

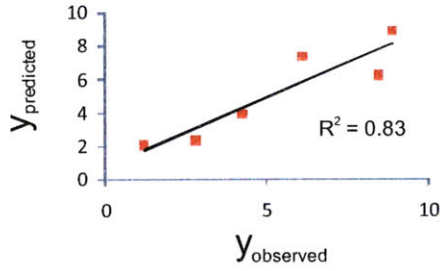


**Supplementary Figure 3-24.** ***(A)*** Full model equation for a combined time-point model using top signal correlates from the TI-SWR analysis set investigating the change in the percentage of apoptosis between 12 and 24 hr following treatment (Δ %apoptosis (CC3+), 12-24 hr) as the response variable, as the explanatory variable set. A subset has been chosen to decrease the number of potential explanatory variables to be less that the number of observations in the dataset (6 observations). The full explanatory variable set is listed (top table) along with the $R^2$ of each within the time-point specific model in which they were determined to be top signal correlates with the cellular response of interest. The response variable for this model is Δ %apoptosis (CC3+), 12-24 hr. The full model as determined by OLS (Ordinary Least squares) regression does not reach a required level of significance ($p<0.05$). ***(B)*** Model equation and regression plot for a regression model relating two of the potential explanatory signal measurements in the "combined time-point" model investigating Δ %apoptosis (CC3+), 12-24 hr (Response variable is p-ERK1/2 at 12 hr; explanatory variable is p-p53 at 8 hr). A high degree of collinearity is demonstrated between the two signal measurements.

A

Y: perk1/2, 12 hr
X: pakt, 4 hr

**OLS**

y = -0.96 + 4.2 pakt, 4hr

| $R^2$ | F stat | p val |
|---|---|---|
| 0.91 | 45.9 | **0.002** |

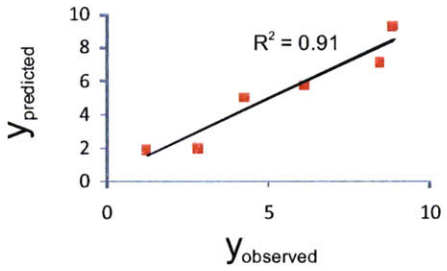


B

Y: perk1/2, 12 hr
X: pakt, 0.25 hr

**OLS**

y = -3.4 + 10.85 pakt, 0.25hr

| $R^2$ | F stat | p val |
|---|---|---|
| 0.86 | 26.2 | **0.006** |

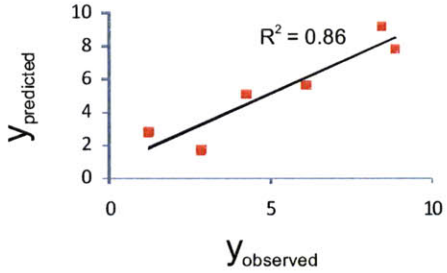


**Supplementary Figure 3-25.** ***(A)*** Model equation and regression plot for a regression model relating two of the potential explanatory signal measurements in the "combined time-point" model investigating Δ %apoptosis (CC3+), 12-24 hr. (Response variable is p-ERK1/2 at 12 hr; explanatory variable is p-Akt at 4 hr). A high degree of collinearity is demonstrated between the two signal measurements. ***(B)*** Model equation and regression plot for a regression model relating two of the potential explanatory signal measurements in the "combined time-point" model investigating Δ %apoptosis (CC3+), 12-24 hr (Response variable is p-ERK1/2 at 12 hr, explanatory variable is p-Akt at 0.25 hr). A high degree of collinearity is demonstrated between the two signal measurements.

A

Y: Δ % CC3+, 12-24 hr
X: X, 16 hr

**y = 0.03 + 0.09 pp38, 16hr**

| | Entry p-value |
|---|---|
| pp38 | 0.03 |

**Regression plot**

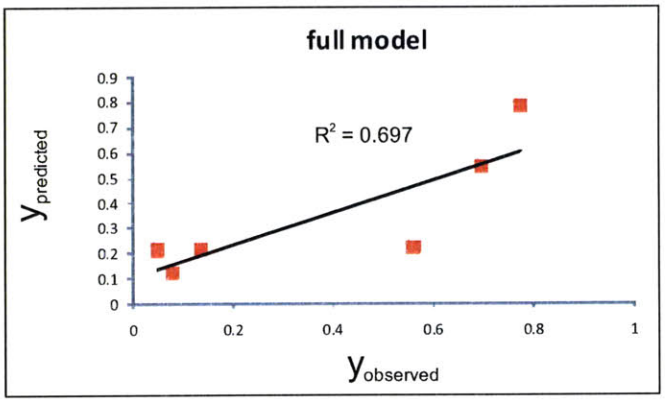


B

**Residuals plot**

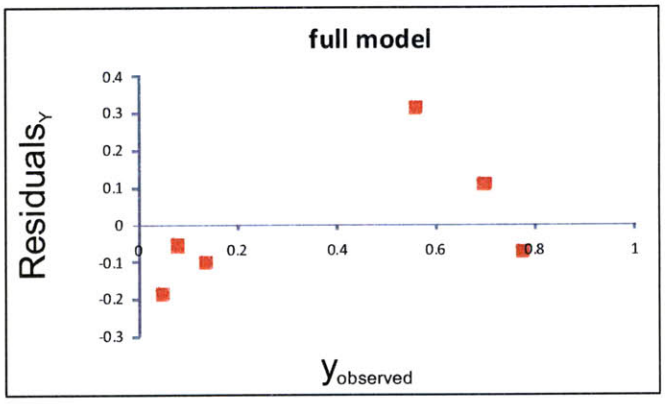


**Supplementary Figure 3-26.** ***(A)*** Full model equation and regression plots for the first time-point specific, Time-Interval model from the "walk back" TI-SWR analysis that starts by investigating the change in the percentage of apoptosis in the cell-population between 12 and 24 hr following treatment (Δ %apoptosis (CC3+), 12-24 hr) as the response variable. The potential explanatory variable set for this first step model is all of the signaling measurements taken at 16 hr following treatment. The full model as determined by a Stepwise regression algorithm includes only one signal. The regression plot for the full model is shown. ***(B)*** Residuals plot for the first step "walk back" model.

A

Y: Δ p-p38, 12-16 hr
X: X, 12 hr

**y = 0.1 - 0.16 pp38, 12hr+ 0.14 pakt, 12hr**

| | Entry p-value |
|---|---|
| pp38 | 8e-6 |
| pakt | 0.01 |

**Regression plot**

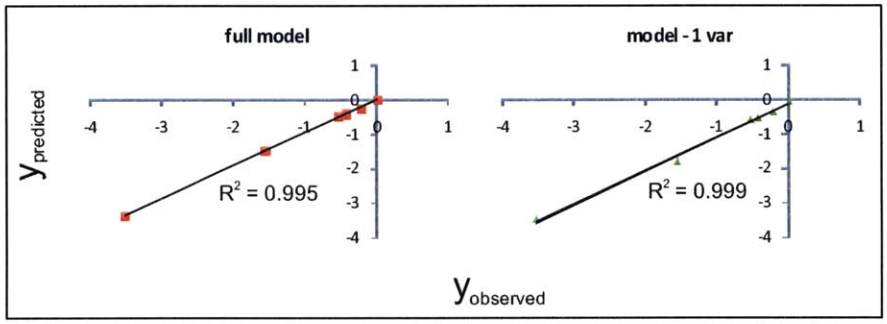


B

**Residuals plot**

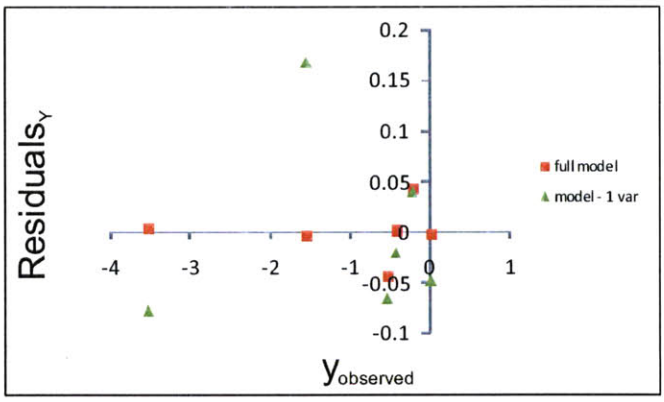


**Supplementary Figure 3-27.** ***(A)*** Full model equation and regression plots for the second time-point specific, Time-Interval model from the "walk back" TI-SWR analysis that starts by investigating the change in the percentage of apoptosis in the cell-population between 12 and 24 hr following treatment (Δ %apoptosis (CC3+), 12-24 hr) as the response variable. The response variable for this second step model is the change in the signal, p-p38, between 12 and 16 hr following treatment. The potential explanatory variable set for the second step model is all of the signaling measurements taken at 12 hr following treatment. The full model as determined by a Stepwise regression algorithm includes 2 signals and these ***signals are listed in decreasing order of $R^2$ (ability to explain variability in the response variable) in the full model equation***. The regression plot for the full model and the model minus one variable ("model – 1 var") is shown where variables are subtracted starting with the signal with the lowest $R^2$. ***(B)*** Residuals plot for the second step "walk back" model.

A

Y: Δ p-p38, 8-12 hr
X: X, 8 hr

y = 0.8 - 0.11 nfkb, 8hr

| | Entry p-value |
|---|---|
| nfkb | 0.03 |

**Regression plot**

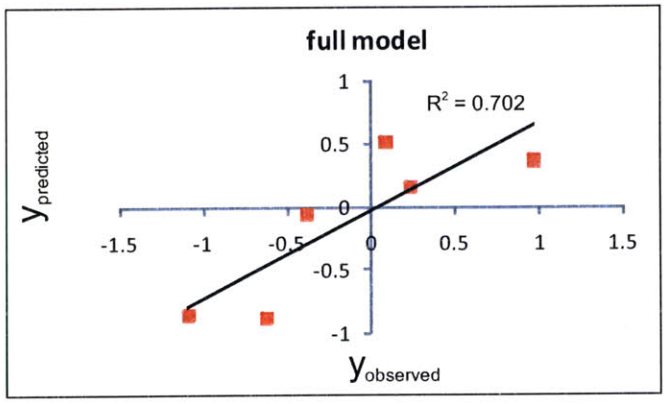


B

**Residuals plot**

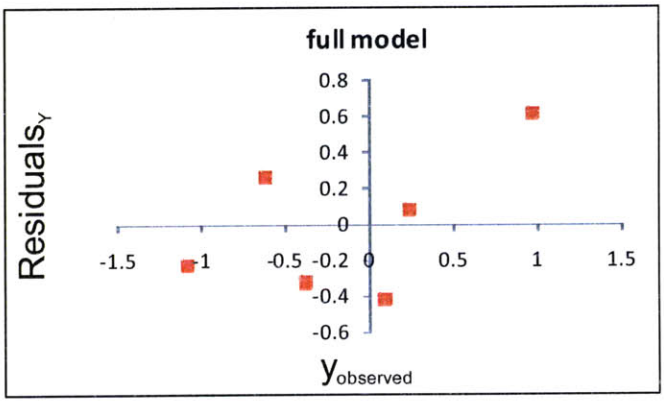


**Supplementary Figure 3-28.** ***(A)*** Full model equation and regression plots for the third time-point specific, Time-Interval model from the "walk back" TI-SWR analysis that starts by investigating the change in the percentage of apoptosis in the cell-population between 12 and 24 hr following treatment (Δ %apoptosis (CC3+), 12-24 hr) as the response variable. The response variable for this third step model is the change in the signal, p-p38, between 8 and 12 hr following treatment. The potential explanatory variable set for the third step model is all of the signaling measurements taken at 8 hr following treatment. The full model as determined by a Stepwise regression algorithm includes only one signal. The regression plot for the full model is shown. ***(B)*** Residuals plot for the third step "walk back" model.

A

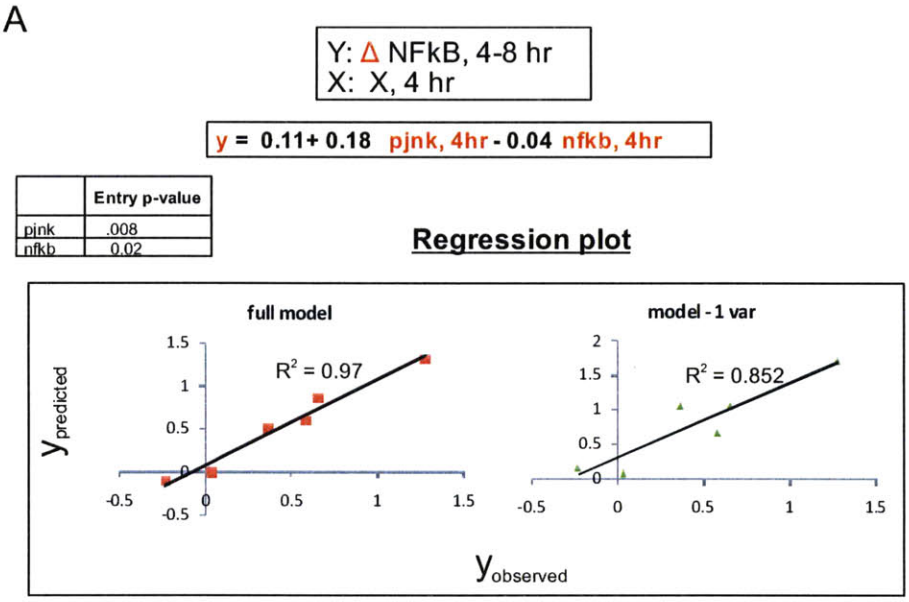


B

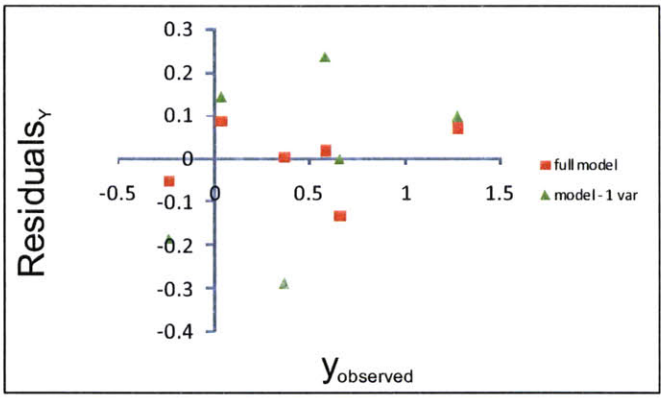


**Supplementary Figure 3-29.** ***(A)*** Full model equation and regression plots for the fourth and last time-point specific, Time-Interval model from the "walk back" TI-SWR analysis that starts by investigating the change in the percentage of apoptosis in the cell-population between 12 and 24 hr following treatment (Δ %apoptosis (CC3+), 12-24 hr) as the response variable. The response variable for this last step model is the change in the signal, NFkB, between 4 and 8 hr following treatment. The potential explanatory variable set for the second step model is all of the signaling measurements taken at 4 hr following treatment. The full model as determined by a Stepwise regression algorithm includes 2 signals and these ***signals are listed in decreasing order of $R^2$ (ability to explain variability in the response variable) in the full model equation***. The regression plot for the full model and the model minus one variable ("model – 1 var") is shown where variables are subtracted starting with the signal with the lowest $R^2$. ***(B)*** Residuals plot for the last step "walk back" model.

| Var ID (Primary) | PC1 (w*c) | PC2 (w*c) |
|---|---|---|
| 'pAkt_Mean' | 0.0766923 | -0.014505 |
| 'pAkt_AUC_whole' | 0.0204662 | 0.0265492 |
| 'pAkt_Max' | 0.0595703 | -0.0446348 |
| 'pAkt_Equilibrium' | -0.00666398 | 0.0332758 |
| 'pAkt_data_t=1' | 0.107059 | -0.0101096 |
| 'pAkt_data_t=2' | 0.119636 | -0.0473851 |
| 'pAkt_data_t=3' | 0.0871647 | -0.0869112 |
| 'pAkt_data_t=4' | 0.113139 | -0.0513266 |
| 'pAkt_data_t=5' | 0.0814595 | -0.0788701 |
| 'pAkt_data_t=6' | 0.0813528 | 0.0253494 |
| 'pAkt_data_t=7' | 0.00965596 | 0.0445957 |
| 'pAkt_data_t=8' | 0.00904189 | -0.00147601 |
| 'pAkt_data_t=9' | -0.0434384 | 0.0627332 |
| 'pERK1_Mean' | 0.095137 | 0.0831913 |
| 'pERK1_AUC_whole' | 0.0606129 | 0.14634 |
| 'pERK1_Max' | 0.0927355 | 0.0999107 |
| 'pERK1_Equilibrium' | 0.0494843 | 0.151895 |
| 'pERK1_data_t=1' | 0.111903 | -0.0570618 |
| 'pERK1_data_t=2' | 0.0722888 | -0.0422239 |
| 'pERK1_data_t=3' | 0.0904217 | -0.0708525 |
| 'pERK1_data_t=4' | 0.0613205 | -0.0126994 |
| 'pERK1_data_t=5' | 0.0960219 | -0.0166218 |
| 'pERK1_data_t=6' | 0.090664 | 0.107524 |
| 'pERK1_data_t=7' | 0.045574 | 0.166503 |
| 'pERK1_data_t=8' | 0.112151 | 0.0436375 |
| 'pERK1_data_t=9' | 0.00282157 | 0.160112 |
| 'pERK1_data_t=10' | -0.00566365 | 0.139255 |
| 'pERK2_Mean' | 0.0916302 | -0.0344579 |
| 'pERK2_AUC_whole' | 0.0708667 | 0.0408568 |
| 'pERK2_Max' | 0.0838336 | -0.0119485 |
| 'pERK2_Equilibrium' | 0.0570299 | 0.0488411 |
| 'pERK2_data_t=1' | 0.0928178 | -0.100231 |
| 'pERK2_data_t=2' | 0.0613373 | -0.0945423 |
| 'pERK2_data_t=3' | 0.043174 | -0.0998411 |
| 'pERK2_data_t=4' | 0.0232599 | -0.0776807 |
| 'pERK2_data_t=5' | 0.0666345 | -0.0882125 |
| 'pERK2_data_t=6' | 0.115778 | 0.0508879 |
| 'pERK2_data_t=7' | 0.0423215 | 0.13004 |
| 'pERK2_data_t=8' | 0.0969654 | -0.0587174 |

| | | |
|---|---|---|
| 'pERK2_data_t=9' | -0.00851311 | 0.0597861 |
| 'pERK2_data_t=10' | 0.0442096 | 0.0951585 |
| 'pJNK_Mean' | 0.126297 | -0.0165364 |
| 'pJNK_AUC_whole' | 0.112916 | 0.00827909 |
| 'pJNK_Max' | 0.112041 | 0.0456533 |
| 'pJNK_Equilibrium' | 0.105124 | 0.0148431 |
| 'pJNK_data_t=1' | 0.0873464 | -0.0706922 |
| 'pJNK_data_t=2' | 0.0970943 | -0.0558031 |
| 'pJNK_data_t=3' | 0.0773869 | -0.0593712 |
| 'pJNK_data_t=4' | 0.0954801 | -0.0435324 |
| 'pJNK_data_t=5' | 0.114913 | -0.0840816 |
| 'pJNK_data_t=6' | 0.122495 | 0.0248564 |
| 'pJNK_data_t=7' | 0.117411 | 0.0579847 |
| 'pJNK_data_t=8' | 0.0945526 | -0.018945 |
| 'pJNK_data_t=9' | 0.0137758 | -0.0296354 |
| 'pJNK_data_t=10' | 0.0623715 | 0.0262006 |
| 'pp38_Mean' | 0.114669 | -0.0866432 |
| 'pp38_AUC_whole' | 0.114872 | -0.07726 |
| 'pp38_Max' | 0.115669 | -0.0780101 |
| 'pp38_Equilibrium' | 0.114264 | -0.0770403 |
| 'pp38_data_t=1' | 0.0981512 | -0.114956 |
| 'pp38_data_t=2' | 0.0662563 | -0.127869 |
| 'pp38_data_t=3' | 0.0757371 | -0.106417 |
| 'pp38_data_t=4' | 0.110141 | -0.0658864 |
| 'pp38_data_t=5' | 0.092967 | -0.10299 |
| 'pp38_data_t=6' | 0.11726 | -0.0611587 |
| 'pp38_data_t=7' | 0.119745 | -0.070052 |
| 'pp38_data_t=8' | 0.108375 | -0.0833421 |
| 'pp38_data_t=9' | 0.102993 | -0.0832459 |
| 'pp38_data_t=10' | 0.080869 | -0.0238244 |
| 'pp53_Mean' | 0.0433363 | 0.0688544 |
| 'pp53_AUC_whole' | 0.0379095 | 0.0753371 |
| 'pp53_Max' | 0.0328096 | 0.0878792 |
| 'pp53_Equilibrium' | 0.0380201 | 0.0720704 |
| 'pp53_data_t=1' | 0.0894899 | -0.0498191 |
| 'pp53_data_t=2' | 0.015101 | -0.0919611 |
| 'pp53_data_t=3' | 0.0736769 | -0.063662 |
| 'pp53_data_t=4' | 0.0747815 | -0.0183732 |
| 'pp53_data_t=5' | 0.0727038 | 0.0243274 |
| 'pp53_data_t=6' | 0.0733811 | 0.0609477 |

| | | |
|---|---|---|
| 'pp53_data_t=7' | 0.0764451 | 0.0347365 |
| 'pp53_data_t=8' | 0.0424254 | 0.0497278 |
| 'pp53_data_t=9' | 0.0246655 | 0.093866 |
| 'pp53_data_t=10' | 0.0261524 | 0.0805183 |
| 'pH2AX_Mean' | 0.12546 | 0.0138202 |
| 'pH2AX_AUC_whole' | 0.126011 | 0.00627863 |
| 'pH2AX_Max' | 0.123314 | 0.00586229 |
| 'pH2AX_Equilibrium' | 0.126688 | 0.00132365 |
| 'pH2AX_data_t=1' | 0.0936551 | -0.0763857 |
| 'pH2AX_data_t=2' | 0.0598721 | -0.0189971 |
| 'pH2AX_data_t=3' | 0.119808 | 0.035917 |
| 'pH2AX_data_t=4' | 0.0863975 | 0.0512064 |
| 'pH2AX_data_t=5' | 0.0796534 | 0.113911 |
| 'pH2AX_data_t=6' | 0.0630143 | 0.131218 |
| 'pH2AX_data_t=7' | 0.124566 | 0.00210757 |
| 'pH2AX_data_t=8' | 0.123064 | 0.0290324 |
| 'pH2AX_data_t=9' | 0.123134 | -0.0153377 |
| 'pH2AX_data_t=10' | 0.123895 | -0.0190178 |
| 'pNbs1_Mean' | 0.0497286 | 0.150925 |
| 'pNbs1_AUC_whole' | 0.0444652 | 0.153754 |
| 'pNbs1_Max' | 0.0409786 | 0.167641 |
| 'pNbs1_Equilibrium' | 0.0512999 | 0.140348 |
| 'pNbs1_data_t=1' | -0.0390361 | 0.059506 |
| 'pNbs1_data_t=2' | -0.0657994 | -0.0796637 |
| 'pNbs1_data_t=3' | 0.08647 | -0.138719 |
| 'pNbs1_data_t=4' | 0.0991373 | 0.0576839 |
| 'pNbs1_data_t=5' | 0.0455679 | 0.156514 |
| 'pNbs1_data_t=6' | 0.0184445 | 0.171426 |
| 'pNbs1_data_t=7' | 0.0638898 | 0.128861 |
| 'pNbs1_data_t=8' | 0.0549268 | 0.142453 |
| 'pNbs1_data_t=9' | 0.0334798 | 0.152542 |
| 'pNbs1_data_t=10' | 0.0463671 | 0.127887 |
| 'totp53_Mean' | 0.0990397 | 0.102793 |
| 'totp53_AUC_whole' | 0.0756552 | 0.138595 |
| 'totp53_Max' | 0.0412768 | 0.165547 |
| 'totp53_Equilibrium' | 0.0723455 | 0.141659 |
| 'totp53_data_t=1' | 0.0982903 | -0.121443 |
| 'totp53_data_t=2' | 0.0513974 | -0.143972 |
| 'totp53_data_t=3' | 0.0799011 | -0.125725 |
| 'totp53_data_t=4' | 0.0969752 | -0.123551 |

| | | |
|---|---|---|
| 'totp53_data_t=5' | 0.0939553 | -0.100494 |
| 'totp53_data_t=6' | 0.12648 | -0.0068935 |
| 'totp53_data_t=7' | 0.110666 | 0.0675255 |
| 'totp53_data_t=8' | 0.0927668 | 0.102548 |
| 'totp53_data_t=9' | 0.0350112 | 0.169226 |
| 'totp53_data_t=10' | 0.0677989 | 0.143908 |
| 'nfkb_Mean' | 0.0975071 | -0.0203919 |
| 'nfkb_AUC_whole' | 0.114095 | -0.00669309 |
| 'nfkb_Max' | 0.112778 | -0.00846476 |
| 'nfkb_Equilibrium' | 0.121455 | -0.00579431 |
| 'nfkb_data_t=1' | 0.0328073 | -0.0698916 |
| 'nfkb_data_t=2' | 0.0698606 | -0.021097 |
| 'nfkb_data_t=3' | 0.055974 | -0.0518483 |
| 'nfkb_data_t=4' | 0.0525114 | -0.05682 |
| 'nfkb_data_t=5' | 0.0473927 | -0.0342764 |
| 'nfkb_data_t=6' | 0.0844364 | 0.0313593 |
| 'nfkb_data_t=7' | 0.114403 | 0.0221515 |
| 'nfkb_data_t=8' | 0.120637 | 0.00465474 |
| 'nfkb_data_t=9' | 0.1075 | -0.0372827 |
| 'nfkb_data_t=10' | 0.115234 | -0.0423155 |
| 6h_CC3+CParp+' | 0.111449 | -0.0683459 |
| 6h_CC3-Cparp-' | -0.110015 | 0.0741083 |
| 12h_CC3+CParp+' | 0.115099 | -0.00163132 |
| 12h_CC3-Cparp-' | -0.118013 | 0.0365518 |
| % G1, 24h | -0.0686022 | -0.135821 |
| % S, 24h | 0.0254471 | 0.141786 |
| % G2-M, 24h | 0.0148521 | 0.169928 |

**Supplementary Table 3-1.** Table of PLSR model Principal component loadings in Principal component 1 (PC1) and Principal component 2 (PC2), unsorted. (t=1,2,3,4,5,6,7,8,9,10 translates to time-points: 0.25, 0.5, 1, 1.5, 2, 4, 8, 12, 16 and 24 hr following treatment)

| Var ID (Primary) | PC1 (w*c) | PC2 (w*c) |
|---|---|---|
| 'pH2AX_Equilibrium' | 0.126688 | 0.00132365 |
| 'totp53_data_t=6' | 0.12648 | -0.0068935 |
| 'pJNK_Mean' | 0.126297 | -0.0165364 |
| 'pH2AX_AUC_whole' | 0.126011 | 0.00627863 |
| 'pH2AX_Mean' | 0.12546 | 0.0138202 |
| 'pH2AX_data_t=7' | 0.124566 | 0.00210757 |
| 'pH2AX_data_t=10' | 0.123895 | -0.0190178 |
| 'pH2AX_Max' | 0.123314 | 0.00586229 |
| 'pH2AX_data_t=9' | 0.123134 | -0.0153377 |
| 'pH2AX_data_t=8' | 0.123064 | 0.0290324 |
| 'pJNK_data_t=6' | 0.122495 | 0.0248564 |
| 'nfkb_Equilibrium' | 0.121455 | -0.00579431 |
| 'nfkb_data_t=8' | 0.120637 | 0.00465474 |
| 'pH2AX_data_t=3' | 0.119808 | 0.035917 |
| 'pp38_data_t=7' | 0.119745 | -0.070052 |
| 'pAkt_data_t=2' | 0.119636 | -0.0473851 |
| 'pJNK_data_t=7' | 0.117411 | 0.0579847 |
| 'pp38_data_t=6' | 0.11726 | -0.0611587 |
| 'pERK2_data_t=6' | 0.115778 | 0.0508879 |
| 'pp38_Max' | 0.115669 | -0.0780101 |
| 'nfkb_data_t=10' | 0.115234 | -0.0423155 |
| '12h_CC3+CParp+' | 0.115099 | -0.00163132 |
| 'pJNK_data_t=5' | 0.114913 | -0.0840816 |
| 'pp38_AUC_whole' | 0.114872 | -0.07726 |
| 'pp38_Mean' | 0.114669 | -0.0866432 |
| 'nfkb_data_t=7' | 0.114403 | 0.0221515 |
| 'pp38_Equilibrium' | 0.114264 | -0.0770403 |
| 'nfkb_AUC_whole' | 0.114095 | -0.00669309 |
| 'pAkt_data_t=4' | 0.113139 | -0.0513266 |
| 'pJNK_AUC_whole' | 0.112916 | 0.00827909 |
| 'nfkb_Max' | 0.112778 | -0.00846476 |
| 'pERK1_data_t=8' | 0.112151 | 0.0436375 |
| 'pJNK_Max' | 0.112041 | 0.0456533 |
| 'pERK1_data_t=1' | 0.111903 | -0.0570618 |
| '6h_CC3+CParp+' | 0.111449 | -0.0683459 |
| 'totp53_data_t=7' | 0.110666 | 0.0675255 |
| 'pp38_data_t=4' | 0.110141 | -0.0658864 |
| 'pp38_data_t=8' | 0.108375 | -0.0833421 |
| 'nfkb_data_t=9' | 0.1075 | -0.0372827 |

| | | |
|---|---|---|
| 'pAkt_data_t=1' | 0.107059 | -0.0101096 |
| 'pJNK_Equilibrium' | 0.105124 | 0.0148431 |
| 'pp38_data_t=9' | 0.102993 | -0.0832459 |
| 'pNbs1_data_t=4' | 0.0991373 | 0.0576839 |
| 'totp53_Mean' | 0.0990397 | 0.102793 |
| 'totp53_data_t=1' | 0.0982903 | -0.121443 |
| 'pp38_data_t=1' | 0.0981512 | -0.114956 |
| 'nfkb_Mean' | 0.0975071 | -0.0203919 |
| 'pJNK_data_t=2' | 0.0970943 | -0.0558031 |
| 'totp53_data_t=4' | 0.0969752 | -0.123551 |
| 'pERK2_data_t=8' | 0.0969654 | -0.0587174 |
| 'pERK1_data_t=5' | 0.0960219 | -0.0166218 |
| 'pJNK_data_t=4' | 0.0954801 | -0.0435324 |
| 'pERK1_Mean' | 0.095137 | 0.0831913 |
| 'pJNK_data_t=8' | 0.0945526 | -0.018945 |
| 'totp53_data_t=5' | 0.0939553 | -0.100494 |
| 'pH2AX_data_t=1' | 0.0936551 | -0.0763857 |
| 'pp38_data_t=5' | 0.092967 | -0.10299 |
| 'pERK2_data_t=1' | 0.0928178 | -0.100231 |
| 'totp53_data_t=8' | 0.0927668 | 0.102548 |
| 'pERK1_Max' | 0.0927355 | 0.0999107 |
| 'pERK2_Mean' | 0.0916302 | -0.0344579 |
| 'pERK1_data_t=6' | 0.090664 | 0.107524 |
| 'pERK1_data_t=3' | 0.0904217 | -0.0708525 |
| 'pp53_data_t=1' | 0.0894899 | -0.0498191 |
| 'pJNK_data_t=1' | 0.0873464 | -0.0706922 |
| 'pAkt_data_t=3' | 0.0871647 | -0.0869112 |
| 'pNbs1_data_t=3' | 0.08647 | -0.138719 |
| 'pH2AX_data_t=4' | 0.0863975 | 0.0512064 |
| 'nfkb_data_t=6' | 0.0844364 | 0.0313593 |
| 'pERK2_Max' | 0.0838336 | -0.0119485 |
| 'pAkt_data_t=5' | 0.0814595 | -0.0788701 |
| 'pAkt_data_t=6' | 0.0813528 | 0.0253494 |
| 'pp38_data_t=10' | 0.080869 | -0.0238244 |
| 'totp53_data_t=3' | 0.0799011 | -0.125725 |
| 'pH2AX_data_t=5' | 0.0796534 | 0.113911 |
| 'pJNK_data_t=3' | 0.0773869 | -0.0593712 |
| 'pAkt_Mean' | 0.0766923 | -0.014505 |
| 'pp53_data_t=7' | 0.0764451 | 0.0347365 |
| 'pp38_data_t=3' | 0.0757371 | -0.106417 |

| | | |
|---|---|---|
| 'totp53_AUC_whole' | 0.0756552 | 0.138595 |
| 'pp53_data_t=4' | 0.0747815 | -0.0183732 |
| 'pp53_data_t=3' | 0.0736769 | -0.063662 |
| 'pp53_data_t=6' | 0.0733811 | 0.0609477 |
| 'pp53_data_t=5' | 0.0727038 | 0.0243274 |
| 'totp53_Equilibrium' | 0.0723455 | 0.141659 |
| 'pERK1_data_t=2' | 0.0722888 | -0.0422239 |
| 'pERK2_AUC_whole' | 0.0708667 | 0.0408568 |
| 'nfkb_data_t=2' | 0.0698606 | -0.021097 |
| 'totp53_data_t=10' | 0.0677989 | 0.143908 |
| 'pERK2_data_t=5' | 0.0666345 | -0.0882125 |
| 'pp38_data_t=2' | 0.0662563 | -0.127869 |
| 'pNbs1_data_t=7' | 0.0638898 | 0.128861 |
| 'pH2AX_data_t=6' | 0.0630143 | 0.131218 |
| 'pJNK_data_t=10' | 0.0623715 | 0.0262006 |
| 'pERK2_data_t=2' | 0.0613373 | -0.0945423 |
| 'pERK1_data_t=4' | 0.0613205 | -0.0126994 |
| 'pERK1_AUC_whole' | 0.0606129 | 0.14634 |
| 'pH2AX_data_t=2' | 0.0598721 | -0.0189971 |
| 'pAkt_Max' | 0.0595703 | -0.0446348 |
| 'pERK2_Equilibrium' | 0.0570299 | 0.0488411 |
| 'nfkb_data_t=3' | 0.055974 | -0.0518483 |
| 'pNbs1_data_t=8' | 0.0549268 | 0.142453 |
| 'nfkb_data_t=4' | 0.0525114 | -0.05682 |
| 'totp53_data_t=2' | 0.0513974 | -0.143972 |
| 'pNbs1_Equilibrium' | 0.0512999 | 0.140348 |
| 'pNbs1_Mean' | 0.0497286 | 0.150925 |
| 'pERK1_Equilibrium' | 0.0494843 | 0.151895 |
| 'nfkb_data_t=5' | 0.0473927 | -0.0342764 |
| 'pNbs1_data_t=10' | 0.0463671 | 0.127887 |
| 'pERK1_data_t=7' | 0.045574 | 0.166503 |
| 'pNbs1_data_t=5' | 0.0455679 | 0.156514 |
| 'pNbs1_AUC_whole' | 0.0444652 | 0.153754 |
| 'pERK2_data_t=10' | 0.0442096 | 0.0951585 |
| 'pp53_Mean' | 0.0433363 | 0.0688544 |
| 'pERK2_data_t=3' | 0.043174 | -0.0998411 |
| 'pp53_data_t=8' | 0.0424254 | 0.0497278 |
| 'pERK2_data_t=7' | 0.0423215 | 0.13004 |
| 'totp53_Max' | 0.0412768 | 0.165547 |
| 'pNbs1_Max' | 0.0409786 | 0.167641 |

| | | |
|---|---|---|
| 'pp53_Equilibrium' | 0.0380201 | 0.0720704 |
| 'pp53_AUC_whole' | 0.0379095 | 0.0753371 |
| 'totp53_data_t=9' | 0.0350112 | 0.169226 |
| 'pNbs1_data_t=9' | 0.0334798 | 0.152542 |
| 'pp53_Max' | 0.0328096 | 0.0878792 |
| 'nfkb_data_t=1' | 0.0328073 | -0.0698916 |
| 'pp53_data_t=10' | 0.0261524 | 0.0805183 |
| % S, 24h | 0.0254471 | 0.141786 |
| 'pp53_data_t=9' | 0.0246655 | 0.093866 |
| 'pERK2_data_t=4' | 0.0232599 | -0.0776807 |
| 'pAkt_AUC_whole' | 0.0204662 | 0.0265492 |
| 'pNbs1_data_t=6' | 0.0184445 | 0.171426 |
| 'pp53_data_t=2' | 0.015101 | -0.0919611 |
| % G2-M, 24h | 0.0148521 | 0.169928 |
| 'pJNK_data_t=9' | 0.0137758 | -0.0296354 |
| 'pAkt_data_t=7' | 0.00965596 | 0.0445957 |
| 'pAkt_data_t=8' | 0.00904189 | -0.00147601 |
| 'pERK1_data_t=9' | 0.00282157 | 0.160112 |
| 'pERK1_data_t=10' | -0.00566365 | 0.139255 |
| 'pAkt_Equilibrium' | -0.00666398 | 0.0332758 |
| 'pERK2_data_t=9' | -0.00851311 | 0.0597861 |
| 'pNbs1_data_t=1' | -0.0390361 | 0.059506 |
| 'pAkt_data_t=9' | -0.0434384 | 0.0627332 |
| 'pNbs1_data_t=2' | -0.0657994 | -0.0796637 |
| % G1, 24h | -0.0686022 | -0.135821 |
| 6h_CC3-Cparp-' | -0.110015 | 0.0741083 |
| 12h_CC3-Cparp-' | -0.118013 | 0.0365518 |

**Supplementary Table 3-2.** Table of PLSR model Principal component loadings in Principal component 1 (PC1) and Principal component 2 (PC2), sorted on ***PC1***, descending order of weight. (t = 1 ,2 ,3 ,4 ,5 ,6, …, 7 ,8 ,9 ,10 translates to time-points: 0.25, 0.5, 1, 1.5, 2, 4, 8, 12, 16 and 24 hr following treatment)

| Var ID (Primary) | PC1 (w*c) | PC2 (w*c) |
|---|---|---|
| 'pNbs1_data_t=6' | 0.0184445 | 0.171426 |
| % G2-M, 24h | 0.0148521 | 0.169928 |
| 'totp53_data_t=9' | 0.0350112 | 0.169226 |
| 'pNbs1_Max' | 0.0409786 | 0.167641 |
| 'pERK1_data_t=7' | 0.045574 | 0.166503 |
| 'totp53_Max' | 0.0412768 | 0.165547 |
| 'pERK1_data_t=9' | 0.00282157 | 0.160112 |
| 'pNbs1_data_t=5' | 0.0455679 | 0.156514 |
| 'pNbs1_AUC_whole' | 0.0444652 | 0.153754 |
| 'pNbs1_data_t=9' | 0.0334798 | 0.152542 |
| 'pERK1_Equilibrium' | 0.0494843 | 0.151895 |
| 'pNbs1_Mean' | 0.0497286 | 0.150925 |
| 'pERK1_AUC_whole' | 0.0606129 | 0.14634 |
| 'totp53_data_t=10' | 0.0677989 | 0.143908 |
| 'pNbs1_data_t=8' | 0.0549268 | 0.142453 |
| % S, 24h | 0.0254471 | 0.141786 |
| 'totp53_Equilibrium' | 0.0723455 | 0.141659 |
| 'pNbs1_Equilibrium' | 0.0512999 | 0.140348 |
| 'pERK1_data_t=10' | -0.00566365 | 0.139255 |
| 'totp53_AUC_whole' | 0.0756552 | 0.138595 |
| 'pH2AX_data_t=6' | 0.0630143 | 0.131218 |
| 'pERK2_data_t=7' | 0.0423215 | 0.13004 |
| 'pNbs1_data_t=7' | 0.0638898 | 0.128861 |
| 'pNbs1_data_t=10' | 0.0463671 | 0.127887 |
| 'pH2AX_data_t=5' | 0.0796534 | 0.113911 |
| 'pERK1_data_t=6' | 0.090664 | 0.107524 |
| 'totp53_Mean' | 0.0990397 | 0.102793 |
| 'totp53_data_t=8' | 0.0927668 | 0.102548 |
| 'pERK1_Max' | 0.0927355 | 0.0999107 |
| 'pERK2_data_t=10' | 0.0442096 | 0.0951585 |
| 'pp53_data_t=9' | 0.0246655 | 0.093866 |
| 'pp53_Max' | 0.0328096 | 0.0878792 |
| 'pERK1_Mean' | 0.095137 | 0.0831913 |
| 'pp53_data_t=10' | 0.0261524 | 0.0805183 |
| 'pp53_AUC_whole' | 0.0379095 | 0.0753371 |
| 6h_CC3-Cparp-' | -0.110015 | 0.0741083 |
| 'pp53_Equilibrium' | 0.0380201 | 0.0720704 |
| 'pp53_Mean' | 0.0433363 | 0.0688544 |
| 'totp53_data_t=7' | 0.110666 | 0.0675255 |

| | | |
|---|---|---|
| 'pAkt_data_t=9' | -0.0434384 | 0.0627332 |
| 'pp53_data_t=6' | 0.0733811 | 0.0609477 |
| 'pERK2_data_t=9' | -0.00851311 | 0.0597861 |
| 'pNbs1_data_t=1' | -0.0390361 | 0.059506 |
| 'pJNK_data_t=7' | 0.117411 | 0.0579847 |
| 'pNbs1_data_t=4' | 0.0991373 | 0.0576839 |
| 'pH2AX_data_t=4' | 0.0863975 | 0.0512064 |
| 'pERK2_data_t=6' | 0.115778 | 0.0508879 |
| 'pp53_data_t=8' | 0.0424254 | 0.0497278 |
| 'pERK2_Equilibrium' | 0.0570299 | 0.0488411 |
| 'pJNK_Max' | 0.112041 | 0.0456533 |
| 'pAkt_data_t=7' | 0.00965596 | 0.0445957 |
| 'pERK1_data_t=8' | 0.112151 | 0.0436375 |
| 'pERK2_AUC_whole' | 0.0708667 | 0.0408568 |
| '12h_CC3-Cparp-' | -0.118013 | 0.0365518 |
| 'pH2AX_data_t=3' | 0.119808 | 0.035917 |
| 'pp53_data_t=7' | 0.0764451 | 0.0347365 |
| 'pAkt_Equilibrium' | -0.00666398 | 0.0332758 |
| 'nfkb_data_t=6' | 0.0844364 | 0.0313593 |
| 'pH2AX_data_t=8' | 0.123064 | 0.0290324 |
| 'pAkt_AUC_whole' | 0.0204662 | 0.0265492 |
| 'pJNK_data_t=10' | 0.0623715 | 0.0262006 |
| 'pAkt_data_t=6' | 0.0813528 | 0.0253494 |
| 'pJNK_data_t=6' | 0.122495 | 0.0248564 |
| 'pp53_data_t=5' | 0.0727038 | 0.0243274 |
| 'nfkb_data_t=7' | 0.114403 | 0.0221515 |
| 'pJNK_Equilibrium' | 0.105124 | 0.0148431 |
| 'pH2AX_Mean' | 0.12546 | 0.0138202 |
| 'pJNK_AUC_whole' | 0.112916 | 0.00827909 |
| 'pH2AX_AUC_whole' | 0.126011 | 0.00627863 |
| 'pH2AX_Max' | 0.123314 | 0.00586229 |
| 'nfkb_data_t=8' | 0.120637 | 0.00465474 |
| 'pH2AX_data_t=7' | 0.124566 | 0.00210757 |
| 'pH2AX_Equilibrium' | 0.126688 | 0.00132365 |
| 'pAkt_data_t=8' | 0.00904189 | -0.00147601 |
| '12h_CC3+CParp+' | 0.115099 | -0.00163132 |
| 'nfkb_Equilibrium' | 0.121455 | -0.00579431 |
| 'nfkb_AUC_whole' | 0.114095 | -0.00669309 |
| 'totp53_data_t=6' | 0.12648 | -0.0068935 |
| 'nfkb_Max' | 0.112778 | -0.00846476 |

| | | |
|---|---|---|
| 'pAkt_data_t=1' | 0.107059 | -0.0101096 |
| 'pERK2_Max' | 0.0838336 | -0.0119485 |
| 'pERK1_data_t=4' | 0.0613205 | -0.0126994 |
| 'pAkt_Mean' | 0.0766923 | -0.014505 |
| 'pH2AX_data_t=9' | 0.123134 | -0.0153377 |
| 'pJNK_Mean' | 0.126297 | -0.0165364 |
| 'pERK1_data_t=5' | 0.0960219 | -0.0166218 |
| 'pp53_data_t=4' | 0.0747815 | -0.0183732 |
| 'pJNK_data_t=8' | 0.0945526 | -0.018945 |
| 'pH2AX_data_t=2' | 0.0598721 | -0.0189971 |
| 'pH2AX_data_t=10' | 0.123895 | -0.0190178 |
| 'nfkb_Mean' | 0.0975071 | -0.0203919 |
| 'nfkb_data_t=2' | 0.0698606 | -0.021097 |
| 'pp38_data_t=10' | 0.080869 | -0.0238244 |
| 'pJNK_data_t=9' | 0.0137758 | -0.0296354 |
| 'nfkb_data_t=5' | 0.0473927 | -0.0342764 |
| 'pERK2_Mean' | 0.0916302 | -0.0344579 |
| 'nfkb_data_t=9' | 0.1075 | -0.0372827 |
| 'pERK1_data_t=2' | 0.0722888 | -0.0422239 |
| 'nfkb_data_t=10' | 0.115234 | -0.0423155 |
| 'pJNK_data_t=4' | 0.0954801 | -0.0435324 |
| 'pAkt_Max' | 0.0595703 | -0.0446348 |
| 'pAkt_data_t=2' | 0.119636 | -0.0473851 |
| 'pp53_data_t=1' | 0.0894899 | -0.0498191 |
| 'pAkt_data_t=4' | 0.113139 | -0.0513266 |
| 'nfkb_data_t=3' | 0.055974 | -0.0518483 |
| 'pJNK_data_t=2' | 0.0970943 | -0.0558031 |
| 'nfkb_data_t=4' | 0.0525114 | -0.05682 |
| 'pERK1_data_t=1' | 0.111903 | -0.0570618 |
| 'pERK2_data_t=8' | 0.0969654 | -0.0587174 |
| 'pJNK_data_t=3' | 0.0773869 | -0.0593712 |
| 'pp38_data_t=6' | 0.11726 | -0.0611587 |
| 'pp53_data_t=3' | 0.0736769 | -0.063662 |
| 'pp38_data_t=4' | 0.110141 | -0.0658864 |
| 6h_CC3+CParp+' | 0.111449 | -0.0683459 |
| 'nfkb_data_t=1' | 0.0328073 | -0.0698916 |
| 'pp38_data_t=7' | 0.119745 | -0.070052 |
| 'pJNK_data_t=1' | 0.0873464 | -0.0706922 |
| 'pERK1_data_t=3' | 0.0904217 | -0.0708525 |
| 'pH2AX_data_t=1' | 0.0936551 | -0.0763857 |

| | | |
|---|---|---|
| 'pp38_Equilibrium' | 0.114264 | -0.0770403 |
| 'pp38_AUC_whole' | 0.114872 | -0.07726 |
| 'pERK2_data_t=4' | 0.0232599 | -0.0776807 |
| 'pp38_Max' | 0.115669 | -0.0780101 |
| 'pAkt_data_t=5' | 0.0814595 | -0.0788701 |
| 'pNbs1_data_t=2' | -0.0657994 | -0.0796637 |
| 'pp38_data_t=9' | 0.102993 | -0.0832459 |
| 'pp38_data_t=8' | 0.108375 | -0.0833421 |
| 'pJNK_data_t=5' | 0.114913 | -0.0840816 |
| 'pp38_Mean' | 0.114669 | -0.0866432 |
| 'pAkt_data_t=3' | 0.0871647 | -0.0869112 |
| 'pERK2_data_t=5' | 0.0666345 | -0.0882125 |
| 'pp53_data_t=2' | 0.015101 | -0.0919611 |
| 'pERK2_data_t=2' | 0.0613373 | -0.0945423 |
| 'pERK2_data_t=3' | 0.043174 | -0.0998411 |
| 'pERK2_data_t=1' | 0.0928178 | -0.100231 |
| 'totp53_data_t=5' | 0.0939553 | -0.100494 |
| 'pp38_data_t=5' | 0.092967 | -0.10299 |
| 'pp38_data_t=3' | 0.0757371 | -0.106417 |
| 'pp38_data_t=1' | 0.0981512 | -0.114956 |
| 'totp53_data_t=1' | 0.0982903 | -0.121443 |
| 'totp53_data_t=4' | 0.0969752 | -0.123551 |
| 'totp53_data_t=3' | 0.0799011 | -0.125725 |
| 'pp38_data_t=2' | 0.0662563 | -0.127869 |
| % G1, 24h | -0.0686022 | -0.135821 |
| 'pNbs1_data_t=3' | 0.08647 | -0.138719 |
| 'totp53_data_t=2' | 0.0513974 | -0.143972 |

**Supplementary Table 3-3.** Table of PLSR model Principal component loadings in Principal component 1 (PC1) and Principal component 2 (PC2), sorted on ***PC2***, descending order of weight. (t = 1 ,2 ,3 ,4 ,5 ,6, ..., 7 ,8 ,9 ,10 translates to time-points: 0.25, 0.5, 1, 1.5, 2, 4, 8, 12, 16 and 24 hr following treatment)

Y : Δ % apoptosis (CC3+), 12-24h

| Time-point (hr) | Signal correlates in decreasing order of $R^2$ |
|---|---|
| 0.25h | + pAkt |
| 0.5h | + total Nbs1 |
| 1h | ---- |
| 1.5h | ---- |
| 2h | ---- |
| 4h | + pAkt |
| 8h | + pp53, + pp38 |
| 12h | + pERK1/2 |
| 16h | + pp38 |
| 24h | + pH2AX, + total Nbs1 |

**Supplementary Table 3-4.** Table of results from a TI-SWR (Time-Interval Stepwise regression) analysis investigating the change in apoptosis between 12 and 24 hr following treatment (Δ % apoptosis (CC3+), 12-24 hr) as the cellular response variable. Here cells staining positively for one apoptotic marker (CC3+) regardless of whether they stain positively for another apoptotic marker (+/- CParp) are considered apoptotic. Rows present an overview of the results for each of the 10 time-point specific Time-Interval models constructed (For each of the time-point specific Time-Interval models, the response variable is Δ %apoptosis, 12-24 hr and the explanatory variable set is all signals measured at that time-point). For each Time-interval model, signal names are listed in order of decreasing $R^2$ (ability to explain the variability in the response variable). Where no signals are listed, no signal-response relationships reached an acceptable level of significance ($p < 0.05$). p-ERK1/2 at 12 hr is positively correlated with Δ %apoptosis between 12-24 hr following treatment. These data suggest that ERK1/2 activity between 8 and 12 hr following treatment may have a role in promoting apoptosis following DNA damage, and further supports a dual role for p-ERK1/2 in mediating both cell-cycle regulatory and apoptotic responses following DNA damage. For further details on individual Time-Interval models in this set, and on the full TI-SWR analysis, reference Supplemental Figure 3-16 through 3-25.

# References


1. Kastan, M. and J. Bartek, *Cell-cycle checkpoints and cancer.* Nature, 2004. **432**: p. 316-323.
2. Khanna, K. and S. Jackson, *DNA double-strand breaks: signaling, repair and the cancer connection.* Nature Getnetics, 2001. **27**(3): p. 247-54.
3. Liang, Y., et al., *DNA damage response pathways in tumor suppression and cancer treatment.* World J Surg, 2009. **33**(4): p. 661-6.
4. Menoyo, A., et al., *Somatic mutations in the DNA damage-response genes ATR and CHK1 in sporadic stomach tumors with microsatellite instability.* Cancer Res, 2001. **61**(21): p. 7727-30.
5. Eyfjord, J.E. and S.K. Bodvarsdottir, *Genomic instability and cancer: networks involved in response to DNA damage.* Mutat Res, 2005. **592**(1-2): p. 18-28.
6. Litman, R., et al., *BRCA-FA pathway as a target for anti-tumor drugs.* Anticancer Agents Med Chem, 2008. **8**(4): p. 426-30.
7. Powell, S.N. and L.A. Kachnic, *Therapeutic exploitation of tumor cell defects in homologous recombination.* Anticancer Agents Med Chem, 2008. **8**(4): p. 448-60.
8. Turner, N., A. Tutt, and A. Ashworth, *Targeting the DNA repair defect of BRCA tumours.* Curr Opin Pharmacol, 2005. **5**(4): p. 388-93.
9. Mamon, H.J., et al., *Differing effects of breast cancer 1, early onset (BRCA1) and ataxia-telangiectasia mutated (ATM) mutations on cellular responses to ionizing radiation.* Int J Radiat Biol, 2003. **79**(10): p. 817-29.
10. Baldwin, E. and N. Osheroff, *Etoposide, topoisomerase II and cancer.* Current Med Chem Anti-Canc Agents, 2005. **5**(4): p. 363-72.
11. Zhou, B. and J. Bartek, *Targeting the checkpoint kinases: chemosensitization versus chemoprotection.* Nature Reviews, 2004. **4**.
12. Bakkenist, C.J. and M.B. Kastan, *DNA damage activates ATM through intermolecular autophosphorylation and dimer dissociation.* Nature, 2003. **421**(6922): p. 499-506.
13. Tibbetts, R., et al., *A role for ATR in the DNA damage-induced phosphorylation of p53.* Genes and Development, 1999. **13**(2): p. 152-7.
14. van den Bosch, M., R.T. Bree, and N.F. Lowndes, *The MRN complex: coordinating and mediating the response to broken chromosomes.* EMBO Rep, 2003. **4**(9): p. 844-9.
15. Helmink, B.A., et al., *MRN complex function in the repair of chromosomal Rag-mediated DNA double-strand breaks.* J Exp Med, 2009. **206**(3): p. 669-79.
16. Burma, S., et al., *ATM phosphorylates histone H2AX in response to DNA double-strand breaks.* Journal of Biological Chemistry, 2001. **276**(45): p. 42462-7.
17. Friesner, J., et al., *Ionizing radiation-dependent gamma-H2AX focus formation requires ataxia telangiectasia mutated and ataxia telangiectasia mutated and Rad3-related.* Molecular Biology of the Cell, 2005. **16**: p. 2566-2576.
18. Celeste, A., et al., *Histone H2AX phosphorylation is dispensable for the initial recognition of DNA breaks.* Nat Cell Biol, 2003. **5**(7): p. 675-9.
19. Banath, J. and P. Olive, *Expression of phosphorylated histone H2AX as a surrogate of cell killing by drugs that create double-strand breaks.* Cancer Research, Advances in brief, 2003. **3**: p. 4346-4350.
20. Williams, R.S., J.S. Williams, and J.A. Tainer, *Mre11-Rad50-Nbs1 is a keystone complex connecting DNA repair machinery, double-strand break signaling, and the chromatin template.* Biochem Cell Biol, 2007. **85**(4): p. 509-20.

21. Paull, T.T. and J.H. Lee, *The Mre11/Rad50/Nbs1 complex and its role as a DNA double-strand break sensor for ATM.* Cell Cycle, 2005. **4**(6): p. 737-40.
22. Lee, J.H. and T.T. Paull, *Direct activation of the ATM protein kinase by the Mre11/Rad50/Nbs1 complex.* Science, 2004. **304**(5667): p. 93-6.
23. Lee, J.H. and T.T. Paull, *Activation and regulation of ATM kinase activity in response to DNA double-strand breaks.* Oncogene, 2007. **26**(56): p. 7741-8.
24. Taylor, A.M., A. Groom, and P.J. Byrd, *Ataxia-telangiectasia-like disorder (ATLD)-its clinical presentation and molecular basis.* DNA Repair (Amst), 2004. **3**(8-9): p. 1219-25.
25. Jazayeri, A., et al., *Mre11-Rad50-Nbs1-dependent processing of DNA breaks generates oligonucleotides that stimulate ATM activity.* EMBO J, 2008. **27**(14): p. 1953-62.
26. Dupre, A., L. Boyer-Chatenet, and J. Gautier, *Two-step activation of ATM by DNA and the Mre11-Rad50-Nbs1 complex.* Nat Struct Mol Biol, 2006. **13**(5): p. 451-7.
27. Kitagawa, R., et al., *Phosphorylation of SMC1 is a critical downstream event in the ATM-NBS1-BRCA1 pathway.* Genes Dev, 2004. **18**(12): p. 1423-38.
28. Kang, J., et al., *Functional interaction of H2AX, NBS1, and p53 in ATM-dependent DNA damage responses and tumor suppression.* Mol Cell Biol, 2005. **25**(2): p. 661-70.
29. Mochan, T., et al., *53BP1, an activator of ATM in response to DNA damage.* DNA Repair (Amst.), 2004. **3**(8-9): p. 945-52.
30. Bartek, J. and J. Lukas, *Chk1 and Chk2 kinases in checkpoint control and cancer.* Cancer Cell, 2003. **2**(5): p. 421-9.
31. Zhou, B., et al., *Caffeine abolishes the mammalian G(2)/M DNA damage checkpoint by inhibiting ataxia-telangiectasia-mutated activity.* Journal of Biological Chemistry, 2000. **275**(14): p. 10342-8.
32. Matsuoka, S., et al., *Ataxia telangiectasia-mutated phosphorylates Chk2 in vivo and in vitro.* PNAS, 2000. **97**(19): p. 10389-94.
33. Caspari, T., *How to activate p53.* Current Biology, 2000. **10**(8): p. R3115-7.
34. O'Connell, M., N. Walworth, and A. Carr, *The G2-phase DNA-damage checkpoint.* Trends in Cell Biology, 2000. **10**(7): p. 296-303.
35. Vousden, K., *p53: death star.* Cell, 2000. **103**(5): p. 691-4.
36. Appella, E. and C. Anderson, *Post-translational modifications and activation of p53 by genotoxic stresses.* European Journal of Biochemistry, 2001. **268**(10): p. 2764-72.
37. Yoon, H., X. Chen, and V. Yang, *Kruppel-like factor 4 mediates p53-dependent G1/S cell cycle arrest in response to DNA damage.* Journal of Biological Chemistry, 2003. **278**(4): p. 2101-5.
38. Yoon, H. and V. Yang, *Requirement of Kruppel-like factor 4 in preventing entry into mitosis following DNA damage.* Journal of Biological Chemistry, 2004. **279**(6): p. 5035-5041.
39. Giaccia, A. and M. Kastan, *The complexity of p53 modulation: emerging patterns from divergent signals.* Genes and Development, 1998. **12**(19): p. 2973-83.
40. Prives, C. and P. Hall, *The p53 pathway.* Journal of Pathology, 1999. **187**(1): p. 112-26.
41. Bassing, C., et al., *Histone H2AX: A dosage-dependent suppressor of oncogenic translocations and tumors.* Cell, 2003. **114**: p. 359-370.
42. Taylor, A. and P. Byrd, *Molecular pathology of ataxia telangiectasia.* Journal of Clinical Pathology, 2005. **58**(10): p. 1009-15.
43. Orton, R., et al., *Computational modelling of the receptor-tyrosine-kinase-activated MAPK pathway.* Biochemical Journal, 2005. **392**(part 2): p. 249-61.
44. Chang, L. and M. Karin, *Mammalian MAP kinase signalling cascades.* Nature, 2001. **410**(6824): p. 37-40.

45. Sumbayev, V. and I. Yasinska, *Regulation of MAP kinase-dependent apoptotic pathway: implication of reactive oxygen and nitrogen species.* Archives of Biochemistry and Biophysics, 2005. **436**(2005): p. 406-12.
46. Yung, Y., et al., *Detection of ERK activation by a novel monoclonal antibody.* FEBS Letters, 1997. **408**(3): p. 292-6.
47. Fritz, G. and B. Kaina, *Late activation of stress kinases (SAPK/JNK) by genotoxins requires the DNA repair proteins DNA-PKcs and CSB.* Molecular Biology of the Cell, 2005. **Epub ahead of print**.
48. Bose, B., L. Motiwale, and K. Rao, *DNA damage and G2/M arrest in Syrian hamster embryo cells during malachite green exposure are associated with elevated phosphorylation of ERK1 and JNK1.* Cancer Letters, 2005. **230**: p. 260-70.
49. Widmann, C., et al., *Mitogen-activated protein kinase: conservation of a three-kinase module from yeast to human.* Physiology Review, 1999. **79**(1): p. 143-80.
50. Solhaug, A., M. Refsnes, and J. Holme, *Role of cell signalling involved in induction of apoptosis by benzo[a]pyrene and cyclopenta[c,d]pyrene in Hepa1c1c7 cells.* Journal of Cellular Biochemistry, 2004. **93**: p. 1143-1154.
51. Deacon, K. and J. Blank, *Characterization of the mitogen-activated protein kinase kinase 4 (MKK4)/c-Jun NH2-terminal kinase 1 and MKK3/p38 pathways regulated by MEK kinases 2 and 3.* Journal of Biological Chemistry, 1997. **272**(22): p. 14489-96.
52. Manke, I., et al., *MAPKAP Kinase-2 is a cell cycle checkpoint kinase that regulates the G2/M transition and S phase progression in response to UV irradiation.* Molecular Cell, 2005. **17**: p. 37-48.
53. Xia, Y., et al., *MEK kinase 1 is critically required for c-Jun N-terminal kinasse activation by proinflammatory stimuli and growth factor-induced cell migration.* PNAS, 2000. **97**(10): p. 5243-8.
54. Song, G., G. Ouyang, and S. Bao, *The activation of Akt/PKB signaling pathway and cell survival.* J Cell Mol Med, 2005. **9**(1): p. 59-71.
55. Kandel, E.S. and N. Hay, *The regulation and activities of the multifunctional serine/threonine kinase Akt/PKB.* Exp Cell Res, 1999. **253**(1): p. 210-29.
56. Burgering, B.M. and P.J. Coffer, *Protein kinase B (c-Akt) in phosphatidylinositol-3-OH kinase signal transduction.* Nature, 1995. **376**(6541): p. 599-602.
57. Sarbassov, D.D., et al., *Phosphorylation and regulation of Akt/PKB by the rictor-mTOR complex.* Science, 2005. **307**(5712): p. 1098-101.
58. Hresko, R.C. and M. Mueckler, *mTOR.RICTOR is the Ser473 kinase for Akt/protein kinase B in 3T3-L1 adipocytes.* J Biol Chem, 2005. **280**(49): p. 40406-16.
59. Toker, A. and A.C. Newton, *Cellular signaling: pivoting around PDK-1.* Cell, 2000. **103**(2): p. 185-8.
60. Plas, D.R. and C.B. Thompson, *Akt activation promotes degradation of tuberin and FOXO3a via the proteasome.* J Biol Chem, 2003. **278**(14): p. 12361-6.
61. Furukawa-Hibi, Y., et al., *FOXO transcription factors in cell-cycle regulation and the response to oxidative stress.* Antioxid Redox Signal, 2005. **7**(5-6): p. 752-60.
62. Cross, D.A., et al., *Inhibition of glycogen synthase kinase-3 by insulin mediated by protein kinase B.* Nature, 1995. **378**(6559): p. 785-9.
63. Datta, S.R., et al., *Akt phosphorylation of BAD couples survival signals to the cell-intrinsic death machinery.* Cell, 1997. **91**(2): p. 231-41.
64. Manning, B.D. and L.C. Cantley, *AKT/PKB signaling: navigating downstream.* Cell, 2007. **129**(7): p. 1261-74.

65. Tokunaga, E., et al., *Deregulation of the Akt pathway in human cancer.* Curr Cancer Drug Targets, 2008. **8**(1): p. 27-36.
66. Nassif, N.T., et al., *PTEN mutations are common in sporadic microsatellite stable colorectal cancer.* Oncogene, 2004. **23**(2): p. 617-28.
67. Samuels, Y. and K. Ericson, *Oncogenic PI3K and its role in cancer.* Curr Opin Oncol, 2006. **18**(1): p. 77-82.
68. Wang, C.Y., M.W. Mayo, and A.S. Baldwin, Jr., *TNF- and cancer therapy-induced apoptosis: potentiation by inhibition of NF-kappaB.* Science, 1996. **274**(5288): p. 784-7.
69. Manna, S.K., A. Mukhopadhyay, and B.B. Aggarwal, *Resveratrol suppresses TNF-induced activation of nuclear transcription factors NF-kappa B, activator protein-1, and apoptosis: potential role of reactive oxygen intermediates and lipid peroxidation.* J Immunol, 2000. **164**(12): p. 6509-19.
70. Karin, M. and F.R. Greten, *NF-kappaB: linking inflammation and immunity to cancer development and progression.* Nat Rev Immunol, 2005. **5**(10): p. 749-59.
71. Hacker, H. and M. Karin, *Regulation and function of IKK and IKK-related kinases.* Sci STKE, 2006. **2006**(357): p. re13.
72. Rothwarf, D.M. and M. Karin, *The NF-kappa B activation pathway: a paradigm in information transfer from membrane to nucleus.* Sci STKE, 1999. **1999**(5): p. RE1.
73. Wu, Z., et al., *Molecular linkage between the kinase ATM and the NF-kappaB signaling in response to genotoxic stimuli.* Science, 2006. **311**(5764): p. 1141-6.
74. Grosjean-Raillard, J., et al., *ATM mediates constitutive NF-kappaB activation in high-risk myelodysplastic syndrome and acute myeloid leukemia.* Oncogene, 2009. **28**(8): p. 1099-109.
75. Ahmed, K.M. and J.J. Li, *ATM-NF-kappaB connection as a target for tumor radiosensitization.* Curr Cancer Drug Targets, 2007. **7**(4): p. 335-42.
76. Stergiou, L. and M.O. Hengartner, *Death and more: DNA damage response pathways in the nematode C. elegans.* Cell Death Differ, 2004. **11**(1): p. 21-8.
77. Clarke, P.R. and L.A. Allan, *Cell-cycle control in the face of damage--a matter of life or death.* Trends Cell Biol, 2009. **19**(3): p. 89-98.
78. Hengartner, M.O., *The biochemistry of apoptosis.* Nature, 2000. **407**(6805): p. 770-6.
79. Reed, J.C., *Dysregulation of apoptosis in cancer.* J Clin Oncol, 1999. **17**(9): p. 2941-53.
80. Reed, J.C., *Mechanisms of apoptosis avoidance in cancer.* Curr Opin Oncol, 1999. **11**(1): p. 68-75.
81. Zimmermann, K.C., C. Bonzon, and D.R. Green, *The machinery of programmed cell death.* Pharmacol Ther, 2001. **92**(1): p. 57-70.
82. Voll, R.E., et al., *Immunosuppressive effects of apoptotic cells.* Nature, 1997. **390**(6658): p. 350-1.
83. Scaffidi, P., T. Misteli, and M.E. Bianchi, *Release of chromatin protein HMGB1 by necrotic cells triggers inflammation.* Nature, 2002. **418**(6894): p. 191-5.
84. Erlandsson Harris, H. and U. Andersson, *Mini-review: The nuclear protein HMGB1 as a proinflammatory mediator.* Eur J Immunol, 2004. **34**(6): p. 1503-12.
85. Martin, S.J. and D.R. Green, *Apoptosis as a goal of cancer therapy.* Curr Opin Oncol, 1994. **6**(6): p. 616-21.
86. Fulda, S. and K.M. Debatin, *Targeting apoptosis pathways in cancer therapy.* Curr Cancer Drug Targets, 2004. **4**(7): p. 569-76.
87. Milas, L., L.C. Stephens, and R.E. Meyn, *Relation of apoptosis to cancer therapy.* In Vivo, 1994. **8**(5): p. 665-73.
88. Czabotar, P.E., P.M. Colman, and D.C. Huang, *Bax activation by Bim?* Cell Death Differ, 2009.
89. Burz, C., et al., *Apoptosis in cancer: Key molecular signaling pathways and therapy targets.* Acta Oncol, 2009: p. 1-11.

90. Schultz, D.R. and W.J. Harrington, Jr., *Apoptosis: programmed cell death at a molecular level.* Semin Arthritis Rheum, 2003. **32**(6): p. 345-69.
91. Strasser, A., L. O'Connor, and V.M. Dixit, *Apoptosis signaling.* Annu Rev Biochem, 2000. **69**: p. 217-45.
92. Meiler, J. and M. Schuler, *Therapeutic targeting of apoptotic pathways in cancer.* Curr Drug Targets, 2006. **7**(10): p. 1361-9.
93. Zhou, B.B. and S.J. Elledge, *The DNA damage response: putting checkpoints in perspective.* Nature, 2000. **408**(6811): p. 433-9.
94. Jeggo, P.A. and M. Lobrich, *Contribution of DNA repair and cell cycle checkpoint arrest to the maintenance of genomic stability.* DNA Repair (Amst), 2006. **5**(9-10): p. 1192-8.
95. Cordon-Cardo, C., *Mutations of cell cycle regulators. Biological and clinical implications for human neoplasia.* Am J Pathol, 1995. **147**(3): p. 545-60.
96. Sellers, W.R. and W.G. Kaelin, Jr., *Role of the retinoblastoma protein in the pathogenesis of human cancer.* J Clin Oncol, 1997. **15**(11): p. 3301-12.
97. Goodyear, S. and M.C. Sharma, *Roscovitine regulates invasive breast cancer cell (MDA-MB231) proliferation and survival through cell cycle regulatory protein cdk5.* Exp Mol Pathol, 2007. **82**(1): p. 25-32.
98. Grant, S. and J.D. Roberts, *The use of cyclin-dependent kinase inhibitors alone or in combination with established cytotoxic drugs in cancer chemotherapy.* Drug Resist Updat, 2003. **6**(1): p. 15-26.
99. Senderowicz, A.M., *Small-molecule cyclin-dependent kinase modulators.* Oncogene, 2003. **22**(42): p. 6609-20.
100. Schwartz, G.K. and M.A. Shah, *Targeting the cell cycle: a new approach to cancer therapy.* J Clin Oncol, 2005. **23**(36): p. 9408-21.
101. Blasina, A., et al., *Breaching the DNA damage checkpoint via PF-00477736, a novel small-molecule inhibitor of checkpoint kinase 1.* Mol Cancer Ther, 2008. **7**(8): p. 2394-404.
102. Zabludoff, S.D., et al., *AZD7762, a novel checkpoint kinase inhibitor, drives checkpoint abrogation and potentiates DNA-targeted therapies.* Mol Cancer Ther, 2008. **7**(9): p. 2955-66.
103. Nayak, S., et al., *A test of highly optimized tolerance reveals fragile cell-cycle mechanisms are molecular targets in clinical cancer trials.* PLoS One, 2008. **3**(4): p. e2016.
104. Carvalho, C., et al., *Doxorubicin: the Good, the Bad and the Ugly Effect.* Curr Med Chem, 2009.
105. Weiss, R.B., *The anthracyclines: will we ever find a better doxorubicin?* Semin Oncol, 1992. **19**(6): p. 670-86.
106. Cortes-Funes, H. and C. Coronado, *Role of anthracyclines in the era of targeted therapy.* Cardiovasc Toxicol, 2007. **7**(2): p. 56-60.
107. Tewey, K.M., et al., *Adriamycin-induced DNA damage mediated by mammalian DNA topoisomerase II.* Science, 1984. **226**(4673): p. 466-8.
108. Binaschi, M., et al., *Anthracyclines: selected new developments.* Curr Med Chem Anticancer Agents, 2001. **1**(2): p. 113-30.
109. Moro, S., et al., *Interaction model for anthracycline activity against DNA topoisomerase II.* Biochemistry, 2004. **43**(23): p. 7503-13.
110. Mukhopadhyay, P., et al., *Role of superoxide, nitric oxide, and peroxynitrite in doxorubicin-induced cell death in vivo and in vitro.* Am J Physiol Heart Circ Physiol, 2009. **296**(5): p. H1466-83.
111. Kalyanaraman, B., et al., *Doxorubicin-induced apoptosis: implications in cardiotoxicity.* Mol Cell Biochem, 2002. **234-235**(1-2): p. 119-24.

112. Kurz, E.U., P. Douglas, and S.P. Lees-Miller, *Doxorubicin activates ATM-dependent phosphorylation of multiple downstream targets in part through the generation of reactive oxygen species.* J Biol Chem, 2004. **279**(51): p. 53272-81.
113. Momparler, R.L., et al., *Effect of adriamycin on DNA, RNA, and protein synthesis in cell-free systems and intact cells.* Cancer Res, 1976. **36**(8): p. 2891-5.
114. Potmesil, M., et al., *Relationship of adriamycin concentrations to the DNA lesions induced in hypoxic and euoxic L1210 cells.* Cancer Res, 1983. **43**(8): p. 3528-33.
115. Hortobagyi, G.N., *Anthracyclines in the treatment of cancer. An overview.* Drugs, 1997. **54 Suppl 4**: p. 1-7.
116. Capranico, G., et al., *Role of DNA breakage in cytotoxicity of doxorubicin, 9-deoxydoxorubicin, and 4-demethyl-6-deoxydoxorubicin in murine leukemia P388 cells.* Cancer Res, 1989. **49**(8): p. 2022-7.
117. Sinha, B.K. and P.M. Politi, *Anthracyclines.* Cancer Chemother Biol Response Modif, 1990. **11**: p. 45-57.
118. Ben-Baruch, A., *Host microenvironment in breast cancer development: inflammatory cells, cytokines and chemokines in breast cancer progression: reciprocal tumor-microenvironment interactions.* Breast Cancer Res, 2003. **5**(1): p. 31-6.
119. Szlosarek, P., K.A. Charles, and F.R. Balkwill, *Tumour necrosis factor-alpha as a tumour promoter.* Eur J Cancer, 2006. **42**(6): p. 745-50.
120. Naylor, M.S., et al., *Tumor necrosis factor and its receptors in human ovarian cancer. Potential role in disease progression.* J Clin Invest, 1993. **91**(5): p. 2194-206.
121. Sheen-Chen, S.M., et al., *Serum concentration of tumor necrosis factor in patients with breast cancer.* Breast Cancer Res Treat, 1997. **43**(3): p. 211-5.
122. Balkwill, F. and A. Mantovani, *Inflammation and cancer: back to Virchow?* Lancet, 2001. **357**(9255): p. 539-45.
123. Dunning, A.M., et al., *A systematic review of genetic polymorphisms and breast cancer risk.* Cancer Epidemiol Biomarkers Prev, 1999. **8**(10): p. 843-54.
124. Popivanova, B.K., et al., *Blocking TNF-alpha in mice reduces colorectal carcinogenesis associated with chronic colitis.* J Clin Invest, 2008. **118**(2): p. 560-70.
125. Goossens, V., et al., *Direct evidence for tumor necrosis factor-induced mitochondrial reactive oxygen intermediates and their involvement in cytotoxicity.* Proc Natl Acad Sci U S A, 1995. **92**(18): p. 8115-9.
126. Lejeune, F., et al., *Rationale for using TNF alpha and chemotherapy in regional therapy of melanoma.* J Cell Biochem, 1994. **56**(1): p. 52-61.
127. Obrador, E., et al., *Possible mechanisms for tumour cell sensitivity to TNF-alpha and potential therapeutic applications.* Curr Pharm Biotechnol, 2001. **2**(2): p. 119-30.
128. Lynch, T.J., et al., *Activating mutations in the epidermal growth factor receptor underlying responsiveness of non-small-cell lung cancer to gefitinib.* N Engl J Med, 2004. **350**(21): p. 2129-39.
129. Helfrich, B.A., et al., *Antitumor activity of the epidermal growth factor receptor (EGFR) tyrosine kinase inhibitor gefitinib (ZD1839, Iressa) in non-small cell lung cancer cell lines correlates with gene copy number and EGFR mutations but not EGFR protein levels.* Clin Cancer Res, 2006. **12**(23): p. 7117-25.
130. Mukohara, T., et al., *Expression of epidermal growth factor receptor (EGFR) and downstream-activated peptides in surgically excised non-small-cell lung cancer (NSCLC).* Lung Cancer, 2003. **41**(2): p. 123-30.

131. Yu, C., et al., *Induction of apoptosis in human leukemia cells by the tyrosine kinase inhibitor adaphostin proceeds through a RAF-1/MEK/ERK- and AKT-dependent process.* Oncogene, 2004. **23**(7): p. 1364-76.
132. Metro, G., et al., *Epidermal growth factor receptor (EGFR) targeted therapies in non-small cell lung cancer (NSCLC).* Rev Recent Clin Trials, 2006. **1**(1): p. 1-13.
133. Ferrer-Soler, L., et al., *An update of the mechanisms of resistance to EGFR-tyrosine kinase inhibitors in breast cancer: Gefitinib (Iressa) -induced changes in the expression and nucleo-cytoplasmic trafficking of HER-ligands (Review).* Int J Mol Med, 2007. **20**(1): p. 3-10.
134. Eichhorn, P.J., et al., *Phosphatidylinositol 3-kinase hyperactivation results in lapatinib resistance that is reversed by the mTOR/phosphatidylinositol 3-kinase inhibitor NVP-BEZ235.* Cancer Res, 2008. **68**(22): p. 9221-30.
135. She, Q.B., et al., *Breast tumor cells with PI3K mutation or HER2 amplification are selectively addicted to Akt signaling.* PLoS One, 2008. **3**(8): p. e3065.
136. Yamasaki, F., et al., *Acquired resistance to erlotinib in A-431 epidermoid cancer cells requires down-regulation of MMAC1/PTEN and up-regulation of phosphorylated Akt.* Cancer Res, 2007. **67**(12): p. 5779-88.
137. Hickson, I., et al., *Identification and characterization of a novel and specific inhibitor of the ataxia-telangiectasia mutated kinase ATM.* Cancer Res, 2004. **64**(24): p. 9152-9.
138. Helleday, T., et al., *DNA repair pathways as targets for cancer therapy.* Nat Rev Cancer, 2008. **8**(3): p. 193-204.
139. Shiloh, Y., E. Tabor, and Y. Becker, *Abnormal response of ataxia-telangiectasia cells to agents that break the deoxyribose moiety of DNA via a targeted free radical mechanism.* Carcinogenesis, 1983. **4**(10): p. 1317-22.
140. Barlow, C., et al., *Atm-deficient mice: a paradigm of ataxia telangiectasia.* Cell, 1996. **86**(1): p. 159-71.
141. Chun, H.H. and R.A. Gatti, *Ataxia-telangiectasia, an evolving phenotype.* DNA Repair (Amst), 2004. **3**(8-9): p. 1187-96.
142. Tribius, S., A. Pidel, and D. Casper, *ATM protein expression correlates with radioresistance in primary glioblastoma cells in culture.* Int J Radiat Oncol Biol Phys, 2001. **50**(2): p. 511-23.
143. Haidar, M.A., et al., *ATM gene deletion in patients with adult acute lymphoblastic leukemia.* Cancer, 2000. **88**(5): p. 1057-62.
144. Ripolles, L., et al., *Genetic abnormalities and clinical outcome in chronic lymphocytic leukemia.* Cancer Genet Cytogenet, 2006. **171**(1): p. 57-64.
145. Austen, B., et al., *Mutation status of the residual ATM allele is an important determinant of the cellular response to chemotherapy and survival in patients with chronic lymphocytic leukemia containing an 11q deletion.* J Clin Oncol, 2007. **25**(34): p. 5448-57.
146. Carbone, D.P., *Epidermal growth factor receptor overexpression: the importance of context.* J Clin Oncol, 2003. **21**(23): p. 4268-9.
147. Grimwade, D., et al., *The importance of diagnostic cytogenetics on outcome in AML: analysis of 1,612 patients entered into the MRC AML 10 trial. The Medical Research Council Adult and Children's Leukaemia Working Parties.* Blood, 1998. **92**(7): p. 2322-33.
148. Kitano, H., *Systems biology: a brief overview.* Science, 2002. **295**(5560): p. 1662-4.
149. Kitano, H., *Computational systems biology.* Nature, 2002. **420**(6912): p. 206-10.
150. Ideker, T., L.R. Winslow, and D.A. Lauffenburger, *Bioengineering and systems biology.* Ann Biomed Eng, 2006. **34**(7): p. 1226-33.
151. Janes, K.A. and M.B. Yaffe, *Data-driven modelling of signal-transduction networks.* Nat Rev Mol Cell Biol, 2006. **7**(11): p. 820-8.

152. Janes, K.A. and D.A. Lauffenburger, *A biological approach to computational models of proteomic networks.* Curr Opin Chem Biol, 2006. **10**(1): p. 73-80.
153. Aldridge, B.B., et al., *Physicochemical modelling of cell signalling pathways.* Nat Cell Biol, 2006. **8**(11): p. 1195-203.
154. Janes, K.A., et al., *A systems model of signaling identifies a molecular basis set for cytokine-induced apoptosis.* Science, 2005. **310**(5754): p. 1646-53.
155. Geladi, P. and B. Kowalski, *Partial least-squares regression: a tutorial.* Anal. Chim. Acta, 1986. **185**: p. 1-17.
156. Mevik, B. and R. Wehrens, *The pls Package: Principal Component and Partial Least Squares Regression in R.* Journal of Statistical Software, 2007. **18**(2).
157. Miller-Jensen, K., et al., *Common effector processing mediates cell-specific responses to stimuli.* Nature, 2007. **448**(7153): p. 604-8.
158. Gaudet, S., et al., *A compendium of signals and responses triggered by prodeath and prosurvival cytokines.* Mol Cell Proteomics, 2005. **4**(10): p. 1569-90.
159. Gaudet, S., et al., *A compendium of signals and responses triggered by prodeath and prosurvival cytokines.* Molecular and Cellular Proteomics, 2005.
160. Kemp, M.L., et al., *Quantitative network signal combinations downstream of TCR activation can predict IL-2 production response.* J Immunol, 2007. **178**(8): p. 4984-92.
161. Kumar, D., et al., *Capturing cell-fate decisions from the molecular signatures of a receptor-dependent signaling response.* Mol Syst Biol, 2007. **3**: p. 150.
162. Kumar, N., et al., *Modeling HER2 effects on cell behavior from mass spectrometry phosphotyrosine data.* PLoS Comput Biol, 2007. **3**(1): p. e4.
163. Cary, N.C., *SAS/STAT User's Guide, Version 6, Fourth Edition*. Vol. 2. 1989: SAS Institute Inc. .
164. Bendel, R. and A.A. Afifi, *Comparison of Stopping Rules in Forward "Stepwise" Regression.* Journal of the American Statistical Association, 1977. **72**(357): p. 46-53.
165. Janes, K.A., et al., *The response of human epithelial cells to TNF involves an inducible autocrine cascade.* Cell, 2006. **124**(6): p. 1225-39.
166. Janes, K.A., H.C. Reinhardt, and M.B. Yaffe, *Cytokine-induced signaling networks prioritize dynamic range over signal strength.* Cell, 2008. **135**(2): p. 343-54.
167. Sachs, K., et al., *Causal protein-signaling networks derived from multiparameter single-cell data.* Science, 2005. **308**(5721): p. 523-9.
168. Sachs, K., et al., *Learning cyclic signaling pathway structures while minimizing data requirements.* Pac Symp Biocomput, 2009: p. 63-74.
169. Junttila, M.R., S.P. Li, and J. Westermarck, *Phosphatase-mediated crosstalk between MAPK signaling pathways in the regulation of cell survival.* FASEB J, 2008. **22**(4): p. 954-65.
170. Ballif, B.A. and J. Blenis, *Molecular mechanisms mediating mammalian mitogen-activated protein kinase (MAPK) kinase (MEK)-MAPK cell survival signals.* Cell Growth Differ, 2001. **12**(8): p. 397-408.
171. Meloche, S. and J. Pouyssegur, *The ERK1/2 mitogen-activated protein kinase pathway as a master regulator of the G1- to S-phase transition.* Oncogene, 2007. **26**(22): p. 3227-39.
172. Chambard, J.C., et al., *ERK implication in cell cycle regulation.* Biochim Biophys Acta, 2007. **1773**(8): p. 1299-310.
173. Tsakiridis, T., et al., *Association of phosphorylated epidermal growth factor receptor with survival in patients with locally advanced non-small cell lung cancer treated with radiotherapy.* J Thorac Oncol, 2008. **3**(7): p. 716-22.
174. Nishioka, C., et al., *Inhibition of MEK signaling enhances the ability of cytarabine to induce growth arrest and apoptosis of acute myelogenous leukemia cells.* Apoptosis, 2009.

175. Tang, D., et al., *ERK activation mediates cell cycle arrest and apoptosis after DNA damage independently of p53.* J Biol Chem, 2002. **277**(15): p. 12710-7.
176. Yan, Y., C.P. Black, and K.H. Cowan, *Irradiation-induced G2/M checkpoint response requires ERK1/2 activation.* Oncogene, 2007. **26**(32): p. 4689-98.
177. McCubrey, J.A., et al., *Roles of the RAF/MEK/ERK and PI3K/PTEN/AKT pathways in malignant transformation and drug resistance.* Adv Enzyme Regul, 2006. **46**: p. 249-79.
178. Roberts, P.J. and C.J. Der, *Targeting the Raf-MEK-ERK mitogen-activated protein kinase cascade for the treatment of cancer.* Oncogene, 2007. **26**(22): p. 3291-310.
179. Li, Q. and Z. Yang, *Expression of phospho-ERK1/2 and PI3-K in benign and malignant gallbladder lesions and its clinical and pathological correlations.* J Exp Clin Cancer Res, 2009. **28**: p. 65.
180. Warrener, R., et al., *Tumor cell-selective cytotoxicity by targeting cell cycle checkpoints.* FASEB J, 2003. **17**(11): p. 1550-2.
181. Albanese, C., et al., *Transforming p21ras mutants and c-Ets-2 activate the cyclin D1 promoter through distinguishable regions.* J Biol Chem, 1995. **270**(40): p. 23589-97.
182. Winston, J.T., et al., *Regulation of the cell cycle machinery by oncogenic ras.* Oncogene, 1996. **12**(1): p. 127-34.
183. Aktas, H., H. Cai, and G.M. Cooper, *Ras links growth factor signaling to the cell cycle machinery via regulation of cyclin D1 and the Cdk inhibitor p27KIP1.* Mol Cell Biol, 1997. **17**(7): p. 3850-7.
184. Cheng, M., et al., *Assembly of cyclin D-dependent kinase and titration of p27Kip1 regulated by mitogen-activated protein kinase kinase (MEK1).* Proc Natl Acad Sci U S A, 1998. **95**(3): p. 1091-6.
185. Vanhaesebroeck, B., et al., *Phosphoinositide 3-kinases: a conserved family of signal transducers.* Trends Biochem Sci, 1997. **22**(7): p. 267-72.
186. Diehl, J.A., et al., *Glycogen synthase kinase-3beta regulates cyclin D1 proteolysis and subcellular localization.* Genes Dev, 1998. **12**(22): p. 3499-511.
187. Sherr, C.J., *Mammalian G1 cyclins.* Cell, 1993. **73**(6): p. 1059-65.
188. Hatakeyama, M., et al., *Collaboration of G1 cyclins in the functional inactivation of the retinoblastoma protein.* Genes Dev, 1994. **8**(15): p. 1759-71.
189. Harbour, J.W., et al., *Cdk phosphorylation triggers sequential intramolecular interactions that progressively block Rb functions as cells move through G1.* Cell, 1999. **98**(6): p. 859-69.
190. Calbo, J., et al., *G1 cyclin/cyclin-dependent kinase-coordinated phosphorylation of endogenous pocket proteins differentially regulates their interactions with E2F4 and E2F1 and gene expression.* J Biol Chem, 2002. **277**(52): p. 50263-74.
191. Leng, X., et al., *Reversal of growth suppression by p107 via direct phosphorylation by cyclin D1/cyclin-dependent kinase 4.* Mol Cell Biol, 2002. **22**(7): p. 2242-54.
192. Sherr, C.J., *Cancer cell cycles.* Science, 1996. **274**(5293): p. 1672-7.
193. Lin, D.I., et al., *Phosphorylation-dependent ubiquitination of cyclin D1 by the SCF(FBX4-alphaB crystallin) complex.* Mol Cell, 2006. **24**(3): p. 355-66.
194. Okabe, H., et al., *A critical role for FBXW8 and MAPK in cyclin D1 degradation and cancer cell proliferation.* PLoS One, 2006. **1**: p. e128.
195. Alt, J.R., et al., *Phosphorylation-dependent regulation of cyclin D1 nuclear export and cyclin D1-dependent cellular transformation.* Genes Dev, 2000. **14**(24): p. 3102-14.
196. Gladden, A.B. and J.A. Diehl, *Location, location, location: the role of cyclin D1 nuclear localization in cancer.* J Cell Biochem, 2005. **96**(5): p. 906-13.
197. Gladden, A.B., et al., *Expression of constitutively nuclear cyclin D1 in murine lymphocytes induces B-cell lymphoma.* Oncogene, 2006. **25**(7): p. 998-1007.
198. Moreno-Bueno, G., et al., *Cyclin D1 gene (CCND1) mutations in endometrial cancer.* Oncogene, 2003. **22**(38): p. 6115-8.

199. Benzeno, S., et al., *Identification of mutations that disrupt phosphorylation-dependent nuclear export of cyclin D1.* Oncogene, 2006. **25**(47): p. 6291-303.
200. Kultz, D., et al., *Distinct regulation of osmoprotective genes in yeast and mammals. Aldose reductase osmotic response element is induced independent of p38 and stress-activated protein kinase/Jun N-terminal kinase in rabbit kidney cells.* J Biol Chem, 1997. **272**(20): p. 13165-70.
201. Kultz, D., S. Madhany, and M.B. Burg, *Hyperosmolality causes growth arrest of murine kidney cells. Induction of GADD45 and GADD153 by osmosensing via stress-activated protein kinase 2.* J Biol Chem, 1998. **273**(22): p. 13645-51.
202. Kurata, S., *Selective activation of p38 MAPK cascade and mitotic arrest caused by low level oxidative stress.* J Biol Chem, 2000. **275**(31): p. 23413-6.
203. Casanovas, O., et al., *Osmotic stress regulates the stability of cyclin D1 in a p38SAPK2-dependent manner.* J Biol Chem, 2000. **275**(45): p. 35091-7.
204. Santra, M.K., N. Wajapeyee, and M.R. Green, *F-box protein FBXO31 mediates cyclin D1 degradation to induce G1 arrest after DNA damage.* Nature, 2009. **459**(7247): p. 722-5.
205. Bouchard, C., P. Staller, and M. Eilers, *Control of cell proliferation by Myc.* Trends Cell Biol, 1998. **8**(5): p. 202-6.
206. Sears, R., et al., *Multiple Ras-dependent phosphorylation pathways regulate Myc protein stability.* Genes Dev, 2000. **14**(19): p. 2501-14.
207. Charron, J., et al., *Embryonic lethality in mice homozygous for a targeted disruption of the N-myc gene.* Genes Dev, 1992. **6**(12A): p. 2248-57.
208. Davis, A.C., et al., *A null c-myc mutation causes lethality before 10.5 days of gestation in homozygotes and reduced fertility in heterozygous female mice.* Genes Dev, 1993. **7**(4): p. 671-82.
209. Coppola, J.A. and M.D. Cole, *Constitutive c-myc oncogene expression blocks mouse erythroleukaemia cell differentiation but not commitment.* Nature, 1986. **320**(6064): p. 760-3.
210. Evan, G.I., et al., *Induction of apoptosis in fibroblasts by c-myc protein.* Cell, 1992. **69**(1): p. 119-28.
211. Benaud, C.M. and R.B. Dickson, *Adhesion-regulated G1 cell cycle arrest in epithelial cells requires the downregulation of c-Myc.* Oncogene, 2001. **20**(33): p. 4554-67.
212. Janardhanan, R., N.L. Banik, and S.K. Ray, *N-Myc down regulation induced differentiation, early cell cycle exit, and apoptosis in human malignant neuroblastoma cells having wild type or mutant p53.* Biochem Pharmacol, 2009.
213. Hann, S.R. and R.N. Eisenman, *Proteins encoded by the human c-myc oncogene: differential expression in neoplastic cells.* Mol Cell Biol, 1984. **4**(11): p. 2486-97.
214. Ramsay, G., et al., *Human proto-oncogene N-myc encodes nuclear proteins that bind DNA.* Mol Cell Biol, 1986. **6**(12): p. 4450-7.
215. Ciechanover, A., et al., *Degradation of nuclear oncoproteins by the ubiquitin system in vitro.* Proc Natl Acad Sci U S A, 1991. **88**(1): p. 139-43.
216. Flinn, E.M., C.M. Busch, and A.P. Wright, *myc boxes, which are conserved in myc family proteins, are signals for protein degradation via the proteasome.* Mol Cell Biol, 1998. **18**(10): p. 5961-9.
217. Salghetti, S.E., S.Y. Kim, and W.P. Tansey, *Destruction of Myc by ubiquitin-mediated proteolysis: cancer-associated and transforming mutations stabilize Myc.* EMBO J, 1999. **18**(3): p. 717-26.
218. Sears, R., et al., *Ras enhances Myc protein stability.* Mol Cell, 1999. **3**(2): p. 169-79.
219. Yeh, E., et al., *A signalling pathway controlling c-Myc degradation that impacts oncogenic transformation of human cells.* Nat Cell Biol, 2004. **6**(4): p. 308-18.
220. Escamilla-Powers, J.R. and R.C. Sears, *A conserved pathway that controls c-Myc protein stability through opposing phosphorylation events occurs in yeast.* J Biol Chem, 2007. **282**(8): p. 5432-42.

221. Kumar, A., M. Marques, and A.C. Carrera, *Phosphoinositide 3-kinase activation in late G1 is required for c-Myc stabilization and S phase entry.* Mol Cell Biol, 2006. **26**(23): p. 9116-25.
222. Sears, R.C. and J.R. Nevins, *Signaling networks that link cell proliferation and cell fate.* J Biol Chem, 2002. **277**(14): p. 11617-20.
223. Jones, S.M., et al., *PDGF induces an early and a late wave of PI 3-kinase activity, and only the late wave is required for progression through G1.* Curr Biol, 1999. **9**(10): p. 512-21.
224. Jones, S.M. and A. Kazlauskas, *Growth-factor-dependent mitogenesis requires two distinct phases of signalling.* Nat Cell Biol, 2001. **3**(2): p. 165-72.
225. Garcia, Z., et al., *Phosphoinositide 3-kinase controls early and late events in mammalian cell division.* EMBO J, 2006. **25**(4): p. 655-61.
226. Seth, A., et al., *Signal transduction within the nucleus by mitogen-activated protein kinase.* J Biol Chem, 1992. **267**(34): p. 24796-804.
227. Pulverer, B.J., et al., *Site-specific modulation of c-Myc cotransformation by residues phosphorylated in vivo.* Oncogene, 1994. **9**(1): p. 59-70.
228. Kinoshita, T., et al., *Raf/MAPK and rapamycin-sensitive pathways mediate the anti-apoptotic function of p21Ras in IL-3-dependent hematopoietic cells.* Oncogene, 1997. **15**(6): p. 619-27.
229. Erhardt, P., E.J. Schremser, and G.M. Cooper, *B-Raf inhibits programmed cell death downstream of cytochrome c release from mitochondria by activating the MEK/Erk pathway.* Mol Cell Biol, 1999. **19**(8): p. 5308-15.
230. Le Gall, M., et al., *The p42/p44 MAP kinase pathway prevents apoptosis induced by anchorage and serum removal.* Mol Biol Cell, 2000. **11**(3): p. 1103-12.
231. Davies, H., et al., *Mutations of the BRAF gene in human cancer.* Nature, 2002. **417**(6892): p. 949-54.
232. Balmanno, K. and S.J. Cook, *Tumour cell survival signalling by the ERK1/2 pathway.* Cell Death Differ, 2009. **16**(3): p. 368-77.
233. Adams, J.M. and S. Cory, *The Bcl-2 apoptotic switch in cancer development and therapy.* Oncogene, 2007. **26**(9): p. 1324-37.
234. Puthalakath, H. and A. Strasser, *Keeping killers on a tight leash: transcriptional and post-translational control of the pro-apoptotic activity of BH3-only proteins.* Cell Death Differ, 2002. **9**(5): p. 505-12.
235. Weston, C.R., et al., *Activation of ERK1/2 by deltaRaf-1:ER* represses Bim expression independently of the JNK or PI3K pathways.* Oncogene, 2003. **22**(9): p. 1281-93.
236. Fu, Z. and D.J. Tindall, *FOXOs, cancer and regulation of apoptosis.* Oncogene, 2008. **27**(16): p. 2312-9.
237. Yang, J.Y., et al., *ERK promotes tumorigenesis by inhibiting FOXO3a via MDM2-mediated degradation.* Nat Cell Biol, 2008. **10**(2): p. 138-48.
238. Ley, R., et al., *Activation of the ERK1/2 signaling pathway promotes phosphorylation and proteasome-dependent degradation of the BH3-only protein, Bim.* J Biol Chem, 2003. **278**(21): p. 18811-6.
239. Ley, R., et al., *Extracellular signal-regulated kinases 1/2 are serum-stimulated "Bim(EL) kinases" that bind to the BH3-only protein Bim(EL) causing its phosphorylation and turnover.* J Biol Chem, 2004. **279**(10): p. 8837-47.
240. Ewings, K.E., et al., *ERK1/2-dependent phosphorylation of BimEL promotes its rapid dissociation from Mcl-1 and Bcl-xL.* EMBO J, 2007. **26**(12): p. 2856-67.
241. Hubner, A., et al., *Multisite phosphorylation regulates Bim stability and apoptotic activity.* Mol Cell, 2008. **30**(4): p. 415-25.

242. Luciano, F., et al., *Phosphorylation of Bim-EL by Erk1/2 on serine 69 promotes its degradation via the proteasome pathway and regulates its proapoptotic function.* Oncogene, 2003. **22**(43): p. 6785-93.
243. Ewings, K.E., C.M. Wiggins, and S.J. Cook, *Bim and the pro-survival Bcl-2 proteins: opposites attract, ERK repels.* Cell Cycle, 2007. **6**(18): p. 2236-40.
244. Domina, A.M., et al., *MCL1 is phosphorylated in the PEST region and stabilized upon ERK activation in viable cells, and at additional sites with cytotoxic okadaic acid or taxol.* Oncogene, 2004. **23**(31): p. 5301-15.
245. Maurer, U., et al., *Glycogen synthase kinase-3 regulates mitochondrial outer membrane permeabilization and apoptosis by destabilization of MCL-1.* Mol Cell, 2006. **21**(6): p. 749-60.